Increasing the Capacity of the Low Voltage Distribution Networks using All-SiC AC-AC Converters

Evangelos Dimitrios Zacharis

Doctor of Philosophy

Aston University

July 2015

Thesis Summary

Aston University
Increasing the Capacity of the Low Voltage Distribution Networks using All-SiC AC-AC Converters
Evangelos Dimitrios Zacharis
PhD in Electronic Engineering
July 2015

Towards 2020, future energy scenarios predict an excessive penetration of distributed generation (DG) in low voltage (LV) networks as well as a significant uptake of electric vehicles (EVs) and electro-heating. The Distribution Network Operators (DNOs) in UK will face significant challenges towards this de-carbonised electricity generation and consumption shift. The deployment of these so-called low carbon technologies (LCTs) will impact the performance of the distribution network in such way where solutions will be needed to maintain capacity, reliability and the availability of the electricity supply to customers. The practise to put more copper on the ground – reinforcement - in order to facilitate these changes is found to be expensive and disruptive to the public and business. An innovative solution proposed in this thesis is to increase the voltage along the distribution feeders and step it back down at a customer's premises. Results show that a significant increase at the hosting capacity of the existing network can be achieved and power quality problems such as overvoltage caused by DG can be avoided. The voltage step-down device, which is termed a voltage control unit (VCU), is to be located in the meter-box of each house. This location raises challenges around the temperature rise in the box caused by VCU losses, and the subsequent effect on the electricity meter and cut-out fuse. It also imposes constraints on the size and weight of the VCU so that a very high efficiency design is required, with high power density and small mass. The optimum VCU design was found to be a power electronic AC Chopper using new Silicon Carbide (SiC) MOSFETs and diodes. The technology was demonstrated by designing, constructing and testing two interleaved, parallel operation, 1 kW AC Chopper modules. Results from the prototype were compared against Spice simulation results and theory and confirmed that the target efficiency of 99% was achieved.

Keywords: Low Carbon Technologies, AC Chopper, Silicon Carbide, High Efficiency

To my parents,
Dimitris and Eleni

“Δεν ελπίζω τίποτα. Δεν φοβάμαι τίποτα. Είμαι ελεύθερος.”

Νίκος Καζαντζάκης

“Our virtues and our failings are inseparable, like force and matter. When they separate, man is no more.”
Nicola Tesla

Acknowledgments

I owe an enormous debt of gratitude to my supervisor, Dr Andrew Cross, for his patience, support, guidance and belief during my study as well as my life throughout the last four years. He taught me something beyond just techniques for solving problems and led me to a new world full of challenges and opportunities. His profound knowledge, gentle personality and rigorous attitude toward research will benefit my career as well as my whole personal life.

I wish also to express my thanks to my second supervisor Dr Dani Strickland for her advices and encouragement throughout my study. Also, to my examiners Dr Jin Yang and Prof Sarath Tennakoon for the evaluation of my work and an enjoyable viva.

A special thank goes to the other members of the Power Engineering and Power Electronics research group, staff in the School of Engineering & Applied Science and my "PhD mates" at Aston University who have provided a friendly working atmosphere.

I am grateful for the support of Western Power Distribution, both financially and in their support of the work throughout.

A big thank also to the company I work for, Arup, and especially to Richard Pearce for the support I received throughout the writing up period.

I would like to thank my family and friends for supporting me and bearing with me during times of stress and hard work. A special thanks to my mother Eleni and my father Dimitris for believing in me and supporting my dreams and decisions.

Finally I owe much to Valia, who manages a very complicated relationship with grace and generosity and without whose love, understanding and encouragement I would not have completed this work.

Contents

List of Figures

List of Tables

1 Introduction

1.1 Motivation

The world faces huge problems around an increasing demand for energy, and electricity networks are the main conduit through which energy is distributed and delivered to us. Making this network more efficient, and allowing it to connect to more environmentally friendly, sustainable energy sources in a secure manner is a significant challenge. This makes it an incredibly exciting research area to be involved in from a scientific and engineering point of view.

1.2 Research Aim and Objectives

The aim of this doctoral thesis is to develop and verify an effective method to increase the amount of Distributed Generation and Low Carbon Technologies that can be connected to existing LV distribution grids.

To achieve this goal, the objectives of this research project are identified as:

- Analysing the role of electricity in developed and developing economies today and tomorrow and the challenges that the electrical power network will face towards a decarbonised future in generation and consumption.
- Evaluating the applicability of a voltage increase in the existing LV network infrastructure and determining the requirements of the device to step back down the voltage within the statutory limits at the point of common coupling of each customer.
- Determining the most suitable power electronic topology for this application by conducting literature review, analysis and simulations.
- Developing and demonstrating an adequate high efficiency and high power density prototype in order to prove the concept

1.3 Research Beneficiaries

Different stakeholders will benefit from the research presented in this thesis:

- **Distribution Network Operators:** The research enables DNOs to recognise the influence that LCTs bring to LV networks regarding load profile variation and effects on purely technical aspects. Also, the network modelling studies allow the DNOs to

estimate what capacity remains on the existing infrastructure in order to host EV charging and the magnitude of feeder voltage drops due to DG. Furthermore, the research also identifies the potential techno-economic benefits DNOs can experience if the proposed VCU solution was implemented.

- **Regulators:** The research discusses how regulators create policies that promote a shift towards low carbon energy future. Regulators will benefit from this research work by appreciating the wider concerns that DNOs have, and how they might better support DNOs in order to successfully achieve an integration of LCTs into present and future network design.
- **Academic society:** The proposed solution can open a new field of research for academics as it is the first to propose an increase in network voltage in order to better utilise the hosting capacity of the existing LV networks.
- **Manufacturers:** Results from this work supports the co-operation between manufacturers from different and/or similar industries. Especially, this research work showcases the significant potential of power electronics in LV network and supports collaboration between Power Systems and Power Electronic companies.
- **Society:** The so-called energy "Trilemma" faced by society can be addressed by an increased use of LCTs. This will result in a cheaper, more reliable and clean, sustainable energy supply. Benefits will be though for example lower energy bills and reduced local pollution level.

1.4 Thesis Outline

Chapter 2: Following the Introduction, Chapter 2 discusses the issues around the UK's so-called energy "Trilemma", giving the research background related to LCTs and introduces what their impact is likely to be on electricity distribution networks. A solution to overcome the associated problems that these impacts will have is presented.

Chapter 3: Provides a literature review on LV distribution network design. Also, uses simulation studies to assess the effect of the proposed solution will have on the capacity of the existing LV network and outlines a specification for a VCU.

Chapter 4: Presents a literature review and an analysis of selected power electronic based topologies and compares them in terms of their VA rating and their power quality benefits in order to derive to a number of most suitable candidate circuits.

Chapter 5: Presents detailed Spice simulation studies of the candidate topologies and a comparison in terms of the associated semiconductor losses.

Chapter 6: Describes the design and implementation of a single-phase AC Chopper converter using Silicon Carbide semiconductor devices.

Chapter 7: Presents and discusses the results from testing the AC Chopper prototype.

Chapter 8: Includes the conclusions, contributions of this research and a discussion of future research.

2 The Role of Electricity and Future Challenges

This chapter discusses the drivers for electricity as the dominant form of energy transport within different energy scenarios, and investigates how it will contribute towards a decarbonised, affordable and secure energy future. Electricity distribution networks are the means by which electricity is delivered from the transmission system to a customer, and these networks will face significant challenges in the near future. The uptake of Low Carbon Technologies (LCTs), such as electric vehicles and photo-voltaic arrays, which is being driven by legal requirements around Climate Change, will make future electricity grids operate close to their designed capacity as well as causing additional power quality problems. Western Power Distribution (WPD) who are the largest distribution network operator (DNO) in the UK, are the sponsor for this research project and are interested in understanding what drives these changes, what problems they cause to the distribution network and what are the potential solutions. This research works identifies a power electronic solution to the problems described above as it is found that the benefits of such a state – of – the – art technology are not limited to the main objective of this thesis but can open a new world of opportunities in how the future distribution networks will operate. This project is just one in a number of studies that WPD are actively investigating the aspects outlined above and potential solutions through funding from the Office of Gas and Electricity Markets (Ofgem) Low Carbon network funding scheme and the Innovation Fund Initiative (IFI).

2.1 The Energy Trilemma

In most countries, whether regulated or liberalised, the energy sector is shaped by a range of energy policies, market designs, and regulations. These are implemented to reach policy targets and stimulate investment in energy supply, distribution and demand. The ultimate goal of these interventions is to make progress on the three dimensions of the so-called "energy trilemma" - increasing energy security, making energy services accessible and affordable while limiting the environmental impact of the way energy is produced and consumed. The correlation between these three dimensions is illustrated in Figure 2.1 [7].

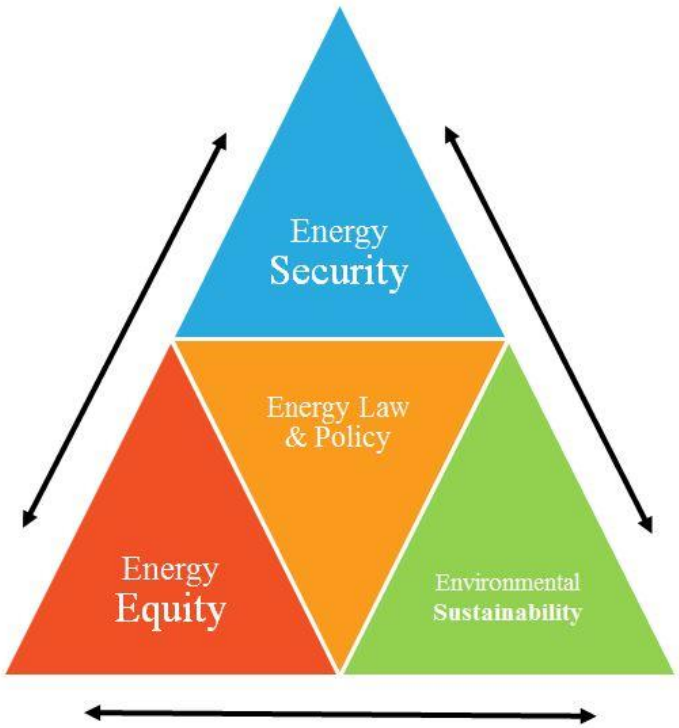

Figure 2.1: ***The Energy Trilemma Balance***

Further to this, in 1997 the United Nations Framework Convention on Climate Change (UNFCCC) established an agreement under which thirty seven initially industrialised countries –including UK, set targets to tackle the climate change by the agreement on the Kyoto Protocol [24]. As a result many of the energy policies developed in the last 10 years are driven from this initiative and reflect a shift towards a low carbon energy infrastructure, where electricity will become a key to solving the energy trilemma. European Union Directives have a straight impact in UK legislation and policy in the context of emission reductions. The previously mentioned legislations and initiatives led the UK parliament to implement the "Climate Change Act 2008" [1], which has led to so-called "Carbon Budgets" and the National Emissions Reduction Plan, which is due to the European Union Large Combustion Plant Directive [3], and the Electricity Market Reform (EMR) bill [4]. EMR is the response of the UK Government to the energy trilemma facing the UK. These policies have resulted in a growing role for electricity in future energy networks. In particular, the Renewables Obligation Order [5], the Feed in Tariff and Renewable Heat incentives have been driven by The Energy Act [6], which has resulted in a drive toward renewable electricity generators, electrically driven heat pumps and electric vehicles.

2.1.1 Drivers from an Energy Economics Perspective

Electricity is generally accepted as having the highest ability of its unit of energy to produce goods and services for people or in other words has the best energy quality followed by refined oil products [8-10]. Energy intensity is a measure of the energy efficiency of a country's economy to produce a unit of Gross Domestic Product (GDP); hence low energy intensity indicates a lower input of energy into an economy to produce one unit of GDP. The energy intensity of electricity is determined by the fuel mix of the generator that is producing the electricity. Therefore economic growth can be further decoupled from energy consumption needed to produce goods and services. This can be achieved by engaging electricity as the "link" energy form, where generation technologies with lower energy intensities can substitute previous energy sources [11-13].

Mackay in [14] clearly states that, there is a correlation between energy consumption per capita and GDP per capita. As can been seen in Figure 2.2 a higher GDP correlates to greater energy consumption. As the energy intensity of a country's energy mix drops, the amount of energy per unit of GDP reduces; energy usage is decoupled from the economy. Schurr and Netschert in [15] were the first to claim that a shift to higher quality fuels reduces the energy intensity and hence a real growth in the economy can be achieved. Further to this, by observing trends in the past five decades, researchers in [16] show that energy intensity has steadily declined in advanced economies, principally due to the shift in using higher quality fuels and the engagement of electricity. Moreover, from a climate change perspective this is desirable, because as economic growth decouples, relative decoupling of emissions from growth also follows.

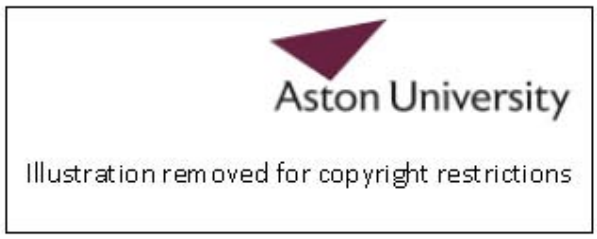

Figure 2.2: ***Power consumption per capita versus GDP per capita, in purchasing-power-parity US dollars. Data from UNDP Human Development Report, 2007. Squares show countries having "high human development;" circles, "medium" or "low."*** **[14]**

Policy makers from both climate change and energy security perspectives see electricity as a form of energy that can enable lowered emissions, and increased economic growth, due to the possibility of a lowered energy intensity, facilitated by the electricity generation mix [17]. Actually, in [17] the authors claim that a large proportion of current energy modelling research, advises that electricity will play a majority role in the delivery of heat and transport by 2050. While in many countries there is agreement that changes in energy infrastructure need to happen, there is much less agreement about the future structure of these energy models or how and who to pay for the shift. Rising energy bills for industry and consumers are becoming particularly contentious in many European countries including UK, and leading to debates on how to maintain economic affordability [7]. For example, in the UK, the average prices electricity paid by end users between 2007 and 2012 increased by around 20%. These figures put UK Government in a difficult position on how to respond to consumer concerns over energy companies' profits and renewable targets. As a result in 2012 the UK Government published the Energy Bill and the updated version of the Electricity Market Reform (EMR) in order to enable the shift to electricity with respect to customers' bills. This can be achieved by maximising benefits and minimising costs to the economy as a whole and to taxpayers and consumers. The

Governments' target is to maintain affordable electricity bills while delivering the investment needed towards decarbonisation [18].

2.1.2 Drivers from a Climate Perspective

Worldwide emissions of greenhouse gases (GHG), in particular CO_2, are speeding up climate change according to the Working Group III which was formed in 2007 to discuss the issue of Climate Change and the ways to mitigate it [19, 20]. In particular, the continued emissions of CO_2 over the last fifty years have caused numerous changes in global climate. These changes will lead to serious consequences in natural systems globally. To name a few, there are impacts on clean water resources, ecological systems, food, forests, coastal areas, human health and industry and society which use climate sensitive resources [21]. Anthropogenic GHG emissions have increased at 49 (± 4.5) $GtCO_2^{eq}$ per year which is an 80 % rise between the last forty years; Further, between 2000 and 2010 GHG emissions were the highest in human history. In particular, GHG emissions increased by an average of 1 $GtCO_2^{eq}$ (2.2 %) per year between 2000 and 2010, compared to 0.4 $GtCO_2^{eq}$ (1.3 %) per year between 1970 and 2000. A major source of CO_2 emissions is the supply of energy from fossil fuels not just within the electricity system but within the heating and transport sectors as well. Specifically, fossil fuel-related CO_2 emissions for energy purposes increased consistently over the last 40 years reaching $32GtCO_2^{eq}$ per year, or 69 % of global GHG emissions in 2008 as shown in Figure 2.3. These have continued to increase every year onwards by about 3 % between 2010 and 2011 and by about 1 – 2 % between 2011 and 2012 [22, 23].

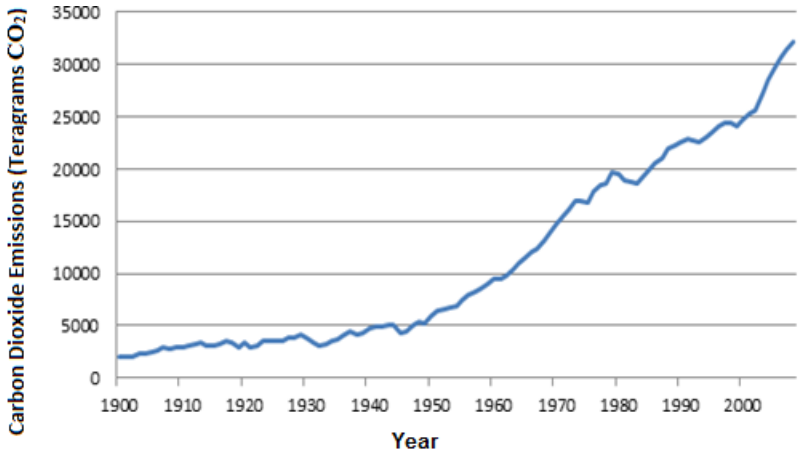

Figure 2.3: ***CO2 emissions over the between 1900 and 200, Source of data: Boden, T.A., G. Marland, and R.J. Andres (2010). Global, Regional, and National Fossil-Fuel CO_2 Emissions. Carbon Dioxide Information Analysis Center, Oak Ridge National Laboratory, U.S. Department of Energy, Oak Ridge, Tenn., U.S.A.***

The Kyoto Protocol [24], an international agreement linked to the United Nations Framework Convention on Climate Change (UNFCCC), was established in order to reduce global emissions of greenhouse gases. The protocol sets a target for which 37 industrialised countries members and the European Union have committed to reduce emissions. Climate mitigation, including meeting the commitments agreed under the UNFCCC, requires the energy systems to move towards decarbonisation, a reduction of fossil fuels reliance and acceleration of renewables technologies penetration [25]. The UK Government, in order to achieve the 80% CO_2 reduction target by 2050, has signed and is legally bound by the UNFCCC Framework and Kyoto protocol agreements. In addition the UK is legally forced under the EU Renewable Energy proposal Directive [26] to generate one fifth of total energy from renewable sources by 2020. In general, the mandatory targets in Europe are to achieve 20% portion of renewables in its input mix, along with a further 20% reduction in greenhouse gases emissions and 20% more energy efficiency infrastructure [27, 28]. As suggested in the UK Renewable Energy Strategy report [29], the UK's short term plan is to ensure that 15% of its energy generation is produced from renewable resources by 2020. This target could be achieved by using an energy scenario which comprises 30% of electricity generation, 12% of heating and 10% of transport energy produced from renewable energy sources.

In 2004, the global electricity and heating generation sector accounted for 12.*7* $GtCO_2^{eq}$ of GHG emissions which results to 26% of total emissions [19]. In the UK in 2006, 30% of energy consumption and 35% of total electricity used was within the residential sector, with the majority of this energy being supplied by fossil fuels [30]. Grubb et al highlight the need for progressive steps towards sustainability in energy systems. They recommend, to achieve even a 60% reduction in CO_2 emissions by 2050 at least a 2% per year reductions in carbon emissions is needed [25].

The technologies that have been developed in the last few decades that are able to substitute current energy technologies are dependent on electricity as a means of supply. Oil for transport can in part be substituted by electric vehicles and similarly gas for heating can be substituted by heat pumps or electro-heat. These new delivery technologies offer a way by which electricity can become the form of decarbonised energy supply. This can be achieved by introducing renewable generators such as, wind turbines and solar PV, or by requiring conventional fuel fired electrical generators to utilise carbon capture technologies to power stations now and in the future [31, 32].

2.1.3 Drivers from an Energy Security Perspective

Since the industrial revolution energy has been relatively abundant. There is therefore a major concern among politicians and policy makers that in the first quarter of 2013 the amount of imported foreign energy in the UK reached 44 %, which is its highest level since 1976 [33], and is illustrated in Figure 2.4. An additional concern is that the capacity margin for heat and electricity must be readily available to meet the growth demand. From 1990 to 2007, world energy demand increased by approximately 1.3 % per year, with the net demand expected to grow until 2035. Predictions beyond this point are considered as non-accurate [34].

Figure 2.4: ***Import dependency, 1970 to 2013*** **[35]**

In the UK in particular, there is a continuing increase in electricity demand, as shown in Figure 2.5. Between 1980 and 2008, it is observed that electricity consumption in services, domestic and industrial sectors grew almost every year [35]. Despite increased energy efficiencies, total energy consumption in the residential sector increased by roughly 1% per annum from 1970 until the recent economic recession in 2008 [36], indicating significant demand for future energy services. Regardless of the uncertain situations that can affect electricity demand such as the economic recession in 2008, the trend of continuing increase in demand suggests a need to ensure that sufficient electricity supply can be achieved.

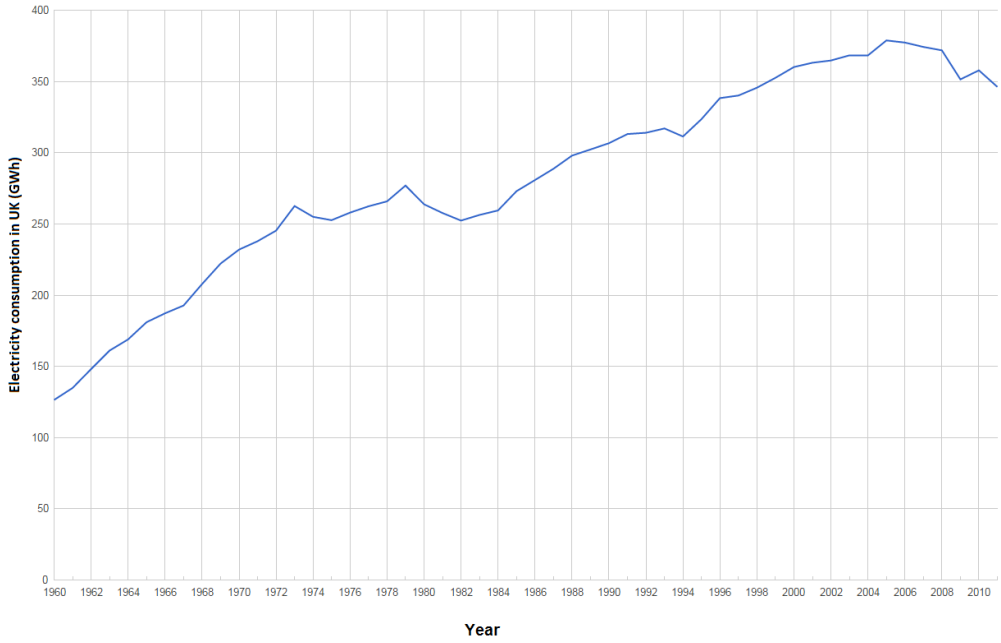

Figure 2.5: ***Electricity consumption in UK between 1960 and 2012. Data from World Bank, ©2014 Google Public Data***

At the same time, around 20 % (19 GW) of existing capacity is expected to come off the system between now and 2020 (compared to around 6 GW of capacity coming off in the last decade), mainly due to EU environmental regulation and ageing plants closure. In particular, 8*GW* of coal power stations are about to retire in 2015, due to the European Directive for Large Combustion Plant [37]. Consequently, the government is keen to make sure new flexible gas generators are in position to facilitate the meeting of demand. On the other hand, a 2012 report from the Department of Energy and Climate Change (DECC) highlights problems with the ability of industry to build new power stations [38]. The report illustrates that national load factors for gas generators have fallen from a 1996 level of 71% to 48% in 2011. The same trend followed in the next two years, generation from gas fell by 4.5%, from 100 TWh in 2012 to 96 TWh in 2013. The reason for this reduction is mainly the higher gas prices, which were equal with coal prices and thus more expensive to generate. As a result, several stations have been running at low output levels or have been temporarily closed and future plans for gas fired power station were postponed in 2013.

The UK government is aware of the need to "keep the lights on", but with coal power stations being taken offline, the economics of gas not encouraging energy companies to build the power stations and the trend of an increased energy demand the UK is resulting in a difficult situation concerning the UKs energy security. In June 2013 Ofgem announced that the UK could face power-blackouts by 2015, unless the industry achieved an effective increase in electricity

production [39]. The chance of electricity blackouts has been increasing from approximately one in fifty years to one in four years as capacity margin has fallen to around 2% at peak times.

Further inspection of the latest energy tendencies in UK shows that in the first quarter of 2013 fossil fuel dependency was 88.3%, oil production fell 15% compared to the first quarter of 2012 and natural gas fell 14.5%. Almost the same percentage fall in gas and oil production was experienced for the year 2012 compared to 2011 [33]. In the first quarter of 2013, two-thirds of gas supply was imported from foreign markets [35]. Moreover, the UK dependency on oil and gas imports appears negatively in other energy sectors. In particular, this has led to price rises for the UK population in heating their homes and transport costs.

The concerns over increased reliance on imported gas and oil and the constraints that shortages of energy supply can have on the growth of the economy, has resulted in policy makers and government to progressively shift to electricity as the form of energy that can enable a diversity of supply technologies that are not reliant on any one particular fuel. The Chair of Energy and Climate Change Committee back in 2011 stated clearly a strong message concerning the UK energy future:

"In an uncertain world the UK needs to think hard about its energy security.
The UK will become more dependent on energy imports as North Sea oil and gas declines, but prudent planning can ensure this doesn't reduce our energy security too drastically.
To keep the lights on and our transport moving we need a diverse energy portfolio that does not rely too heavily on fossil fuels from unstable parts of the world or any one single technology at home."

(Energy and Climate Change Committee, 2011)

2.1.4 Summary

With demand for energy showing no signs of slowing down, and a pressing need for an international effort to combat climate change, the trilemma framework is more pertinent than ever. Due to electricity being a high grade form of energy supply, enabling the use of new delivery technologies, together with the principles and interpretation of mainstream economics, then policy makers and politicians have been guided towards utilising and planning for an electric future in order to solve the energy trilemma.

2.2 Future Energy Scenarios

Within an anticipated shift to a more electric energy network this section explores the results of recent studies about future generation and demand profiles within the UK energy sector and its anticipated impact on the electricity distribution network. This is in the context of decarbonisation levels and electrification which is being driven by the economic theory, climate change and the energy security drivers which were presented in the previous section.

2.2.1 Electricity Generation & Decarbonisation Targets

Much of the current academic literature [41-43, 52] and government policy [44, 45] is based on national supply side scenario analysis. For instance Skea et al, in [40], estimate that if supply side decarbonisation is highlighted, electricity will be substantially decarbonised by 2030. The generator mix within all scenarios is in part influenced by existing and planned generators. Of the 72 *GW* total installed generating capacity in 2004, 57.1 *GW* was provided by fossil fuel generators. By 2020 24.9 *GW* of these generators will be in charge for more than 50 years [42]. The National Grid Seven Year Statement gives a detailed short-range forecast of the UK electricity system [46]. The up to date version from National Grid [47] also provides details of all new generation projects contracts with energy suppliers. It provides an indication of likely future generating technologies and capacities. The authors of SuperGen scenarios note that by 2020 the majority of existing central fossil fuel based power plants will still be in existence. By 2050 most will have been replaced and the rate of replacement will depend on economic factors [48]. The 2020 “Gone Green" scenario proposed by The National Grid Company in 2014 [49], forecasts 22% wind, 5% coal, 31% gas and 18% nuclear generation output as it can be seen in Figure 2.6. National Grid states that current and future generators will facilitate 15% of the 80% reduction in emissions required by the Climate Change Act and this will be deployed by 15% penetration of renewables in 2020. Also under the Gone Green scenario UK power output is less dependent on imports as the imported electricity via interconnection is predicted to be at 11% in 2020 with a trend to minimise to 1% in 2035. The penetration of renewables towards the 80% target of 2050 is 23% in 2030 and 39% in 2050. Onshore and offshore wind, are generally considered to be the largest contribution towards decarbonised generation among the majority of energy scenarios.

Figure 2.6: ***Predictions of UK power output in 2020 under the Gone Green scenario*** **[49]**

In 2010 DECC published the "2050 Pathways Analysis", with seven main scenarios which focus on supply side considerations. These scenarios were developed by DECC using their online calculator tool [45]. If the energy sector remains unchanged, in term of tendencies in production, consumption and the technology evolution, in 2050 the UK will achieve only a 3% of reduction in GHG emissions which will mainly come from the increased energy efficiency in sectors related to energy. For the same relative parameters in the "No Progression" National Grid scenario GHG emissions will be reduced by around 50%, but under this scenario quite a large penetration of renewables is still under consideration. The above comparison is a good example that highlights that for predictions of future energy scenarios there are a lot of parameters that can affect the outcomes and it is up to the scenario developers to quantify and qualify these parameters.

Looking out to 2050, there is a greater opportunity to change the generation mix. Despite the differences, among all energy scenarios, there is an agreement that the future energy sector will be much more different than it looks like nowadays. It is expected that a significant proportion of the generation would be produced from renewable energy sources. In the UK, large-scale Distributed Generation (DG) technologies, for example onshore and offshore wind, hydro generation and combined heat and power CHP, are potential sources that will contribute to the improvement of hosting capacity so as to provide a generation mix to improve system reliability, affordability and efficiency. Smaller scale generation such as solar photovoltaic and micro-generation will also play an important role in meeting the decarbonisation of electricity [50]. In particular, National Grid argues that there is a potential for micro-generation scenarios of sub-1 MW wind, solar PV and hydro installations. For solar PV, falling installation and

equipment costs have resulted in an increase in PVs penetration growth. While similar effects have been experienced in the wind and hydro industries, they have not been as dramatic and therefore a much slower growth is expected. Moreover, micro generation by utilising solar energy will exceed the 14GW installed capacity by 2035 as is illustrated in Figure 2.7. Development of micro-generation is an important consideration for the future energy scenarios, as it reduces the transmission demand and can have localised impact on the wider electricity network. This trend toward PV solar panels is raising challenges to the DNO as will be discussed in more detail later in this chapter.

Figure 2.7: ***Predictions of UK micro-generation installed capacity in 2020 under the Gone Green scenario*** **[49]**

2.2.2 Electrification and Demand Targets

Electricity demand will also change in the long term future with growth in GDP, employment and population, combined with greater levels of LCTs. The Carbon Plan 2050 scenarios also includes possible demand up to 2050, with varying levels of electrification of heat and transport as well as of energy efficiency technologies implementation [50].

The traditional way for future power systems planning involves historic demand profiles and future predictions, which affects the planning of generation and hosting capacity. Therefore, the need to consider how national demand will evolve toward 2050 is an important factor in future energy scenarios. For instance, if a scenario of highly decarbonised national supply and

high demand growth is projected, then future household demand patterns will be highly impacted.

There are a number of UK focused 2050 future scenario studies which include demand as well as supply side projections [41-45]. Across all five scenarios in the Long-Term Electricity Network Scenarios (LENS) project [51], - a forward looking scenarios project sponsored and led by Ofgem - the total energy consumption of the UK drops by around 11% relative to year 2000 levels, but electricity consumption rises by an average of 21%. The same result can be found for the residential sector in three out of the four National Grid scenarios. For example "Gone Green" where the annual electricity demand increases by 50%, to "No Progression" scenario where the annual electricity demand increases by 7%, as is shown Figure 2.8.

Figure 2.8: ***Historic presentation and predictions of UK residential power demand under several scenarios*** **[49]**

The electrification of heating plays a major role in the results presented above regarding the increase in annual electricity demand. Across the nine energy scenarios developed by the UK Energy Research Council (UKERC) [52], an average of 42% of 2050 heating demand is delivered by heat pumps. This is a representative example of the degree of heat electrification apparent within the majority of scenarios. Furthermore, the number of installed Heat Pumps to cover heating demands will reach 10 million by 2035 according to the National Grid Gone Green scenario. The level of electrification of heating and transport within the Transition Pathways [31] – a follow on energy scenario project from the Ofgem LENS project [51] - is different within the three scenarios. The lowest level of electrification of heating is 24.5% within the Conservative scenario, meaning that 24.5% of heat delivered to the domestic consumer will be

supplied by heat pumps. This ratio increases to 76.2% for the Extreme scenario. The scenarios above consider that an increase in resistive heating is not significant.

The DECC 2050 Pathways Analysis report [45] details heat delivery technology breakdowns, with heat pumps and resistive heating playing a role in 12 out of 16 sub-scenarios, 10 of these specifying 25% or more of heat to be delivered by electrified heating technologies. Moreover, 80% or more of heat will be delivered through electrified heating technologies, in 5 of the 16 sub-scenarios. Within the three DECC Calculator scenarios of "Higher renewables, more energy efficiency", "Higher nuclear, less energy efficiency" 48-90% of heating demand is delivered by heat pumps and 36 – 49 *TWh per year* of electrical demand is due to electric vehicles in 2050.

Figure 2.9: ***Predictions of UK EVs uptake in 2035 according to National Grid*** **[49]**

Within the UKERC 2013 energy scenarios [52] resistive heating and heat pumps make a major contribution to heating in all scenarios, whereas electric vehicles are not projected to place significant extra demands on the system. But again this is subjective, because National Grid in [49] strongly advices its stakeholders that electrification of transport and in particular the electric vehicles will play an important role in the future energy profiles. Especially as Figure 2.9 illustrates, it is stated that the number of electric vehicles will exceed 1 million by 2030 and may reach 5.5 million in 2035 with an annual demand predicted to be 14 TWh.

2.3 Moving to a Decarbonised Electricity System

Moving towards a decarbonised electricity future with a high penetration of heating, distributed generation and transport electrification will lead to several impacts which electrical grids will face. In this section an attempt made to understand the features of these LCTs - from the generation and consumption point of view, and their impact on the distribution network.

The power grid of the future will be fundamentally different to the one presently operated in the UK. As described in the previous section, in order to solve the energy trilemma, there is a need for a secure, sustainable and affordable electrical system. Consequently, there will be challenges using the UK electricity network to deliver electricity to points of consumption. Ignoring the future generation mix, the grid should have sufficient hosting capacity to meet the peak demands; provide highly reliable delivery; and provide stable voltage quality [53]. As a consequence, there are expected to be a number of challenges in future distribution networks and particularly for Distribution Network Operators (DNOs).

2.3.1 The UK Transmission & Distribution System

The aim of the UK electricity network is to generate and deliver electricity to the place and at the time that is demanded. Functionally, the system can be divided into three categories, which are generation, transmission and distribution of electricity and as a whole it can be considered as an islanded system, with small connections to Northern Ireland, France and the Netherlands through High Voltage Direct Current (HVDC) links of 500 MW, 2000 MW and 1200 MW respectively. These links can be compared to the total UK installed capacity of 85 GW [54].

The generation of electricity is a liberal market and companies from private sector own the power stations which are mainly coal, gas and nuclear fired stations. Electricity is generated at the power stations at low voltages and then stepped up to high voltages of 400kV, 275kV and 132kV to be transmitted through 25,000km of High Voltage (HV) overhead lines and 2,000km HV underground cables to Grid Supply Points(GSP) [55]. The four transmission networks in UK can be likened to the motorway system enabling the bulk transfer of HV electricity around the country. The owners of these transmission networks are National Grid, Northern Ireland Electricity, SP Energy Networks and the Scottish and Southern Energy companies.

Power is carried at high voltages in order to prevent excessive losses during the transmission over long distances. Before power is supplied to the customers and after it exits the Transmission system, it enters the 14 UK distribution regions operated by eight Distribution Network Operators (DNOs) as shown in Figure 2.10. In the distribution network the voltages

are stepped down back from a 132kV High Voltage (HV) distribution grid, progressively to 66kV and 33kV - usually named as the Medium Voltage (MV) distribution grid, and then to 11 kV and 6.6kV the secondary distribution grid and eventually power is delivered to residential, commercial and light industrial customers using a 400V LV distribution grid.

Figure 2.10: ***Geographical presentation of Distribution Network Operators in GB and details of the largest DNO, Western Power Distribution – reproduction from http://www.energynetworks.org***

Generally, Transmission and Distribution (T&D) of power is carried out using Alternating Current (AC) system with the frequency of supply used in UK to be 50 Hz. The T&D grid design philosophy provides redundancy, so that if any asset of the network - overhead lines, underground cables, transformers or generators fails, power can be provided from other sources via a different route through the interconnected electricity network. This has resulted in huge vertically integrated power systems which make the UK electricity supply system quite complex. In particular the UK national electricity network handles approximately 359TWh of energy per

year, through more than 27,000 km of transmission and 800,000 km of distribution infrastructure [47].

Western Power Distribution's (WPD) network is the largest in the UK, covering every kind of geography and demography from heavily populated residential areas to widely spread rural societies. WPD obtain four DNO licenses for the geographic regions of East Midlands, West Midlands, South West and South Wales as it is shown in Figure 2.10. Some key facts about the WPD distribution networks are presented in this figure as well.

2.4 Distributed Generation

Despite the extensive penetration of DG technologies around the world, there has not been a specific definition given to clearly describe DG. DG may be defined as any generation of low-carbon sources including CHP which are connected directly to the distribution network and where the electricity generated is used by the local community [56]. In the UK, the Energy Network Association (ENA) [57] gave in 2010 a short and simple definition for DG such as a generating unit which is directly connected into a distribution network. Ackermann et al in [58] have examined various definitions of DG and its characteristics that are used in different countries. In order to avoid confusion from the various meanings seen by different countries, the authors suggest the following general definition of DG:

"*Distributed generation is an electric power source connected directly to the distribution network or on the customer side of the meter"*

Since climate change is becoming a significant issue, this definition could be extended so that DG becomes a low carbon emissions generation which is connected to a distribution network. According to the authors of several papers, DG relies on a range of factors which can be summarised as [58, 59]:

- Purpose of distributed generation;
- Connection Voltage Level;
- Location of the generation;
- Type of technologies;
- Maximum power rating of the generator;
- Role of the generator for dispatching;
- Ownership;
- National electricity market regulations;

Ackermann *et al* [58] introduce four categories of DG based upon the maximum generation rating as follows:

- Micro DG a few Watts < 5 kW;
- Small DG 5 kW < 5 MW;
- Medium DG 5 MW < 50 MW;
- Large DG 50 MW < 300 MW.

2.4.1 Impacts of DG on the Low Voltage Distribution Network

As described in the previous section the integration of different DG technologies can have different impacts on the distribution network. This thesis considers focuses on a particular type of DG, which is defined as:

- DG with a maximum capacity from micro to small-scale, being capable of producing active and reactive power and connected to a distribution network at 400V three phase or 230V single phase voltage level. In addition the DG is owned by the end-user.

Further, due to the high interest of grid connected PVs in residential LV distribution networks resulting from UK policy to promote the development of PVs connected to distribution networks, there is predicted to be a high penetration of this technology as was shown in Figure 2.7. Therefore this project has focused on the impact of PV on the LV distribution network.

Technical and non-technical factors have been studied concerning the potential impacts of integrated distributed generation [59-64]. Generally, from a technical point of view, DG can reduce system losses, enhance system reliability and improve voltage profiles (voltage sags). However DG can cause problems related to voltage limits and power quality [65, 66]. Application of grid connected PVs is increasing in residential LV Distribution Networks globally. Incentives by different countries promote the development of PVs connected to distribution networks. By generating electricity closer to the residential customers, transmission and distribution losses can be reduced, which is a benefit from a climate change perspective [66, 67].

Co-generation

The by-products of DG may also be utilised since DG is often connected close to the load demand. For example, there are loads, such as residential and industrial, which have a heat demand as well as an electricity demand. Technology like micro turbines, biomass engines which form the (CHP) plants produce heat as a sub-product. This waste heat can be used to supply holistically or partly the residential and industrial customer's heating demand [68, 69].

Reliability

A highly-reliable network can satisfy the majority of the demand connected to the power system even under difficulties, such as loss of transmission lines or transformers. Reliability of generation can be improved by using DG. For example, a typical power-station may be generating 1GW of power while a DG unit may only be generating 1 MW of power. If the fossil-fuel fired generator were to fail, the system would be required to either produce an extra 1 GW of power or disconnect 1GW of load in order to maintain the power system in balance. However, the loss of 1 MW of DG can be managed much easier. In addition, if the 1GW of generation is spread over a large number of micro-generation units the likelihood of all small DG units failing is less than the likelihood of one unit failing. Therefore, the spread of power generation into many more units gives a higher reliability when compared to one large generation unit. Under critical circumstances when it is impossible to deliver the power to meet the demand holistically, load-shedding has to take place to mitigate stress on the network and avoid total collapse of the electricity supply grid. The unsupplied demand leads directly in economic losses. Incentives from electricity regulators to DNOs to design and maintain a more reliable network has led in the UK to Ofgem's strategic decision for a new electricity distribution price control known as the RIIO-ED1. This control is based on the previous Distribution Price Control Review (DPCR). In particular, end-users rely on the DNOs to maintain a safe network while reducing the number and duration of power interruptions. Thus, DNOs are obligated to provide an equal or equivalent reduction in loading risk to their assets in order to facilitate a higher penetration of DG [70]. In [71] and [72], DG was utilised along with purposeful islanding to improve the system reliability. In [73], an algorithm has been developed to strategically place DG to minimise the costs incurred during rotating and load-shedding.

Transmission and Distribution Losses

Transmission and distribution (T&D) losses are the difference between the energy generated and the energy delivered through the system to the customer. Technical losses are those caused by the physical properties of the system such as lines and transformer losses while non-technical losses are more quantitative losses such as theft or non-accurate meter readings [74]. DG will affect these technical losses because of the change in the magnitude and direction

of the power flow. For instance, if more demand is met with a closer placement of electricity generation to the load, power flows in the LV distribution network are decreased and so are the losses. Electricity from a large power station may be transported over long transmission lines and through a number of transformers. Each kilometre of transmission line and each transformer between the generation and the load reduces the efficiency due to equipment losses such conduction, iron and corona. The gain from reducing the amount of generation required to be transported over long distances, is to increase the efficiency of the power grid. A study in [75] analyses the reduction of losses from integrating DG at the feeder ends. It found that the main factors which affect the line loss reduction are the rating, the location, and the operating power factor of the DG units. For example, if the ratio of DG power output to the amount of load increases beyond the suitable point, the DG that installed near the load will cause more electrical line loss than the one that installed close to the substation.

Each feeder of a distribution network has a demand profile that ranges between an average minimum and an average maximum, but there are also periods of time during the day where the demand exceeds the average maximum significantly, which is known as the Peak Demand. During these periods, there is evidence that DG is able to reduce the LV peak demand [76]. Having the ability to reduce the peak demand may allow for more generation to be connected to that feeder without having to reinforce the feeder with a larger transformer or larger cross section conductor. However, if the power output of DG increases to the point where it exceeds local demand, there will be increasing amounts of reverse power flow and distribution losses can increase [77- 79].

2.4.2 Photovoltaic micro-generation – Impacts

As discussed previously, PVs are expected to be the most widely installed form of DG in the UK distribution grid network in the near future. These will turn such networks from being "passive" to "active". A simplified diagram of a "passive" LV power is illustrated in Figure 2.11.

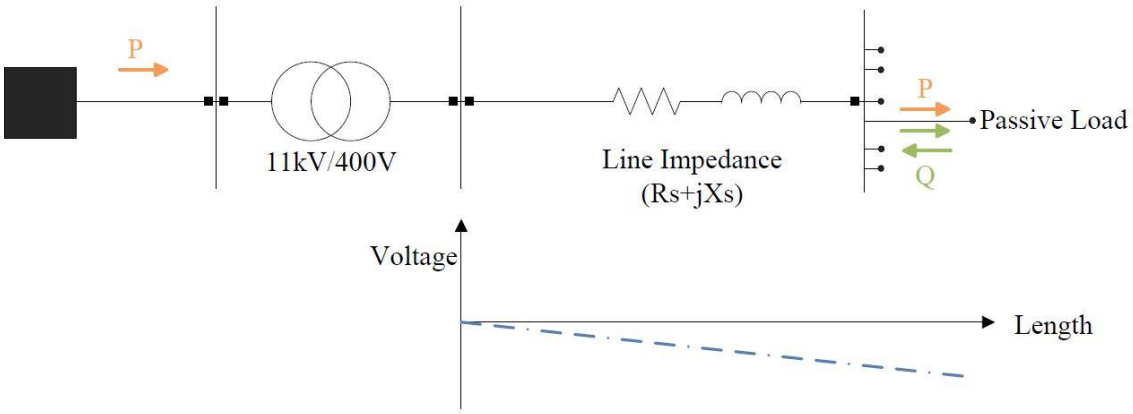

Figure 2.11: ***A "passive"- traditional Low Voltage Distribution Network with unidirectional power flow***

The network consists of:

- The 11kV/400V substation which consists a transformer to reduce the voltage of the medium voltage (MV) grid to that of the 400V three phase LV network. These transformers are typically set to a fixed voltage ratio as there is no flexibility for an automatic, on-load tap changer.
- Loads, such as domestic properties, commercial buildings and small scale industrial customers with LV supplies.
- Mainly overhead line in rural areas and/or underground LV cables in urban regions, having predominantly resistive and inductive behaviour.

In an existing passive LV network the power flow is unidirectional from the high voltage to the low voltage network. The performance of these networks is managed by a number of technical constraints and regulations placed by authorities as will be described later.

2.4.2.1 Active Networks

Reverse Power Flow

A simplified diagram of an "active" LV power network with active loads such as residential, rooftop photovoltaics systems is shown in Figure 2.13. In this network, it can no longer be assumed that power will only flow into each load since the PV generation might exceed local demand. The end user from being a passive consumer starts being an active one, a so-called "prosumer" [80]. In this case electric current might flow from the load end of the line in an upstream direction towards the distribution transformer during times of high power output or low power demand. Reverse power flow can then cause a violation of thermal constraints in the network feeders. The maximum current capacity of the cable, commonly known in the industry as ampacity, is the thermal threshold of the cable. If there is a significant overload of the cable

then there is a risk that the conductor will overheat and damage its insulation. LV networks are designed so that the current under the highest demand will not exceed the thermal limits of the cable and other equipment. Thus the hosting capacity of the LV networks is determined by the thermal stress on the LV cables [81].

Voltage Variation

There are a number of regulatory constraints on LV networks which need to be maintained by the network operator companies by both the transmission network operators (TSOs) or DNOs. Regarding the Voltage Limits, the nominal magnitude of the input voltage in the LV network is 230V, phase-to-neutral in 4 wire systems or 400 V phase-to-phase in 3 a wire systems. LV Voltage level can fluctuate with different loading conditions [63]. This variation must not be 10% above (i.e. 253V) or 6% below (i.e. 216V) the statutory limit of 230V [82]. Overvoltage occurs if the upper steady state voltage limit is violated. Regulations state that 95% of the 10 minute mean rms voltages in a week should be within these limits, and absolutely no overvoltage is allowed according to BS EN 50160:2007 [83].

Under normal power flow, the voltage at the input site of the LV network close to the secondary substation, will be higher than that at the Point of Common Coupling (PCC) which is the point at which of the majority of the loads connect to the LV grid. The difference between these voltages is named feeder voltage drop. This is largest when the power flows is greatest. If the voltage drop is sufficient to exceed regulatory voltage limit i.e. Vmin=216V (-6%), this is termed an undervoltage as shown in Figure 2.12.

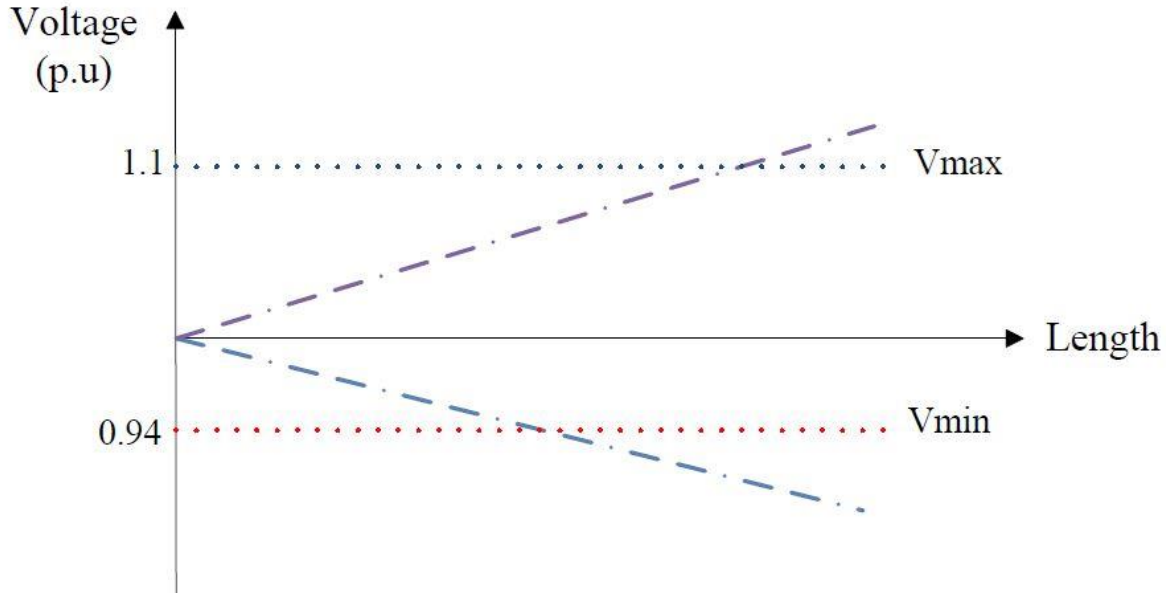

Figure 2.12: ***Voltage drop and rise along a LV feeder in correlation with the length of feeder.***

Under reverse power flow, the voltage at the input point of the LV network will be higher than that at the PCC. This is termed a voltage rise and this phenomenon is illustrated in Figure 2.13 where an "active" load triggers the bidirectional power flow into the LV network. If the voltage rise is sufficient to violate the upper voltage limit Vmax=253V (+10%) then this is called overvoltage as shown in Figure 2.12.

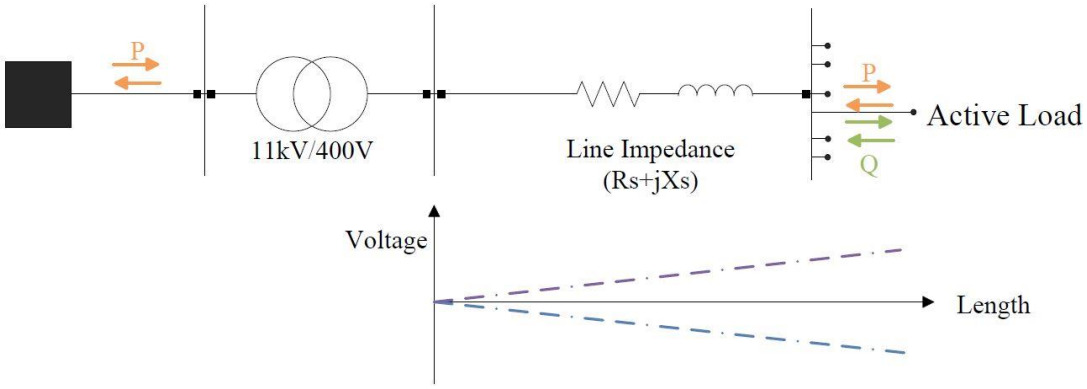

Figure 2.13: ***An "active" Low Voltage Distribution Network with bidirectional power flow.***

Modern LV networks can be affected by either overvoltage or under-voltage. The severity of the voltage change caused by DG again depends on its location and relative output compared with the load demand. The impact of overvoltage through residential PV installations is a thoroughly studied subject and is considered to be the main problem for DNOs in conjunction with the exceeding of power flow limits [84, 85]. Indeed, it results in a limitation of the LV distribution grid hosting capacity for future DG technologies penetration. In [86] it is explained that overvoltage is a major concern with PVs. Voltage rise from PV is most likely to be worst in the middle of the day when there is a mismatch between generation and demand [87, 88]. However, this can change depending on regional weather conditions and consumer's demand trends. Voltage rise is only a problem if this causes overvoltage and can sometimes be constructive in mitigating under-voltage [89]. Furthermore, it is concluded in [90] that in a region of an LV distribution network where there is an issue of under-voltage during the day, PV installations could support the network by increasing the local voltage. This means that, it may be considered that PV is most suitable for power systems when the PV generation is integrated in a LV network with loads that are relative heavy and predictable such as mid-day peaks. For example, in hot climate countries which have a high solar irradiance at noon hours, there is an extensive load demand for air conditioning cooling at the same time which PVs generation can nicely match it.

The structure of the grid and its assets can also affect how severe voltage rise is. It is commonly known that urban networks are less likely than rural networks to have overvoltage issues [85]. This is due to the higher value of the impedance in rural feeders, where feeder runs are generally much longer than with the urban networks. However, the overvoltage is not a phenomenon which occurs only in rural networks. Power quality issues due to increasing PV levels in Flanders, Belgium were investigated in [90]. Specifically the power quality issues of overvoltage, under-voltage and voltage unbalance was studied. As discussed by Gonzalez et al. overvoltage can occur in a considerable amount, but not at all urban networks. The other difference between the two types of networks except of the impedance of the line is the load demand. Urban networks are heavily loaded and the power needed from the customers is much higher. So it is not as common to experience an overvoltage in respect with a normal penetration of PVs when compared with rural networks. Also, different networks will be affected by different PV profiles, such as the number of units and their output rating. This indicates that, when assessing the impact of PV across a large distribution network, it is not technically correct to accept that all networks will be affected, or that the location and the number of PVs that will cause a problem can be easily determined. In [91], an increasing amount of PVs on a real UK distribution network is modelled and shows that voltage limits are violated when there is a large amount of PV installations. This is because the magnitude of the voltage rise is affected by both the output and the location of the PVs [92]. It was found that none of the overvoltage studies enable network operators to calculate the voltage rise, due to the uncertainty about where the DG will be located. This is particularly problematic for UK DNOs who cannot prevent where residential photovoltaics will be installed under current UK regulation. UK DNOs cannot refuse installation of residential PVs. DNOs have started considering the issue of voltage rise recently and several attempts have been made in UK to define the "hot" points of the distribution grids [93]. Recently WPD issued distribution generation network constrains maps for the 4 licensed areas for the HV and MV networks. Such stochastic work from a purely academic point of view was completed in [94, 95]. In particular, Navarro et al [95] carried out a stochastic analysis of two real LV networks in the North West region of England with different PV penetration level. It is found that for long feeders with high load, voltage issues can start in average at 40% of PV penetration. This picture can change depending on location, population's density and type of network of the place.

Voltage unbalance occurs because of a difference in impedances of the three conductors across the phases or because of the uneven placement of single phase DG or load [96]. The installation of PV panels which are typically single-phase can increase the amount of unbalance in the network. This would cause higher neutral losses as the return current is increased. The impact of PV on voltage unbalance, is studied in [97] by using a Monte Carlo analysis of

domestic distribution grids with arbitrarily rating, location and number of PVs. The unbalance is found to be worse when PV with a higher rating is located at the very end of feeders as these points of common coupling are most sensitive to voltage changes due to the length. In contrast to the Shania et al. study [97] , a recent project from Electricity North West – the DNO in North West region of UK, found that the voltage unbalance due to PV generation is negligible, whereas the main problem of overvoltage followed by poor power factor [98].

Power Quality

Voltage flicker as a result of domestic PV installations is considered by the authors in [99]. Flicker is undesirable for customers as they can cause damages to sensitive equipment. Such a fluctuation is designated as a power quality issue and is caused by transient changes in the PV output by clouds or shading.

A limiting factor on the number of PVs that can be installed in LV networks is the injection of harmonic currents [100, 101]. Harmonics can disturb or damage sensitive equipment, distort the supply voltage and overload equipment [102]. For example, in a study of the impact of harmonics on an LV grid, limits are violated under the most extreme scenario of PV penetration in the network – all houses with rooftop PV systems [103]. On the other hand, experimental measurements were taken in a study in [104] considering several day output profiles on a three phase 20 kW residential PV system in Greece. The researchers measured harmonic current and then built a simulation tool to model the impact of this harmonic current on the feeder that the PV inverter was connected to. They concluded that the PV panels cause an increase in the harmonic current. However the PV system did not cause any limit violations. Harmonics themselves are injected by the switching behaviour of the power electronic inverter which acts as a nonlinear load. There is significant amount of research work has been carried out with the purpose of reducing this harmonic injection to the grid. This means that harmonic reduction can be achieved to certain extent by improving the inverter design and control such as through Harmonic Elimination Pulse-Width Modulation for Voltage Source Inverters [63,105].

2.5 Low Carbon Technologies

As it was discussed earlier, electricity is not the only industry which needs decarbonising in order to meet UK climate change targets. In 2013, provisional figures showed that electricity supply accounted for 38.4% of CO_2 emissions, with transport and residential heating accounting for 41.6% [106]. These two sectors will need to be decarbonised in order for the UK to meet its emission reduction targets. Therefore, the UK expects these loads to be increasingly met using a low carbon electricity system [49]. Delivery of domestic heat is expected to be achieved using

heat pumps since these have much lower energy demand than resistive heating. In particular, National Grid predicts a quite significant increase in the number of heat pumps installed in the UK. Moreover the same National Grid scenario illustrates the replacement of the existing heating technology trends. It shows that oil and electric systems are expected to be replaced before gas boilers. Pathways for decarbonisation of transport results in an increase number of EVs as shown in Figure 2.9 and it can be seen that there is expected to be an increase in electric vehicles being used in the UK. If demand from these LCTs is sufficiently grouped, they can increase peak demands which can overload cables and transformers and also cause voltage to drop below limits [107, 108].

2.5.1 Impacts from Electric Vehicles

In [109] the result of different EV penetration levels in a part of the Bornholm island network in Denmark was investigated in terms of equipment loading and voltage variations for both the LV and MV grid. The result is that the LV grid is most sensitive with voltage drops being the major problem. In [110] large scale EV integration affects quality of service and may cause significant technical problems. In particular, the congestion problems increase in the case of unpredictable or non-regulated charging consideration and in combination or not with rural network topologies. The effect network topology has on simulation studies is also noticeable in [111] and [112] respectively. Shao [111] demonstrates that a strong urban distribution grid supports a 100% EV integration considering all the technical aspects such as, voltage limits, harmonics and thermal loading of equipment. On the other hand, the author in [112] clearly states that the feeder and the transformer of a very rural residential network can be overloaded even with a relatively low EV uptake.

Under two different EV uptake scenarios Papadopoulos et al [113] examined the impacts of EVs penetration to the UK LV distribution grid. The low and high EV uptake is 7% and 48%. Under minimum load and maximum load conditions during winter and summers extremes, the voltage exceeds the lower statutory limit and resulted to the under-voltage phenomenon. Secondary transformer and feeders of the LV network are found to be overloaded only for the high EVs uptake scenario. This is translated to further distribution losses which result in a 10% increase. Concerning the peak demand, the proliferation of EVs in the LV distribution network under a high EV uptake scenario will result in a 60% rise in peak demand.

In order to have an understanding of the load that is related to an EV charging, Figure 2.14 shows the current waveform from a typical EV charger. This measurement was taken from the EV used by Aston universities' estate's department. The continuous load is around 3.2 kW. It can be seen also that the waveform is distorted due to the harmonics injection but whilst the

total THD it is found to be within the statutory limits, the notches at the zero crossings may be problematic for other sensitive electronic loads.

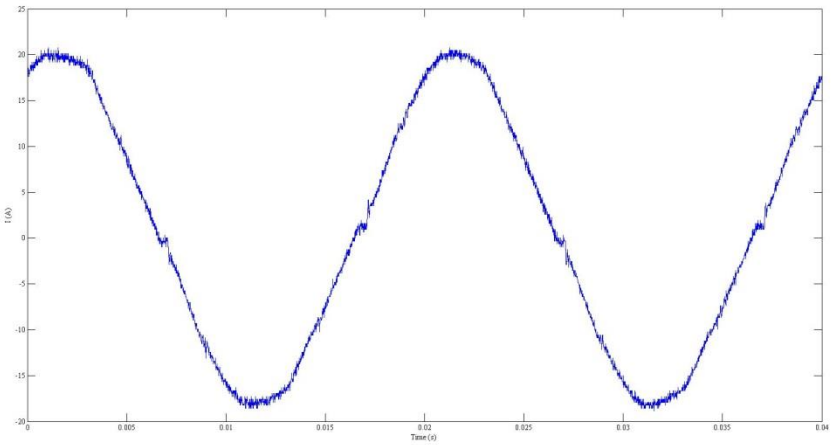

Figure 2.14: ***EV charger current waveform***

Despite the fact that this particular EV charger meets existing power quality requirements, there is lot of research considering the power quality characteristics of several types of EV chargers and their impact on distribution network power quality. Most of this literature is summarised by Kutt et all in this review paper [114]. Briefly, the power electronic EV charger injects harmonic currents, and if single-phase chargers are used, the voltage unbalance is coming up as an issue. The presence of either current and/or voltage harmonics can cause further stress on the network equipment in terms of increased losses. The components to suffer the most are the distribution transformers, cables and fuses, in this order.

UK Power Networks the DNO for London and South UK commissioned a trial during the recent Olympic Games in London, 2012 to measure the characteristics of EV charging in different areas of the London city, from demand and power quality point of view [115]. These EV trials have confirmed the assumption made in previous research studies that if EV charging is not controlled and regulated, the extra demand will result in high load peaks which broadly match with the time of existing system peak demand. This puts the LV distribution network under further stress. In addition, it is found that there is a large proportion of low order harmonics caused by EV charging injected to the grid.

2.5.2 Impacts from Heat Pumps

Heat pumps (HPs), like EVs, are expected to cause capacity constrains in the future and under the scenario of high penetration of such technology in LV networks. The impact of heat

pumps on the LV distribution network was investigated in [107] where the load and generation of both electricity and heat were modelled. An algorithm based on fractals was used to model generic networks with different topologies and characteristics. The work considered both an urban network and a rural network that had different peak load densities with different electrical and heat demands. Results from this study indicated that there was a potential impact on the network loading from the HP. This causes overloading of substations for penetration levels of around 30 %. This study observed that for a penetration level of 50 %, the network peak increased by 50 % which will require network reinforcement. It is noted that this study only considered power flows and not power quality.

Work in [116] modelled a generic urban UK distribution network in each cluster of 24 consumers on a 400V feeder with heat pumps, using the software package DIgSILENT Power Factory. Parameters such as starting current, voltage variations, active and reactive power and the impact of single phase inductive loading were considered. Results from [116] demonstrated that the network could accommodate 20 % additional loading. After this LV transformers start to become overloaded. The study found that for a typical feeder the steady-state voltage dropped below by more than 5% of nominal voltage when the penetration was 40 %. In a recent study Akmal et al [116] found that if 20% of customers install heat pumps, the grid under investigation will not be overloaded. Nevertheless, the transient voltage drops exceed statutory limits, as in many cases the voltage is observed to fall below 90% of nominal. There is also a problem of HP inrush current, which is often higher than 20 times the normal current during the start-up and this was investigated in a recent study from Northern Power Grid, the DNO who services the North region of England. It was found that in a very rural LV network the neighbour loads were suffering from voltage fluctuations – flicker as a result of the operation of a large HP unit close by. In the same study the Total Harmonic Distortion at the affected feeder was recorded as being within the limits [117]. The measurement of THD is not always useful in order to quantify the distortion that a HP or any other LCT will cause to the grid. The harmonic amplitude should also be recorded to provide this information as is recommended in [115] where 20 HP from different manufacturers were studied.

Moreover, in [115] the amount of low order harmonics caused by the penetration of heat pumps is significant. In particular, the HPs that were examined on this trial produced a large amount of 3^{rd} and 5^{th} harmonic current as it can be seen in Figure 2.15. Especially the 3^{rd} harmonic for 2 different HPs is close to the statutory limits. The harmonic current slightly increased with output power but did not significantly decrease when the demand from the heat pump was reduced. This will present a constant harmonic current to the distribution network. The third harmonic is of a major concern because looking across all distorting loads, it tends to

be in-phase with the fundamental and therefore the 3rd harmonic contributions of all loads add together.

Figure 2.15: ***Mean current magnitude of the 3rd, 5th, 7th, 9th, 11th, 13th harmonics for 20 heat pumps from different manufactures*** **[115]**

2.6 Solutions to Constrained Capacity and Power Quality Problems

Various studies have also been carried out into alternative solutions to capacity limits and voltage variations:

- Upgrading distribution feeder's cross-section [86]. Lowering the network impendence through cable replacement reduces the voltage variations and can improve the hosting capacity of the network [63]. However, this is expensive, disruptive and not innovative, which the DNOs have a regulatory incentive to be [93].

- In [118], it is proposed to switch the distribution transformer between two pre-defined tap settings. But it is based on historical loading data which is not at all a reliable process. Further, in order to eliminate overvoltages from the PV generation a solution is to

reduce the voltage at the point of the distribution transformer by changing the taps. However, the voltage at the secondary transformer can only be lowered if this does not cause undervoltages. This is much likely to happen when there is no reverse power flow and at the same time the demand for power is at its peak [86]. A trend in the markets is to develop, test and install on-load tap changers into MV/LV substation transformers [119]. Hereby, the ratio between primary and secondary equipment is adjusted dynamically now depending on the actual, local consumption and generation profiles. In [120] a coordinated control of energy storage with on-line tap changer (OLTC) is studied. However OLTC needs monitoring devices along the LV busbar in order to facilitate a continuous voltage adjustment [121].

- LV Grid reconfiguration is also possible [122], although there is no guarantee that there is enough flexibility in a given network to achieve this. In addition there may not be enough space to install additional equipment such as cables and link boxes for reconfiguration. Despite the fact that this is more economical than total reinforcement, it requires complicated control techniques and often affects the coordination of the protective devices [123].

- Auto-transformers may be installed along the feeder if there is physical space in the network [124], due to the fast changing load profiles this devices could see a significant stress and may this reduce their life time. Moreover, putting additional transformers on the LV grid will result to higher distribution losses [125]. Flexible AC Transmission Systems (FACTS), such as static compensators, use reactive power for voltage control [126]. However, because of the low presence of inductive loads in the LV network, these are not very effective for voltage management as it is on the transmission network [127].

- Curtailment is the reduction of real or reactive power from the generator and can be used to avoid overvoltage and/or undervoltage [128]. This is studied for an urban, residential network using reactive power in [129]. As it is discussed above, the impedance of LV networks is mainly resistive. Therefore, voltage is much more sensitive to variations of active than reactive power, so using reactive power to regulate voltage in LV is not the best option. Consequently, in the UK, active power curtailment is likely to be required. In practical networks, the voltage is higher at the ends of feeders and so some systems are curtailed more than others. To conclude, active power curtailment is counterproductive and violates the actual reason of PV installation, which is to generate maximum power from

sunshine. This is not a fair solution from the end user perspective as it can cause a loss of revenue [130,131].

- Smart load management is another option to manage the voltage/power quality in distribution network [132]. In general there are two types of load management schemes – direct and indirect and usually defined in literature as Demand Side Management (DSM) or Demand Side Response (DSR). Typically the direct DSR makes use of a control signal from utility to directly control loads. Using a real time price as the control signal, it triggers an automated action from home automation controller [133]. The indirect demand schemes use price as a control variable to influence consumers' behaviour and thus indirectly control the load. Demand side response (DSR) is an alternative active way to improve the hosting capacity and cope with the voltage variation issues. Rather than restricting the energy production, changes the time that equipment is used or adjusts the power consumption of devices. This can be achieved through changing customer behaviour and/or automated control of loads [134]. As studied in [135], customers might be encouraged to shift demand to increase the load on the network at the time when DG generation is high. Sensitivity analysis shows that this is most effective when customers at the end of feeders are encouraged to load shifting because they have a larger impact on network voltages. However, this is not desirable if the energy market needs to treat all customers in a fair way. A good review of the barriers to DSR is presented in [136] including the customers being sceptical that changing behaviour will reduce their bills, the high cost of such appliances, technical and aesthetic suitability of older housing stock, privacy and data security and difficulties in actually being flexible with demand. These present major uncertainties to DNOs about how flexible and responsive DSR can be.

- By storing electricity during off-peak hours and discharging the stored energy during peak hours, the peak power demand from the power plant is reduced. In [137] it shows that by adding fairly small energy storage, the peak power demand from the grid is substantially reduced and the grid sees a very smooth load instead of a very dynamic power demand with fast changing spikes. Moreover by utilising energy storage units, it is possible to provide active power control in LV networks in order to solve any voltage related issues. Energy storage is a good solution to prevent voltage violations but does not cover the need for a holistic improvement of LV network capacity under the scenario of a high penetration of LCTs. For example, the distribution substation presented by Melnik et al. in [138] combines 'intelligent' components, such as power electronics for voltage regulation, an

electricity storage system and a measurement system in one substation, to improve the power quality for the connected customers.

In general, except for network reinforcement, the previously mentioned trends of introducing more intelligent technologies and using information and communication technology (ICT) also in the distribution grid goes along with the so-called 'Smart Grid' vision. There is a significant amount of research presently being carried out around Smart-Grids; however the technology remains complex and relatively immature.

This thesis considers a new alternative to the above solutions around limited hosting capacity problem on the existing infrastructure. This solution proposes an increase in the existing local 230 V LV network phase-to-neutral voltage to a higher level with respect to the existing underground cable rating which is 600 V. This voltage is stepped down at each consumer using an electrical and/or electronic device. The device can also be used to provide a tightly regulated 230 V to each customer regardless of variations in the supply voltage. This would therefore relieve some the voltage limit violations that are anticipated with a large number of LCTs. In this thesis such a device is named a Voltage Control Unit (VCU). This can be achieved be either utilising AC or DC feeder configurations. An illustration of the proposed solution is shown in Figure 2.16.

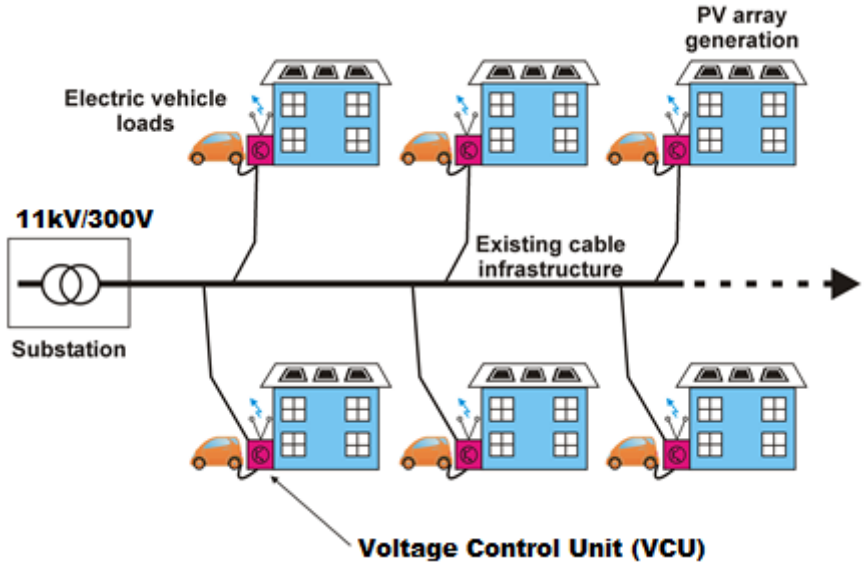

Figure 2.16: ***The proposed solution concept***

The concept of a higher distribution voltage level was considered in the early 1980's by G.A. Hazelrigg et al [139] in order to increase the capacity of the network in urban areas and reduce the losses in rural networks. The study considered the primary to secondary network in the United States [139]. According to the authors, the increase of the LV network voltage from 120 V to a higher one does not have a significant impact in reduction of losses and in addition

can cause safety issues to the customers. The study proposed a higher voltage to enter the customer premises and for direct use with appliances. Other past studies [140-145] have also considered a voltage uprating. However the work described in this thesis differences in the following respects:

- This study is applicable to the 400 V LV network from the distribution substation to the point of common coupling (PCC). Previous studies examined a higher voltage at the 11 kV network and above.
- This study looks at how an increase in capacity will facilitate EV charging and solve the voltage rise issues around DG.
- A device such the VCU can provide secondary benefits to the DNO and the end user. For example, elimination of load current harmonics, fundamental power factor improvement. In addition, communication between loads would enable active demand response.
- The use of a power electronic VCU could allow DC transmission from the substation, with inversion back to AC at the VCU. This would also require an AC-DC converter at the substation. The benefit of DC distribution is that a higher capacity can be achieved over the same conductors than AC.

2.7 Alternative Project

Western Power Distribution have also funded Strathclyde University to independently carry out a similar study to that described in this thesis, and Strathclyde's findings have been presented in [146,147]. It is worth mentioning that the research work which is presented in this thesis, has been published earlier than the Strathclyde University's work. In addition, their work differs in a number of ways:

- Capacity loading assumes a very simple demand model.
- DC distribution is not considered.
- It considers only a single type of VCU device namely an AC chopper power electronic converter. The proposed back-to-back converter discussed in the study does not provide a continuous neutral connection, which is mandatory for safety and protection requirements.
- The location of the VCU at a property is not considered, whereas this has a significant impact on the VCU viability and design.
- More importantly the work in this thesis utilises new Silicon Carbide (SiC) MOSFETs, which prove to be an enabling technology in terms of performance and cost for this type of application.

2.8 Summary

This chapter has discussed the issues around the UKs so-called energy "Trilemma". DNOs will face significant challenges in the near future towards a decarbonised electricity generation and consumption. The deployment of the LCTs will impact the performance distribution network in such way where solutions will be needed to maintain a safe and reliable delivery of electricity to the customers. The practise to put more copper on the ground in order to facilitate these changes is found to be expensive and disruptive. This thesis, proposes an innovative solution to increase the voltage along the distribution feeders and step it back down at the PCC of each customer. By that, a significant increase at the hosting capacity of the existing network can be achieved and power quality problems such as the overvoltage issues can be avoided.

The next chapter will describe the residential LV network in more detail in order to identify the issues that affect the VCU requirements. In particular the results from load-flow simulations of typical networks will be presented that determine the rating of the VCU.

3 Analysis of the LV Residential Network & Identification of a new Voltage Level

In order to evaluate the feasibility of increasing the voltage on the LV network, by using either AC or DC as a solution to the congestion and secondly to power quality problem issues described in Chapter 2, there is first a need to understand the structure and the features of the LV distribution network in order to assess its suitability for such a voltage increase or change to DC and the requirements for an appropriate device to execute this.

3.1 Distribution Network Design Aims

Distribution networks are designed within a strict set of regulatory policies and legislation as well as engineering recommendations that ensure that the electricity in the UK remains robust and reliable. The fundamental aims of the system design philosophy are [14]:

- Develop an efficient, co-ordinated and economical system for the distribution of electricity.
- Provide a system capable of being operated to exceed the minimum overall standards of performance set by the office of Regulation – OFGEM.
- Maximise asset utilisation within the minimum capital investment whilst improving the quality of supply to customers.
- Develop a system which can operate within equipment design ratings.

These aims are directed by various legal, primary Regulatory Mechanisms [148], and these mechanisms are related to the issues around raising the network voltage as proposed in this thesis. The primary regulations are:

- The Electricity Safety, Quality and Continuity Regulations 2002
- The Electricity Supply Regulations 1994 – Amendment No. 2
- Electricity Act 1989 as amended by the Utilities Act 2000
- Distribution Licence Conditions
- Distribution Code
- Grid Code
- Electricity at Work Regulations 1989
- Health & Safety at Work Act 1974
- Construction (Design and Management) Regulations 2002
- Engineering Recommendations
- Energy Network Association Technical Specifications (ENA)

3.2 Distribution Network Structure

An illustration of the UK electricity network is shown in Figure 3.1. The transmission network transmits power at a voltage range of 275 to 400 kV, EHV level. Further substations reduce the voltage level to a 132 kV HV level for distribution. In the HV/MV substations, the voltage is stepped down to a 33 kV MV level which then feeds the primary distribution substations. The distribution network is divided from this point at 11 kV MV, feeding large and small industrial loads and secondary substations. After the point of the secondary substation, the 400V feeders start to supply power to each end user customer either in rural or urban environments and is designated LV.

Typical MV distribution grids consist of different types of topology. This happens because of several factors such as the necessary of need for security of supply, the installation cost and the potential fault levels. A ring or meshed configuration is found in higher load density MV networks such as in urban areas as illustrated in Figure 3.2a. Such networks are used at 11 kV and above. However 400 V circuits use a radial feeder configuration due to the low cost and low fault level as shown in figure 3.2b. On the other hand this topology has the lowest level of supply security with the absence of redundancy. It should be noted that radial feeders can also be found at 11 kV in very rural and rural areas where the load density is lower than 75 kW/mile^2 [149]. To increase the level of reliability, an LV network can be supplied by two transformers as shown in Figure 3.2c. In the likely event of one of the transformers is tripped or cut off for maintenance, the load may still be served by the other transformer.

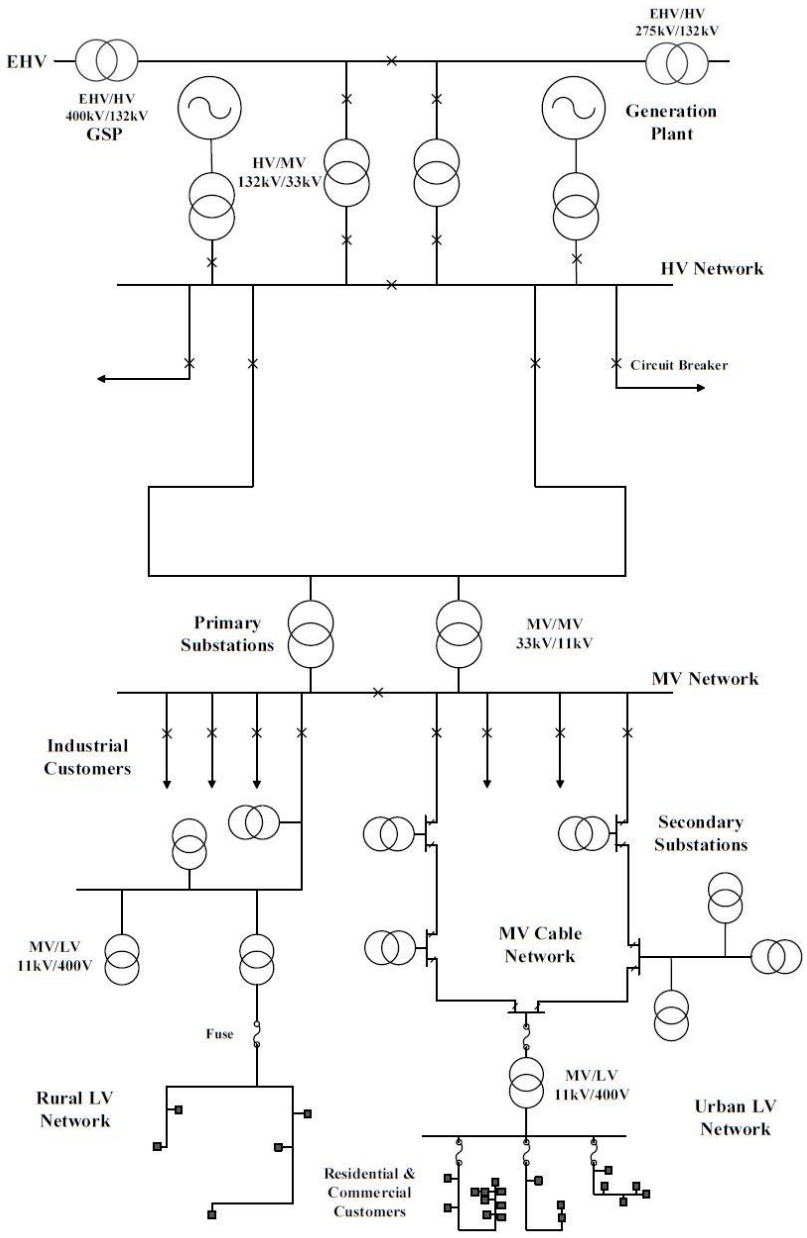

Figure 3.1: ***The structure of the Distribution Network in UK***

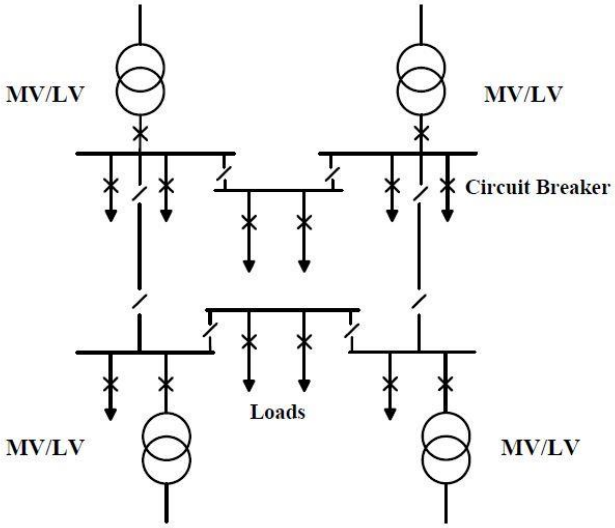

(a)

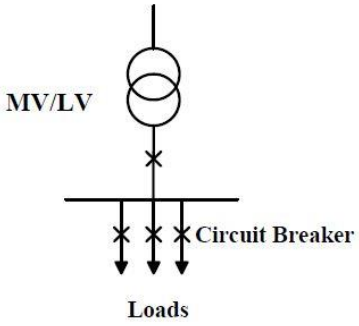

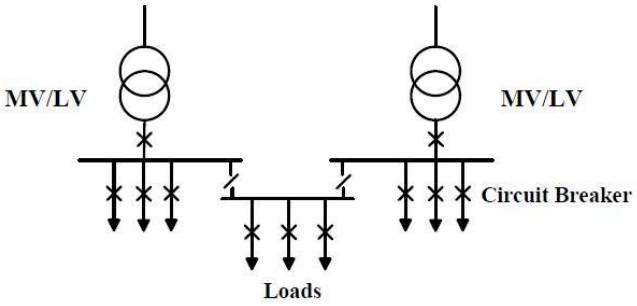

(b) **(c)**

Figure 3.2: ***(a) LV Ring configuration, (b) LV Radial configuration, (c) LV Interconnected Radial configuration***

The 400 V LV lines consist of three phase underground cables or overhead lines suspended from wooden poles. In urban areas where the density is high, the common rule is that 100 customers are connected to each LV feeder. In rural areas, it is recommended that not more than 100 customers are connected to each LV circuit to avoid under-voltages [150].

Single-phase services are directly connected to the main cables via a service cable, and these services are then distributed across the phases of the main feeder in a uniform way in order to maximally equalise the load and avoid unbalance issues [150]. Three-phase services are normally used in larger commercial and industrial properties. However, this thesis only considers purely residential networks, where all of the loads are single-phase.

3.3 Low Voltage Earthing

Earthing can affect the voltage at a particular property, for example depending on the earthing arrangement, a phase-to-earth fault at the LV distribution transformer can cause an overvoltage at the customer's installation.

According to the Low Voltage earthing policy, all new constructions should be consistent with Protective Multiple Earthing (PME) specification, whereas existing networks should be changed to PME only if the PME terminals are requested by the customers. The method of earthing used at a customer's supply is dependent on the Low Voltage (LV) system earthing arrangement, the LV earth resistance and the nature of the customer's installation. The four types of customer earthing are:

- Protective Multiple Earthing (PME)
- Protective Neutral Bonding (PNB)
- Separate Neutral and Earth (SNE)
- Direct Earthing

The majority of UK installations are PME derived systems, which directly take the earth of the distribution system network [3]. Any system decoupling the customer load from the distribution network must maintain the earthing provision in order to protect the customer's installation. Where customer's use direct earthing they are often required to fit a Residual Current Device (RCD) to meet safety requirements specified in BS7671[151]. Under the PME earthing scheme, the neutral conductor is also used as the protective conductor and is referred to as a Protective Earth and Neutral (PEN) conductor. This system is not permitted for conductors of less than 10 mm^2 or for not fixed equipment. The PME system which is shown in Figure 3.3 requires an effective equipotential environment within the installation with distributed earth electrodes spaced as frequently as possible since the conductor is both the neutral conductor and at the same time carries phase unbalance currents as well as 3^{rd} order harmonic currents and their multiples.

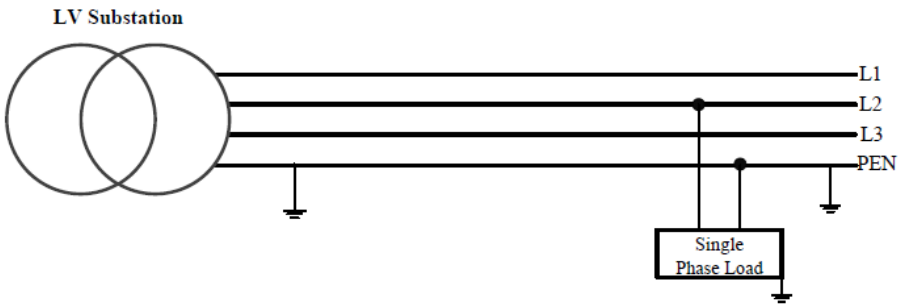

Figure 3.3: ***A PME configuration***

3.4 Low Voltage Protection

The LV designers' goal is to provide the best quality of supply, as well as safe fault clearance times. This means that beside maximum short-circuit current, it is necessary to calculate minimum phase to neutral short-circuit current. The proposed VCU that drops the voltage at each house will therefore need to comply with protection requirements in terms of over-currents and over-voltages.

LV lines are protected by High Rupture Capacity (HRC) fuses up to 630 A that comply with IEC 60269-5. These fuses are located at the secondary substation so that phase to neutral faults on main and service cables are cleared within 100 seconds, allowing for a 15% voltage reduction for arc resistance [150]. This limits the length of main and service cables according to the combined loop impedance of the transformer, main and service cable and substation fuse size. In residential sectors and especially in single-phase servicing, cut out boxes are fused at 80 A and 100 A depending on the absence or the presence of electric heating. Low Voltage lines are protected by High Rupturing Capacity (HRC) fuses. The designed clearance time for LV phase to neutral faults is 30 seconds maximum. At the cut-out the earth loop impedance and fault level are considered so that maximum clearance time for the fuse will be 5 seconds for any fault occurring on the customer side [151]. For discrimination, the minimum pre-arcing I^2t of a feeder circuit fuse must be greater than the maximum total I^2t of any protection device downstream. [152]

3.5 Low Voltage Meter Box

The VCU, which will be owned by the DNO, needs to be located as close to the customer's premises as possible in order to take advantage of the increased network voltage. The most obvious position is in the electricity meter box, prior to the meter itself. Here there is an easy access and installation point for the DNO, and it offers the least intrusive location to the customer. This was the position that Western Power Distribution finally selected as being the preferred solution.

Service terminations in the new and re-serviced domestic property are placed in the outdoor cut-out boxes firmly fixed on external walls on the front or side elevation of the property. The boxes are placed as recessed or surface mounted. The suitable dimensions of cut out boxes used for single-phase services are: 1) 600mm high x 410mm wide x 210mm deep 2) 830mm high x 275mm wide x 210mm deep, see Figure 3.4.

Figure 3.4: ***Cut-out Boxes for a single phase domestic property. From left to the right 1) 600mm high by 410mm wide and 2) 830mm high by 275mm wide*** **[150]**

The meter box can accommodate a single-phase cut out, a time switch, a double rating meter and an isolator, while there are configurations which consist of a single-phase cut out and a single meter with a DNO's owned isolator as can be seen in Figure 3.5.

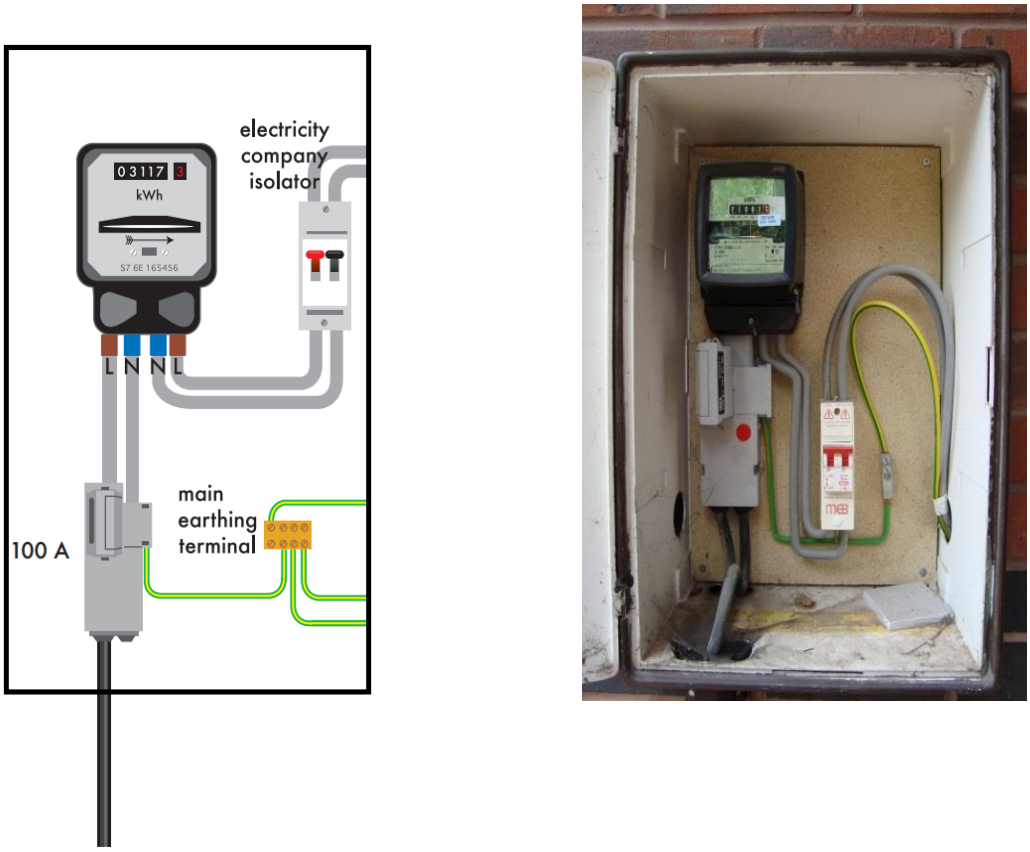

(a) **(b)**

Figure 3.5: ***A representation (a) of a typical UK single phase property meter box - reproduced from*** **[151]** ***- with PME configuration and a close up of a 4-bedroomed dwelling in Midlands (b).***

3.6 Low Voltage Network Policy

The LV network must comply with several regulations in order to maintain nominal values for voltage, frequency and current. Since the last automatic element of the network can be found at the primary substations such as the on load tap changers (OLTCs), the design of the network after this point is crucial in order to prevent any disturbances. The only way to adjust the voltage on the LV network is by manually changing the taps of the 11kV/400V transformer. A summary of nominal values under normal feeding arrangements and their limits are presented at Table 3-1.

Factor	Nominal Value	Range	Regulation
Voltage	230V	+10% /-6%	Electricity Safety, Quality and Continuity Regulations 2002
Voltage Step change-connection/disconnection of user's equipment/customer's demand		± 3%	
Current (maximum for single-phase supply)	100A		
Frequency	50Hz	± 1%	Distribution Code
Exceptional circumstances Frequency		47-52 Hz	Distribution Code
Flicker	$P_{Is} \leq 1$ for 95% of 1 week		BS EN50160. Normal operation conditions
Voltage (Harmonic) Distortion	Total = 8% 3^{rd} =5% 5^{th} = 6% 7^{th} = 5% All for 95% of 1 week		BS EN50160. Normal operation conditions
Voltage (Harmonic) Distortion – for planning purposes	Total = 5% 3^{rd} =4% 5^{th} = 4% 7^{th} =4%		G5/4-1 Planning Limits
Voltage Unbalance	3% for 95% of 1 week		BS EN50160. Normal operation conditions
Voltage Unbalance – for planning purposes	≤ 1.3% sustained ≤ 2% < 1 minute		P29 Planning Limits
Voltage Dips	Few tens to one thousand, majority duration <1s and depth <60%		BS EN50160. Indicative Value
Temporary Overvoltage	<1.5 kV		BS EN50160. Indicative Value
Short Interruptions (up to 3 minutes)	Few tens to several hundreds , 70% for duration <1s		BS EN50160. Indicative Value
Long Interruptions	Less than ten up to fifty not prearranged		BS EN50160. Indicative Value
Transient Overvoltage	<6kV		BS EN50160. Indicative Value

Table 3-1: ***Typical Network Values***

3.7 Types of Low Voltage Network Conductors

In order to benchmark the ability to raise the LV system voltage, a number of typical reference LV network templates are required. These templates inform the models used to analyse the effects of DG and LCTs in particular the benefits accrued in hosting capacity or in reduction of losses by utilising a higher voltage.

The existing underground cables on the network adhere to the Distribution Network Operators for Low Voltage three core mains cables or single core service cables. The mains cables are 600/1000 V (Line to Line / Line to Neutral) three core cables, solid aluminium phase conductors 95, 185 or 300 mm^2 , XPLE insulated coloured brown, black and grey, copper CNE conductors on a bedding comprising only as underlying rubber layer, to British Standard Specification BS 7870 Part 3.40, Table1.

The service cables are 600/1000 Volt four core polymeric insulated aerial bundled conductors (ABCs) with phase and neutral conductors of equal size and type, conductor sizes are from 25mm^2 up to and including 120 mm^2 complying with the British Standards BS 7870- 5:2011.

All low voltage cables and conductors are rated to voltage 0.6/1/2 kV, where the voltages are expressed in the form U_o /U (U_m). The voltages are designated by U_o, U and U_m, where U_o is the rated voltage between conductors and U_m is the maximum permissible voltage according to IEC60038 [153].

It is clear for the cables characteristics described in the previously that it is technically feasible to raise the voltage across the 400 V LV network to around 1000 V, as the assets are in place and there is an opportunity of better utilisation.

3.8 Domestic Loads at LV

As discussed in Chapter 1, an issue arising in the modern load profile is the growth of energy demand due to an increase of electrification in transport and heating. However there is also an opportunity for feeders to provide the Low Voltage Network with power by producing electricity from renewable energy sources such as PV units. The main question nowadays is whether the LV Networks are able to satisfy these demands. In the last couple of decades the profile of a typical residential load has changed dramatically. This trend is shown in Figure 3.6, along with a breakdown of load type.

Figure 3.6: ***Consumption data of appliances in UK*** **[154]**

It can be seen that there is a significant increase in power electronic loads such as consumer electronics, home computing and lighting. These loads can be characterized as non-linear as they normally include an input AC-DC converter. In 2011 and according to UK National Statistics non-linear electronic loads were 54% of the total domestic loading [154]. By the term non-linear load, scientists and engineers mean any electronic device, creating harmonics by drawing current in abrupt short pulses, rather than in a smooth sinusoidal manner. The power quality of Low Voltage networks is severely affected by the flow of these generated harmonics. Harmonics cause increased losses in the customer and utility power system components [155]. Moreover, they can give rise to augmented costs as a result of maintenance issues, occurring failures or transformer de-rating and life-span reduction of both feeders and utility power system components. Users will also experience difficulties from distorted voltage waveforms caused by harmonic currents flowing in the power distribution network. In particular in a recent study the 3rd, 5th, 7th, 11th and 13th harmonics measurements at the PCC were found to exceed the statutory limits. [156].

A typical example of non-linear load is a domestic micro-wave oven, where the supply current waveform drawn by the input rectifier is shown in Figure 3.7a and has a current THD of 5.4%. Figure 3.7b shows the corresponding frequency spectrum where it can be seen there is a large amount of 3^{rd} and 5^{th} harmonic(s).

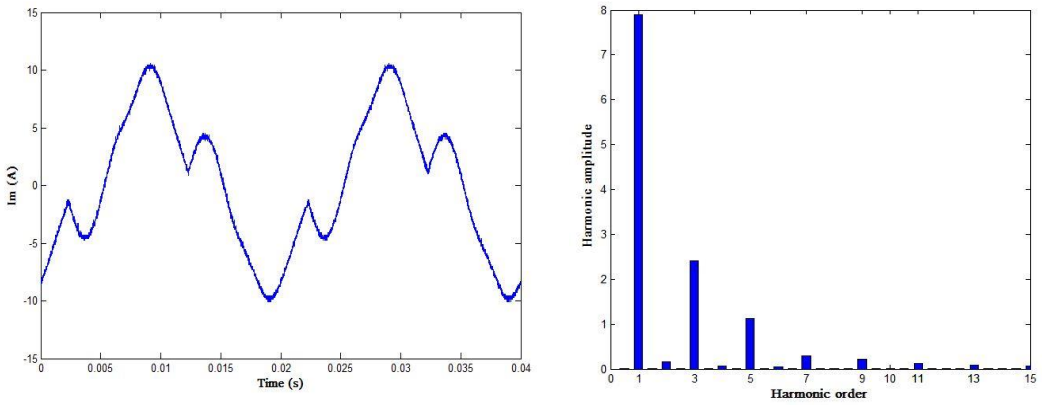

(a) **(b)**

Figure 3.7: ***Microwave oven (a) measured current waveform (A) against time (s) and (b) corresponding magnitude of higher order harmonics (A)***

In [157] it has been reported that non-linear loads like PCs, Televisions and Compact fluorescent lamps (CFLs) could generate power quality problems for the Low Voltage Network of New Zealand that would cause the THD to exceed the 5% statutory limit, and the fundamental power factor to drop below 0.95. On the other hand this study does not mention anything about the existence of linear (resistive) loads or the capacitance and inductance of the service cables.

3.9 Residential Distribution Network Modelling and Simulation

In order to initially approximate the increase in LV network capacity that a higher network voltage would provide, a basic analysis can be carried out by assuming all of the loads can be represented as a single lumped load halfway along a feeder. The details of this analysis are presented in Appendix B. For a typical urban network of 100 houses, with an ADMD load of 3 kW per house, a VCU efficiency of 99%, and a supply voltage increase from 230 V to 300 V, this analysis suggest typical network capacity gains of 40%, can be achieved. This result gives an initial indication that the proposed solution is worthwhile. However, a number of more detailed load-flow simulations were carried out using Micro-Cap Spice in order to validate this value. In particular the gains in capacity were appraised in terms of the amount of EV charging that would be realised on the network as well as the effect of voltage rise due to DG.

A difficulty arises with load-flow studies of LV networks in obtaining representative data of the residential load. Whilst recordings of the aggregated load are available, measurements of individual properties cannot in general be recorded due to concerns around data protection issues of the customer. Therefore, in order to calculate the load demand from individual houses for the

following studies, the Excel based model - "A high-resolution energy demand model" [158-159] was used, which has been developed by Loughborough University and Eon under a previous EPSRC Supergen project. This model allows the user to set the number of occupants of a house along with a range of electrical appliances and generates an electricity demand profile with a one minute time resolution over a twenty-four hour period for either winter or summer. In particular, the Loughborough model has been validated against data from a study that was granted permission to carry out recordings over a period of one year within 22 dwellings in the Midlands, UK. The list of electrical appliance settings for this model along with a typical occupancy and electricity usage waveforms are shown in Figure 3.8 and Figure 3.9 respectively. Factors that are included for example are the external iridescence during the day, which is used to calculate lighting demand within a property.

Appliance category	**Appliance type**	**Dwelling configuration** Presence
Cold	**Chest freezer**	NO
	Fridge freezer	YES
	Refrigerator	YES
	Upright freezer	YES
Consumer Electronics + ICT	**Answer machine**	YES
	Cassette / CD Player	YES
	Clock	YES
	Cordless telephone	YES
	Hi-Fi	YES
	Iron	YES
	Vacuum	YES
	Fax	NO
	Personal computer	YES
	Printer	NO
	TV 1	YES
	TV 2	YES
	TV 3	NO
	VCR / DVD	YES
	TV Receiver box	YES
Cooking	**Hob**	YES
	Oven	YES
	Microwave	YES
	Kettle	YES
	Small cooking (group)	YES
Wet	**Dish washer**	NO
	Tumble dryer	YES
	Washing machine	YES
	Washer dryer	NO
Water heating	**DESWH**	NO
	E-INST	NO
	Electric shower	YES
Electric Space Heating	**Storage heaters**	NO
	Other electric space heating	NO
Lighting	**Lighting**	YES

Figure 3.8 : ***Typical electrical appliance settings for a 3- bedroomed dwelling***

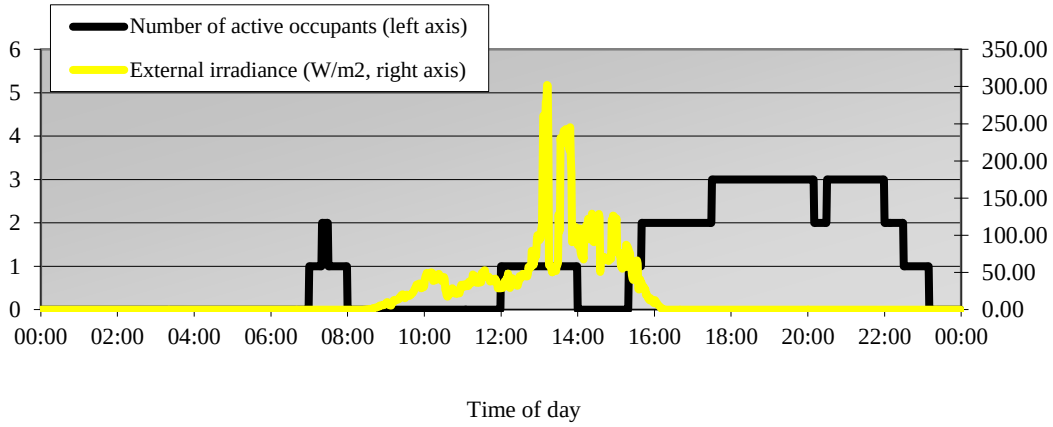

(a)

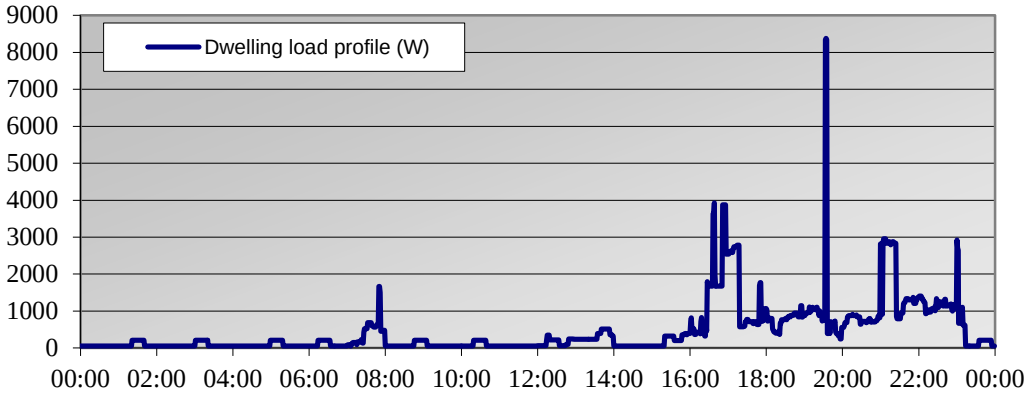

(b)

Figure 3.9: ***Calculated occupancy and electricity demand for a typical 3-bedroomed dwelling during a winter day***

It can be seen in Figure 3.9 that because the model has a one minute resolution, then high peak demands such as 8.5 kW electric showers are apparent. The LV distribution network studies were divided into three distinct topologies namely (1) Very Rural, (2) Rural and (3) Urban, with weekday January load demands and the hosting capacity of each were evaluated under different operating voltage levels for slow, fast or rapid EV charging scenarios. Unfortunately at the time of carrying out the project, the Loughborough model had not been developed enough to include DG or heat pumps.

3.9.1 LV Services Connections

Each property is connected to the nearest LV mains cable or Overhead Line (OHL) by approximately 20 meters of 35 mm^2 single phase hybrid service cables with specific characteristics as presented in Table 1 in Appendix A. For the purpose of the study, each property was split equidistantly across the total length of the mains cable.

3.9.2 Very Rural Network

Typically, a very rural network consists of a single phase 100 kVA Pole Mounted Transformer feeding 15 customers connected off a single-phase, 50 mm^2 Aerial Bundled Conductor (ABC), 250 meters in length. The pole transformer complies with the ENATS 35-1 Distribution transformers (from 16 kVA to 100 kVA) Technical Specification [160]. Typical values for the conductor and the transformer output impedance were derived from WPD Design Manual [150] and are presented in Table 2 and Table 3 in Appendix A.

The predicted power use in kW calculated using the Loughborough load model for a weekday in January [159] for the 15 houses in a Very Rural network is shown in Figure 3.10 a and b.

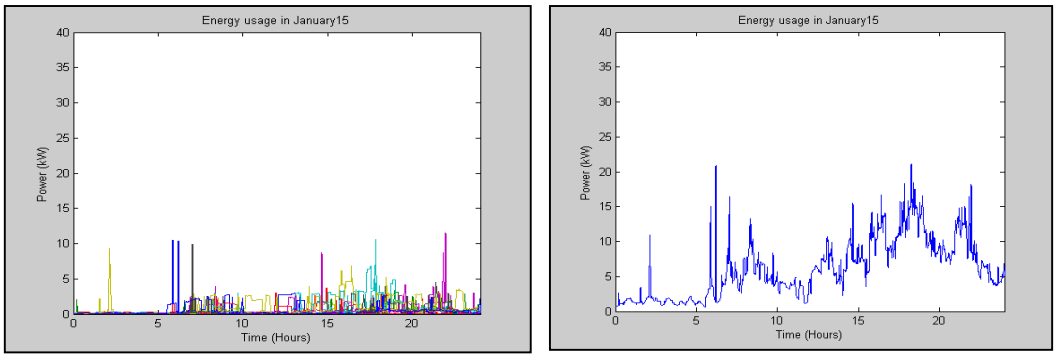

(a) **(b)**

Figure 3.10: ***Predicted power use (kW) for 15 houses in a Very Rural network over 24-hours (a) individual houses and (b) total summation of 15 houses.***

The peak demand from an individual house can be obtained from the curve in Figure 3.10a and the peak aggregated power demand over the 15 houses from the curve in Figure 3.10b, and these peaks are shown in Table 3-2:

Peak power demand from an individual house (kW)	Peak of aggregated power demand for the network (kW)
11.5	21.1

Table 3-2: ***Peak power demand from an individual house and peak aggregated network power demand for the Very Rural Network***

With current ratings of 144 A and 115 A for the main overhead line feeder and service cable respectively, calculation shows that even at the current 250 V the main overhead line and service cables are operating well below their existing capacity:

- 21.1 kW compared with a maximum of 103 kW capacity for the main OHL
- 11.5 kW compared with 26 kW capacity for the service cable

The results from the Loughborough model shown in Table 3-3 can be compared against those obtained using WPD's traditional estimation method, which is based on statistical/historical data as described in [161] and gives 11.4 kW and 22.5 kW respectfully. This shows that there is close agreement between the two methods.

A Micro-Cap load-flow simulation for the Very Rural network was then used to determine the maximum capacity of the main and service cables for a range of network voltages above 250 V up to a hypothetical voltage of 1000 V. The lower 250 V is the typical open-circuit voltage of the LV distribution transformer. The Micro-Cap simulation uses a non-linear numerical optimiser to vary the load until the current flowing into the main OHL is equal to its rated value for a given supply voltage. The load is assumed to be spread evenly amongst the 15 houses with a typical domestic fundamental power factor of unity. The Micro-Cap simulation, single-line schematic is shown in Figure 3.11. A number of circuit models have been developed at Aston University to enable Micro-Cap Spice to run traditional, balanced load-flow simulations. In Figure 3.11, the PQ block is a constant power load that can source or sink active, P and reactive Q, power. Each PQ block represents 3 houses spread across the feeder phases. The brown coloured cylindrical components shown in the Figure 3.11 are used to model cable, overhead line, mains and service cable impedances and consist of fully-distributed, distribution line models of the lines. The network is fed from an ideal, three-phase voltage source, which is represented by the Slack Generator component and corresponds to the grid connection. Simulation schematics shown further in the thesis such as Figure 3.12 also include the three-phase Transformer model, with adjustable tap-settings. The corresponding results from the simulation are summarised in Table 3-3.

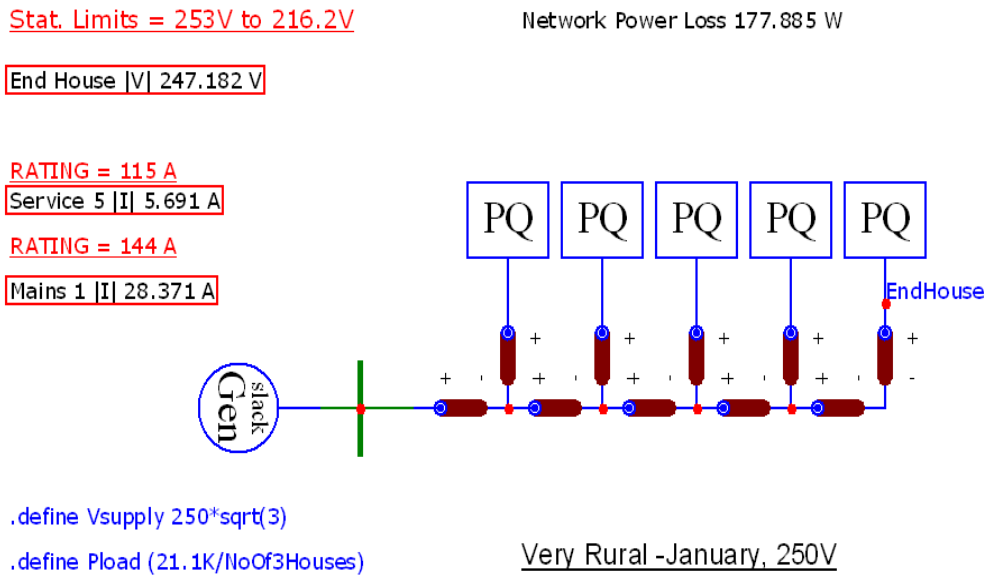

Figure 3.11: ***Simulation schematic for Very Rural network at 250 V***

Network Voltage (V) RMS (Peak)	Power (kW), based on 144 A OHL Rating		Network Loss (kW)	Network Loss as a % of Capacity (%)	Last 3 houses at 115 A Service Rating – Network at max. power. House power (kW)
	Network max.	ADMD/ house			
250 (354)	103	6.87	4.58	4.45	26
300 (424)	124	8.27	4.53	3.65	31
400 (566)	168	11.20	4.59	2.73	43
500 (707)	211	14.07	4.58	2.17	54
600 (849)	254	16.93	4.57	1.80	66
700 (990)	297	19.80	4.56	1.53	77
800 (1131)	341	22.73	4.59	1.34	89
900 (1273)	384	25.60	4.58	1.19	100
1000 (1414)	427	28.47	4.58	1.07	112

Table 3-3: ***Load flow calculations from simulation for a range of network phase voltages between 250 V and 1000 V RMS***

The results for Table 3-3 are laid out as follows:

- Column 1 : The substation network voltage in Volts RMS (peak in brackets)
- Column 2a : The maximum theoretical capacity of the network in kW calculated by the Micro-Cap optimiser routine, which gives rated OHL feeder current
- Column 2b : The maximum capacity from column 2a divided by the number of houses to give the equivalent maximum ADMD load capacity for each house

- Column 3 : The network loss calculated from the load flow simulation
- Column 4 : How this loss translates as a percentage of the maximum capacity in column 2a
- Column 5 : The maximum load in kW that an individual end-house can draw without overloading the service cable, whilst the overall network draws the maximum theoretical capacity from column 2a. The end house is used as the worst case because due to feeder voltage drops it has the lowest voltage and therefore draws the highest current.

The important data in the table is the maximum network capacity in column 2a, which is based on the main OHL feeder rating. This can be subtracted from the peak aggregated demand from Table 3-2 to calculate the spare capacity that is available for EV charging. Also column 5 gives the maximum allowable load demand from an individual house, which is limited by the service cable rating.

In the UK there are three different Modes of EV charging: Slow=3.7 kW, Fast=7.5 kW and Rapid=34 kW according to UK Electric Vehicle Supply Equipment (UKEVSE) [170]. If future electric vehicle charging is to be taken into account then the total loading on the network for 15 houses can be determined from Tables 3-2:

	EV charging load		House load		Total load	
•	15 x 3.7 kW	+	21.1 kW	=	76.6 kW	for slow charging
•	15 x 7.5 kW	+	21.1 kW	=	133.6 kW	for fast charging
•	15 x 34 kW	+	21.1 kW	=	531.1 kW	for rapid charging

Therefore based on these totals, from Table 3-3, column 2a it can be concluded that both main and service cables would be capable of supplying a Very Rural network with Slow charging for every house with the existing 250 V as this load has a total of 76.6 kW, whereas the network has a maximum capacity of 103 kW. However, Fast charging for the complete network is only possible with a network voltage of between 300 V and 400 V. The Rapid charging scenario has a 531.1 kW demand and this cannot be supplied to the entire network even with the higher 1000 V supply, as the maximum network capacity is limited to 427 kW. A small number of houses could be hosted Rapid charging, which requires a peak of 34 + 11.5 = 45.5 kW per house, but due to service cable limits shown in Table 3-3, column 5, this is only possible with network voltages of approximately 500 V and above.

It should be noted that as well as a capacity increase then raising the network voltage also reduces energy losses as a percentage of capacity as shown in column 4. This would therefore have a contribution in terms of overall CO_2 emissions.

The second simulation investigates the voltage rise issue that occurs with embedded generation. In this scenario, every house is generating a maximum of 3.7 kW power back into the grid, this figure was suggested by WPD as representative of current PV technology. The substation transformer tap is set to give an output voltage of 250 V with the maximum ADMD load from Table 3-3 of 21.1 kW with a typical residential 0.95 power factor.

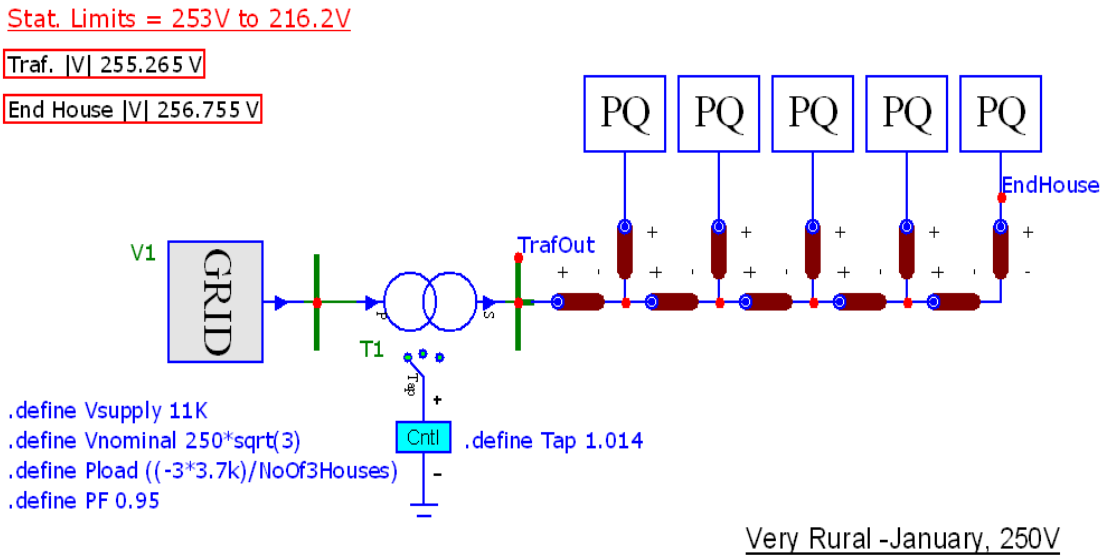

Figure 3.12: ***Simulation schematic for a Very Rural network with DG loads***

It can be seen from the above simulation schematic that the voltage calculated at the end three houses is 256.8 V, which violates the specified maximum voltage of 253 V [161]. However, this problem could be mitigated by increasing the network voltage and using the proposed VCU as a voltage controlled device to regulate the voltage at each property to within the statutory limits.

3.9.3 Rural Network

A typical rural network consists of a 100kVA Pole Mounted transformer, feeding 50 customers connected off 2 three-phase 95 mm^2 ABC conductors with specific characteristics. Each feeder is on average 250 meters distance from the distribution transformer, and the conductor and transformer data is given in Table 4 and Table 5 in Appendix A.

The predicted power use in kW calculated using the Loughborough load model for a weekday in January [159] for the 27 houses in a Rural network is shown in Figure 3.13a and b.

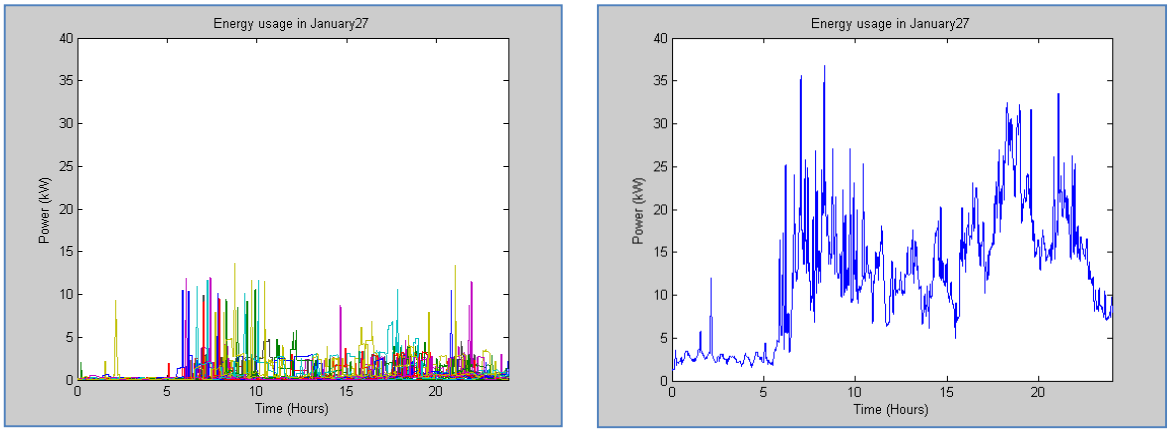

(a) **(b)**

Figure 3.13: ***Predicted power use (kW) over 24 hours for 27 houses in a Rural network (a) individual houses and (b) total summation of 27 houses.***

The peak demand from an individual house can be obtained from the curve in Figure 3.13a and the peak aggregated power demand over the 27 houses from the curve in Figure 3.13b, and these peaks are shown in Table 3-4:

Peak power demand from an individual house (kW)	**Peak of aggregated power demand for the network (kW)**
13.7	36.8

Table 3-4: ***Peak power demand from an individual house and peak aggregated network power demand for the Very Rural Network***

With current ratings of 228 A and 115 A for the main overhead line feeder and service cable respectively, calculation shows that even with the current 250 V the main overhead line and service cables are operating well below their existing capacity:

- 36.8 kW compared with a maximum of 165 kW capacity for the main OHL
- 13.7 kW compared with 26 kW capacity for the service cable

The results from the Loughborough model shown in Table 3-4 can be compared against those obtained using WPD's traditional estimation method, which is based on statistical/historical data as described in [161] and gives 11.4 kW and 45.9 kW respectfully. This shows that there is reasonable agreement between the two methods.

The same Micro-Cap load-flow simulation that was carried out for the Very Rural network was repeated for the Rural network in order to determine the maximum capacity of the main and

service cables. The Micro-Cap simulation schematic is shown in Figure 3.14, and the corresponding results from the simulation are summarised in Table 3-5.

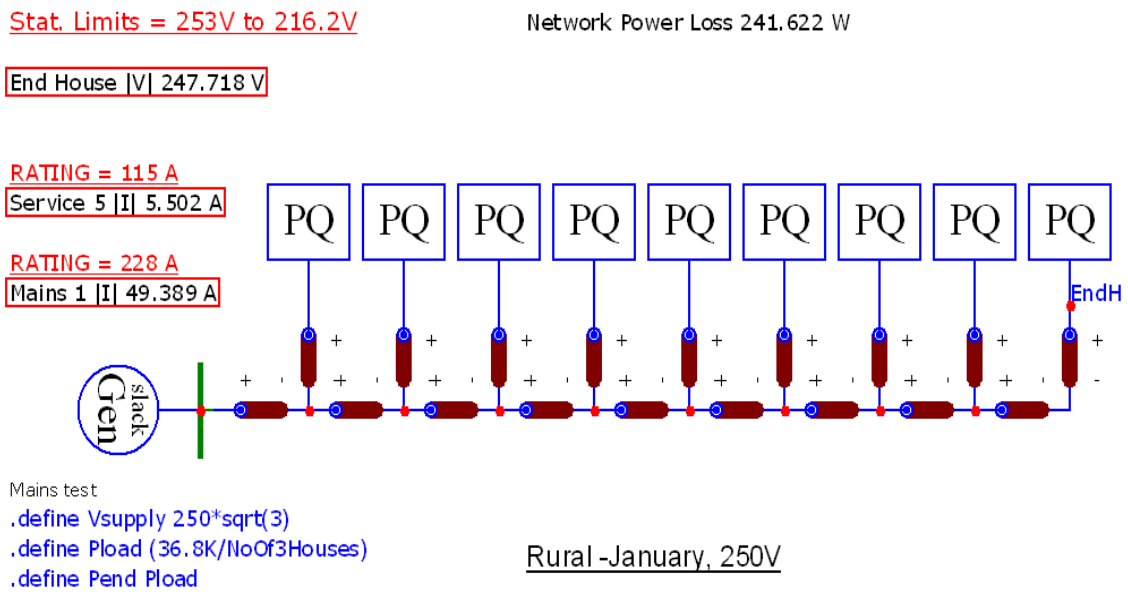

Figure 3.14: ***Simulation schematic for Rural network at 250 V***

Network Voltage (V) RMS (Peak)	Power (kW), based on 228 A OHL Rating		Network Loss (kW)	Network Loss as a % of Capacity	Last 3 houses at 115 A Service Rating – Network at max. power. House power (kW)
	Network max.	ADMD/ house			
250 (354)	165	6.11	5.13	3.11	26
300 (424)	199	7.37	5.12	2.57	32
400 (566)	268	9.92	5.15	1.92	44
500 (707)	336	12.44	5.14	1.53	55
600 (849)	405	15.00	5.15	1.27	67
700 (990)	473	17.50	5.15	1.09	78
800 (1131)	547	20.07	5.15	0.94	90
900 (1273)	610	22.60	5.14	0.84	101
1000 (1414)	678	25.11	5.14	0.76	113

Table 3-5: ***Load flow calculations from simulation for a range of network phase voltages between 250 V and 1000 V RMS***

If future electric vehicle charging is to be taken into account then the total loading on the network for 27 houses would be:

	EV charging load		House load		Total load	
•	27 x 3.7 kW	+	36.8 kW	=	136.7 kW	for slow charging
•	27 x 7.5 kW	+	36.8 kW	=	239.3 kW	for fast charging
•	27 x 34 kW	+	36.8 kW	=	954.8 kW	for rapid charging

Therefore based on these totals, from Table 3-5, column 2a it can be concluded that both main and service cables would be capable of supplying a Very Rural network with Slow charging for every house with the existing 250 V as this load has a total of 136.7 kW, whereas the network has a maximum capacity of 165 kW. However, Fast charging for the complete network is only possible with a network voltage of 400 V and above. The Rapid charging scenario has a 954.8 kW demand and this cannot be supplied to the entire network even with the highest 1000 V supply, as the maximum network capacity is limited to 678 kW. A small number of houses could be hosted with Rapid charging, which requires a peak of 34 + 36.8 = 70.8 kW per house, but due to service cable limits shown in Table 3-5,column 5, this is only possible with network voltages of approximately 700 V and above.

The second simulation investigated the voltage rise issue that occurs with embedded generation. In this scenario, every house is generating a maximum of 3.7 kW power back into the grid. The substation transformer tap is set to give an output voltage of 250 V with the maximum ADMD load of 36.8 kW at 0.95 power factor.

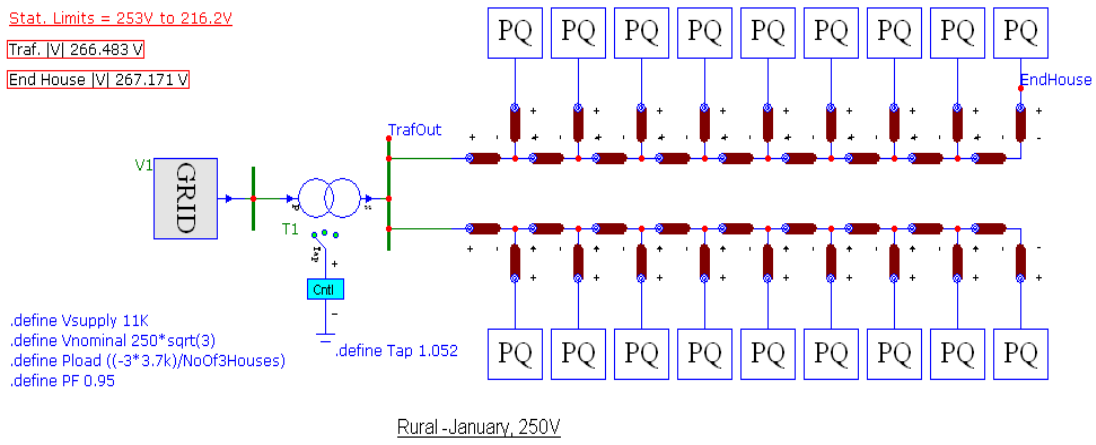

Figure 3.15: ***Simulation schematic for a Rural network with generating loads***

It can be seen from the simulation results that the voltage at the end three houses is 267.2 V, which violates the specified maximum voltage of 253 V [161]. As mentioned for the Very Rural Network, this problem could be mitigated by increasing the network voltage and using the proposed VCU as a voltage controlled device to regulate the voltage at each property to within the statutory limits.

3.9.4 Urban Network

A typical urban LV network consists of an 800kVA Ground Mounted transformer with four feeder ways, each supplying 75 houses from 185 mm^2 Combined Neutral Earth (CNE) three phase underground cables, each of 200 meters in length. It is also common in congested metropolitan city areas for each feeder to supply 100 single phase properties. The distribution transformer and conductor data is given in Table 5 and Table 6 in Appendix A.

The predicted power use in kW calculated using the Loughborough load model for a weekday in January [159] for the 75 houses in an Urban network is shown in Figure 3.16 a and b.

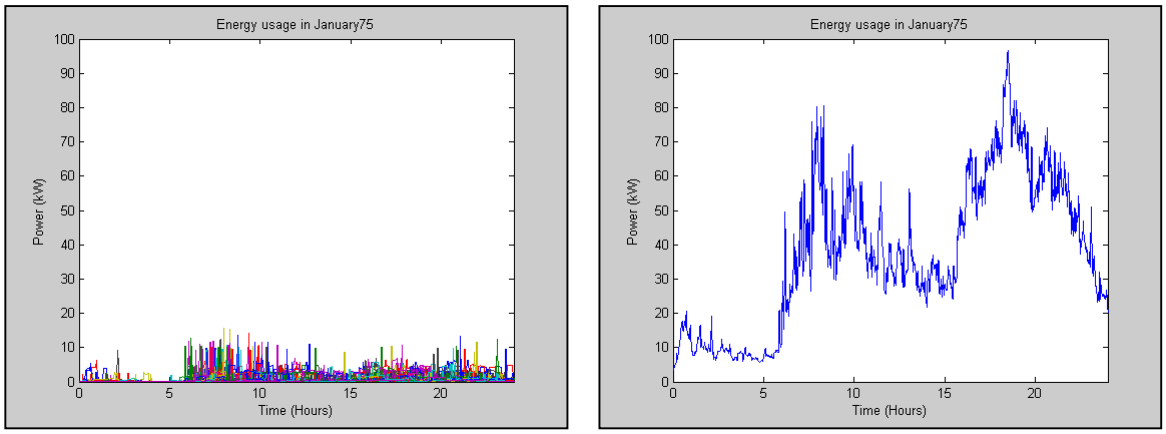

(a) **(b)**

Figure 3.16: ***Predicted power use (kW) over 24 hours for 75 houses in an Urban network (a) individual houses and (b) total summation of 75 houses.***

The peak demand from an individual house can be obtained from the curve in Figure 3.16a and the peak aggregated power demand over the 15 houses from the curve in Figure 3.16b, and these peaks are shown in Table 3-6:

Peak power demand from an individual house (kW)	Peak of aggregated power demand for the network (kW)
15.6	96.6

Table 3-6: ***Peak power demand from an individual house and peak aggregated network power demand for the Very Rural Network***

With current ratings of 292 A and 115 A for the main cable feeder and service cable respectively, calculation shows that even with the current 250 V the main feeder cable and service cables are operating well below their existing capacity:

- 96.6 kW compared with a maximum of 215 kW capacity for the main cable
- 15.6 kW compared with 26 kW capacity for the service cable

The same Micro-Cap load-flow simulation that was carried out for the Rural network was repeated for the Urban network in order to determine the maximum capacity of the main and service cables. The Micro-Cap simulation schematic is shown in Figure 3.17, and the corresponding results from the simulation are summarised in Table 3-7.

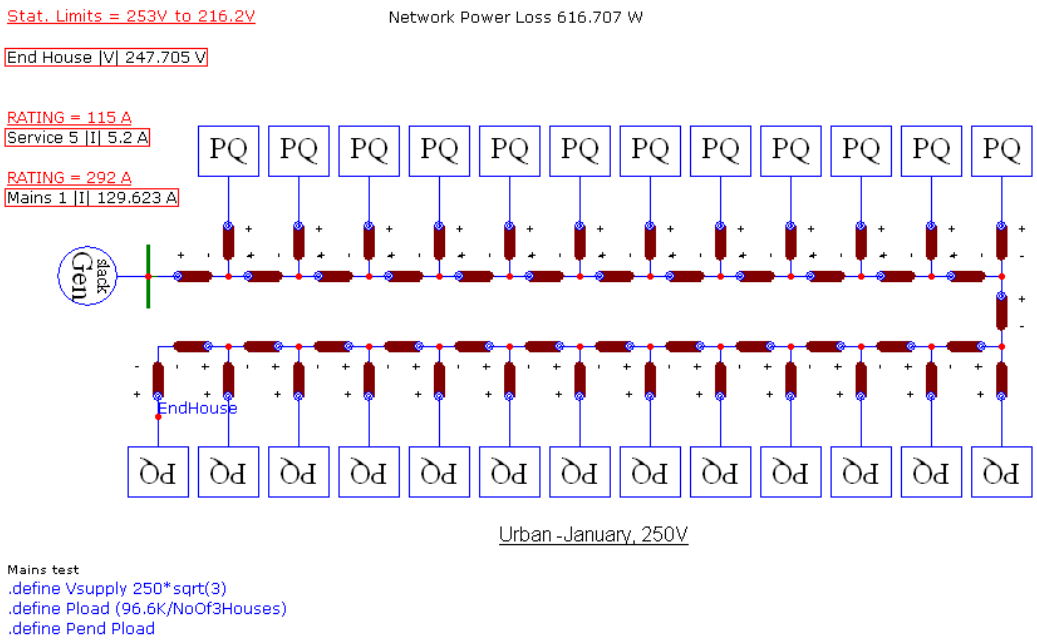

Figure 3.17: ***Simulation schematic for Urban network at 250 V***

Network Voltage (V) RMS (Peak)	Power (kW), based on 292 A Cable Rating		Network Loss (kW)	Network Loss as a % of Capacity	Last 3 houses at 115 A Service Rating – Network at max. power. House power (kW)
	Network max.	ADMD/ house			
250 (354)	215	2.87	3.11	1.44	27
300 (424)	259	3.45	3.12	1.20	33
400 (566)	347	4.60	3.13	0.90	45
500 (707)	435	5.80	3.13	0.72	56
600 (849)	522	6.96	3.12	0.60	68
700 (990)	614	8.19	3.17	0.52	79
800 (1131)	697	9.29	3.12	0.45	91
900 (1273)	785	10.46	3.13	0.40	102
1000 (1414)	872	11.63	3.12	0.36	114

Table 3-7: ***Load flow calculations from simulation for a range of network phase voltages between 250 V and 1000 V RMS***

If future electric vehicle charging is to be taken into account then the total loading on the network for 75 houses would be:

	EV charging load		House load		Total load	
•	75 x 3.7 kW	+	96.6 kW	=	374.1 kW	for slow charging
•	75 x 7.5 kW	+	96.6 kW	=	659.1 kW	for fast charging
•	75 x 34 kW	+	96.6 kW	=	2646.6 kW	for rapid charging

Therefore based on these totals, from Table 3-7, column 2a it can be concluded that the network is incapable of supplying all houses with any of these charging schemes using the existing 250 V. For example Slow charging requires 374.1 kW, whereas the network has a maximum capacity of 215 kW. However Slow charging can be achieved for the complete network at voltages of approximately 450 V and above. Fast and Rapid charging is not possible for the entire network, but could be accommodated for a small number of houses, but due to service cable limits this is only possible with network voltages of approximately 250 V and above for Fast charging and 500 V and above for Rapid charging.

The second simulation investigated the voltage rise issue that occurs with embedded generation. In this scenario, every house is generating a maximum of 3.7 kW power back into the grid. The substation transformer tap is set to give an output voltage of 250 V with the maximum ADMD load of 96.6 kW at 0.95 power factor.

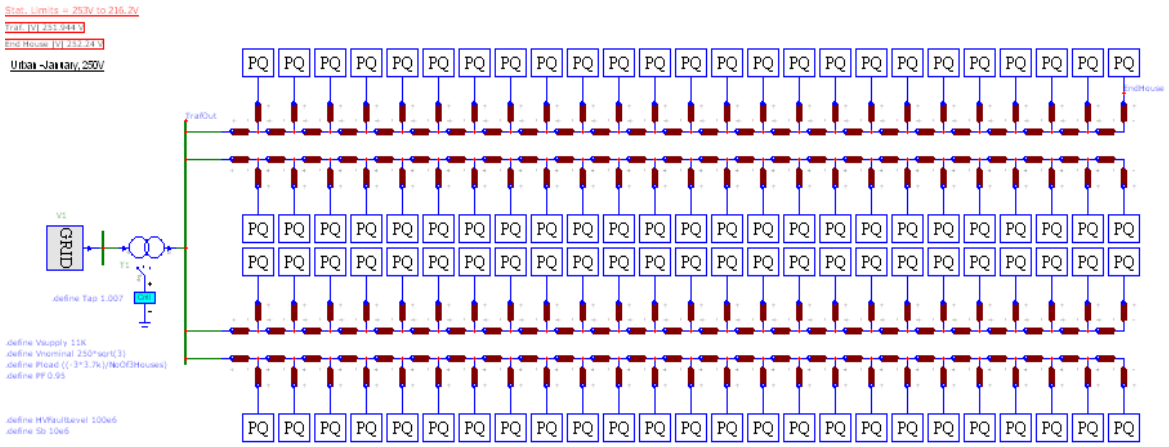

Figure 3.18: ***Simulation schematic for an Urban network with generating loads***

It can be seen from the simulation results that the voltage at the end three houses is 252.2 V, which unlike the Very Rural and Rural networks does not violate the specified maximum voltage of 253 V [161]. This is because whilst the urban network has a higher overall power input from the embedded generation than the Very Rural and Rural networks, its cable and distribution impedances are much lower.

3.9.5 Summary of Very Rural, Rural and Urban Studies

Since this thesis only considers the proposed VCU solution when using existing residential mains cables or overhead lines, which is rated at 600 V, then the previous results are only useful for voltage values below this voltage level. The following general conclusions can then be drawn from the previous results:

- By operating the network voltage at its maximum value of 600 V rather than the existing 250 V, which is an increase by the factor of 2.4, then for all three networks:
    - Network capacity increases by the factor 2.4.
    - The After Diversity Maximum Demand (ADMD) increases by the factor 2.4.
    - Network loss as a percentage of network capacity reduces by the factor 2.4.
    - The capacity of the service cables connecting individuals properties to the main feeder will increase by approximately 2.4
- Network capacity is limited by the main feeder cable rather than the service cables when the load is equally loaded amongst properties.

- The following electric vehicle charging schemes are possible:

	Very Rural	Rural	Urban
Slow Charging	**All** houses at 250 V and above	**All** houses at 250 V and above	**All** houses at 450 V and above
Fast Charging	**All** houses at 350 V and above	**All** houses at 400 V and above	**50%** of the houses at 400 V and above
Rapid Charging	**40%** of the houses at 500 V and above	**35%** of the houses at 500 V and above	**15%** of houses at 500 V and above

Table 3-8: ***Summary of maximum possible electric vehicle charging schemes for Very Rural, Rural and Urban networks.***

- There are over-voltage issues with embedded generation in Very Rural and Rural networks at 250 V.

The simulation results for maximum network cable/OHL and service cable capacity for Very Rural, Rural and Urban networks with supply voltages up to 600 V are summarised in Table 3-9.

Network Voltage (V) RMS (Peak)	Maximum network power (kW)			Max. Individual house
	Very Rural (15 houses)	Rural (25 houses)	Urban (75 houses)	
250 (339)	103	165	215	27
300 (424)	124	199	259	33
400 (566)	168	268	347	45
500 (707)	211	336	435	56
600 (849)	254	405	522	68

Table 3-9: Summary of maximum network capacity and service cable capacity simulation results for Very Rural, Rural and Urban networks

- Using Table 3-8 and 3-9, it can be seen that by choosing a network voltage of 400 V then Slow and Fast charging for all houses can be provided to Very Rural and Rural networks and 50 % of houses in an urban network. Rapid charging is possible for a limited number of houses. This is a good compromise between maximising the hosting of EV charging

and the peak voltage stress on the VCU. For example, it was anticipated that the VCU would be a power electronic converter, and since a 400 V network voltage equates to a 566 V peak VCU input voltage, this voltage level allows a 50% safety margin using industry standard 900 V transistors or above.

Whilst it is concluded that 400 V seems to be the preferred network voltage, no such voltage was available for prototype testing within the university's laboratories. The maximum voltage that could be generated for loads up to 15 kW was 300 V, using a 15 kVA step-up laboratory isolated autotransformer. A voltage of 300 V was therefore used in the subsequent VCU simulation and designs. In addition, the above studies predict a maximum load from individual houses of between 10 kW to 15 kW. These figures comply with WPD load estimations for design and planning of the LV network [150, 161]. Therefore, the target power rating of the VCU was chosen is 15 kW.

3.10 DC Distribution Network

Historically, the first distribution power systems were designed as DC, and then were changed by AC systems due to the advantages of voltage step-up/down using transformers and simpler circuit breaker design. Due to the evolution of power electronics technology, DC has been extensively used in HVDC applications for the transmission of the electricity over long distance, usually greater than 600km [162]. At distribution levels, DC distribution systems are not widely used yet, and their applications are limited to specific areas. On the other hand a significant amount of research has being carried out over the last few years in order to identify the advantages and the disadvantages of the DC utilisation in the distribution grid [163] and especially in Finland. An explanation of this trend can be given by the fact that in Scandinavian countries the majority of the distribution grid feeders run in rural areas in order to serve remote customers. [164-167]. The reason for considering DC for LV grids in this thesis is that the existing overhead lines and cables would then be able to carry a higher power when compared with an AC network. This is because with an AC system the power throughput is a function of the RMS voltage, whereas the insulation has to be rated for the peak voltage. In a DC system the power throughput and insulation are a function of the same DC voltage.

3.10.1 Using DC over the Existing Underground Cable Infrastructure

This section investigates the feasibility of using DC on the existing feeder and service cables. A typical residential area is connected to a local transformer via a three-phase underground cable, or in rural areas this is achieved using an overhead-line. The underground

cable consists of either three individual cables each with its own earthed screen laid in what is known as a trefoil arrangement, or via a single sectored cable with a single earthed outer screen as shown in Figure 3.19a and 3.19b respectively. The cables are rated at 600 V phase to screen, 1000 V phase-phase, with a peak overvoltage rating of 1200 V. An underground feeder cable is referred to in the remainder of this section but the argument equally applies to an overhead line feeder.

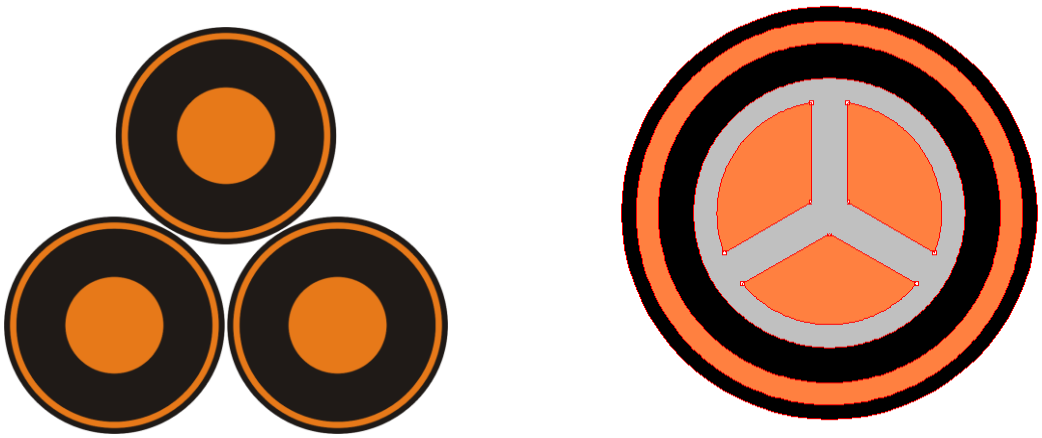

(a) **(b)**

Figure 3.19: ***Cross-section of a three-phase LV distribution cable with earthed outer screen (a) trefoil and (b) self-contained sectored***

Three-phase cables are typically arranged along a residential street and connected to the meter box of individual houses via underground, single-phase, service cables. The two conductors of the service cable connect to one of the three-phases and the earthed screen. The number of connections to each of the three-phases is spread evenly along a street to ensure an equal loading on the feeder cable. A typical connection for the first three houses in a residential area is shown in Figure 3.19, where the thick lines represent the individual phases of the main feeder cable.

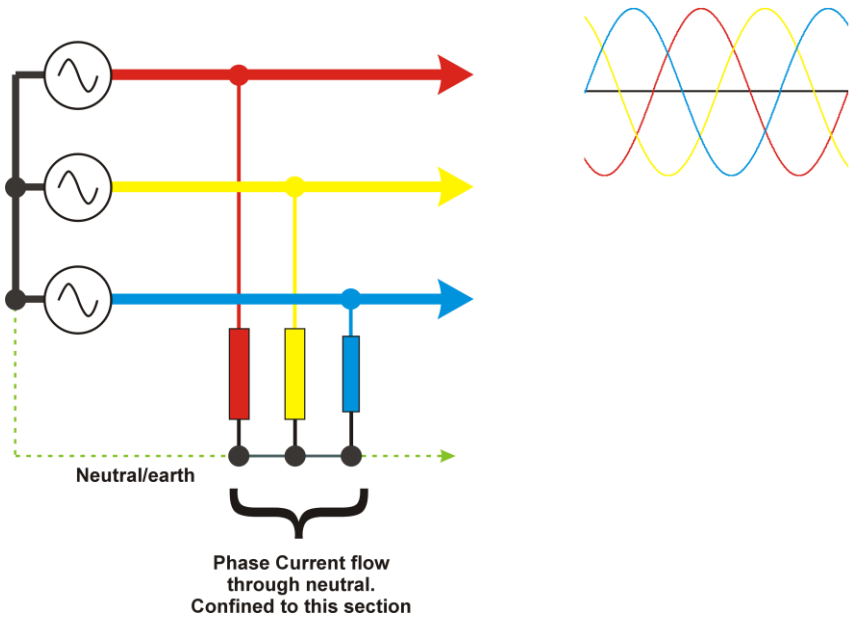

Figure 3.20: ***Connection of three houses to a 3-phase AC cable with outer earthed neutral/screen***

Figure 3.20 also shows ideal, balanced sinusoidal currents that are drawn from each phase by the three-loads. There is no current flow in the neutral conductor (shown dotted), with a balanced load - other than between the small section that spans the three houses (shown solid). In this solid section the current will be equal to the current that flows in each of the three houses. For this reason the neutral conductor is typically rated at just one-third of the phase conductors since the maximum neutral current in this section of the feeder will be equal to the maximum current in an individual house plus any current due to unbalanced loads. If the same cable is used for DC distribution, then there are 2 options. The first option uses the neutral screen as the return conductor as shown in Figure 3.21.

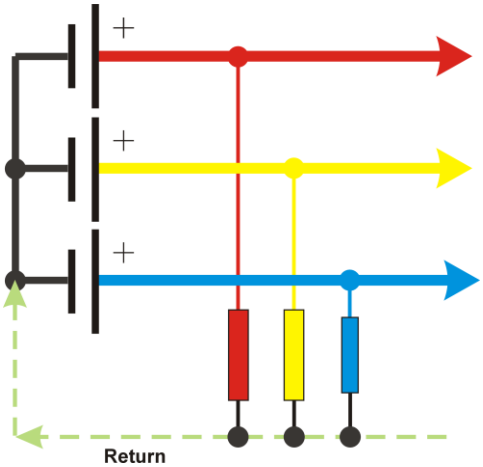

Figure 3.21: 3-phase DC fed cable with outer earthed neutral/screen used as return conductor (option 1)

The second option uses the blue-phase as the return conductor as shown in Figure 3.22; this is a purely arbitrary decision as either the red or yellow phases would serve equally well. The phase-voltage for the blue-phase must be reversed to maintain the supply to the houses on its phase. It can be shown that the total cable losses are a minimum (maximum capacity), when the red and yellow phases have equal currents. This situation is shown superimposed on the original sinusoidal current waveforms in the figure. In this case the blue phase carries twice the current of either the red or yellow phases. Just like the AC case the neutral conductor only has to be rated to carry the current from three houses plus any currents due to unbalanced loads.

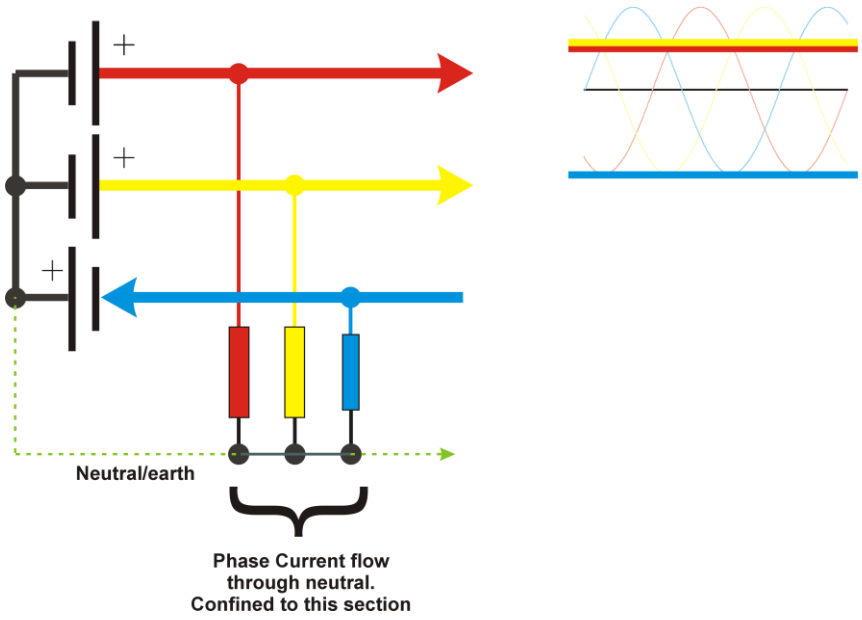

Figure 3.22: ***3-phase DC fed underground cable with blue-phase used as return conductor***

Unfortunately neither option 1 or 2 is a viable solution because under balanced conditions:

- ***Option 1*** is limited by the one-third rating of the neutral so that the phase currents will be limited to one-ninth of their rating. This is a very significant under-utilisation of the cable. The DC voltage would need to be nine-times greater than the equivalent AC RMS phase voltage in order to have the same power throughput. For example, to supply the same power as a 230 V phase AC system, the DC phase voltage would have to be at least 2070 V. This is well above the anticipated 1500 V DC rating of the cable.

  In addition, the neutral is now permanently conducting potentially large currents through what was the earth return. This will have a significant impact on the safety and protection of the network.

- ***Option 2*** is limited by the red/yellow phase currents having to work at one-half rating, which is also a significant under-utilisation of the copper in the cable. The DC voltage would need to be two-times greater than the equivalent AC RMS phase voltage in order to have the same power output. For example, to supply the same power as a 400 V phase AC system, the DC phase voltage would have to be at least 800 V.

The return phase could be cycled equally among the red-yellow-blue phases to form a three-phase square-wave AC system. However, the fast rising edges of the square wave may cause severe transient interference within the network.

Therefore for the reasons outlined above the use of DC over the existing underground cables is not a viable solution. Research work in [168] shows similar results to this study and in addition Antoniou et al add that another drawback of the LVDC scheme is the need to rewire all the nodes connected to the network for power flow optimisation in LV distribution systems. This would be expensive and time consuming from the DNOs perspective. However, for new installations where a bespoke DC cable could be laid then a DC system can provide overall benefits.

3.11 Location of the VCU

The VCU is to be located inside each customer's meter-box, as shown in Figure 3.23b. Cooling for the VCU would need to be by natural ventilation as fans are not allowed in the design due to reliability concerns. The requirement for natural ventilation is a serious issue as the VCU heat loss is directly into the meter box where the electricity meter has a typical maximum operating temperature of range between 55 and 70 ^{0}C [169]. Moreover, an increase of the meter box temperature could affect the cut-out fuse. In particular, a BS88 type of fuses has a de-rating factor of 0.7 in an ambient temperature of 60 ^{0}C [151]. This situation is totally undesirable as it can affect maximum fault current, fault clearance times and discrimination throughout the LV distribution network. For these reasons, the temperature rise inside the meter-box must be limited, which drives the VCU design to one with extremely low losses.

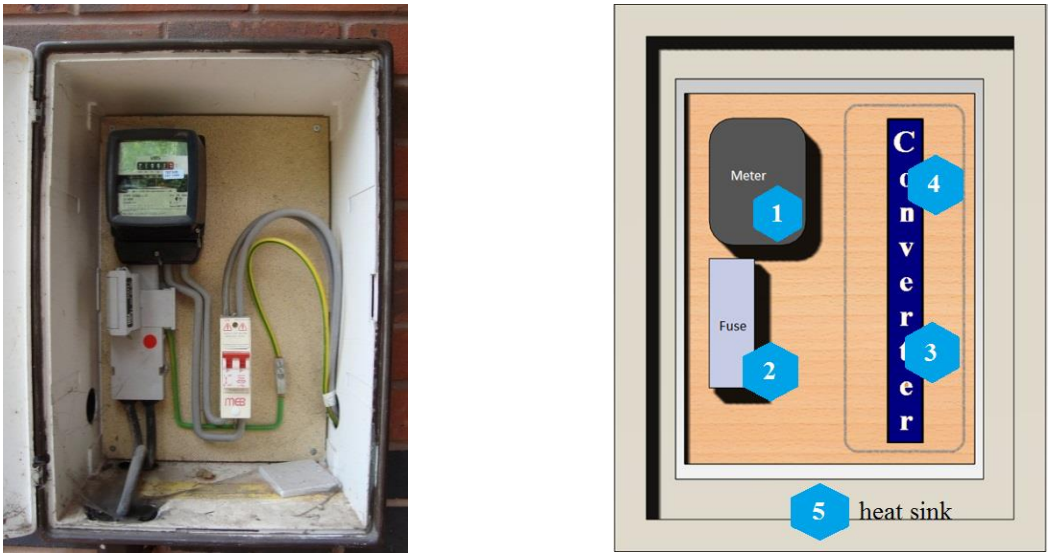

(a) (b)

Figure 3.23: ***(a) Meter box and (b) proposed converter location with placement of thermocouples for experimental tests***

To quantify the effect of VCU heat dissipation on the temperature rise ΔT, within the box, several experiments were undertaken for various cooling scenarios on an actual meter box. Thermocouples were placed at strategic points inside the box as shown in Figure 3.23b, to measure temperature rise, and power resistors were used to represent the VCU thermal losses. The power resistors were mounted on aluminium plates of various shapes and sizes, for example an aluminium door was tested as shown in Figure 3.24a, as well as aluminium surfaces in L-shapes shown Figure 3.24b, where one face of the L was situated on the inner side of the box, and the other face was exposed to the outside, flush with the door. The scenarios that were considered are shown in Table 3-10:

Scenario	Description
1	L - shape Aluminium (40mm outer width)
2	L - shape Aluminium (100mm outer width)
3	Aluminium door - VCU mounted on inside face of door
4	As (3) but door thermally insulated on the inside face (excluding VCU mount)
5	As (4) but additional insulation covering the outside of the VCU
6	As (3) with eight 3inches by 8 inches ventilation slots cut into the door in front of the meter location
7	As (3) with sixteen 3inches by 8 inches ventilation slots cut into the door in front of the meter location

Table 3-10: ***Different VCU cooling arrangements for experimental tests***

(a) **(b)**

Figure 3.24: ***(a) Aluminium door and (b) L-shape Aluminium surfaces***

Figure 3.25 shows as an example the temperature rise above ambient ΔT, against VCU power dissipation for one cooling scenario 5 in Table 3-10. Moreover, it can be seen that there is an almost linear rise in temperature with VCU dissipation, with the hottest location being next to the meter (location 1). This was also true of all the scenarios (1-7), and a plot of the temperature rise ΔT for the most sensitive location – the electricity meter, location 1, against VCU dissipation is shown in Figure 3.26 for all of these scenarios.

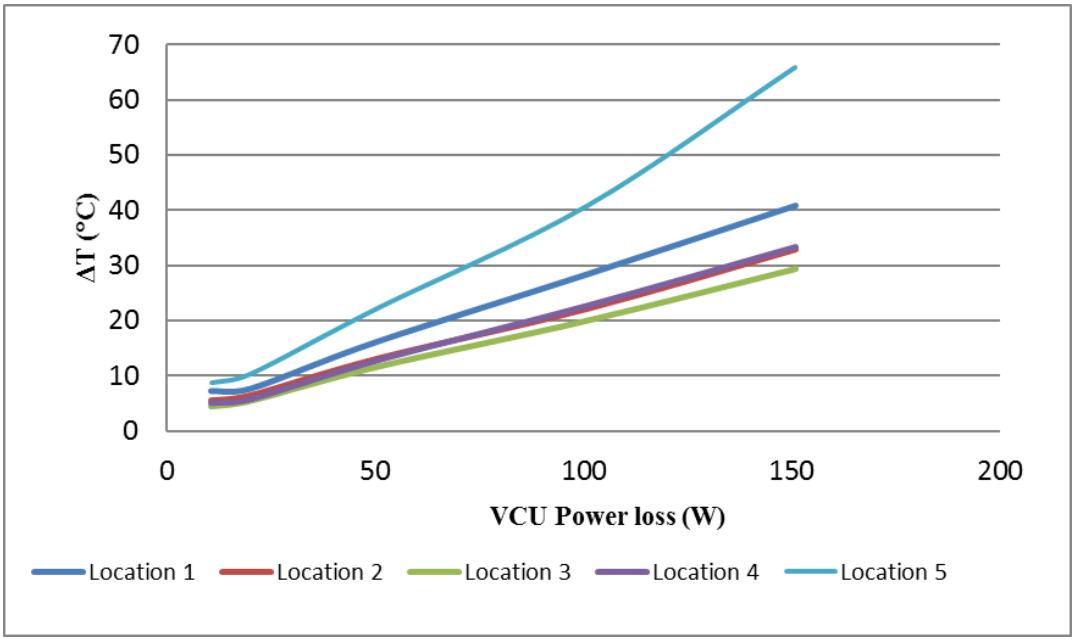

Figure 3.25: ***Temperature rise above ambient ΔT (°C) inside meter-box against VCU power loss (W) for scenario 5 (locations are shown in Figure 2.23b)***

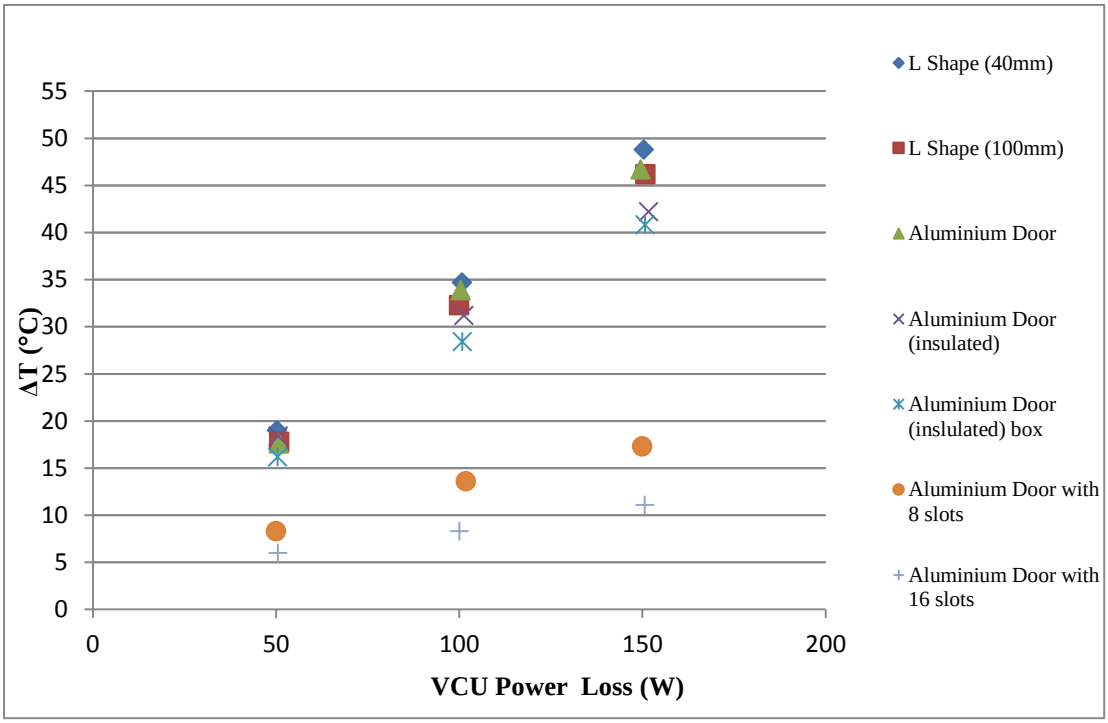

Figure 3.26: ***Temperature rise above ambient ΔT (°C) against PCU power loss (W) for electricity meter (location 1), for scenarios (1-7)***

It can be seen from Figure 3.26 that for the unventilated scenarios (1-5), the aluminium door with insulated VCU, scenario (5), gives the lowest temperature rise across all of the five scenarios. Under scenario (5), in order to keep the internal temperature of the meter box below

its maximum value of 50 °C with say an ambient of 30 °C during a hot day of the UK summer, the maximum VCU loss must be less than approximately 50 W. However, if ventilation slots are cut into the door, the allowable power dissipation increases by around a factor of four for 16-slot scenario for the same temperature rise. This vented scenario is quite beneficial as is it allows a higher relaxation on the VCU's power dissipation to approximately 150W. Even in the rare scenario of an extremely hot day in the UK, for example 10th August 2003 when the ambient temperature reached 38.5 °C in Kent, the temperature inside the meter box would not exceed the 50°C meter specification under full load operation conditions. As long as the slots are louvered as shown by a similar design for gas utility meter box shown in Figure 3.27, then the impact on the water Ingress Protection (IP) should be acceptable.

Figure 3.27: ***Typical gas meter-box with upper and lower louvered ventilation slots*** **[171]**

Whilst the above measurements are all steady-state, the thermal capacitance of the meter-box can also be exploited to provide short-term overloads. The transient thermal step-response for full-load operation condition – 150 W losses - is shown in Figure 3.28, where it can be seen that the meter-box has an approximate first-order time-constant of around 40 minutes.

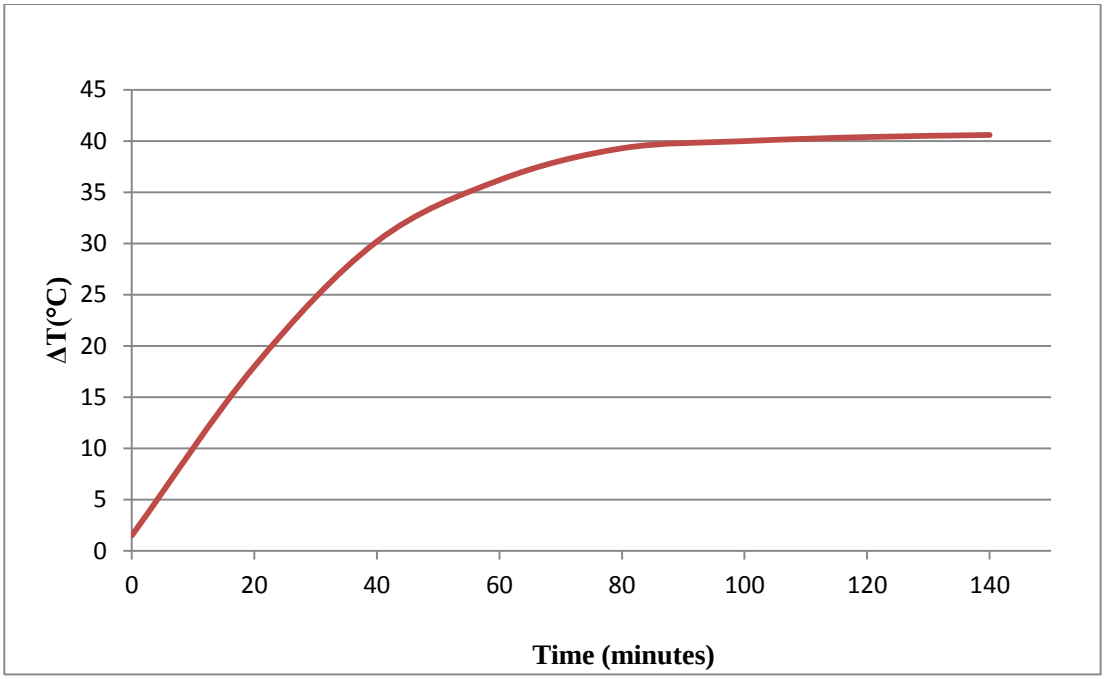

Figure 3.28: ***Meter-box transient thermal step-response for scenario (5) and location (1)***

Such a continuous maximum rating of this duration is not common according to WPD and residential load demand curves, for example it would not be expected that a 10 kW shower would be used for this duration. Finally, as well as thermal constrains, which leads to a high efficiency VCU design, the meter-box also imposes a limit on the size and the weight of the VCU. The available remaining volume within the box for the placement of the VCU is around 14 litres. Consequently, for a 15 kW rated VCU, its volumetric power density be higher than 1.07 kW/litre.

3.12 Summary

This chapter has shown that by raising the LV network voltage, significant increase in capacity could be achieved. In addition, the availability of a VCU would resolve problems of voltage rise caused by embedded generation. The use of a DC distribution is not viable on the existing underground cabling leaving just high-voltage AC system as the only solution. However it is clear that a device is needed to step down the voltage from the 300V to the statutory limits (230V) at customer's premises. This device must have a specific size, weight and efficiency close to 99%.

Care must be taken to ensure any device decoupling the customers' load from the network is able to protect the installation from faults and grade with the existing protection devices. An additional residual current device (RCD) is needed to meet safety requirement specified in

BS7671. A summary as an output of this chapter regarding the VCU specification is presented in Table 3-11.

VCU Characteristics	
Power Output Rating	**15 kVA**
Maximum Input Voltage	**300 V**
Maximum Input Current	**35 A**
Output Voltage	**230 V +10%, -6%**
Frequency	**50 Hz**
Power Factor	**0.95**
Efficiency	**99%**
Volumetric Power Density	**1.07 kW/litre**

Table 3-11: ***VCU Requirement specification***

In terms of VCU cost, Western Power Distribution estimate that the price per household of replacing the main feeder in a residential network including service cable joint would be around £500 to £1000 depending on location, for example soft verges or tarmacked roads. This cost does not include un-quantified expenses such as disruption to business and traffic. Therefore an approximate manufactured target cost for the VCU would be £350 to £400.

4 VCU - Topologies Analysis and Selection

In Chapter 3 a solution was proposed and described to alleviate existing capacity limits of LV networks, which was to increase the LV network phase-voltage from 230 V to 300 V. This is achievable by the deployment of a DNO-owned, low-cost VCU installed in the meter-box of individual properties, which steps-down the voltage to 230 V. However, in order to prevent temperature rises within the meter box from affecting the electricity meter unit and rating of the main fuse, the VCU must have extremely low losses and at the same time a small size and weight. As there is a vast amount of literature on AC- AC converters and in order to reduce the scope of it, in this chapter only the literature of relevant voltage step-down AC-AC power electronic topologies is presented, followed by the study of these topologies in order to identify an optimum candidate solution for this particular application. As it is stated later on the present Chapter, a conventional solution such as the doubly wounded transformer cannot be considered, mainly due to its size and weight restrictions in this particular application.

4.1 Fundamental Topologies

In order to identify the most suitable topology applicable to form the VCU voltage-step down function, several fundamental devices and their main features are presented in this section. In particular, all the devices can be classified into five main topological categories. These categories are different arrangements of AC voltage and current sources, which are here, represented by power electronic Voltage Source Inverters (VSIs) and Current Source Inverters (CSIs). A single-phase full-bridge inverter is shown in Figure 4.1. The inverter consists of two half- bridge inverter legs modulated using sinusoidal pulse-width-modulation (PWM). A DC voltage source or capacitor C, supplies the DC-link, which has a voltage V_{DC}, and an inductor L is used to smooth the output current *i* and connect the VSI to an AC circuit. For a closed-loop control of the VSI the output voltage *v* is fed back and the modulation of the bridge is adjusted accordingly. This makes the VSI output voltage independent of the load current drawn or variations in the DC supply voltage V_{DC}. With a CSI the output current *i* is fed back and the modulation of the bridge is adjusted accordingly and the output voltage *v* is determined by the load impedance.

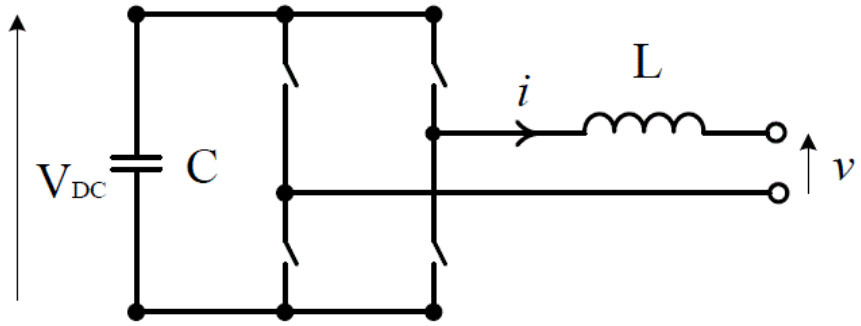

Figure 4.1: ***Single-phase full-bridge inverter***

Figure 4.2 illustrates how an AC input source and output supply of differing voltage levels can be connected using a single-phase *series* VSI, which is represented by a voltage source. This topology is a common circuit for interfacing differing source and supply voltages. The magnitude and phase of the VSI can be used to adjust the voltage appearing at the load side. Consequently, this topology is within the scope of this application as it has a voltage step–up and/or step-down capability.

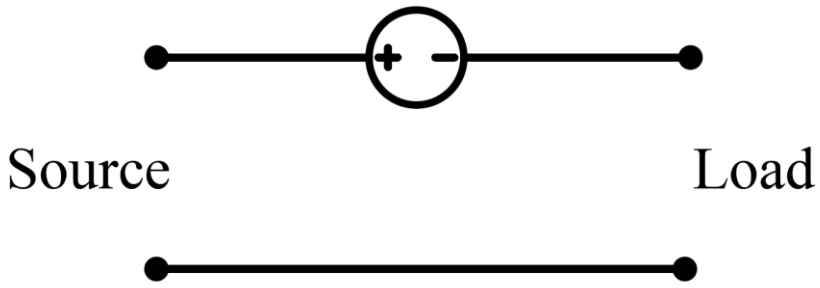

Figure 4.2: ***A series VSI configuration***

Figure 4.3 illustrates the circuit configuration of a *shunt* CSI. The difference between the series VSI and the shunt CSI is that the CSI can compensate current distortion generated by the load from being injected back into the source, also to improve fundamental power factor at the source. On the other hand this type of topology does not have any step-up and step-down voltage capabilities on its own. However, in power systems it is used as a so-called Static Synchronous Compensator (STATCOM), which will be discussed in more detail later. The STATCOM is used to inject reactive current into a transmission line to allow a partial control of the line voltage through the mitigation of voltage drops across the line impedances. Due to the lack of direct

voltage step-up/down capability, this topology in its stand-alone configuration will not be analysed any further in this thesis.

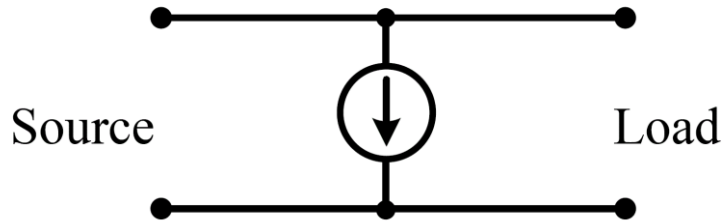

Figure 4.3: ***A shunt CSI configuration***

A *shunt/series* combination of the first two topologies, which is of the form of a shunt CSI and a series VSI, is shown in Figure 4.4. This allows the step-up/down of the voltage as well as power factor improvement. This circuit is designated a SHUnt SEries (SHUSE) converter. The DC-links of the VSI and CSI can be optionally connected through an isolated interface to allow the sharing of active power flow. This is shown by the dotted line which represents an active power link. The VSI and CSI can therefore operate without a common, active DC-link, termed an Independent-SHUSE, or I-SHUSE, or with an active power link so that their operation depends on each other termed a Dependent-SHUSE or D-SHUSE.

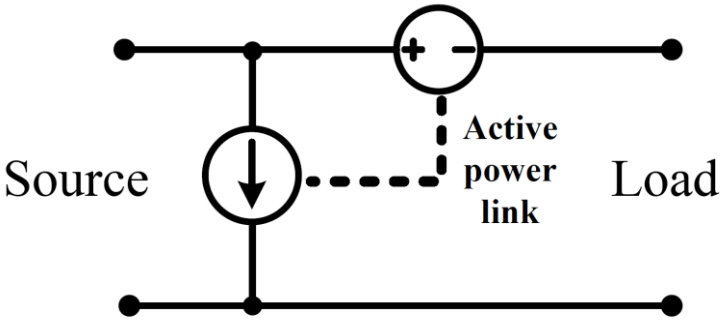

Figure 4.4: ***A shunt CSI and a series VSI configuration (SHUSE)***

Finally in Figure 4.5 a mirrored configuration of the series VSI and shunt CSI topology is shown and is termed a SEries SHUnt (SESHU).

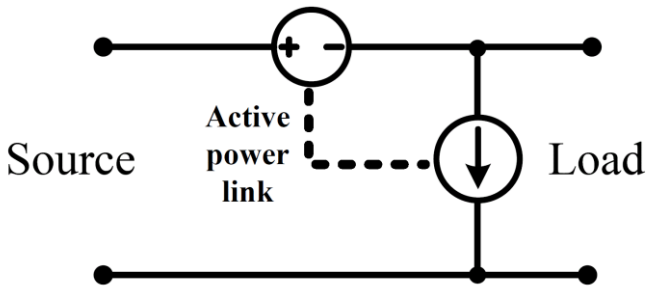

Figure 4.5: ***A series VSI and a shunt CSI configuration (SESHU)***

Again, the VSI and CSI can operate independently denoted by an I-SESHU, or can be connected through an active power link so that their operation depends on each other denoted by D-SESHU.

Whilst there are an infinite number of variations of the above circuits by connecting them in cascade, the overall efficiency of such converters is reduced due to the series processing of power throughput. Therefore only these four fundamental topologies need to be considered in this analysis.

4.2 Topologies Analysis and VA rating

A single equivalent generic circuit can be derived for the series VSI, shunt CSI, SUSHE and SESHU in order to define their circuit voltages and currents. This generic circuit is shown in Figure 4.6 and the corresponding circuit equations for the above topologies are defined by (4.1)-(4.3),

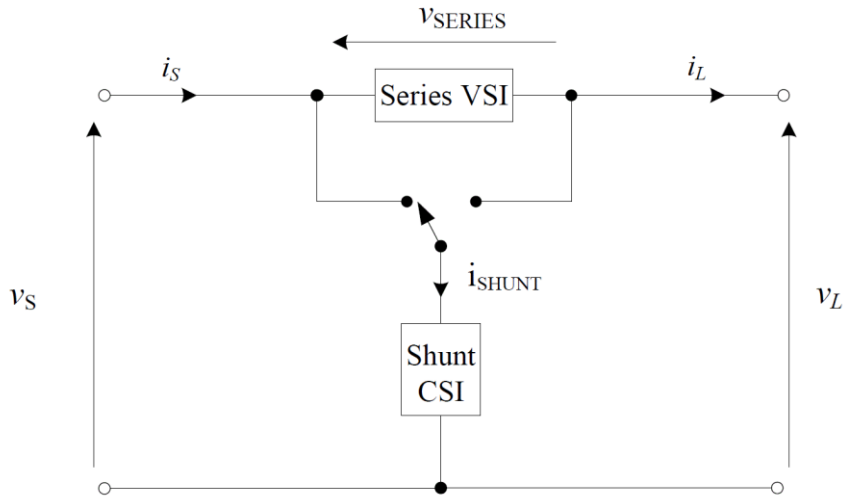

Figure 4.6: ***A generic topology for the series VSI, shunt CSI, SHESU and SHUSE topologies***

where v_S and v_L are the supply and load voltage phasors respectively, i_S and i_L are the supply and load current phasors respectively, v_{SERIES} is the voltage phasor across the series VSI and i_{SHUNT} is current phasor through the shunt CSI.

All topologies

$$v_S + (-v_L) + (-v_{SERIES}) = 0$$
$$i_L + i_{SHUNT} + (-i_S) = 0 \tag{4.1}$$

For the Series VSI

$$i_{SHUNT} = 0 \tag{4.2}$$

For the Shunt CSI

$$v_{SERIES} = 0 \tag{4.3}$$

For the SHUSE topology the changeover switch in Figure 4.6 is in the left-hand position, and for the SESHU topology the changeover switch is in the right-hand position.

In addition, a generic expression that is applicable to all four topologies is the relationship between the magnitude of the supply and load voltages, which is expressed with the term N, and is named the voltage conversion ratio:

$$N = \frac{|V_S|}{|V_L|} \tag{4.4}$$

In the next section, each topology will be compared in terms of its total VSI and CSI VA rating. This gives an indication of the semiconductor requirements for the VCU, and hence its size, weight, complexity and cost. Each section derives expressions for the converter VA rating – see Appendix C for Mathematica derivation.

4.2.1 The Series VSI analysis and VA rating

The VA rating of the series VSI, VA_{SERIES} is given by,

$$VA_{SERIES} = |v_{SERIES}||i_S| \tag{4.5}$$

The VSI series voltage can be found using equation (4.3):

$$v_{SERIES} = v_S - v_L \tag{4.6}$$

Where the supply voltage is used as a reference phasor, $v_S = V_S e^{j0}$ and $v_L = V_L e^{j\varphi_{VL}}$. The current through the VSI is obtained from the power balance between supply and load power assuming the converter losses are zero so that,

$$V_S I_S \cos(\varphi_S) = V_L I_L \cos(\varphi_L)$$

$$I_S = \frac{V_L I_L \cos(\varphi_L)}{V_S \cos(\varphi_S)} \tag{4.7}$$

The ratio V_L/V_S in the above equation can be eliminated by using (3.4), and the load current can be expressed in terms of the load apparent power S_L, so that,

$$I_L = \frac{S_L}{V_L} \tag{4.8}$$

Substituting in (4.6)-(4.8) into (4.5) and simplifying and then normalising the result to the load apparent power S_L, the expression for the normalised VA rating of the converter $VA_{SERIES\ Norm}$ is given by:

$$VA_{SERIES\ Norm} = \frac{\cos(\varphi_L)\sqrt{N^2 - 2N\cos(\varphi_{VL}) + 1}}{N} \tag{4.9}$$

The unknown in this equation is the angle φ_{VL}, this can be obtained by the fact that the VSI DC link cannot absorb active power, so that,

$$Re\left[V_{SERIES} i_S^*\right] = 0 \tag{4.10}$$

Again, substituting in (4.5)-(4.7) and simplifying then gives,

$$\varphi_{VL} = \cos^{-1}\left(N\cos(\varphi_S)\right) + \varphi_S \tag{4.11}$$

For a real solution to this expression it is a necessary condition that the following constraint equation is satisfied,

$$N\cos(\varphi_S) \leq 1 \tag{4.12}$$

Therefore this equation indicates that it is not possible to achieve a unity input power factor $\cos(\varphi_S)$, since for a step-down converter N is greater than one. For example with the proposed

step-down voltage from 300 V to 230 V then the maximum input power factor that can be achieved from equation (4.12) is 0.77, which is far too low to be used on the LV network. Whilst the overall VA rating of this converter is found to be much lower than those studied below, this topology is unsuitable for step-down operation due to its poor power factor and will not be considered as a further option.

4.2.2 Independent SESHU (I-SESHU) analysis and VA rating

The VA rating of the independent SESHU, $VA_{I\text{-}SESHU}$ is given by,

$$VA_{I-SESHU} = \left|v_{SERIES}\, i_S\right| + \left|v_L\, i_{SHUNT}\right| \tag{4.13}$$

The voltage across the series VSI v_{SERIES}, is the same as equation (3.5). The current through the shunt CSI from equation (3.3) is:

$$i_{SHUNT} = i_L - i_S \tag{4.14}$$

Where $i_s = I_S e^{j\varphi_S}$ and $i_L = I_L e^{j\varphi_L}\, e^{j\varphi_{VL}}$. Substituting these equations, simplifying and normalising to the load apparent power S_L, the expression for the normalised VA rating of the I-SESHU converter is $VA_{I\text{-}SESHU\ Norm}$, given by:

$$VA_{I-SESHU\ Norm} = \frac{\cos(\varphi_L)\sqrt{N^2 - 2N\cos(\varphi_{VL}) + 1}}{N} + \frac{\sqrt{1 + 2N^2 + \cos(2\varphi_{VL}) - 4N\cos(\varphi_L)\cos(\varphi_L + \varphi_{VL})}}{\sqrt{2}N} \tag{4.15}$$

The unknown in this equation is the angle φ_{VL}, this can be obtained by the fact that the VSI DC link and the CSI DC-link are independent and therefore cannot absorb active power, so using the VSI power equation,

$$Re\left[v_{SERIES} i_S^*\right] = 0 \tag{4.16}$$

Solving this equation and simplifying,

$$\varphi_{VL} = cos^{-1}\left(N\,cos(\varphi_S)\right) + \varphi_S \tag{4.17}$$

For a real solution to this expression it is a necessary condition that the following constraint equation is satisfied,

$$N\,cos(\varphi_S) \leq 1 \tag{4.18}$$

As with the previous series VSI topology, this equation indicates that it is not possible to achieve a unity input power factor cos(φ_S), since for a step-down converter N is greater than one. For example with the proposed step-down voltage from 300 V to 230 V then the maximum input power factor that can be achieved from equation (4.12) is 0.77, which is far too low to be used on the LV network. This topology is therefore unsuitable for step-down operation due to its poor power factor and will not be considered as a further option.

4.2.3 Independent SHUSE (I- SHUSE) analysis and VA rating

The VA rating of the independent SHUSE, $VA_{I\text{-}SHUSE}$ is given by,

$$VA_{I-SHUSE} = \left|v_S i_{SHUNT}\right| + \left|v_{SERIES} i_L\right| \tag{4.19}$$

The voltage across the series VSI v_{SERIES}, is the same as equation (4.5) and the current through the shunt CSI is the same as equation (4.14). Substituting these equations, simplifying and normalising to the load apparent power S_L, the expression for the normalised VA rating of the I-SHUSE converter is $VA_{I\text{-}SHUSE\ Norm}$, given by:

$$VA_{I-SHUSE\ Norm} = \sqrt{N^2 - 2N\,cos(\varphi_{VL}) + 1} + \frac{\sqrt{2N^2 + cos(2\varphi_L) + 1 - 4N\,cos(\varphi_L)cos(\varphi_L + \varphi_{VL})}}{\sqrt{2}} \tag{4.20}$$

The unknown in this equation is the angle φ_{VL}, this can be obtained by the fact that the VSI DC link and the CSI DC-link are independent and therefore cannot absorb active power, so using the VSI power equation,

$$Re\left[V_{SERIES}\, i_L^*\right] = 0 \tag{4.21}$$

Solving this equation and simplifying then gives,

$$\varphi_{VL} = \cos^{-1}\left(N\cos\left(\varphi_L\right)\right) - \varphi_L \tag{4.22}$$

For a real solution to this equation it is a necessary condition that the following equation must be satisfied,

$$\cos\left(\varphi_L\right) \leq N \tag{4.23}$$

For a step-down converter N is greater 1.0, so that (4.23) is always satisfied. However, unlike the previous converter, the supply power factor angle φ_S does not appear in this constraint equation so it can be set to give unity input power factor. It is interesting to note that since the I-SHUSE and I-SESHU topologies are mirror images, the I-SHUSE can only operate at unity input power factor for step-down applications; in contrast the I-SESHU can only operate at unity input power-factor for step –up applications.

4.2.4 Dependent SESHU (D- SESHU) Analysis and VA rating

The DC-links of the VSI and CSI for the dependent SESHU are linked to allow a flow of active power. This gives greater freedom in ensuring the input power factor operates at unity. However, the disadvantage of the Dependent topologies is that the DC-link connection needs to be isolated. It is therefore assumed in this analysis that this isolation is achieved using two VSIs and a high-frequency transformer to form an isolated DC-AC-DC converter between the two DC-links. The VA rating for this DC-AC-DC converter must be included in the VA rating analysis. This is also true for the analysis of the Dependent SHUSE that follows this section.

The VA rating analysis for the dependent D-SESHU is identical to that for its independent counterpart the I-SESHU, other than it includes the VA rating of the two VSI converters used for the isolated active power DC link. The expression for the normalised VA rating $VA_{D\text{-}SESHU\ Norm}$ is therefore,

$$VA_{D-SESHU\ Norm} = \frac{\cos(\varphi_L)\left(2N + \sqrt{N^2 - 2N\cos(\varphi_{VL}) + 1}\right)}{N} + \frac{\sqrt{1 + 2N^2 + \cos(2\varphi_{VL}) - 4N\cos(\varphi_L)\cos(\varphi_L + \varphi_{VL})}}{\sqrt{2}N} \quad (4.24)$$

However, since the series VSI and shunt CSI can now absorb or source active power, there is no constraint equation such as (4.16), so that the angle between the supply voltage and the load voltage φ_{Vl}, shown in the above equation, can take on any value. It is therefore appropriate to choose a value for φ_{VL} that minimises the converter VA rating, (4.24).

4.2.5 Dependent SHUSE (D-SHUSE) Analysis and VA rating

Again the VA rating analysis for the dependent D-SHUSE is identical to that for its independent counterpart the I-SHUSE, other than it includes the VA rating of the two VSI converters used for the isolated active power DC link. The expression for the normalised VA rating $VA_{D\text{-}SHUSE\ Norm}$ is therefore,

$$VA_{D-SHUSE\ Norm} = 2\cos(\varphi_L) + \sqrt{N^2 - 2N\cos(\varphi_{VL}) + 1} + \frac{\sqrt{2N^2 + \cos(2\varphi_L) + 1 - 4N\cos(\varphi_L)\cos(\varphi_L + \varphi_{VL})}}{\sqrt{2}} \quad (4.25)$$

As with the D-SESHU, there is no constraint equation such as (4.16), and angle φ_{Vl} is therefore chosen to minimise the converter VA rating, (4.25).

4.2.6 Back - to - Back Analysis and VA rating

Another candidate topology for the VCU, which does not fall into any of the categories discussed previously, and which cannot be represented by the generic circuit in Figure 4.6, is the back-to-back combination of a CSI and VSI shown in Figure 4.7. This circuit is commonly referred to as a Back-to-Back converter, because it consists of two full-bridge VSIs sharing a common DC link. Three-phase versions of this arrangement are used universally for example for grid-fed variable-speed drives. Both the source current and load voltage can be controlled independently with the Back-to-Back converter.

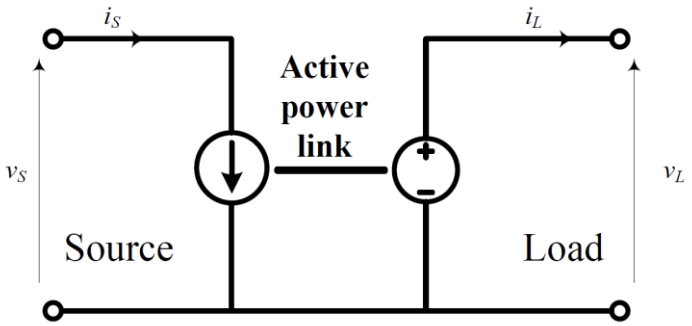

Figure 4.7: ***The Back -to- Back configuration***

However, in its basic form the Back-to-Back circuit does not allow a direct connection of the supply neutral to the load neutral since neither the plus or minus nodes of the DC-link are at the same potential as the supply or load. However a continuous neutral is a fundamental requirement of the VCU because of the safety-earthing requirements in the property. Therefore if this topology was to be used for the VCU it would require two additional VSIs and a high-frequency isolation transformer to form an isolated the DC-AC-DC stage. This would then allow the supply and load neutrals could to be bonded together as shown in Figure 4.7.

Unlike the previous converters, both the CSI and VSI parts must process the total load power. The VA rating of the Back-to-Back configuration VA_{BB}, can therefore be calculated from the expression,

$$VA_{BB} = V_S I_S + V_L I_L + 2V_L I_L \cos(\varphi_L) \tag{4.26}$$

The last term on the right of equation (4.26) represents the two VSIs used in the intermediate isolated DC-AC-DC converter. The normalised VA rating $VA_{BB\,Norm}$, is then given by,

$$VA_{BB\,Norm} = 1 + 3\cos(\varphi_L) \tag{4.27}$$

4.3 Comparison of VA ratings

In this section the normalised VA ratings of the I-SHUSE, D-SESHU, D-SHUSE and the Back-to-Back converter are compared for a number of different voltage conversion ratios N, and load power factor $\cos(\varphi_L)$. However, before this can be done the angle φ_{VL} must be calculated for the normalised VA ratings of each topology, and this is summarised in Table 4-1,

Topology	Normalised Rating Equation	φ_{VL} Equation
I-SHUSE	(4.20)	(4.22)
D-SESHU	(4.24)	Optimised to minimise VA rating – (4.24)
D-SHUSE	(4.25)	Optimised to minimise VA rating – (4.25)
Back-to-Back	(4.27)	N/A

Table 4-1: ***Normalised rating equations and corresponding equations for φ_{VL}***

MATLAB was used to evaluate the angle φ_{VL} for a range of values for the voltage conversion ration N and for various load power factors cos (φ_L). For the I-SHUSE, equation (4.22) was used, whereas for the dependent topologies D-SESHU and D-SHUSE, the MATLAB "fminsearch.m" optimisation routine was used to numerically calculate optimum values of φ_{VL} that minimised the corresponding VA rating equations (4.24) and (4.25) respectively. Plots of the angle φ_{VL} are shown in Figures 4.8 to Figures 4.10 for the I-SHUSE, D-SESHU and D-SHUSE respectively for values of N=1.01, 1.20, 1.30 and 1.70 and for cos(φ_L)=0.8→1.0.

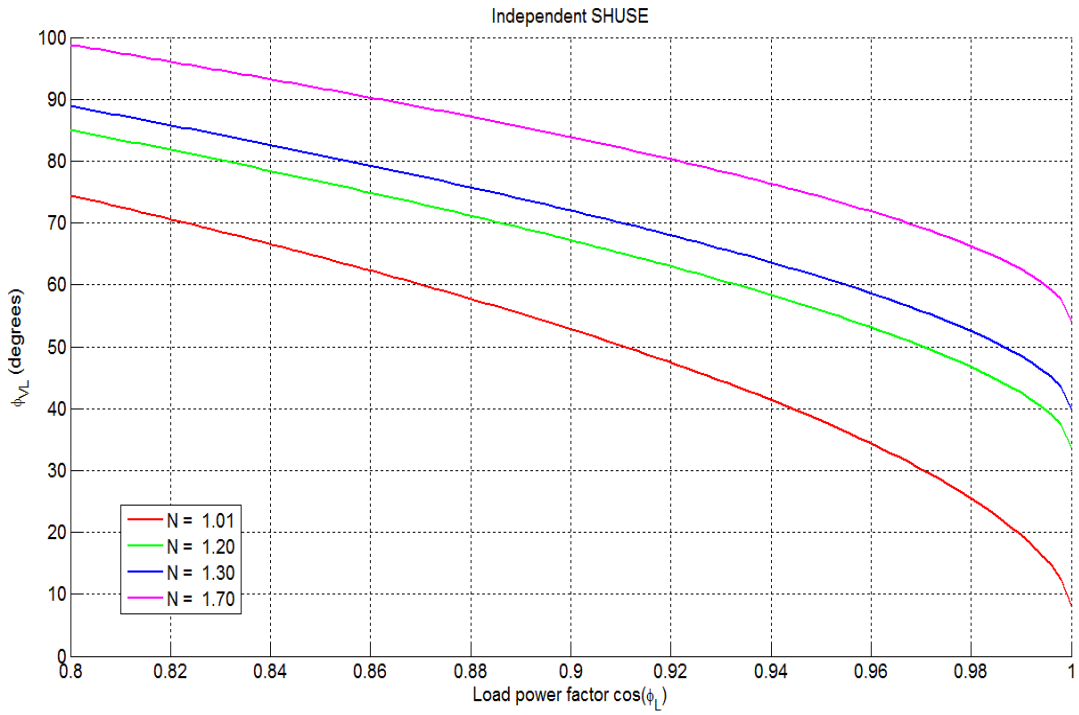

Figure 4.8: ***Angle φ_{VL} calculated for N=1.01, 1.20, 1.30, 1.70 and cos (φ_L) =0.8→1.0 for the I-SESHU configuration***

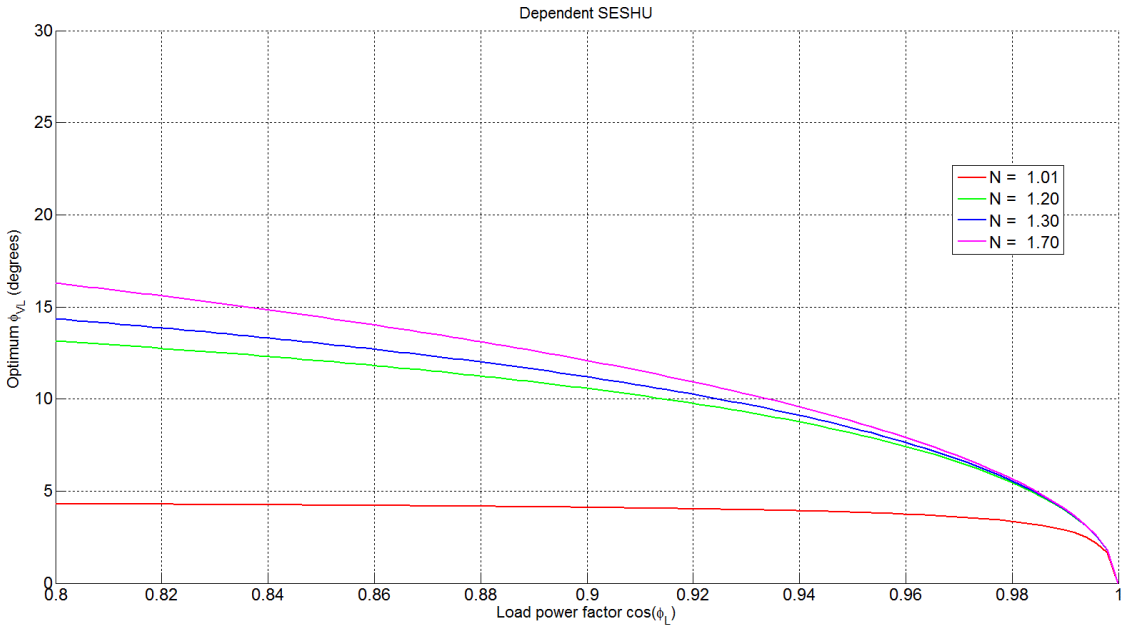

Figure 4.9: Optimised angle φ_{VL} calculated for N=1.01, 1.20, 1.30, 1.70 and cos(φ_L)=0.8→1.0 for the D-SESHU configuration

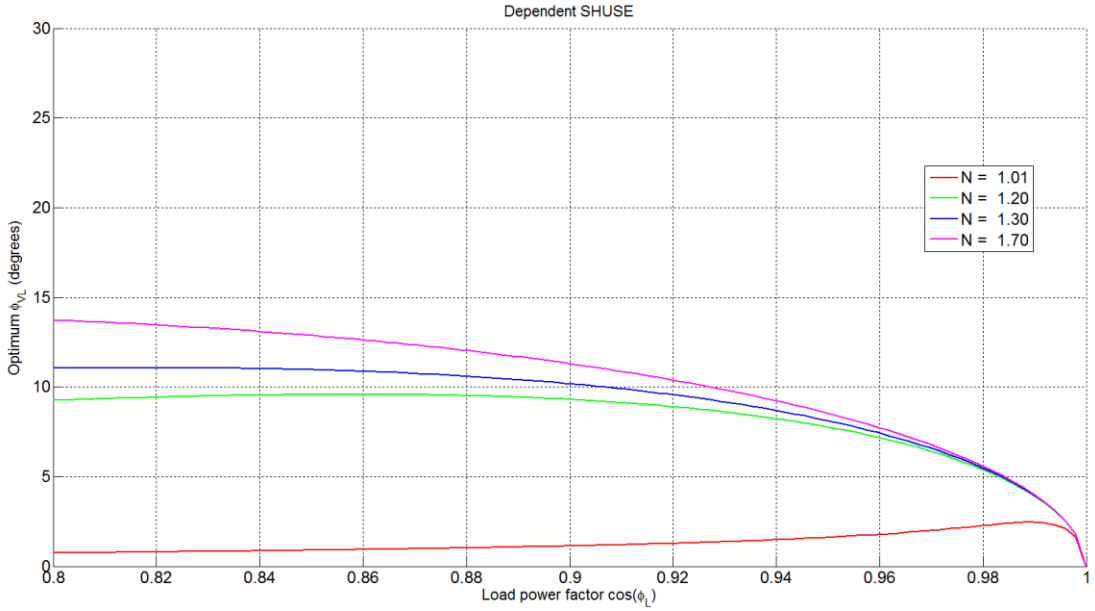

Figure 4.10: Optimised angle φ_{VL} calculated for N=1.01, 1.20, 1.30, 1.70 and cos(φ_L)=0.8→1.0 for the D-SHUSE configuration

Plots of the normalised VA ratings are shown in Figures 4.11 to Figures 4.13 for the I-SHUSE, D-SESHU and D-SHUSE respectively, for values of N=1.01, 1.20, 1.30 and 1.70 and for cos(φ_L)=0.8→1.0. Since the VA rating of the Back-to-Back converter with isolated DC-link is independent of N, it is also shown on all of the following three Figures for comparison.

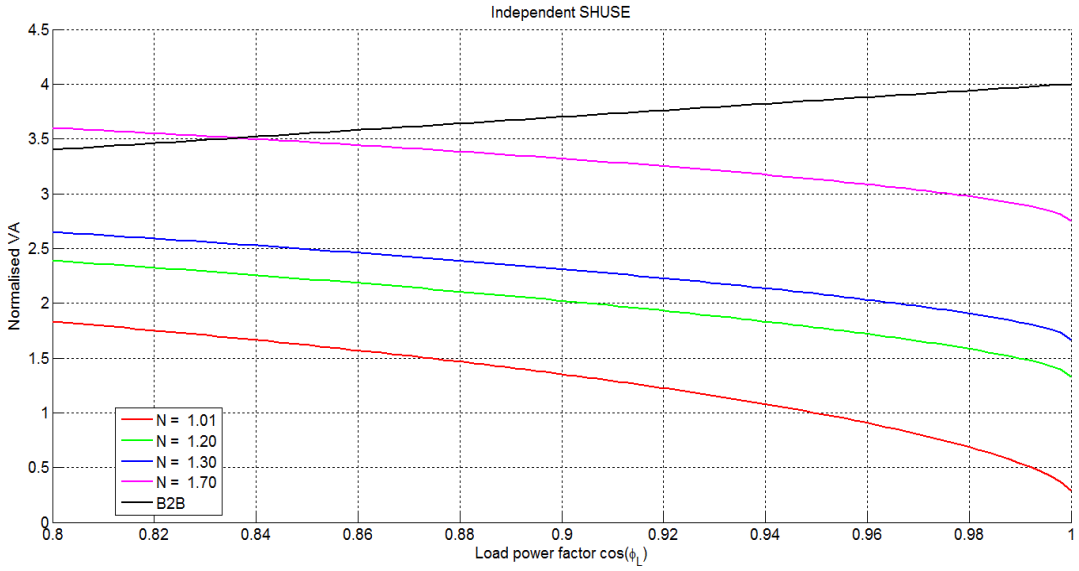

Figure 4.11: Normalised VA rating of the I-SHUSE configuration calculated for N=1.01, 1.20, 1.30, 1.70 and cos(φ_L)=0.8→1.0

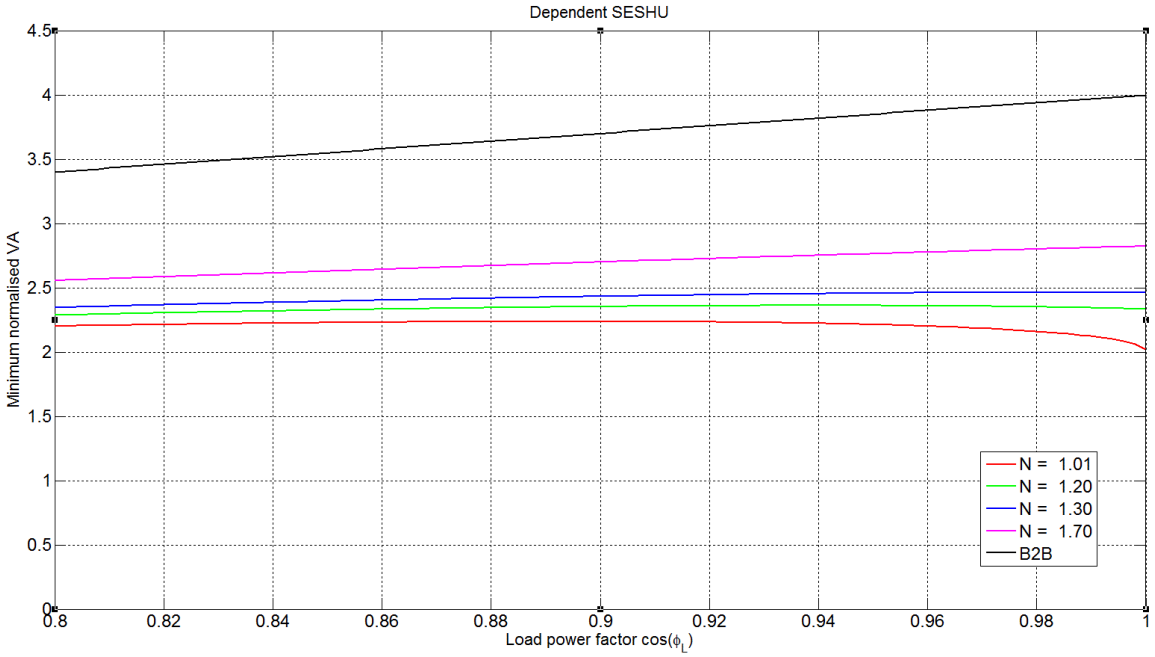

Figure 4.12: Normalised VA rating of the D-SESHU configuration calculated for N=1.01, 1.20, 1.30, 1.70 and cos(φ_L)=0.8→1.0

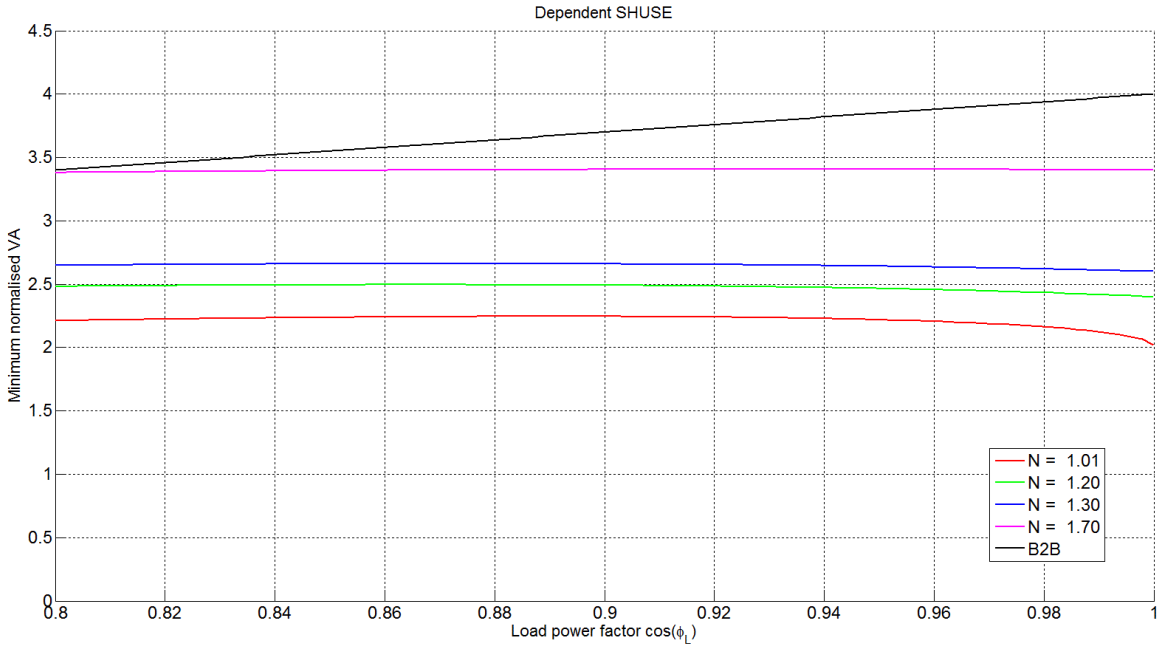

Figure 4.13: Normalised VA rating of the D-SHUSE configuration calculated for N=1.01, 1.20, 1.30, 1.70 and cos(φ_L)=0.8→1.0

It can be seen from Figures 4.12 and 4.13 that for a voltage conversion ratio of N=1.3, which is the value proposed for the VCU in this thesis, the voltage ratings of the D-SESHU and D-SHUSE are fairly insensitive to changes in load power factor. Also the D-SESHU has a slightly lower normalised VA rating than the D-SHUSE, with an approximate value of 2.5 compared with 2.6. Both the dependent converters have a VA rating that is approximately 33% lower than the Back-to-Back converter.

With N=1.3, the I-SHUSE has an almost equal VA rating to the D-SESHU and D-SHUSE for power factors approaching 0.8 and below. However, for higher power factors, the VA rating of the independent converter falls to around 20% of the dependent configurations.

The minimum VA rating of the D-SESHU for an optimum φ_{VL} is presented in Figure 4.12. For this topology the VA rating for a voltage ratio N equals 1.3 and a unity load power factor is 1.5 times lower than the Back-to-Back VA rating. Also, it can be noted that there is not much difference in the VA rating between a poor load power factor scenario and a unity one. Moreover, the topology's VA rating doesn't have a significant difference for a higher voltage ratio, for example 1.7.

4.4 Summary and Discussion of VA Rating analysis

The series VSI and the I-SESHU are not suitable for stepping-down the voltage from 300 V to 230 V at the customer's side as both result in a poor input power factor of less than 0.77. On the other hand, they would be suitable for step-up applications.

The VA rating of the D-SESHU is slightly lower than the D-SHUSE. However, if the function of these topologies were to also include active filtering, the D-SESHU may be the preferred solution in terms of eliminating current harmonics generated by the load. If the load power factor is high, then the lowest VA rating topology is the I-SHUSE. In particular, for a specific voltage ratio of N=1.3 and a load power factor of 0.95, which is the target of this project, this configuration has a normalised VA rating of 2.1 and this is 1.8 times lower than the VA rating of the Back-to-Back topology and around 1.3 times lower than the dependent topologies.

The requirement for an isolated active power link for the Back-to-Back and dependent converters is a serious disadvantage when compared with the I-SHUSE. Moreover the VA rating of the high-frequency isolating transformer that is needed for the isolated converters has not been included in these comparisons, which further increases the attractiveness of the I-SHUSE.

The Back-to- Back configuration which is the reference point for the VA rating comparison has the largest VA rating and this can be explained by the fact that it has to process the total load power flow through the CSI, isolated link and VSI of the converter. The dependent topologies have and approximately 1.4 times lower VA rating when compared to the Back-to-Back converter.

Therefore, circuits that can be categorised as either I-SHUSE, D-SESHU or D-SHUSE are the most likely to offer the highest power density for the VCU, and this conclusion is carried forward into the next section.

4.5 Series VSI, Shunt CSI, SESHU, SHUSE and Back-to-Back circuit Implementations

All the above generic topologies have specific applications in power systems and are expressed in the form of actual circuits. In this section these circuits are studied in terms of their likely merits to form the VCU.

4.5.1 Doubly Wound Transformer

The most common way to step down an AC grid voltage is using a wound transformer. The traditional double-wound power transformer is an indispensable component in electric power systems for voltage conversion and isolation. The conventional transformer is a very reliable,

robust and low-cost device with a very simple operating principle. At first-hand the transformer appears to be the most likely candidate for the VCU. On the other hand, the saturation of the core can produce 3rd harmonics and the magnetising current results in a low power factor. Also it is not able to filter any distorted load currents from flowing into the grid from non-linear loads. More importantly, because of its line-frequency operation it is bulky, heavy and acoustically noisy. For example, Table 4-2 gives the values for the size and the weight of two, single-phase, 300/230 V, 15 kVA double wound transformers from two different manufacturers.

Manufacturer	Rating (kVA)	Width(mm)	Height(mm)	Depth(mm)	Weight (kg)	Volumetric Power Density (kW/lt)
JMS Transformers	15	320	500	240	130	2.6
Majestic Transformer Co	15	320	550	330	107	3.9

Table 4-2: Single-phase conventional Transformers specifications

Table 4-2 shows that the size and weight of these devices are totally unsuitable for locating in the meter-box of a house.

4.5.2 Auto-transformers and Voltage Optimisers

Auto-transformers are an alternative to the doubly wound transformer, and have a lower VA rating. However, the disadvantage is that electrical isolation between source and load is lost. The VA savings are due to savings in the conductors for the windings, according to [172] the copper weight ratio can be expressed as:

$$\frac{Autotransformer \text{ copper weight}}{Two\ winding \text{ transformer copper weight}} = 1 - \frac{N_2}{N_1} \tag{3.28}$$

where N_2 is the number of turns on the load side and $N_1$is the number of turns on the supply side. For this specific application the copper VA rating of the Auto-transformer is 4.3 times lower than the VA rating of the conventional transformer. However, even with this reduction in copper the weight of the autotransformer would still be too heavy for use as a VCU installed in a meter-box. This is because the size and weight of the iron core would remain the same and assuming that the

core accounts for 50 % of the autotransformer weight then Table 4-2 gives a mass of approximately 50 Kg, which is unacceptable.

In the LV power industry there are already units called Voltage Optimisers, which are essentially autotransformers that reduce the voltage into a house to the lower end of the statutory limits. These devices convert the input voltage, which is typically 240 V in the UK to a lower level of 220V. It is claimed that these devices lower a customer's power consumption, which is achieved by reducing the iron losses in motor loads such as pumps, since iron losses are proportional to the square of the voltage.

For single-phase applications, Voltage Optimisers consist of a conventional autotransformer with a turns-ratio of around 1.09 [173, 176]. They are placed between the electricity meter and the customer's consumer unit. With such a modest turns-ratio they are relatively small in size and weight. Nevertheless, as can be seen in Figure 4.14, their size is not insignificant. The typical size of such a device is approximately 265mm W x 310mm H x 148mm D with a weight of 14.5kg [5]. Another disadvantage of these devices is that they do not provide either the utility or the customer with power quality improvement.

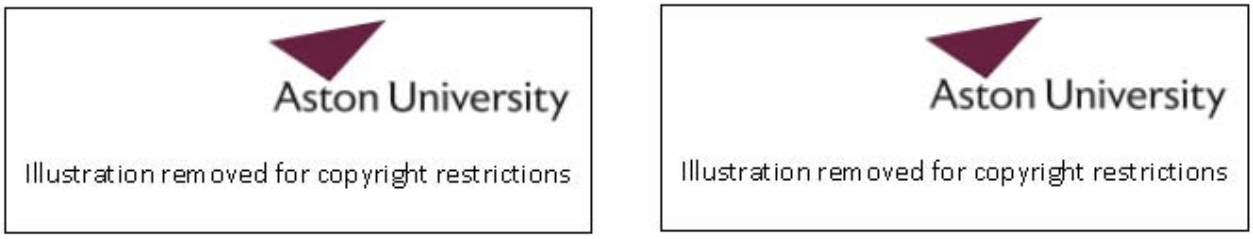

(a) (b)

Figure 4.14: ***Voltage Optimisers – (a) VO4 Home [175] and (b) Vphase*** **[176]**

Three-phase versions of the Voltage Optimiser are used in industry and commercial buildings such as hotels. As well as the energy savings, it is also claimed by the manufacturer's that they extend the lifetime of a customer's equipment [173, 174].

4.5.3 Custom Power Devices

Much work is being done on the use of power-electronic based Custom Power Devices (CPDs), as reliable solutions to the power system quality problems already described in the

literature review. These devices are converter-based topologies named according to their specific power quality features, converter topology and type of connection to the grid [177]. There are two common forms of CPDs, which are used to compensate for voltage drops and rises, one is connected as a CSI current shunt and the other as series voltage VSI [178]. The device which is connected in shunt is named a static compensator (STATCOM) or a D-STATCOM for distribution networks. The series connected device is named a dynamic voltage restorer (DVR). The VSIs and the CSIs are the basic blocks of both these categories. A review of these devices has been carried out in order to assess their suitability as the proposed power-electronic based residential VCU.

4.5.3.1 STATCOMs and Active Power Filters

The Static Synchronous Compensator STATCOM, which is used in transmission and distribution grids, can regulate the voltage at its terminals by controlling the amount of reactive power absorbed or injected into the network and is shown in Figure 4.15. An isolating transformer is used to couple the LV power electronics to the MV/HV grid. The STATCOM is a shunt CSI and is therefore able to improve fundamental power factor and also the transient stability on power grids [179]. The STATCOM can operate to either control line-current or line voltage. The STATCOM regulates line voltage by indirectly controlling the reactive current flowing through the impedance of the line. Its voltage regulation capabilities are therefore limited to the magnitude of this external impedance and it would not be suitable for the proposed residential VCU.

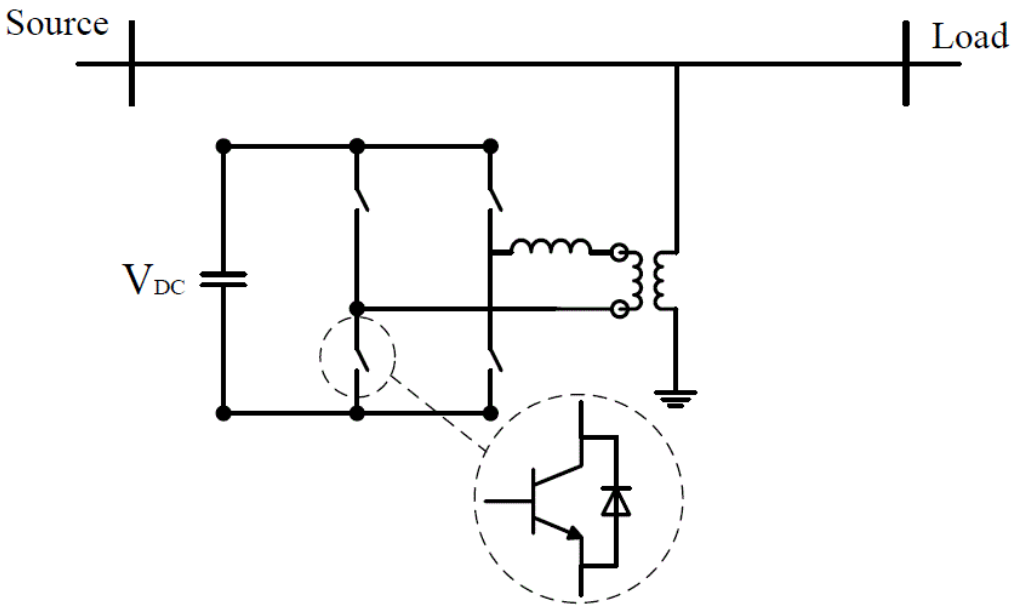

Figure 4.15: ***A STATCOM configuration***

The STATCOM topology can also be used as a shunt Active Power Filters (APFs), which involves compensating voltage distortion and suppressing voltage flicker at the Point of Common Coupling (PCC) by injecting compensating current harmonics [180, 184].

4.5.3.2 Dynamic Voltage Restorer

The Dynamic Voltage Restorer (DVR) is a series voltage device connected between the grid supply voltage and the load. It consists of the series VSI, with a capacitor DC link as shown in Figure 4.16. For medium to high voltage applications, the LV power electronics of the VSI are coupled to the grid via a line frequency isolating transformer. An energy storage unit such as a super-capacitor or battery is connected to the DC-link of the VSI to provide the grid with a long-term active power supply. The VSI's function includes the conversion of DC to AC and injection of the appropriate amount of voltage necessary for the grid. The DVR can be a crucial CPD for voltage sag or swell mitigation, as well as the protection of sensitive loads from voltage fluctuations and power outages. Since DVRs do not operate continuously and for the majority of the time operate in stand-by mode, they have relatively low losses [182]. In the event of an unbalanced three-phase sag/swell on the supply side, the DVR injects unbalanced voltages to maintain the voltage at the load side. The DVR as mentioned previously cannot be considered for the VCU application since the relative high conversion voltage ratio needed for the VCU leads to a very poor input power factor.

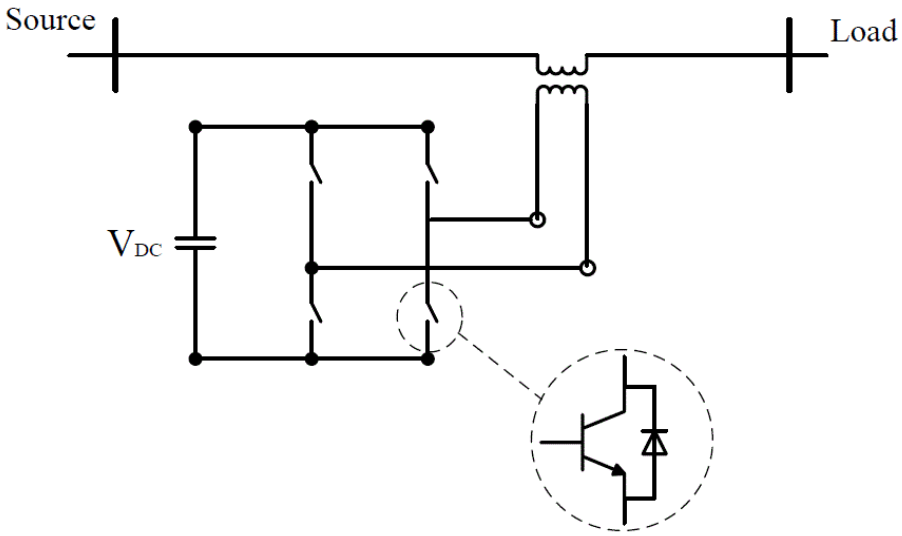

Figure 4.16: A single-phase DVR configuration

The DVR topology can also be used as a series Active Power Filters (APFs), where it is used to inject a distorted voltage to neutralise voltage harmonics [183].

4.5.3.3 Unified Power Quality Conditioner (UPQC)

This type of CPD employs two PWM converters, sharing an isolated DC link, to execute both the series/shunt APFs, DVR and STATCOM functions. This circuit is known as a Unified Power Quality Conditioner (UPQC) as shown in Figure 4.17. The UPQC can achieve voltage and current harmonic elimination, fundamental power factor correction and mitigate voltage amplitude variations such as flicker and longer term variations like sags/swells by utilising an energy storage unit in the DC-link [185]. The DC-link must be isolated from either the series or shunt connections and this is usually achieved using an isolating line-frequency transformer to connect the series VSI. Several approaches have been proposed in the literature for different possible configurations of converters used in a UPQC, for example half-bridge or full-bridge converters or multilevel converter topologies. The combination of a series-shunt converter is known as a UPQC-R, where the R stands for right-hand location of the shunt converter with respect to the series converter. Also discussed in the literature [185-187] is the opposite topology known as UPQC-L, which is a shunt-series configuration, with the shunt to the left of the series converter. This topology is commonly known as a Unified Power Flow Conditioner (UPFC) and is used primarily for transmission lines. The main difference between the two configurations is that the UPQC-L cannot operate in zero current injection modes [178, 186]. Moreover, the UPQC-R provides better compensation by reducing the THD of load voltage and source current than UPQC-L. It can also make the power factor unity at the load terminal, whereas for the UPQC-L the power factor at the load terminal depends on the load characteristics [186,187].

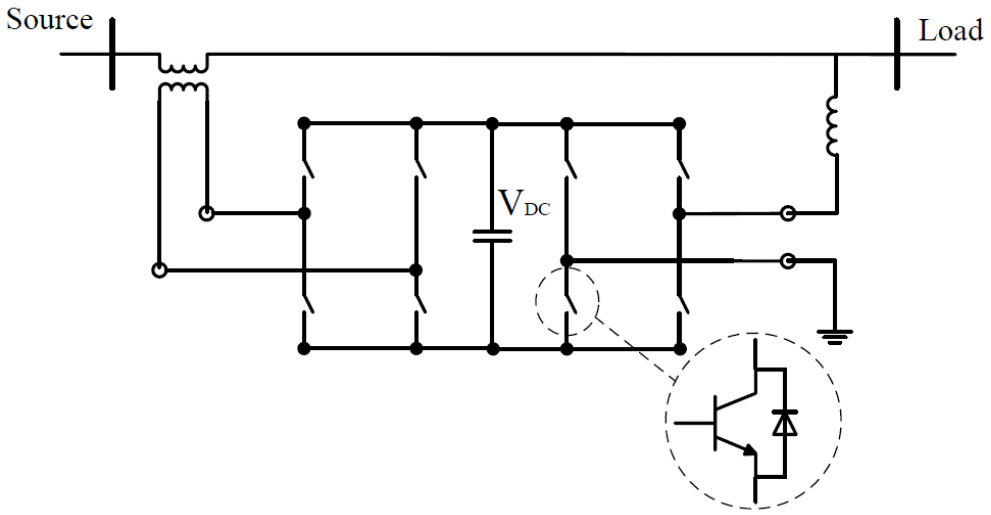

Figure 4.17: A UPQC-R topology

Both the UPQC-R and UPQC-L variations were included in the previous VA rating comparison where they were designated as the dependent D-SESHU and the D- SHUSE topologies. Another variation reported in the literature is the so-called open-UPQC-R [188], which was designated the independent I-SESHU in this thesis. This circuit is not considered further due to its poor input power factor for a step–down application. The I-SHUSE, or open-UPQC-L, which was found to have the lowest VA rating, has not been found in the literature.

4.5.4 Matrix Converters

Matrix converters are a class of direct AC/AC converter topologies, which provide both variable frequency and magnitude control of their output voltage. According to Figure 4.18 the three-phase to three-phase matrix converter includes 9 bi-directional switches allowing any output phase to be connected to any input phase. The converter input is linked to a three-phase voltage-fed system, which is normally the grid, whereas the output is linked to a three-phase current-fed system, such as an inductive motor load. It is essential to have a capacitive filter on the voltage-fed side, as well as the inductive filter on the current-fed side [189]. This type of converter presents a number of advantages compared to conventional rectifier-inverter type power frequency converters. It provides sinusoidal input current and output voltage waveforms, with minimised switching frequency harmonics and no sub-harmonics. It also has inherent bi-directional power flow capability and the input power factor is wholly controllable. Moreover, since there is no intermediated DC-link capacitor, the energy storage requirements for matrix converters are minimal.

Although the matrix converter is sometimes presented as a compact device, there is still a need for the input and output filters as well as voltage clamps, which are needed when there is an incorrect switch commutation. The converter is operated with a sinusoidal PWM but has a restricted ratio of input to output voltage transfer, which is 87% for sinusoidal input and output waveforms. In contrast to a traditional Back-to-Back AC-DC-AC indirect power frequency converter, the matrix converter needs a larger number of semiconductor devices 18 compared with 12 for a Back-to-Back circuit. Lastly, matrix converters are specifically sensitive to the input voltage system disturbances [190].

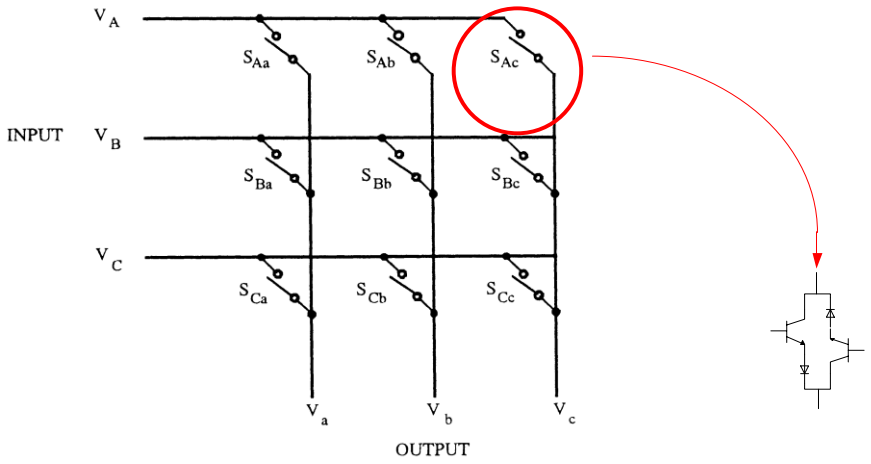

Figure 4.18: ***Switch layout of a 3-phase Matrix converter***

In the literature there are papers which describe a single-phase version of the Matrix converter [191-194], which would be suitable for the proposed VCU device. In its most basic form this circuit is known as an AC chopper as shown in Figure 4.19.

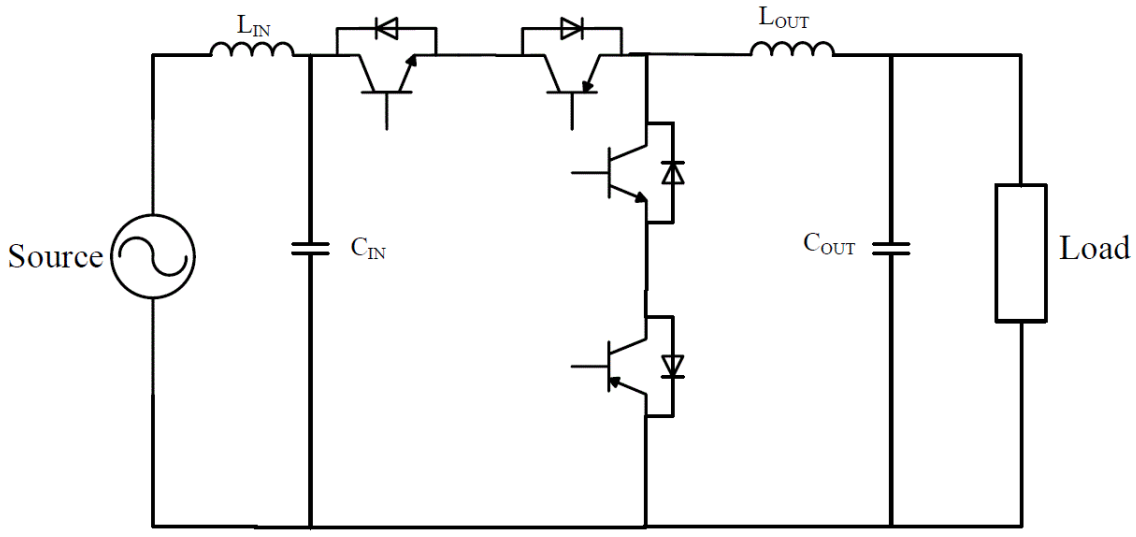

Figure 4.19: A single-phase matrix converter configuration

In input capacitor C_{IN}, decouples the circuit from the source inductance L_{IN}. The switches operate with a simple fixed duty cycle and the high-frequency chopped input voltage is filtered by the inductor L_{OUT} and capacitor C_{OUT} [193]. However, the disadvantage of this circuit is that it cannot provide any additional benefits in the context of the power quality improvements [193, 194].

In terms of VA rating comparison, this topology can be categorised as a D-SESHU. This is because in terms of line frequency sinusoids, the two switches shown at the top of Figure 4.18 operate as an equivalent series voltage source, whereas the remaining pair of switches operates as an equivalent shunt current source. Whilst there then appears to be an active power flow into and out of these sources, the switching harmonics contribute an additional power flow such that the net power flow into the switches is zero. The equation for the normalised VA rating is therefore the same as that for the D-SESHU, (4.24), but with the terms for the two VSIs for the isolated DC-link removed,

$$VA_{D-SESHU\ Norm} = \frac{\cos(\varphi_L)\sqrt{N^2 - 2N\cos(\varphi_{VL})+1}}{N} + \frac{\sqrt{1+2N^2+\cos(2\varphi_{VL})-4N\cos(\varphi_L)\cos(\varphi_L+\varphi_{VL})}}{\sqrt{2}N} \tag{4.29}$$

The normalised VA rating for the AC Chopper for various values of N and load power factor are shown in Figure 4.20.

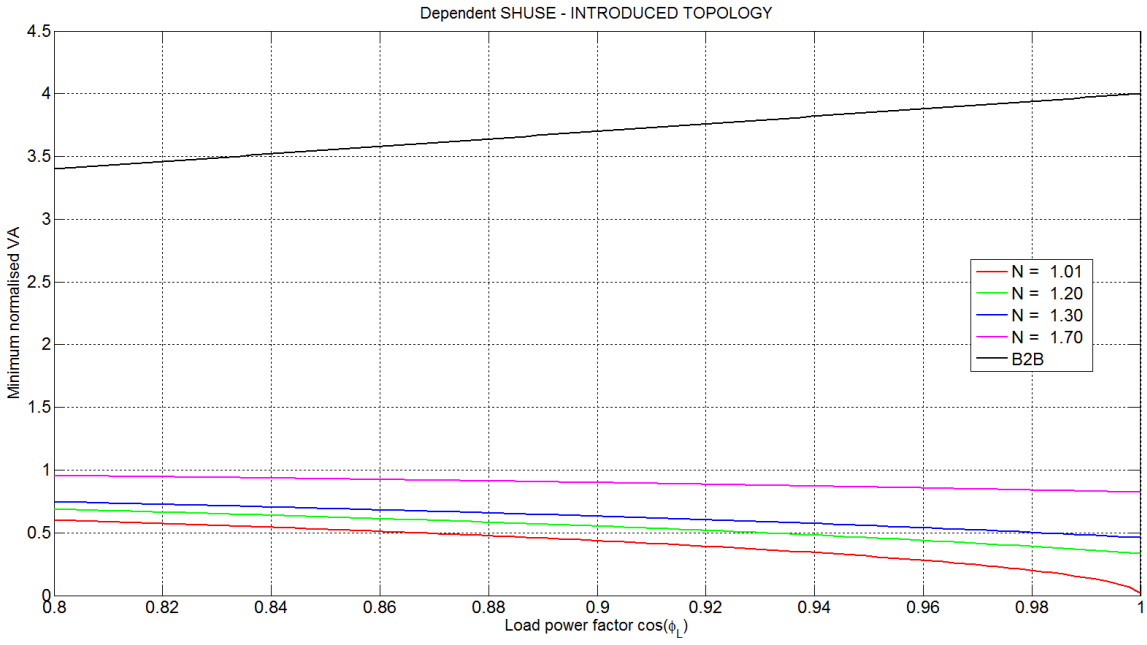

Figure 4.20: Normalised VA rating of the AC Chopper calculated for N=1.01, 1.20, 1.30, 1.70 and cos(φL)=0.8→1.0

It can be seen from Figure 4.19, that the AC Chopper has a much lower VA rating than those presented for the I-SHUSE, D-SESHU and D-SHUSE. For a specific voltage ration of N=1.3 and a load power factor of 0.95 the AC Chopper has a normalised VA rating of 0.6, which is 3.5 times lower than the I-SHUSE, which was found previously to have the lowest VA rating of all the configurations.

4.5.5 Back-to-Back AC-DC-AC converter

The traditional Back-to-Back converter is a combination of two series VSIs sharing a common DC-link as is illustrated in Figure 4.21. This circuit has bidirectional power flow capabilities, operates at high input power factor, and has well-regulated output AC voltage with low THD. The basic topology is a combination of two sinusoidal Pulse Width Modulation (PWM) VSIs sharing a common DC link. The converters employ IGBTs for medium power applications and MOSFETs for low power applications [195]. The main drawback of this topology is the absence of a continuous neutral between the supply and the load, which for safety reasons is not allowed for the VCU application and cannot therefore be considered further.

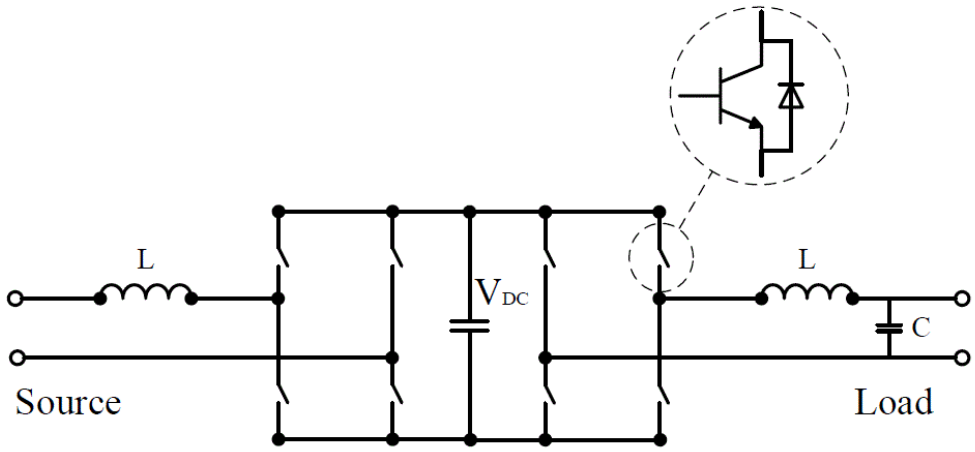

Figure 4.21: Back-to-Back AC-DC-AC converter

A solution to the non-continuous neutral is either the 2-leg [196] or the 3-leg [197] configurations of the Back-to-Back topology, which are shown in Figure 4.22 and Figure 4.23 respectively.

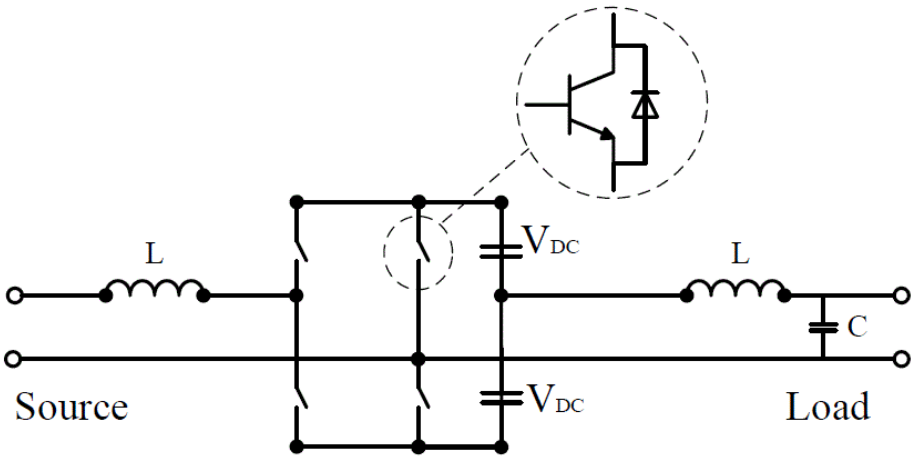

Figure 4.22: A 2-leg AC-DC-AC converter

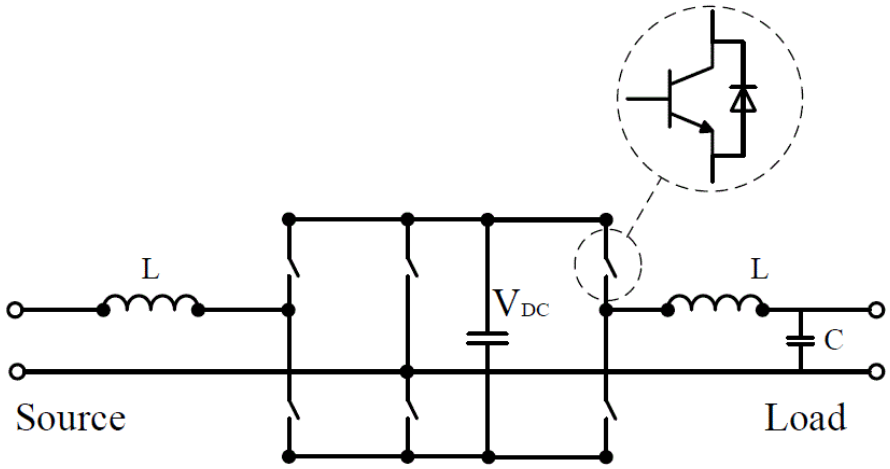

Figure 4.23: A 3-leg AC-DC-AC converter

An expression for the VA rating of these converters is more complex than that for the Back-to-Back topology as the minimum DC-link voltage is a complex function of the modulation indices of each inverter leg. However, the lower number of switches than the Back-to-Back converter as well as the continuous neutral, which is achieved without additional isolation stage [196,197], makes these two converters attractive for the VCU application.

4.5.5.1 Power Electronic Transformer

Several power-electronic based, isolated topologies with a reduced volume and weight have been discussed in the literature, which is made possible by using a high frequency operation of a transformer. These topologies are known as Power Electronic Transformers (PETs) [198] or

more recently as Solid State Transformers (SSTs) [199]. The PET type has two AC-DC-AC converters connected by a high frequency transformer [200], as it is illustrated in Figure 4.24.

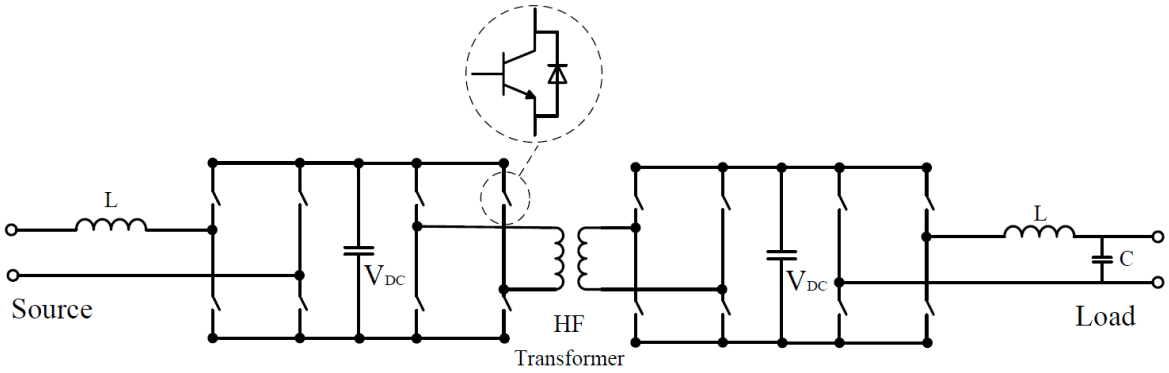

Figure 4.24: A typical PET with a High Frequency transformer

The PET has all the advantages of the previously discussed Back-to-Back AC-DC-AC converter as well as providing isolation. However, the major disadvantage is that it needs a large number of conversion stages (AC/DC and DC/AC) and DC link capacitors, which leads to a high overall VA rating.

4.6 Multilevel converters

Whilst the above power-electronic based devices are shown as two-level circuits all of them can be implemented as multi-level topologies. Multilevel converters bring the benefits of low voltage stresses on the switches, minimised losses at decreased switching frequency while maintaining a similar level of harmonic performance. Multi-level circuits are suited to grid interface topologies which work at voltages with many times that of the rating of individual semiconductor switches [201]. However whilst this project is concerned with an LV application - 230 V, which is well within the voltage rating of a single IGBT based two-level technology, this option can be considered in order to potentially use low-voltage, high-frequency MOSFETs, which have a much higher current handling capability than their high-voltage counterparts. In addition, MOSFETs can switch at much higher frequencies than IGBTs.

Multilevel converters categorised into diode clamped converters (DCCs), flying capacitor converters (FCCs) and cascade H bridge (CHB) converters. Generally they belong to the family of medium voltage and high power converters. DCCs have simple control but higher losses for a

large number of levels. FCCs can be used with a high number of levels, but requires complex control and a large number of storage capacitors. A CHB converter, on the other hand, can reach high voltage and high power levels. It has been reported that the AC supply current THD can be less than 1% even without using the PWM control. [201], on the other hand, for the low power level these converters are quite expensive in comparison with the two level converter topologies [202]. Figure 4.25 shows an example of a series voltage source implemented as a multi-level CHB.

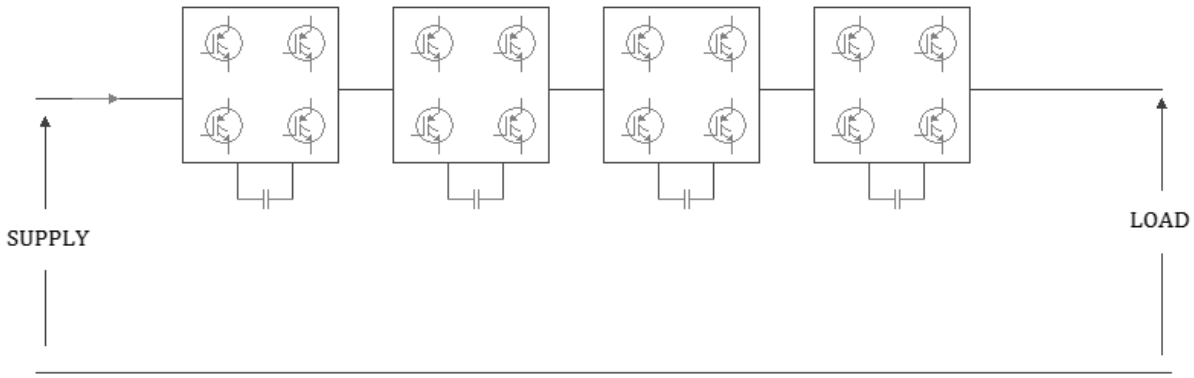

Figure 4.25: ***A typical series Multilevel Cascade Converter for a DVR application***

This circuit along with its current shunt equivalent connected as an I-SHUSE converter is a good candidate for the VCU. Using approximately twenty modules for the shunt stage would allow 20 off MOSFETS with an individual rating of 20 V to be used, which would have extremely low switching and conduction losses.

4.7 Summary

The main features of the circuits discussed above are shown in Table 4-3, where the five-star symbol "*****" means high and the one star symbol "*" is low. The first criterion for the appraisal of the circuit as a candidate VCU is whether it has a continuous neutral, followed by its VA rating. The VA rating is important because the VCU is a very cost-sensitive application, requiring a small size and weight for the meter box location. Finally, secondary benefits such as isolation and power quality improvements are judged last.

	Base Topology	VA Rating	PQ Improvement	Isolation	Suitability VCU application
Transformer	**Back-to-Back**	*****		✓	
Auto-Transformer	**Back-to-Back/DSESHU**	***		✓	
B2B AC-DC-AC	**Back-to-Back**	***	*****		
PET	**Back-to-Back**	*****	*****	✓	✓
DVR	**Series VSI**	**	***		
APF	**Shunt CSI**		**		
STATCOM	**Shunt CSI**		**		
UPQC-R	**D-SESHU**	**	*****	✓	✓
UPQC-L	**D-SHUSE**	**	****	✓	✓
OPEN UPQC-R	**I-SESHU**	*	*****		
OPEN UPQC-L	**I-SHUSE**	*	****		✓
AC CHOPPER	**D-SESHU**	*	*		✓
2-Leg	**Back-to-Back**	*	***	✓	✓
3-Leg	**Back-to-Back**	*	***	✓	✓

Table 4-3: ***A summary categorisation and an appraisal of the circuits studied in this chapter***

Table 4-3, shows that the OPEN UPQC-L, AC-Chopper, 2-Leg and 3-Leg AC-DC-AC converters are the best potential candidates for further study. These circuits appear in Table 4-3 with light blue shading. These four circuits are studied in more detail in the next chapter, which includes detailed simulations for the calculation of conduction and switching losses.

5 Power Loss Evaluation of Candidate AC/AC Converters

5.1 Candidate AC/AC Converters

The selected VCU must comply with the main requirements of the specification presented at the ender of Chapter 4 that is very high efficiency and power-density. Therefore, the main criterion for appraising candidate topologies is the efficiency of the converter. The corresponding losses will be dominated by the conduction and switching losses of the semiconductor components within the converter. To calculate these losses detailed simulations were carried out using manufacturer's Spice models of the transistors and diodes. The four candidate topologies that were selected in Chapter 4 were the I-SHUSE, the 2-Leg and 3-Leg converter and the AC Chopper. The simplicity factor of the operation and control of each topology was been taken into account in order to prioritise the appraisal of each circuit within the timescales of the project. For this reason the I-SHUSE topology was given a low priority due to its more complicated structure and control. Subsequently no further work was carried out on the I-SHUSE due to lack of time.

The 2-Leg and 3-Leg converters can provide a neutral connection between the supply and load. Moreover, they have a lower number of semiconductor devices in comparison with a traditional the Back-to-Back AC-DC-AC converter whilst maintaining the same power quality benefits. If these two circuits represent the highest performance in terms of power quality, then the AC chopper is a an example of low performance device; however it is a near-optimum solution in terms of voltage step-down capability in the context of reduced converter size, weight and control complexity. In terms of power quality, the basic chopper circuit only provides a regulated, sinusoidal voltage to the load.

The converter topologies presented above are assumed to have approximately equal ratings in terms of filter capacitors and inductors and are therefore compared solely in terms of the semiconductor conduction and switching losses. Three different transistor technologies were evaluated namely Si MOSFETs, IGBTs and new Silicon Carbide (SiC) MOSFETs in conjunction with Si and SiC Diodes.

5.2 Power Semiconductor Devices for AC/AC Converters

A recent trend in power electronics is the increasing desire for power semiconductor devices which should have a low on-state voltage in order to reduce the conduction losses. In addition, during the off-state mode, they also should be capable blocking high voltage. From a switching loss point of view they should have high switching speed. Finally, to ensure a robust

solution the semiconductor material should have as lower as possible degradation effects and operate at high temperature levels.

In this section, a brief description of two main semiconductor materials namely Silicon (Si) and Silicon Carbide (SiC) is presented. Moreover, an overview of advanced Si and SiC switching devices, appropriate for low-voltage AC/AC converters that are placed in market, is provided.

5.2.1 Power Electronic Semiconductor Devices

Silicon has been the dominant material for power electronic devices for several decades. However, new materials are now becoming available such as Gallium Nitraide (GaN) and Silicon Carbide. GaN does not have as higher voltage rating compared with Si or SiC, and is a relatively immature technology. It is therefore not considered further in this thesis.

Various Silicon Carbide structures exist, such as 3C-SiC, 4H-SiC, and 6H-SiC, whereas 4H-SiC, and 6H-SiC are typically used for power devices. 4H-SiC is the preferred material due to its higher electron mobility compared with 6H-SiC. Additionally, the much lower thermal minority carrier generation of 4H-SiC results in lower device leakage currents.

Comparing the characteristics of Si and the 4H-SiC devices, it can be concluded that there is a significant difference between the high electric field and the low intrinsic carrier density characteristics of 4H-SiC and Si. These characteristics are the key drivers for enabling the implementation of power semiconductor devices with high blocking voltage and small on-state resistance. SiC also has superior thermal conductivity compared with Si making SiC power devices attractive for operation at high temperatures. Of course, the advantages of SiC devices are reflected in their cost, which is significantly higher than the comparable Si devices. Moreover, due to manufacturing difficulties SiC has a limited range of voltage and current ratings when compared with Si diodes, MOSFETs and IGBTs.

The Metal Oxide Field Effect Transistor (MOSFET) has superior performance when compared to bipolar devices. In particular, they have lower on-state conduction losses and switching losses, for blocking voltages of up to approximately 600V for Si. For higher blocking voltage ratings it is common to utilise bipolar devices such as the Si Insulated Gate Bipolar Transistors (IGBTs), which have significantly lower conduction losses in a smaller package when compared to a MOSFET. In addition, the switching operation performance of the intrinsic body diode of high-voltage MOSFETs is very poor [203], whereas, IGBTs can operate in conjunction with an external fast, anti-parallel diode with superior characteristics. A common technique new being offered in the industry is to replace fast Si common diodes with high-voltage SiC Schottky

diodes, which results in a hybrid configuration of a Si transistor with a SiC freewheeling diode. This configuration leads to significant reduction of the IGBT turn-on losses and the turn-off losses of the diode due to the complete elimination of the reverse recovery charge. One disadvantage of IGBTs when compared with MOSFETs is that the benefit of paralleling devices to reduce conduction losses is limited by the on-state voltage of the bipolar junction, which is insensitive to current levels.

In 2011, CREE released the industry's first commercial SiC power MOSFET, which is designed to replace the Si IGBTs in high-voltage power electronic applications [204]. This type of SiC MOSFET has a voltage rating 1200 V and maximum current rating 50 A in a TO247 package, with on-state resistances of between 80-160 Ωm. In addition the junction can operate at temperatures from 125-150 ^{0}C. One of the CREE's demonstration SiC MOSFET solar inverter test results have shown an average saving in switching losses up to 30% when compared with a high-performance IGBT. Moreover, the overall system efficiency exceeds 98% [205]. In addition, recent research work in [206] shows that the implementation of SiC MOSFETs can reduce the size and the weight of a converter by utilising a higher switching frequency, which results to a lower passive components size. A converter with a power rating of 6 kW achieved an efficiency of 98% and a power density of 5 kW/lt.

The 300 V RMS, 425 V peak input voltage specification for the proposed VCU suggests the use of semiconductor devices rated in excess of 600 V. This occurs mainly due to the safety margin needed for the operation of the VCU on the grid where high over-voltages can occur.

5.3 Power Electronic Circuit Simulation

In order to carry out the appraisal of the different candidate topologies for the VCU, two commercial circuit simulation packages were used. The first, which is an add-on toolbox to MATLAB is known as Piece-Wise Linear Circuit Simulator (PLECS) [207]. The second package was Micro-Cap Spice, where Spice stands for Simulation Program with Integrated Circuit Emphasis, which is a generic circuit simulator, originally developed at Berkeley University in the US [208]. Whilst PLECS is not as accurate as SPICE, it was used initially to give a first order estimate of semiconductor losses so that the different candidate topologies and semiconductor types such as a comparison of Si MOSFETs, IGBTs and SiC MOSFETs could be rapidly evaluated. This initial study suggested that the losses for the different circuits were not that different; therefore Spice was subsequently used to give a more accurate calculation of losses. However, the disadvantage of Spice is that this increased accuracy requires significantly longer simulation run-times.

5.3.1 Piece Wise Linear Circuit Simulator, PLECS

PLECS is an add-on toolbox to MATLAB/SIMULINK. Power electronic semiconductor devices such as diodes, IGBTs and MOSFETs are modelled as ideal switches. The actual switching transition is not modelled in PLECS so that the circuit topologies corresponding to the periods before and after a switch operates are linear. PLECS therefore uses a sophisticated algorithm to detect switch transitions, known as switch toggling. However, this method of modelling means that switching losses cannot be calculated. To overcome this problem PLECS uses the switch voltage and current prior to toggling to estimate switching losses using either a look-up table or a simple loss estimation equation that assumes for example a linear rise/fall in current during the transition. For example, the look-up table method for an IGBT, which can be obtained directly from its data sheet, is shown in Figure 5.1a, whereas the parameter entry dialogue for the equation based method is shown in Figure 5.1b.

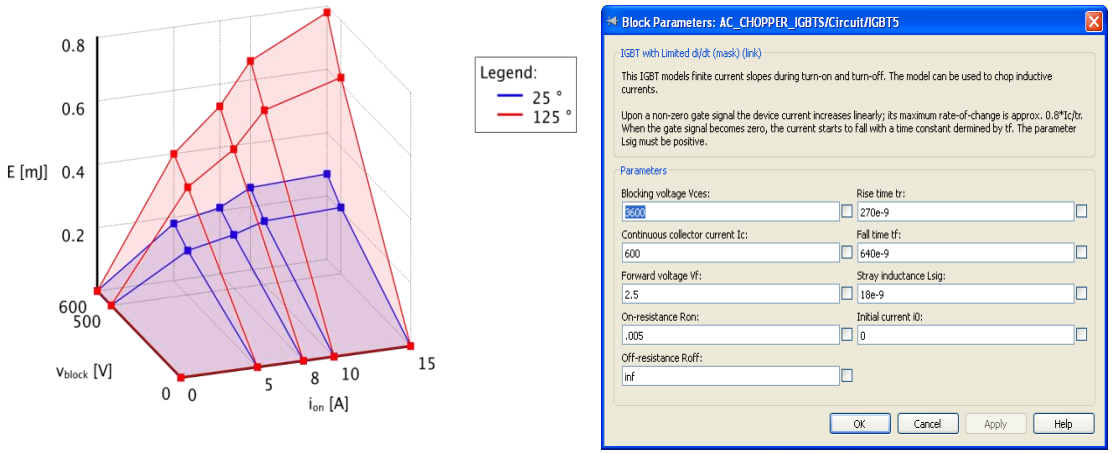

(a) **(b)**

Figure 5.1: ***PLECS data entry methods for power semiconductor device loss calculations (a) 3-dimensional surface from data sheet (b) parameters for loss equations***

It can be seen from Figure 5.1a that a 3-dimensional surface is generated of switching energy losses in mJ, against switched voltage and current. In addition, the device heatsink can be modelled so that junction temperature can be calculated. This then allows the temperature dependent nature of losses such as on-state resistance, to also be included model. However, loss surfaces for a range of temperatures then have to be included in the look-up table, for example

Figure 5.1 shows two sets of surfaces for junction temperatures of 25°C and 125°C. The look-up table method also includes the more complicated switching-loss effects to be modelled such as IGBT tail-currents and diode reverse recovery, which are included in the manufacturer's data sheet loss curves.

The second method of loss calculation is shown in Figure 5.1b, where parameters such as device rise and fall times are used to estimate switching losses. This assumes a simple linear rise/fall of the transistor current and current waveforms V_T and I_T respectively as shown in Figure 5.2.

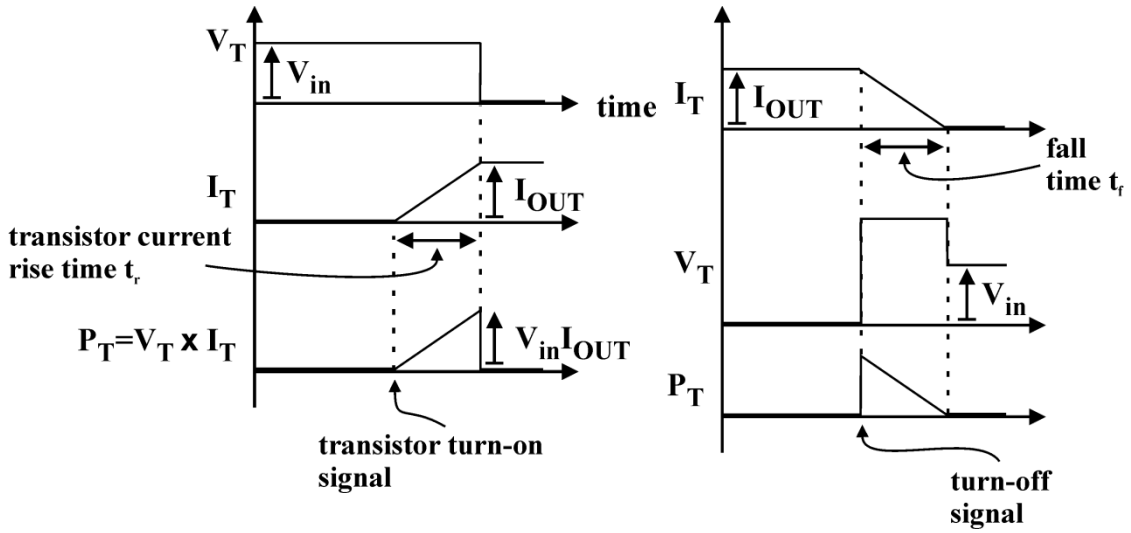

Figure 5.2: ***PLECS simplified switching waveforms (a) turn-on sheet (b) turn-off***

The turn-on and turn-off waveforms shown Figure 5.2a and b respectively assume an inductive load, where the off-state voltage is V_{IN} and the on-state current is I_{OUT}. The corresponding transistor power loss waveform P_T has a trapezoidal shape and the energy loss is therefore given by $V_{IN}I_{OUT}t_{SWITCH}/2$, where t_{SWITCH} is the either the current rise time t_r or fall time t_f, for the turn-on and turn-off waveforms respectively. The turn-off waveform also includes the effect of stray-inductance L_{STRAY}, as shown in Figure 5.2b, which generates an additional energy loss $L_{STRAY}I_{ON}^2/2$.

The PLECS software assumes a simple equivalent on-state resistance to calculate conduction losses for MOSFETs and on-state resistance plus constant on-state voltage for IGBTs.

5.3.2 Spice Simulator

For a more accurate estimate of semiconductor device losses, then device manufacturers provide Spice models of their transistors. These models are based on equations that describe the fundamental physics of diode and FET operation [209]. The equivalent Spice circuit for the NMOS FET is shown in Figure 5.3a.

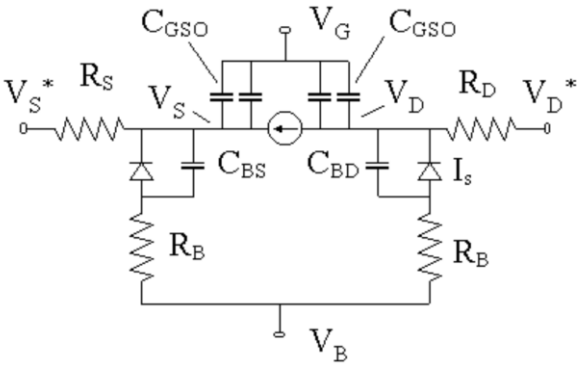


```
**************************************
*Model generated on Jan 31, 97
* MODEL FORMAT: SPICE3
*Symmetry IGBT Model (Version 1.0)
*External Node Designations
*Node 1 -> C
*Node 2 -> G
*Node 3 -> E
M1 9 6 8 8 MSUB L=100u W=100u
* Default values used in MSUB:
* The voltage-dependent capacitances are
* not included. Other default values are:
*   RD=0 RS=0 LD=0 CBD=0 CBS=0 CGBO=0
.MODEL MSUB NMOS LEVEL=1
+VTO=5.94387 KP=0.214059 LAMBDA=1.66093 CGSO=2.00187e-05
RD 7 9 1e-06
RS 4 8 1e-06
Q1 4 7 1 QSUB OFF
.MODEL QSUB PNP
+IS=1e-17 BF=4.47778 NF=0.85 VAF=88.0979
+IKF=493.458 ISE=3.54824e-11 NE=1.47478 BR=10.1202
+NR=0.75 VAR=142.787 IKR=1134.64 ISC=9.98961e-12
+NC=1.98439 RB=0.0001 IRB=1073.98 RBM=0.0001
+RE=1e-08 RC=0.000222891 XTB=0 XTI=3.54269
+EG=1.2 CJC=1.45053e-09 VJC=1.82764 MJC=0.9
+CJE=2.90106e-08 VJE=0.4 MJE=0.9 TF=2.99912e-09
RDS 7 4 1e8
RER 4 3 0.0005
RG 6 2 13.9403
RL 10 11 1
D2 12 11 DCAP
* Default values used in DCAP:
*   RS=0 EG=1.11 XTI=3.0 TT=0
*   BV=infinite IBV=1mA
```

(a) **(b)**

Figure 5.3: ***Spice (a) NMOS equivalent circuit (b) Example Spice IGBT example code Copyright(c) MODPEX for International Rectifier***

The NMOS equivalent circuit consists of a current source and a number of non-linear capacitors and diodes, where the diode model itself consists of a further set of equations and an equivalent circuit. Manufacturer's power device models augment the basic Spice NMOS FET model using further linear and non-linear components to include effects such as package parasitic, IGBT tail currents and Miller capacitance. A Typical example of Spice code for an International Rectifier IGBT is shown in Figure 5.3b.

Spice models give very accurate simulation results for the devices themselves due to the underlying complexity of the model equations. However, the disadvantage of using these models is that simulation run-times can be very long. For example, the simulation of a MOSFET based AC Chopper consisting of four MOSFETs, which is described further on in this chapter, took approximately two hours for a 20 ms simulation time. Figure 5.4 and 5.5 show the corresponding turn on and off waveforms for this simulation for one of the Cree CMF10120 MOSFETs used in the AC Chopper Micro-Cap Spice simulation. The operating conditions were with a switched

voltage of 300 V, a current of 10A and a typical circuit drain-source stay-inductance of 50 nH. The top waveform shows the drain-source voltage V_{DS} and drain current I_D, and the bottom waveform the instantaneous power loss V_{DS} x I_D and energy.

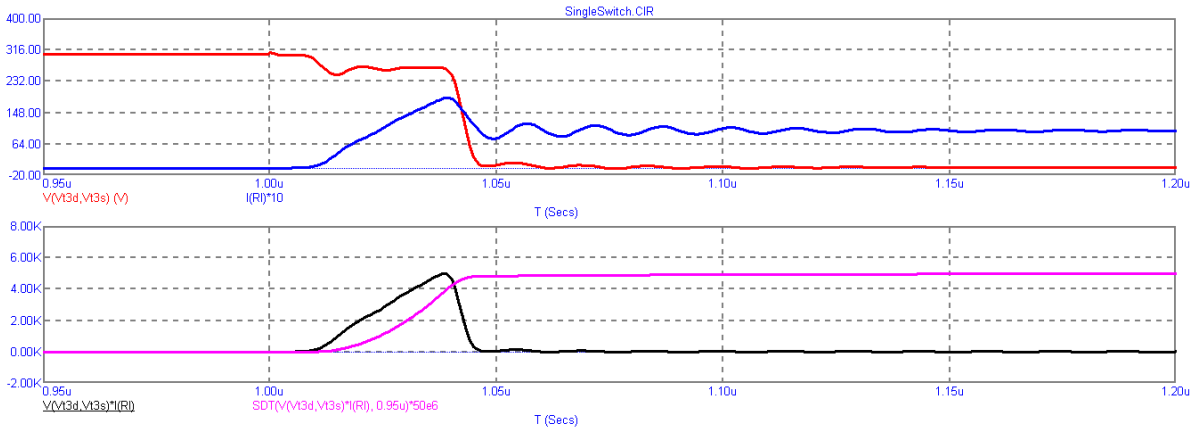

Figure 5.4: ***Micro-cap Spice turn-on waveform for a Cree CMF10120 MOSFET (a) top waveform VDS (red V), ID (blue x10 A) and bottom waveform power (black W) and energy (magenta x50 µJ)***

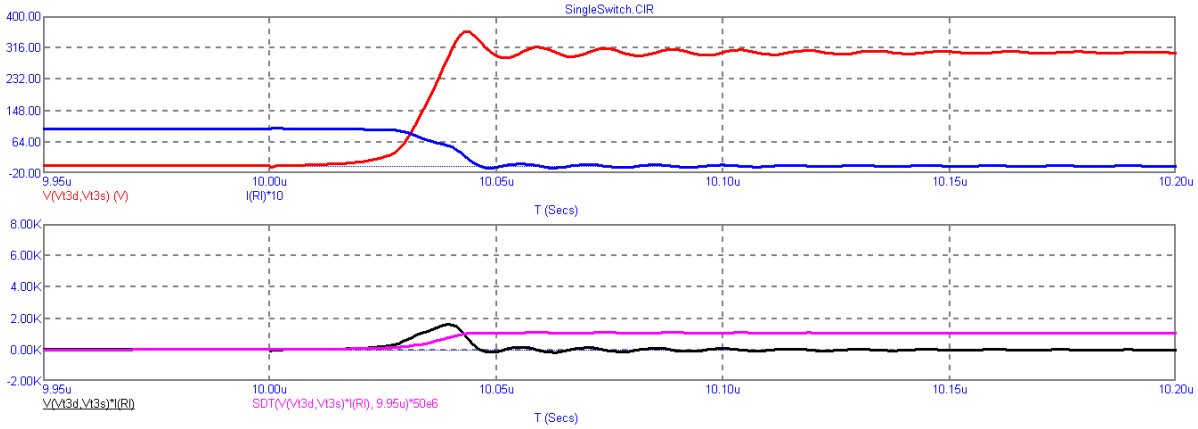

Figure 5.5: ***Micro-cap Spice turn-off waveform for a Cree CMF10120 MOSFET (a) top waveform VDS (red V), ID (blue x10 A) and bottom waveform power (black W) and energy (magenta x50 µJ)***

It can be seen from these figures that the voltage and current waveforms are significantly more complex than those for the PLECS models shown in Figure 5.2. The turn-on waveform, Figure 5.4, displays a significant current overshoot due to the reverse-recovery of the body-diode in the opposing MOSFET within the leg.

5.4 PLECS Simulation Results

Semiconductor device losses were calculated using PLECS for the three candidate circuits for three, low-loss TO247 devices representing: the particular Si MOSFET, IGBT and SiC MOSFET technologies shown in Table 5-1. The simulation results were checked against analytic expressions where possible in terms of conduction loss equations [210] and empirical switching loss equations [211]. As an example, equation (5.1) calculates the conduction loss for a semiconductor device in an inverter leg with sinusoidal PWM, modulation index M, on-state voltage V_{on}, peak inverter leg output current I_m, on-state resistance R_{on} and current phase angle φ with respect to the leg output voltage,

$$Conduction\ Loss = \frac{V_{on} I_m}{2\pi}\left(1 + \frac{\pi}{4} M \cos(\varphi)\right) + \frac{I_m^2 R_{on}}{2\pi}\left(\frac{\pi}{4} + \frac{2M}{3}\cos(\varphi)\right) \tag{5.1}$$

	Si IGBT	**Si MOSFET**	**SiC MOSFET**
	FAIRCHILD SEMICONDUCTOR FGH40N60SMDF	**Advanced Power Technology APT60N60BCS**	**Cree CMF20120**
Voltage Rating	600 V	600 V	1200 V
Current Rating	40 A	60 A	42 A
Package	TO-247-3	TO-247-3	TO-247-3

Table 5-1: The three power semiconductor devices used in the PLECS simulations

The PLECS simulation schematic for the 2-leg topology is shown in Figure 5.6. The blue shading over the bottom semiconductors represents the heatsink model used in PLECS for the calculation of losses and junction temperature rise. All three converters were simulated with a 300 V input voltage, 50 kHz switching frequency and a 230 V, 15 kW load.

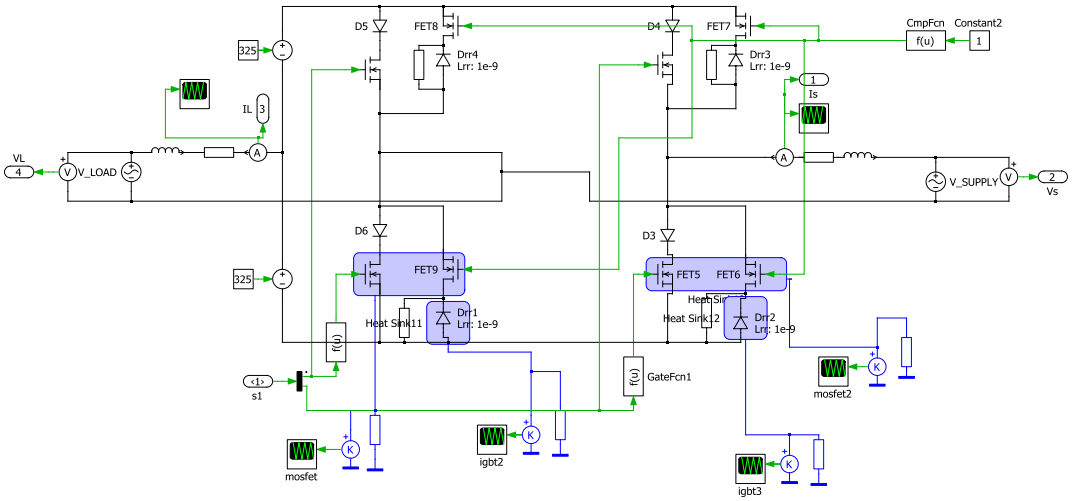

Figure 5.6: PLECS simulation schematic for the 2-leg converter topology with MOSFET switches.

Table 5-2 shows the conduction losses calculated using PLECS and analytic expressions [210, 211] for the FGH40N60SMDF IGBT for the three different converter topologies. These initial studies focused on the conduction loss performance of the different transistors as switching losses can always be reduced using soft-switching techniques if needed. The table also shows that there is reasonable agreement between the PLECS results and calculation using the analytic equations. Similar results were also obtained for the Si MOSFET and SiC MOSFET.

Converter	Total Conduction Losses (W) PLECS Simulation	Total Conduction Losses (W) Analytical Expressions
2-Leg AC/AC	328	298
3-Leg AC/AC	245	240
AC Chopper	266	245

Table 5-2: Conduction losses (W) for the FGH40N60SMDF IGBT

The table also shows that the losses exceed those from the target requirement specification given in the summary at the end of Chapter 2, of 1% of 15 kW = 150 W, and it became clear from this initial study that a single TO247 device would not capable of achieving the target efficiency and that devices would have to be paralleled in order to reduce overall conduction losses. Parallel arrangements can be implemented in one of three-Ways:

- Individual TO247 devices could be connected in parallel
- Individual converter modules containing single TO247 devices could be connected in parallel

- Manufacturer's high-power semiconductor modules with multiple semiconductor dies in parallel could be utilised

The last option is the most promising; however, the cost of these modules especially SiC devices was prohibitively expensive for this project. Therefore, only the first two options were investigated further. Out of these two options, it was decides that the parallel module approach was the most attractive because:

- The switching of individual modules could be interleaved so that the size of passive filter components could be minimised [212, 213].
- In the event of a failure, a modular approach would allow an easier method of hot-swapping a faulty module within the meter-box. This would reduce the amount of time a customer was off supply with a VCU fault.

Increasing the number of parallel devices/modules only reduces *overall* losses up to the point, since any further reduction in conduction losses are negligible compared with the almost constant switching losses, which are relatively insensitive to paralleling. Therefore in order to estimate what the optimum number of parallel modules would be for the VCU, a detailed Spice simulation was carried out for the AC Chopper. In these simulations losses were calculated by reducing the 15 kW target power by an integer factor N, where N represents the number of modules, and the calculated losses represent the loss for one module. Finally the module losses were multiplied by N to get a loss figure for the overall converter. The results of these simulations are shown in Figure 5.7.

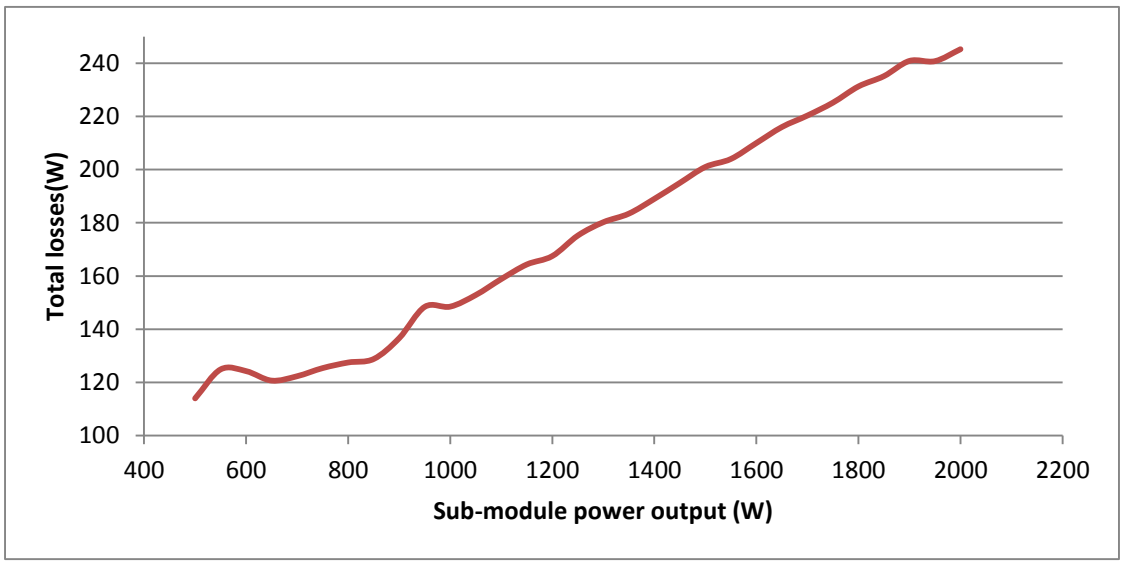

Figure 5.7: Total losses for a range of module' power outputs

It can be seen from Figure 5.7 that as the number of modules N, increases and the individual module power ratings are reduced, then below around 1 kW, the curve tends to flatten out as switching losses become dominant. At this point the benefits from paralleling start to reduce. It was therefore decided that the VCU should be split into 15, 1 kW modules. The following simulations are therefore based on a single module 1 kW module and the module losses are multiplied by 15 to get the overall VCU loss.

The initial PLECS simulations showed that for the IGBT there was also a limit to the reduction in losses that could be gained from paralleling IGBT based module or devices. This was the case for all the candidate AC/AC topologies and is due to the constant on-state voltage characteristic of Si IGBTs – for example the Fairchild FGH40N60SMDF has an on-state voltage of 0.5 V. In particular Table 5-3 shows the value of conduction losses that are asymptotically approached when an increasing number of IGBTs are connected in parallel. These losses were calculated using the analytic expressions for conduction losses validated in Table 5-2 above.

Converter	$P_{conduction\ min}$ (W)
2-Leg AC/AC	83
3-Leg AC/AC	88
AC Chopper	63

Table 5-3: ***Limit of conduction loss reduction using an increasing number of IGBTs***

It is clear from Table 5-3 that the target loss of 150 W cannot be achieved using IGBTs due to their constant on-state voltage characteristic. Therefore they were not considered for further investigation.

Finally it was discovered using the PLECS simulations that high-voltage Si MOSFETs were also unsuitable for this application due to the high-switching losses which arise from the poor reverse recovery characteristics of the body diode - the APT60N60BCS Si MOSFET has t_{rr} = 600ns and Q_{rr} =17.00 μC with a 600 V rating, compared with 220 ns and 0.14 for the CREE 1200 V CMF20120 SiC MOSFET. Therefore it was decided to proceed with just the CREE MOSFET, as not only did this device have superior switching characteristics to the Si device, the 1200 V rating of the SiC MOSFETs are far superior to the 600 V Si device when operating from the proposed 425 V peak supply voltage. Another factor that influenced this decision was that CREE were regularly announcing newer technology in terms of on-state resistance, such that CREEs latest offering at the end of the project was a 25 mΩ, 1200 V device compared to the 45 mΩ, 600 V APT60N60BCS Si MOSFET.

5.5 Spice Simulation Results

Micro-Cap Spice simulations were carried out for the 2-leg, 3-leg and AC Chopper topologies in order to estimate circuit losses. Based on the results of the previous section, these simulations only included results for the CMF20120 SiC MOSFETs, using Spice models from CREE.

5.5.1 2-Leg Converter

The Micro-Cap Spice simulations schematic for the 2-leg converter is shown in Figure 5.8.

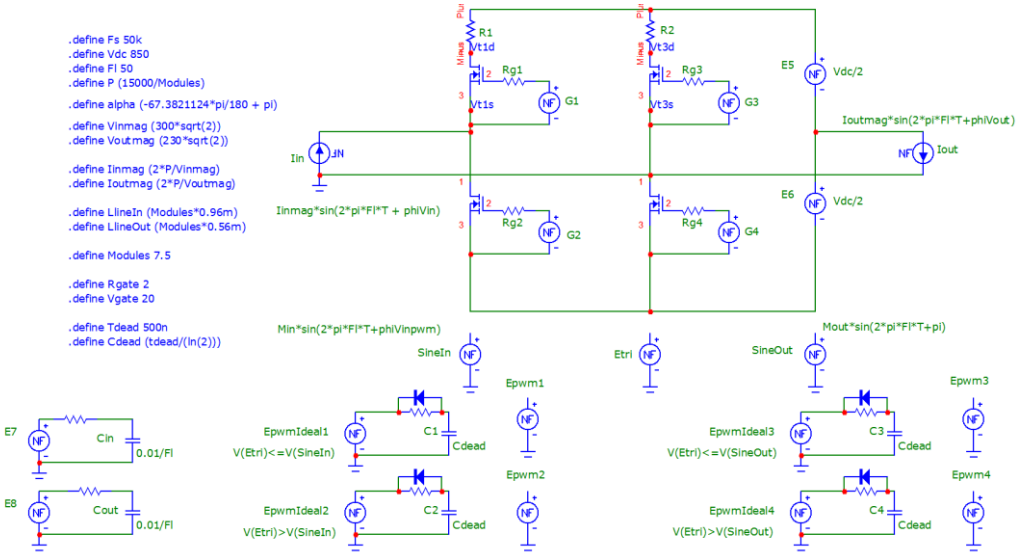

Figure 5.8: Micro-Cap simulation schematic for the 2-leg converter topology with SiC MOSFET switches.

The converter uses a sinusoidal PWM for each leg with a maximum switching frequency of 50 kHz and a 0.5 µs dead-time between the upper and lower transistors. The magnitude and phase-angle for the two-legs of the converter are chosen according to [196] using a DC-link voltage of 850 V. The supply and load were modelled using ideal current sources to represent the input and output line inductors and they both operated at unity power factor. The MOSFET gate was driven by an ideal +20/-5 V voltage source through a 2 Ω gate resistor as recommended by the CREE data sheet. Figure 5.9 shows the input and output voltage waveforms with a supply/load phase angle of 70.39° as described in Table 5-4. Other important parameters are also given in Table 5-4.

	Input leg	Output leg
Line inductance	0.96mH	0.56mH
Supply/load voltage amplitude	425 V	325 V
Supply/load voltage phase angle	70.39°	-2.8547°
Power factor	1	1
Output power	1 kW	
PWM modulation signal	Amp. 1.0000 Phase= -67.4°	Amp.0.7662 Phase =0.0°

Table 5-4: ***2-Leg AC/AC Converter simulation parameters***

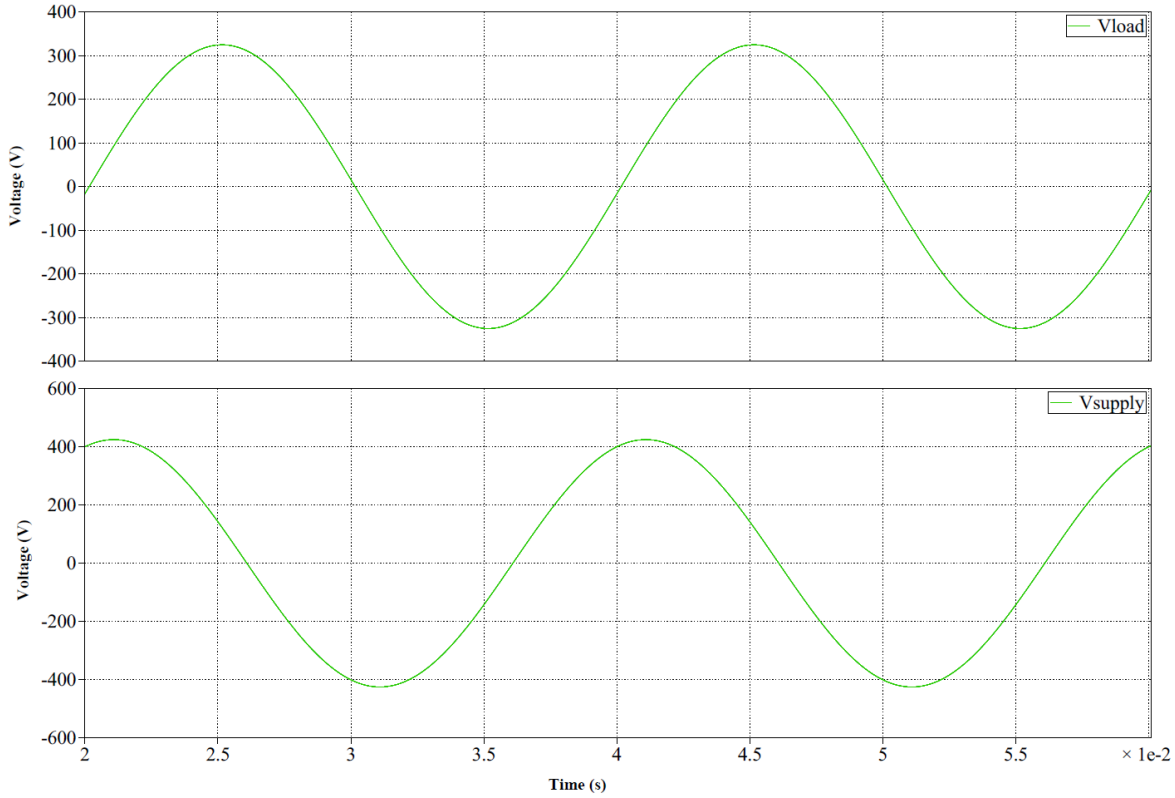

Figure 5.9: ***Micro-Cap Spice input and output voltage waveforms for the 2-leg converter topology***

Simulations were carried out for both 10 kHz and 50 kHz switching frequencies and also a hypothetical switching frequency of 50 Hz, where the total losses at this frequency correspond to conduction losses only as switching losses are negligible. The results for a total of 15 modules are shown in Figure 5.9.

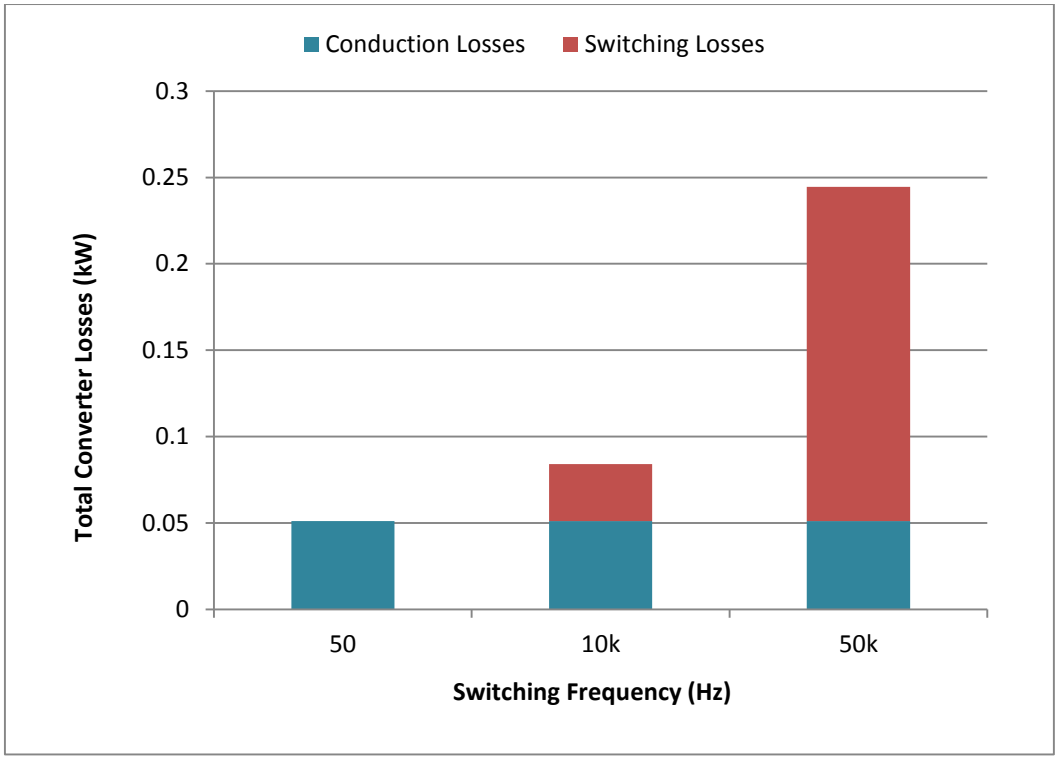

Figure 5.10: ***2-Leg converter total VCU losses (W) against switching frequency for SiC MOSFETs***

Figure 5.10 shows that the total conduction losses for the 15 modules x 4 transistors of the 2-leg converter are 51 W. This is value is taken from the 50 Hz switching frequency results were the switching losses are negligible. As the switching frequency increases the switching losses increase whereas the conduction losses remain the same. The total convert losses with a 10 kHz and 50 kHz switching frequency are 95 W and 244 W respectively.

5.5.2 3-Leg AC/AC Converter

The Micro-Cap Spice simulations schematic for the 2-leg converter is shown in Figure 5.11.

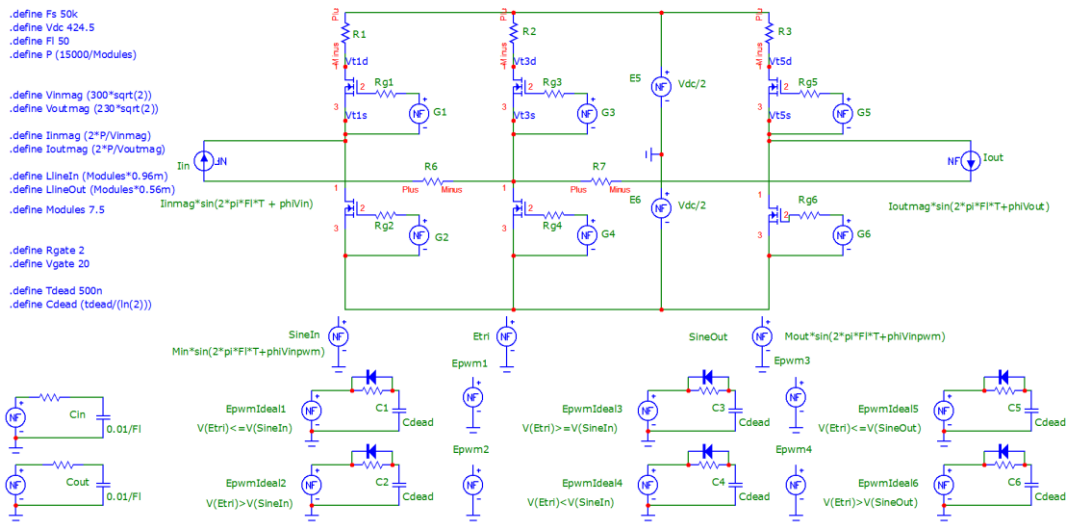

Figure 5.11: Micro-Cap simulation schematic for the 3-leg converter topology with SiC MOSFET switches.

The converter uses a sinusoidal PWM for each leg with a maximum switching frequency of 50 kHz and a 0.5 µs dead-time between the upper and lower transistors. The magnitude and phase-angle for the three-legs of the converter are chosen according to [197] using a DC-link voltage of 425 V. The supply and load were modelled using ideal current sources to represent the input and output line inductors and they both operated at unity power factor. The MOSFET gate was driven by an ideal +20/-5 V voltage source through a 2 Ω gate resistor as recommended by the CREE data sheet. Figure 5.12 shows the input and output voltage waveforms with a supply/load phase angle of 1.91° as described in Table 5-5. Other important parameters are also given in Table 5-5.

	Input leg	**Common leg**	**Output leg**
Inductance	0.96mH		0.56mH
Supply/load voltage amplitude	425.00 V	425.00 V	325.00 V
Supply/load voltage phase angle	1.91°	N/A	-2.86°
Power factor	1	N/A	1
Output power	1 kW		
PWM Modulation Index	Amp. 1.0000 Phase= 0.00°	Amp 1.0000 Phase angle= 180.00°	Amp.0.5344 Phase = 0.00°

Table 5-5: *3-Leg AC/AC Converter simulation parameters*

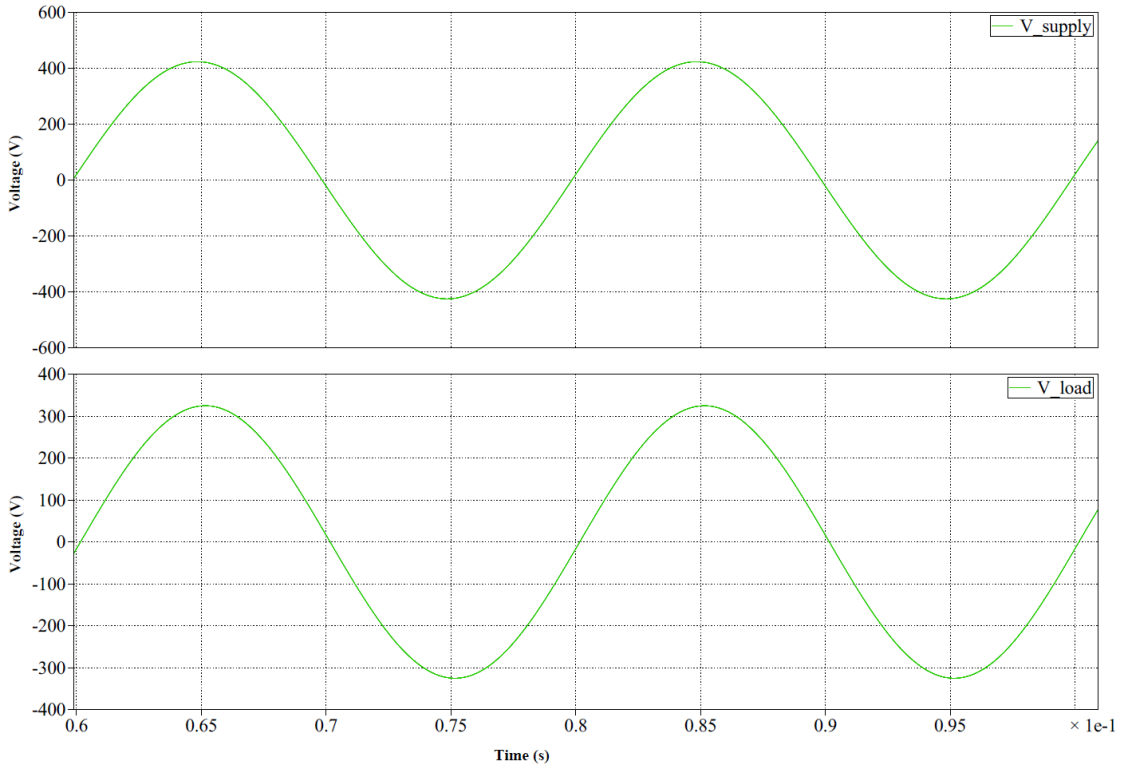

Figure 5.12: ***Micro-Cap Spice input and output voltage waveforms for the 3-leg converter topology***

Simulations were carried out for both 10 kHz and 50 kHz switching frequencies and also a hypothetical switching frequency of 50 Hz, where at this frequency the total losses correspond to conduction losses only as the switching losses are negligible. The results for a total of 15 modules are shown in Figure 5.13.

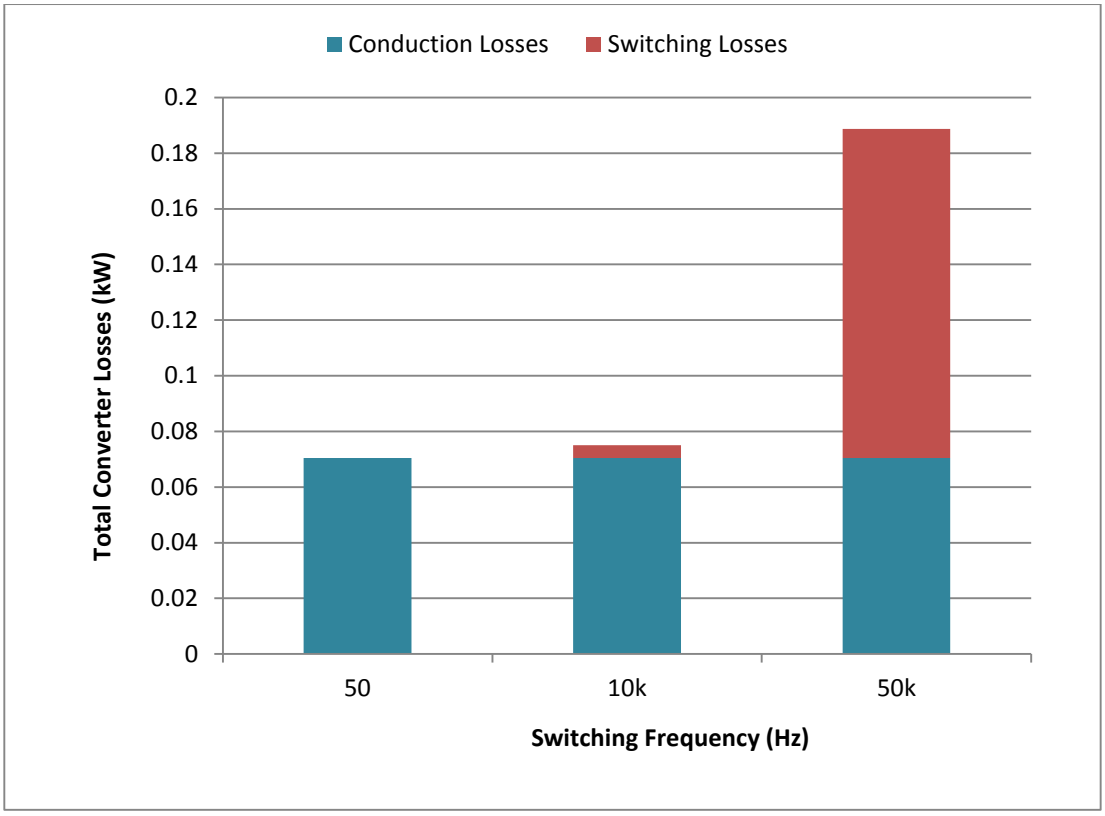

Figure 5.13: ***3-Leg converter total VCU losses (W) against switching frequency for SiC MOSFETs***

Figure 5.13 shows that the total conduction losses for the 15 modules x 6 transistors of the 3-leg converter are 70 W. This is value is taken from the 50 Hz switching frequency results were the switching losses are negligible. As the switching frequency increases the switching losses increase whereas the conduction losses remain the same. The total convert losses with a 10 kHz and 50 kHz switching frequency are 78 W and 189 W respectively.

5.5.3 AC Chopper

The Micro-Cap Spice simulations schematic for the AC Chopper converter is shown in Figure 5.14.

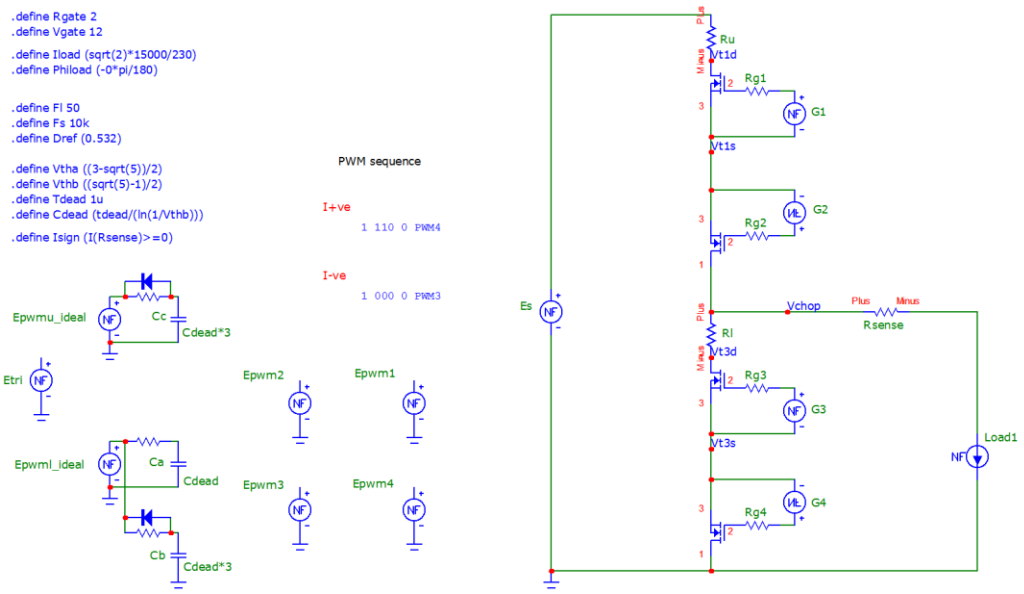

Figure 5.14: ***Micro-Cap simulation schematic for the AC Chopper converter topology with SiC MOSFET switches.***

The converter uses a fixed duty-cycle PWM for the leg given by 2x230/300-1, which corresponds to the voltage step-down ratio of the converter. The maximum switching frequency was 50 kHz with a 1.0 µs dead-time four-step commutation as described in [214]. This commutation will be described in more detail in Chapter 6 of this thesis. The supply source and load were modelled using ideal voltage and current sources respectively, where the output current source represented the output line inductor. Both the supply and source both operated at unity power factor. The MOSFET gate was driven by an ideal +20/-5 V voltage source through a 2 Ω gate resistor as recommended by the CREE data sheet. Other important parameters are given in Table 5-6.

	Input	**Output**
Supply/load voltage amplitude	300 V	230 V
Supply/load phase angle	0°	0°
Power Factor	1	1
Output power	1 kW	
Leg modulation Index	0.532	

Table 5-6: ***AC Chopper converter simulation parameters***

Simulations were carried out for both 10 kHz and 50 kHz switching frequencies and also a hypothetical switching frequency of 50 Hz, where at this frequency the total losses correspond to conduction losses only as the switching losses are negligible. The results for a total of 15 modules are shown in Figure 5.13.

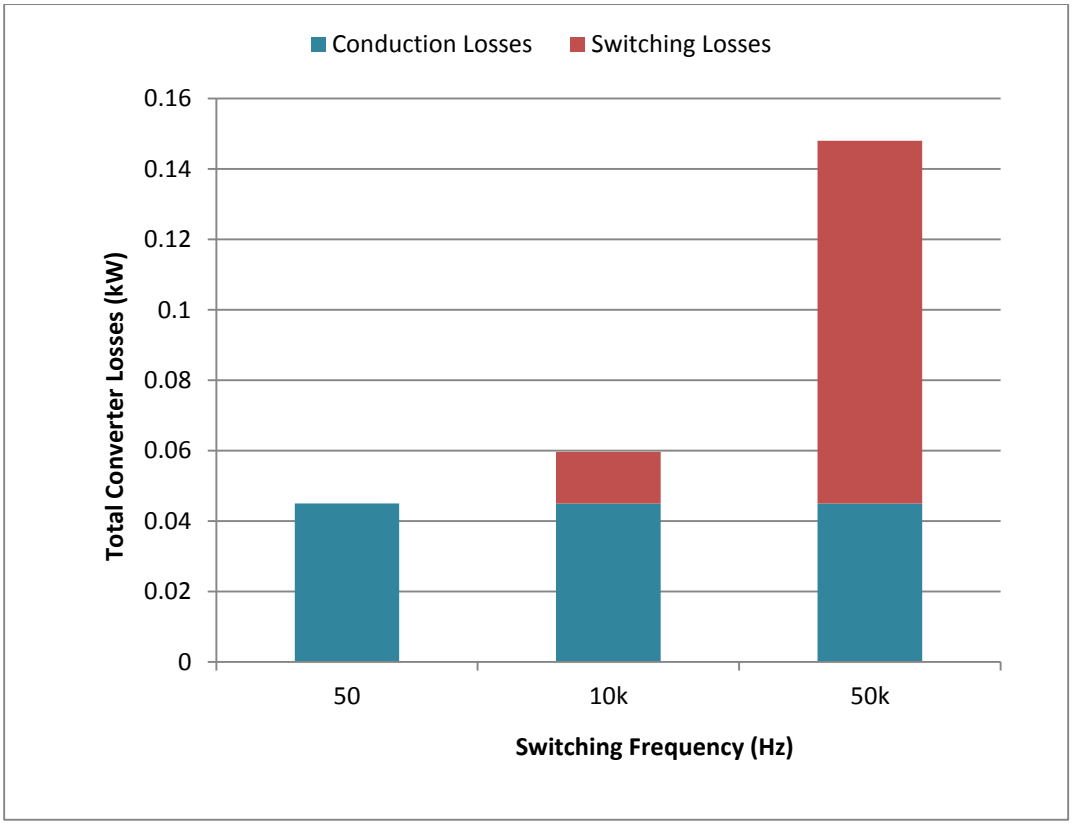

Figure 5.15: AC Chopper converter total VCU losses (W) against switching frequency for SiC MOSFETs

Figure 5.15 shows that the total conduction losses for the 15 modules x 4 transistors of the AC Chopper converter are 45 W. This is value is taken from the 50 Hz switching frequency results were the switching losses are negligible. As the switching frequency increases the switching losses increase whereas the conduction losses remain the same. The total convert losses with a 10 kHz and 50 kHz switching frequency are 58 W and 148 W respectively.

5.5.4 Summary of Spice simulation results

A summary of the Spice simulation results with SiC MOSFETs and a 50 kHz switching frequency for the three candidate topologies are shown in Table 5-7 and Figure 5.16.

Converter Topologies	Total converter semiconductor losses (W)	Comments
2-leg	244	High power quality benefits, complex control
3-leg	189	High power quality benefits, complex control
AC Chopper	148	Low power quality benefits, simple control

Table 5-7: Summary of total converter switching and conduction losses for 50 kHz, SiC MOSFET based converters

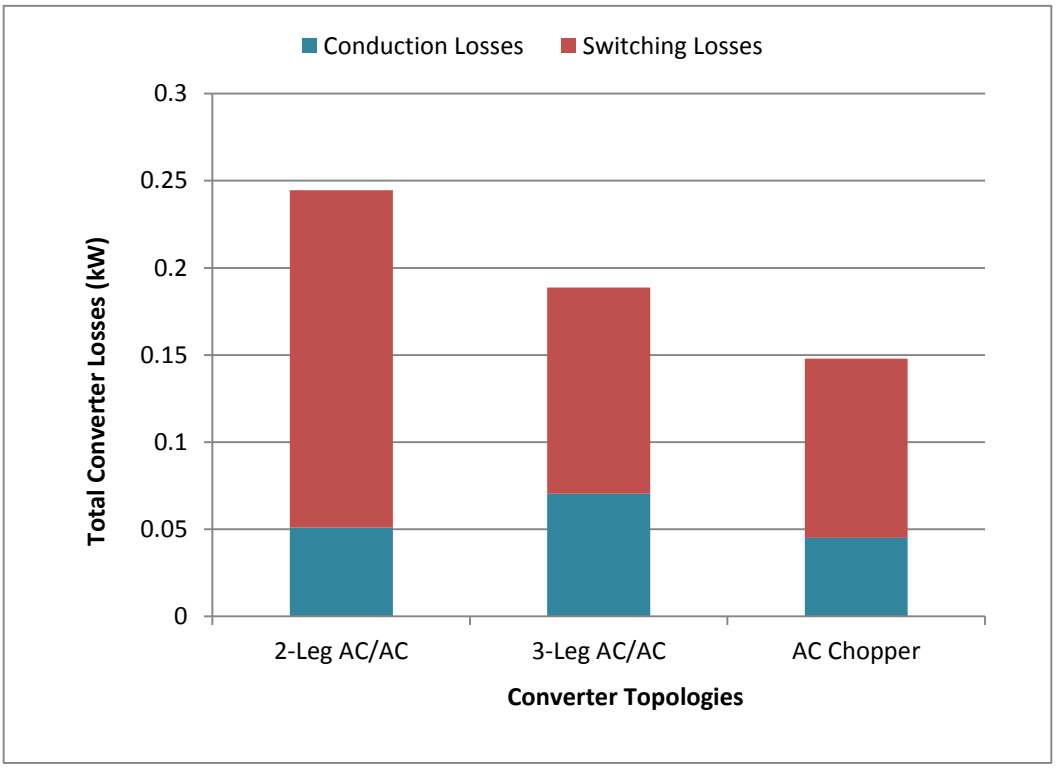

Figure 5.16: ***Summary of total converter switching and conduction losses (W) for 50 kHz, SiC MOSFET based converters***

Table 5-7 and Figure 5.16 shows that the best candidate topology in terms of total losses is the AC chopper circuit followed by the 3-leg converter. However, the power quality benefits of the three-leg converter are much better than those of the AC chopper, whereas the AC chopper has very simple control, a lower number of transistors and it does not require a DC-link capacitor.

Nevertheless the primary objective for the project was to demonstrate the feasibility of installing a VCU into the meter box of a house with a maximum loss of 150 W, and the AC Chopper with its lower losses was the preferred option. Whilst the AC Chopper does not meet the target of 150 W total losses it was anticipated that CREE were releasing better performance devices on a regular basis. Therefore it was decided that a 1 kW, SiC MOSFET based AC Chopper module would be designed and tested. The next chapter describes the design of this hardware prototype.

6 Hardware Design

This chapter presents the hardware design for a 1 kW single-phase AC-AC module converter with the metric of high efficiency. SiC MOSFETs and SiC Schottky diodes were selected in order to achieve high power and high switching frequency with the minimum dissipation of losses. Based on the topology analysis in Chapter 3 and the simulation results in Chapter 4, the AC Chopper was the selected topology for the hardware system. The prototype consisted of the main power devices, isolated gate drives, filter inductor, input and output filter capacitors, over-current protection, voltage clamp, output current direction detector and an FPGA PWM generation. Figure 6.1 shows the main functional schematic of the experimental prototype.

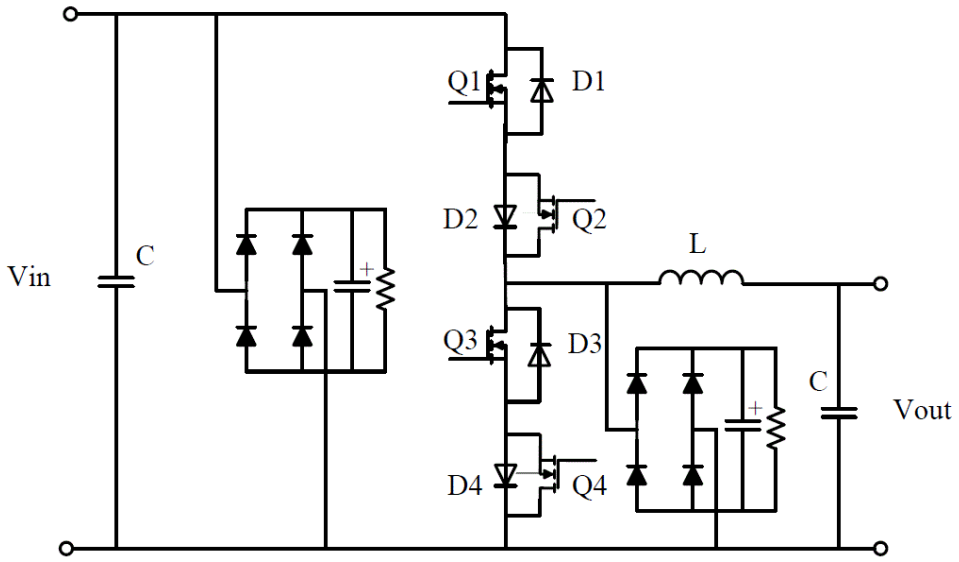

Figure 6.1: ***The AC Chopper experimental rig schematic***

6.1 AC Chopper power circuit

Two bi-directional switches were constructed using four Cree 40 A, 1200 V CMF20120D MOSFETs, TO-247 devices and four Cree 20 A, 1200 V C4D20120A Schottky diodes TO-220-2 devices, and arranged as a 1-phase to 1-phase matrix converter. The supply (V_{in}) is 50Hz, variable voltage, using a 20 kVA, isolated variac, from 0-300 V rms phase, and the output current is controlled by adjusting a variable 3 kW load resistance. A top view of the 1 kW module is shown in Figure 6.2a where the gate drive PCBs, the protection circuits and the four SiC MOSFETs are shown. A bottom view of the module is shown in Figure 6.2b where the input

and output filter capacitors as well as the voltage clamp electrolytic capacitors and the hall-effect current sensor are shown.

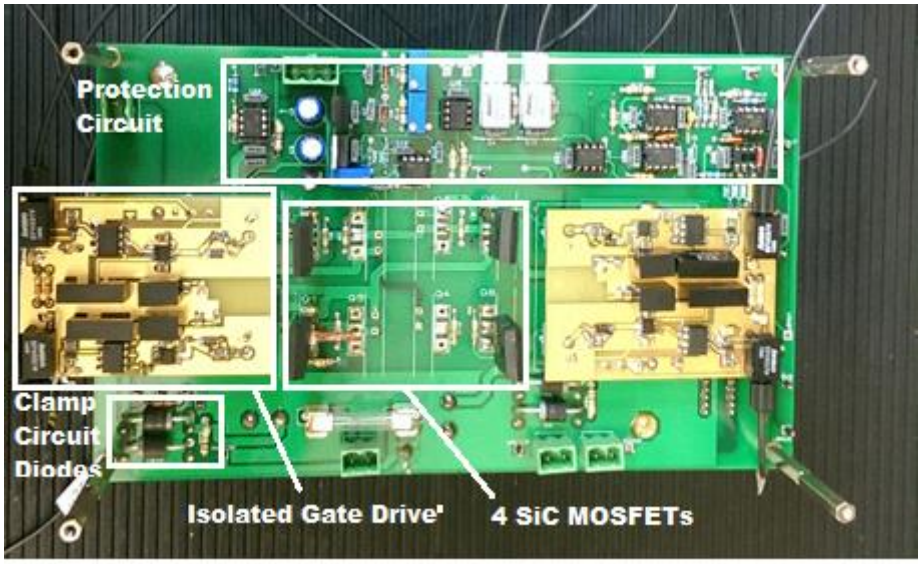

(a)

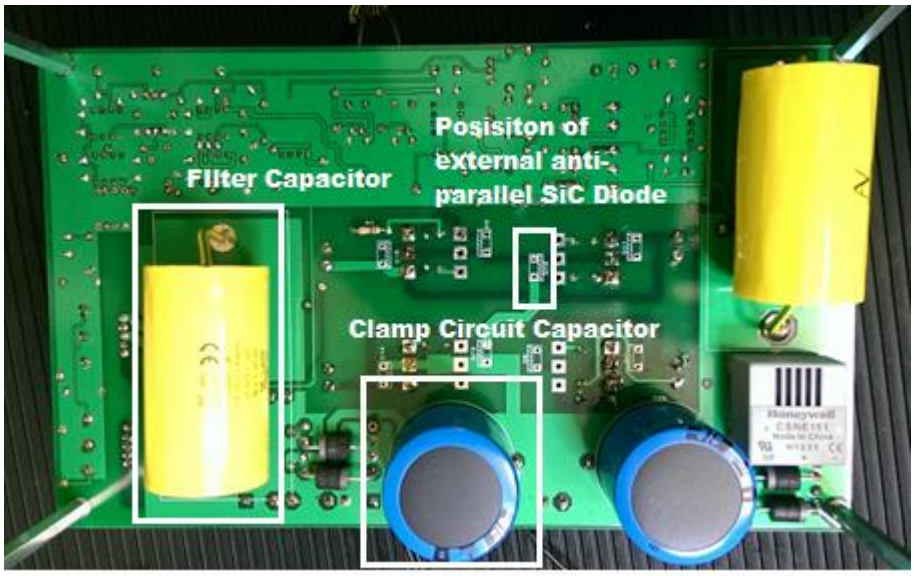

(b)

Figure 6.2: ***A top (a) and a bottom (b) view of the 1 kW laboratory***

In order to get the required efficiency for the 15 kW converter the VCU was divided into 15 off, parallel 1 kW modules. This gave the opportunity to interleave the switching of individual modules, which gives the benefit of a reducing the input and output filter capacitance C, shown in Figure 6.1. To test this concept, 2 off 1 kW modules were constructed and connected in parallel. Figure 6.3 shows the two parallel sub-modules giving a total power output of 2 kW. In addition to this, the experimental prototype was designed to accommodate two parallel TO-247 MOSFETs devices within each module in order to evaluate the benefit of losses reduction by paralleling devices.

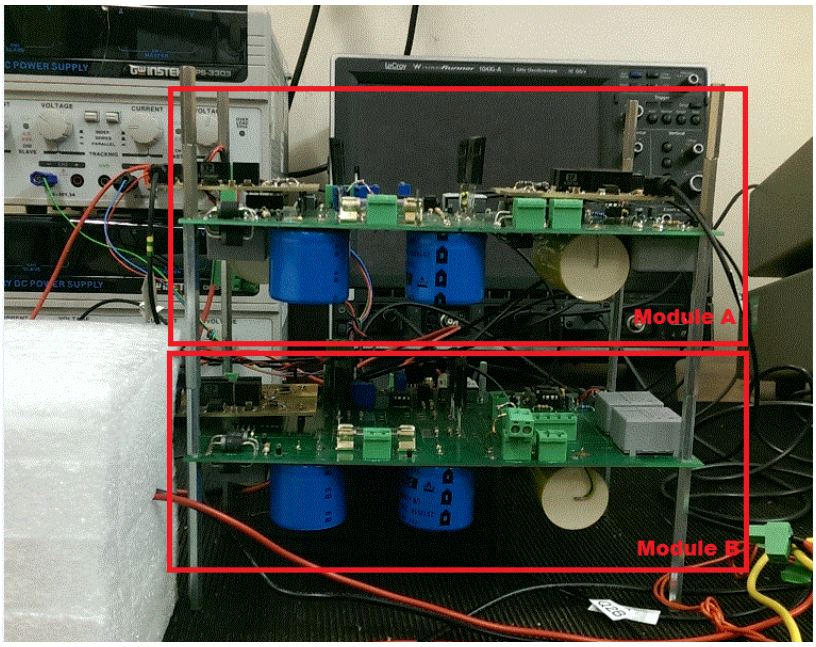

Figure 6.3: A representation of modules A and B operating in parallel with interleaved switching giving a total power output of 2 kW

6.2 Design of the Printed Circuit Board

Because of the very high-speed switching of the SiC MOSFETs, the design of the Printed Circuit Board (PCB) has a critical impact on the behaviour of the converter. For example, the stray inductance and capacitance of the interconnections between the MOSFETs has a significant effect on switching losses. The prototype was therefore constructed using a laminated power-plane approach to minimise the connection inductance, which is a common practise in standard power electronic circuits, whereas the mid-point of the converter leg was separated from the upper and lower nodes to minimise mutual capacitance. In particular, the PCB consists of four layers – one layer for each of the three input/output nodes of the circuit shown in Figure 6.1, and the fourth was used as a ground plane for the control electronics. Sufficient separation

was required between power tracks in order to withstand insulation breakdowns and a "best-practice" figure of 1 mm/100 V was used.

Tracking for the power routes was kept as short as possible, with wide tracks/power-planes to maximise their current handling capability. Connections between the gate drivers and the MOSFETs were kept as short as possible and the gate-source circuit loop area was minimised in order to reduce gate circuit inductance. The layouts of the PCB and the associated schematics are presented in Appendix D.

6.3 Protection Scheme

To prevent the converter from over-voltage faults, a clamp circuit which consists of an ultra-fast diode rectifier bridge, a clamp capacitor and a discharge resistor are connected at the input and the output of the converter module. By utilising such a protection, over-voltages due errors in the commutation of the MOSFETs at the zero-crossing of the filter inductor current are safely limited by the clamp capacitor. Moreover, a free-wheeling path for the inductor current to the electrolytic capacitor in the event of a converter shut-off is provided to avoid damage to the power electronic devices. An ultra-fast fuse at the input of the converter module is also provided to avoid short-circuit faults at the load. Finally, two fast, Honeywell hall-effect sensors are provided to detect MOSFET overcurrents by monitoring the current flowing into the Chopper leg and out of the mid-point of the leg. If the current exceeds a pre-set overcurrent value the Chopper was shut-down.

6.4 Passive Filter Selection and Design

An output filter is needed in order to eliminate the high-frequency switching components appearing at the mid-point of the Chopper leg. The operation of the AC Chopper is similar to a Buck DC-DC converter. However, the 50 Hz, sinusoidal nature of the Chopper waveforms means that traditional design equations that have been developed for the Buck converter cannot be used. Therefore the Micro-Cap Spice simulation presented in Chapter 4 was used to estimate the inductance, where the magnitude of the inductor ripple current was traded against minimising the switching and conduction losses of the MOSFETs. The selected inductor value for the 1 kW converter module was 100 μH. A Micro-metals powder-iron core was chosen, and their on-line design calculator was used to select a core size and calculate the number of turns. With a target converter efficiency of 99%, which equates to 10W, loss for the 1 kW module, a power loss of around 5 W was allocated to the inductor. The Micro-metals design calculator gave predicted losses of 3.8 W with an inductor ripple current of 13%. The volume of the inductor core was

0.01 litres. Figure 6.3 illustrates the final inductor prototype. The copper winding was a single layer, using a twisted pair of insulated conductors to reduce skin and proximity effects and ease the bending of the copper.

Figure 6.3: ***The output inductor with an iron powder core and a 2 stranded 14 AWG wire***

The input capacitor was selected on the basis of the requirements to de-couple the converter from any supply inductance and minimise the stray inductance around the MOSFETs bridge. The capacitor had to be AC as it sees the supply voltage, with at least a 425 V rating, with low Equivalent Series Resistance (ESR) and self-inductance. Low ESR was required to ensure low losses in the converter. Therefore a 600 V, polypropylene film capacitor was chosen, and on the basis of experience a value of 10 µF was selected. Subsequently hardware tests found this value of capacitance to be satisfactory.

The output capacitor value was chosen on the basis of minimising the output voltage ripple to less than 5 %. This was carried out using Micro-Cap Spice simulation and a 10 µF capacitor was selected. Again the capacitor had to be AC with a voltage rating of at least 325 V. Therefore a 10 µF, 600V polypropylene film capacitor was again chosen.

6.5 Prototype Control

Since the chopper consists of the series connection of MOSFETs, the gate drive signals must provide both a dead-time between the upper and lower devices, as well as a conduction path for the free-wheeling current for the output inductor. This requires a four-step switching transition as the upper and lower switches change state under PWM, which is described in more detail in the next section. The four-step commutation sequence depends on the direction of the output filter inductor and therefore the sign this current is needed as an input to the PWM

generator circuit. The PWM with 4-step commutation was implemented in an Altera FPGA using a state-machine design. The Altera Quartus software state-machine is shown in Figure 6.5.

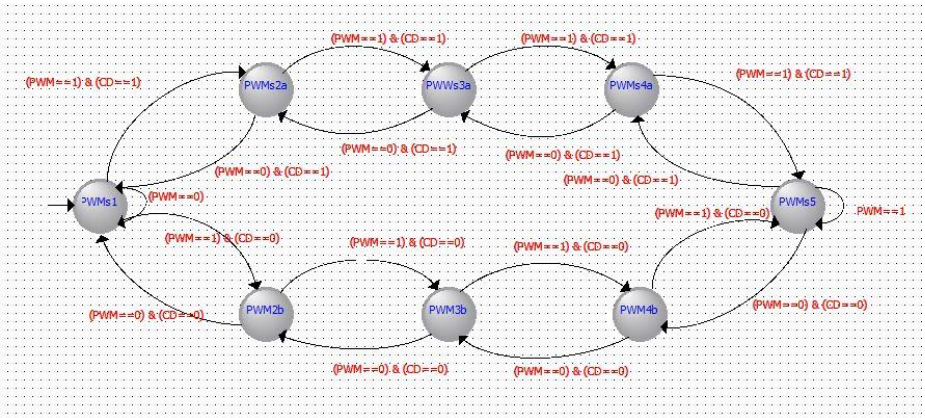

Figure 6.4: ***State-machine representation of the AC chopper PWM control***

Each of the states shown in the above figure has four-outputs, which are used to switch the four MOSFETs in the Chopper leg. A PCB was designed for the Altera FPGA, which included fibre-optic links that were used to interface the FPGA outputs to the Chopper gate-drives. A Figure of the FPGA PCB with fibre-optic links can be seen in Figure 6.6.

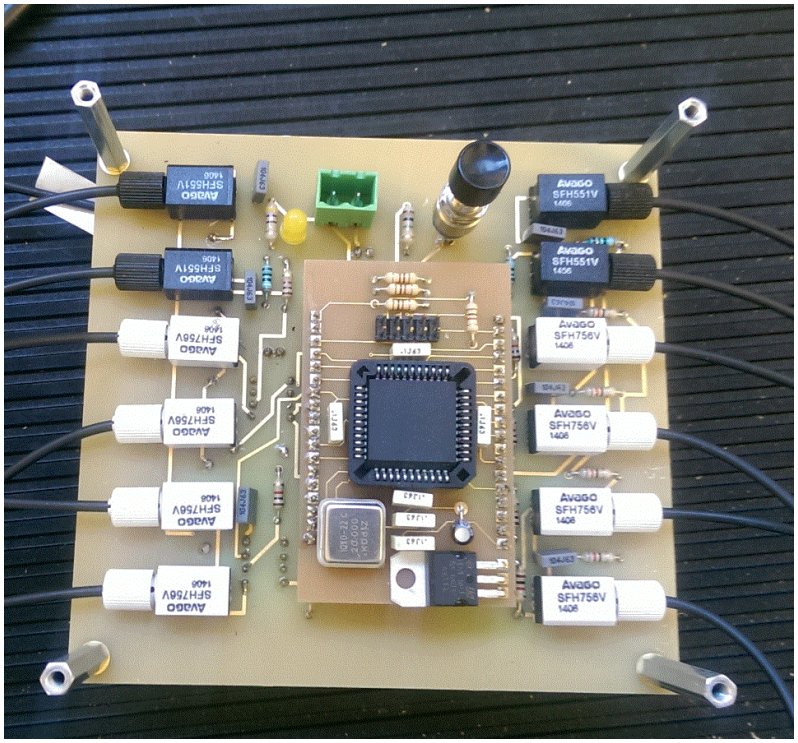

Figure 6.5: The FPGA AC chopper PWM and commutation control board with fibre-optic links

To protect the converter, the FPGA has an optically isolated fault input from the over-current detectors on the main board. If a fault is detected all the power switches are set to their off state. A push-button integrated to the FPGA board switch to reset the trip and re-enable the converter.

6.5.1 Commutation Strategy

The current commutation in an AC Chopper converter is not as straightforward as a traditional converter since the back-to-back arrangement of the switches means there are no freewheeling paths for the filter inductor current. This, together with the requirement to avoid short circuits of the input voltage supply means a 4-step sequence is needed in order to switch between the upper and lower device pair. The commutation period for each step needs to be long enough to allow each MOSFET to turn on/off, since the devices cannot be switch instantaneously due to the finite switching times of the transistors as well as the propagation time delays of their gate signals. It is important also to note that the commutation time needs to be minimised otherwise it can cause distortion of the current waveform. The commutation sequence is dependent on direction of the filter output current. Figure 6.7a shows the sequence for an upper-on/lower-off to upper-off/lower-on transistion for positive input voltage and

positive inductor current and Figure 6.7b its complement for negative output inductor current and positive input voltage. For negative input voltage and negative inductor current the oposite sequence should be followed, from upper off/lower on to upper on/lower off.

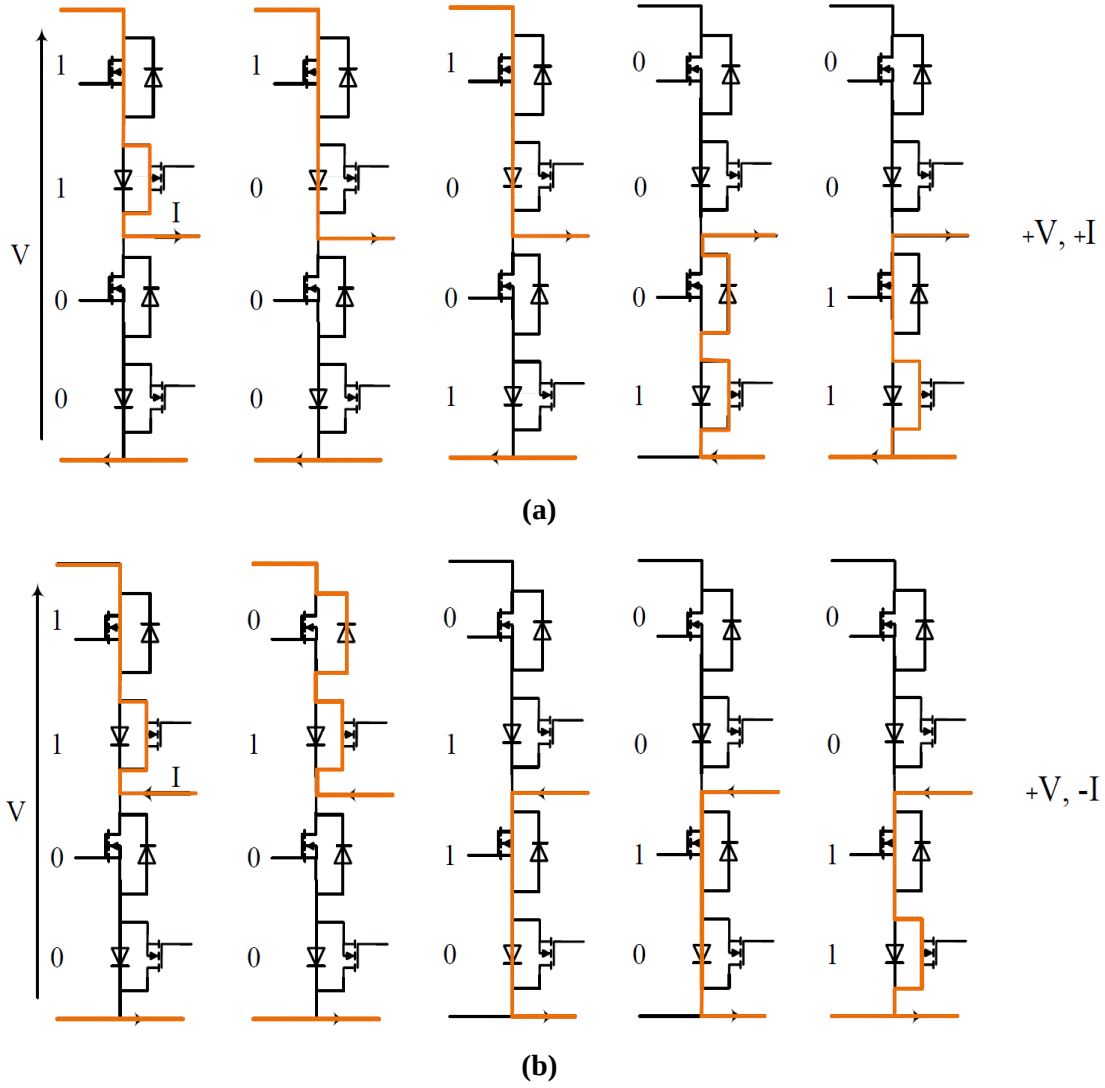

Figure 6.6: ***Sequence of four-step commutation for positive voltage and current (a) and for positive voltage and negative current (b)***

Figure 6.7(a) shows the leg output current, which flows through the output filter inductor is initially passing through the upper MOSFETs. Whilst the lower MOSFET of this pair does not need to switched on as current would flow through its anti-parallel diode, it is enabled to allow reverse-conduction through its channel, which provides a lower on-state loss than the diode.

During the first stage of the commutation sequence, the lower MOSFET of the upper pair is turned off and current flow passes to its anti-parallel diode.

During the second stage, the lower MOSFET of the lower pair is turned on, which allows a free-wheel path to be established for the inductor current through the anti-parallel diode of the upper MOSFET of the lower pair.

The third-stage is when current commutates from the upper pair to the lower pair. During this period the conducting diode of the upper pair undergoes a reverse-recovery.
Finally the lower MOSFET is turned on so that current commutates from its anti-parallel diode to the MOSFET channel in order to minimise conduction losses.

When the output filter current is reversed as shown in Figure 6.7 (b), the switching sequence of the MOSFETs within a pair is swapped over.

6.6 Gate Drive Circuit

A drive circuit is needed to transfer the switching signals generated from the FPGA to the voltage and current levels needed to drive the gate of the MOSFETs. The turn-on voltage of the CREE MOSFET is typically 20 V, and the turn-off voltage is -5 V. The gate circuit of the MOSFET appears as a small capacitor to the gate-drive circuit, and the speed with which this capacitor is charged, determines the switching time of the MOSFET. Typical currents of 1 or 2 A for durations of 50 ns are needed to turn the MOSFET on or off in.

In addition, if the lower node of the Chopper leg is connected to ground, then the gate-source terminals of the devices switch between ground and the input supply voltage, which can have a magnitude of several hundred volts. However, the PWM generation electronics such as the FPGA is also connected to ground, and therefore isolation is required between the FPGA and the gate-drive circuits. This is done using an opto-isolator integrated circuit, with an additional fibre-optic link to the FPGA. The gate drive power is provided through an isolated DC-DC converter module.

The gate drive circuit was based on a recent Cree application note [215], which gives the circuit diagram, parts-list and PCB layout design. The output power of the gate driver is transmitted to the MOSFET gate source pins via a 4 Ω gate resistor, which is recommended in the CREE MOSFET data sheet. The placement of the gate drive is as close as possible to the MOSFET to minimise parasitic effects.

6.7 Summary

This Chapter has described the design of the laboratory prototype single-phase AC Chopper converter. The AC chopper converter PCB power circuit implementation consists of the power devices and diodes, the input and output filters, the clamp circuit, the detection circuit of the

current direction and the protection circuit. The drive circuit has been implemented in separate PCB which was plugged in the main PCB power circuit. The functionality, the construction of the mechanisms and the key components used in each circuit have also been described. The control execution of the prototype has been achieved using the high performance FPGA platform. In the next chapter the results of testing the prototype are presented in terms of voltage step-down performance, waveform quality and efficiency.

7 Power Loss Performance of the AC Chopper Prototype

This chapter describes the results from testing a SiC based AC Chopper prototype that was built in order to demonstrate the technology and the feasibility of locating such a converter in the meter-box of a residential property. In particular the efficiency of the converter was a key target of the design.

7.1 4-Step Commutation Technique

The 50 kHz PWM with fixed duty cycle was generated using an Altera FPGA. The FPGA also included the 4-step commutation sequence that is required for the AC chopper circuit. The sequence depends on the sign of the filter current and this appears as an input to the FPGA. Figure 7.1a shows a measurement of the four gate signals generated by the FPGA for the four SiC MOSFETs, for an upper off/lower on to upper on/lower off transition and Figure 7.1b for its complement with positive output inductor current.

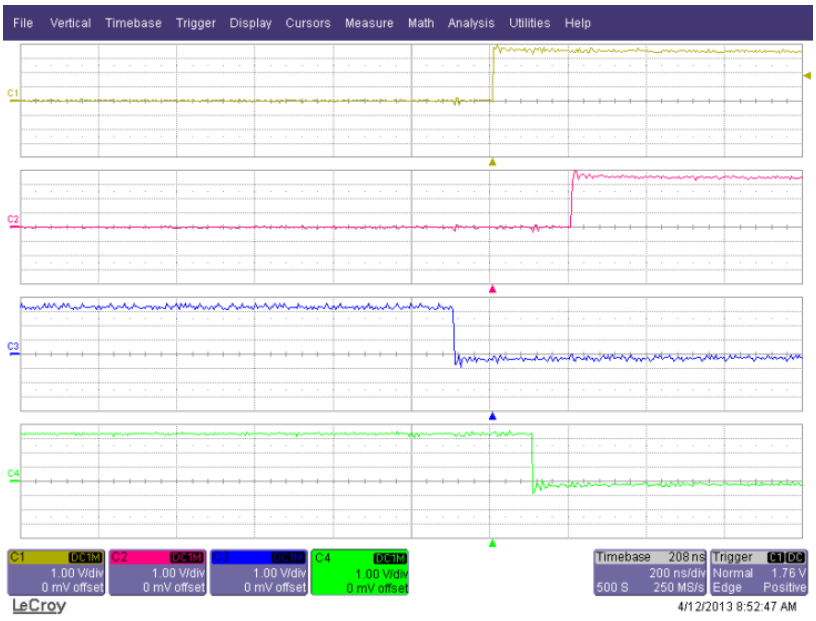

(a)

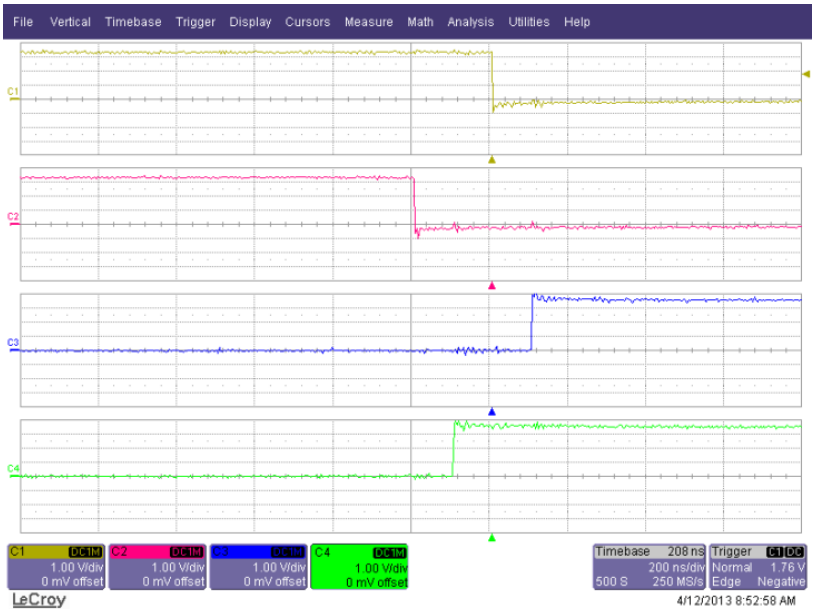

(b)

Figure 7.1: ***(a) upper devices off/lower devices on → upper devices on/lower devices off transition and (b) the complementary transition, with positive output inductor current***

7.2 Switching Performance of SiC MOSFET Prototype

The voltage and current turn-on and turn-off switching waveforms of the SiC MOSFETs used in the AC Chopper were measured when the input voltage is was at its maximum of 425V and the load peak current was 6.2 A. Figure 7.2 and Figure 7.3 show the measured drain-source voltage and drain current waveforms of transistor Q1 - see Figure 6.1, Chapter 6 - for turn-on and turn-off respectively.

Figure 7.2: ***Measured waveforms for Q1 turn -on (Voltage 100 V/div, Current 5 A/div, time 50ns/div)***

Figure 7.3: ***Measured waveforms for Q1 turn -off (Voltage 100 V/div, Current 5 A/div, time 50ns/div)***

The current turn-on time from Figure 7.1 is approximately 10ns with a gate source resistance of 6 Ω. The current increases at a fairly constant di/dt causing a voltage drop across

the parasitic inductance resulting in a plateau in the voltage waveform. The current continues rising above the load peak current due to the reverse recovery characteristics of the anti- parallel diode in the lower pair of devices. The voltage drops rapidly as the diode starts to block and the current falls down toward the nominal load current value. During the hard turn-off shown in Figure 7.3, it can be seen that the current falls towards zero in approximately 15 ns. The drain to source voltage rises rapidly and overshoots due to the parasitic inductance in the circuit. This surge voltage does not exceed the rated voltage of the devices.

The waveforms contain a lot of ringing due to the parasitic inductance and capacitance within the circuit and these oscillations were also predicted by the Spice simulations as shown in Chapter 5, Figures 5.4 and 5.5. It therefore makes it difficult to estimate switching losses from this waveform. In addition, the switched voltage and current vary sinusoidally over half a fundamental, 50 Hz period, which means that each individual switching transient waveform would have to be captured in order to calculate the total switching losses for a device. Therefore alternative methods of calculating converter losses were used as will be described further in this chapter. Whilst the above figures show that the SiC devices were achieving very rapid switching times, the drawback to this was the generation of troublesome EMI/EMC noise throughout the electronics causing circuit mal-operation.

The module input and output voltage and current waveforms when supplying a 1 kW, lagging 0.98 power-factor load are shown in Figure 7.4 and 7.5 respectively.

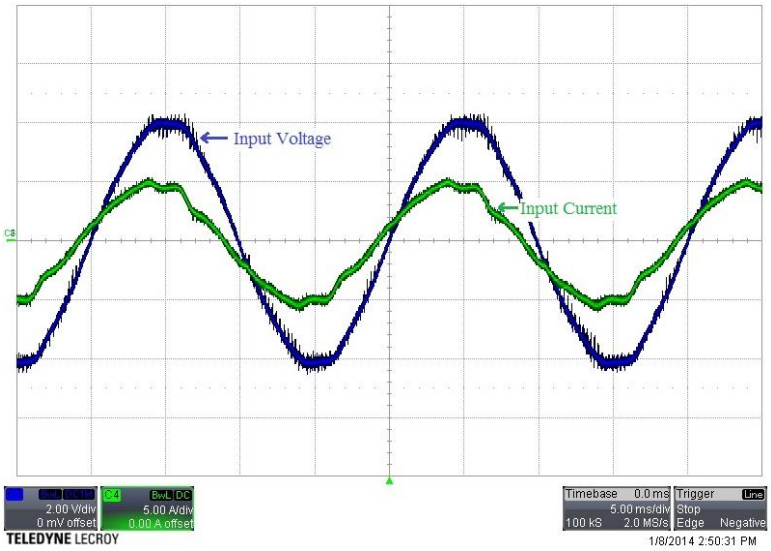

Figure 7.4: Module input voltage (200 V/div) and current (5 A/div) waveforms for 1 kW, 0.98 power factor output power (time 5 ms/div)

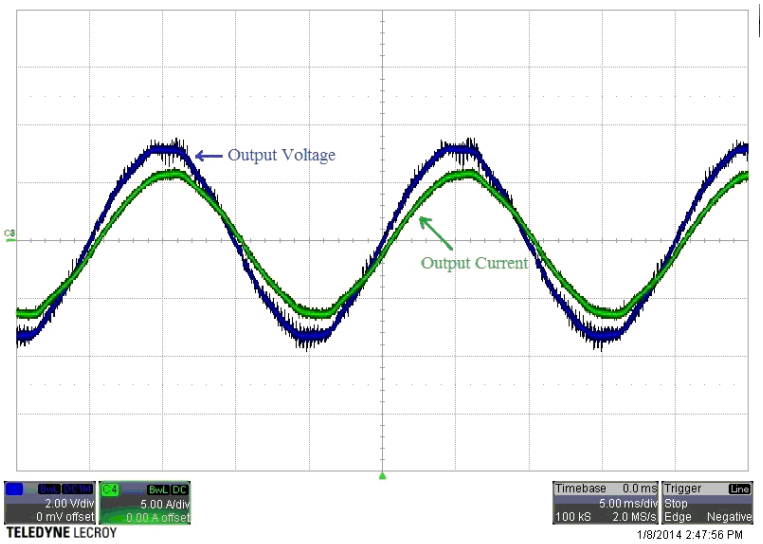

Figure 7.5: ***Module output voltage (200 V/div) and current (5 A/div) waveforms for 1 kW, 0.98 power factor output power (time 5 ms/div)***

It can be seen from Figure 7.4 that the peak voltage is approximately 400 V peak, but there is some distortion on the in-coming laboratory supply voltage, which is the reason that this value is less than the nominal figure of 425 V. In addition, even though the output current is close to sinusoidal as shown in Figure 7.5 the input current is quite distorted. This is thought to be due to errors in the output current-sign detector, which is used to determine the switching sequence for the 4-step current commutation. These errors are apparent from the mid-point output voltage of the Chopper leg as shown in Figure 7.6.

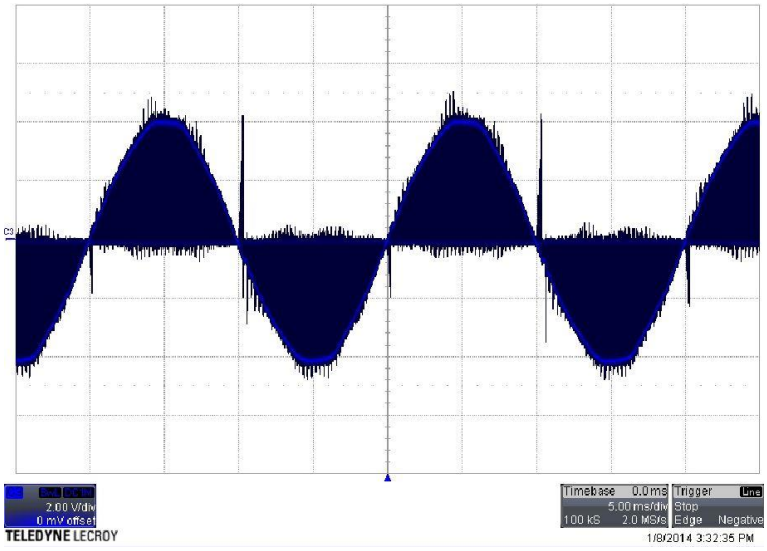

Figure 7.6: ***Chopper leg mid-point voltage (200 V/div) for 1 kW, 0.98 power factor output power (time 5 ms/div)***

It can be seen from the chopper leg mid-point voltage waveform shown in Figure 7.6 that there are large voltage spikes around the voltage zero-crossings. This is caused by noise generated by the fast switching of the SiC MOSFETs entering the current-sign detector circuit. This circuit is then incorrectly measuring the output current direction, which is fed back to the 4-step commutation controller in the FPGA, and causes a commutation failure. During this period the converter output inductor current has no free-wheel path and the inductor voltage rises until it is limited by the converter clamp-circuit. The subsequent disturbance to the circuit that this causes results in a large transient in the input current waveform, which appears as the input current distortion shown in Figure 7.4.

The output inductor current waveform is shown in Figure 7.7. The current ripple is relatively high being almost 50% of the fundamental. But this level of ripple was deliberately chosen based on the Micro-Cap simulation as a trade-off between total module losses and inductor size.

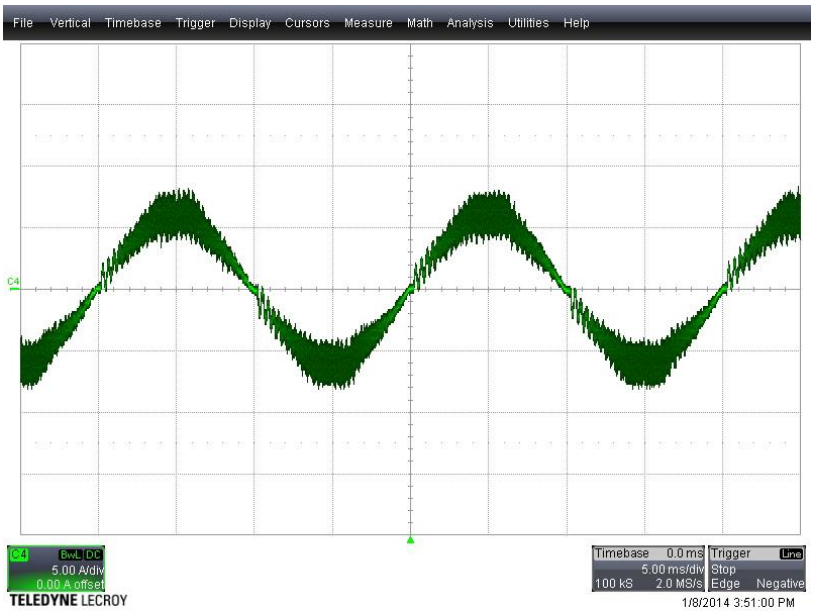

Figure 7.7: Module output inductor current (5 A/div) for 1 kW, 0.98 power factor output power (time 5 ms/div)

The 1kW power modules can be connected in parallel to increase the overall VCU output power level. This concept is shown in Figure 7.8, where two modules, A and B, share a common input and output capacitors C. The PWM generation for each module is then interleaved within the FPGA to give an apparent doubling of switching frequency as seen by the filter capacitors C, which results in a reduced VCU input current ripple and output voltage ripple.

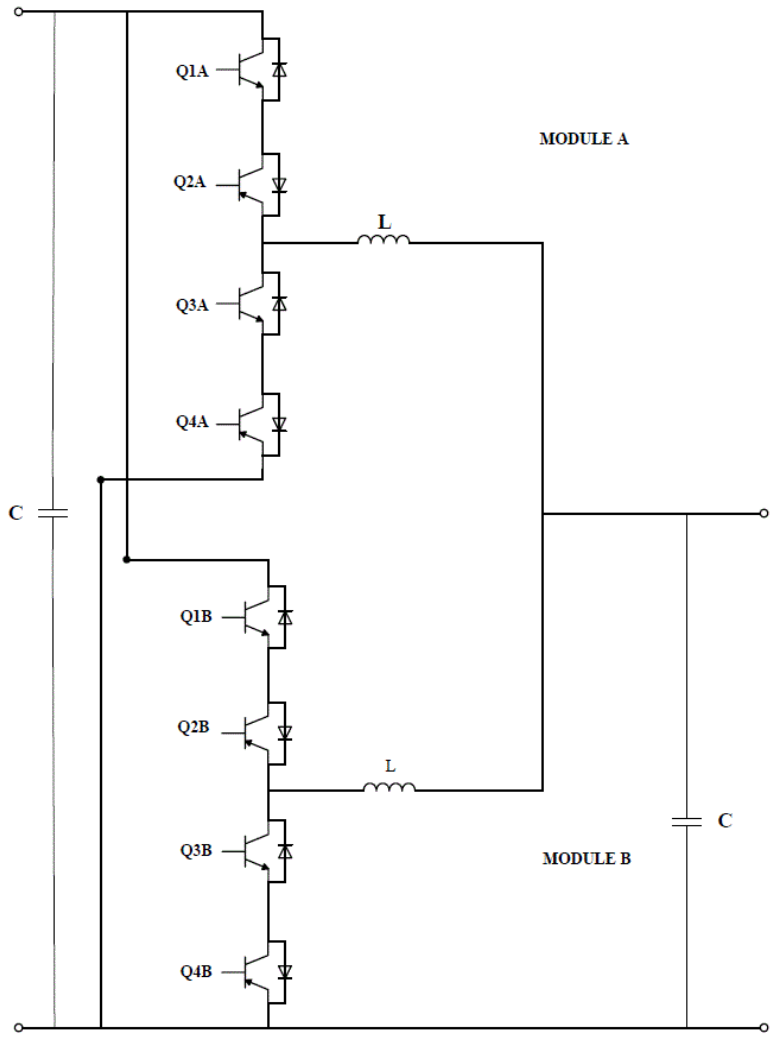

Figure 7.8: ***Parallel module arrangement***

A potential problem with such a parallel connection is that the modules do not share current. However, when a second module was connected to the prototype to give an overall 2 kW power rating, the output currents were equally balanced as demonstrated in Figure 7.9, which shows the inductor currents of each module, and the two waveforms overlay almost identically.

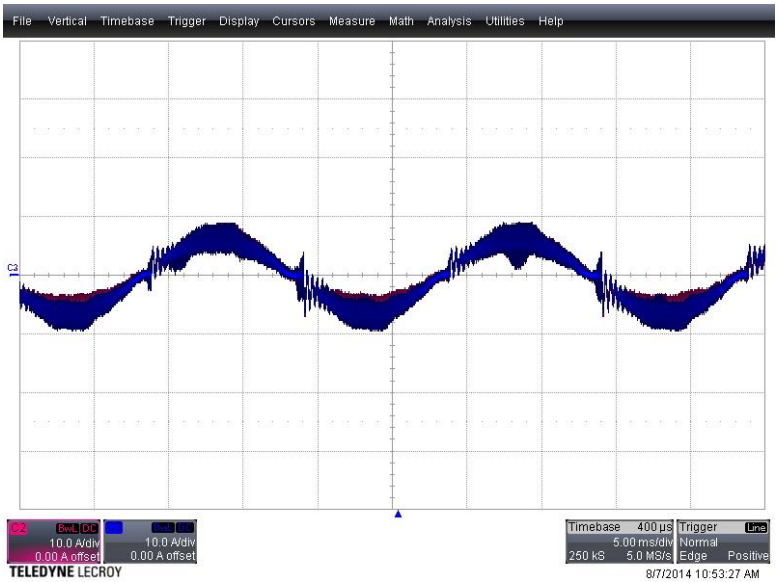

Figure 7.9: Output inductor current waveform with two 1 kW, interleaved modules (current 10 A/div), (time 5 ms/div)

The expansion of the scale on one of the measured current waveforms in Figure 7.9 allows the two waveforms to be distinguish and this is shown in Figure 7.10.

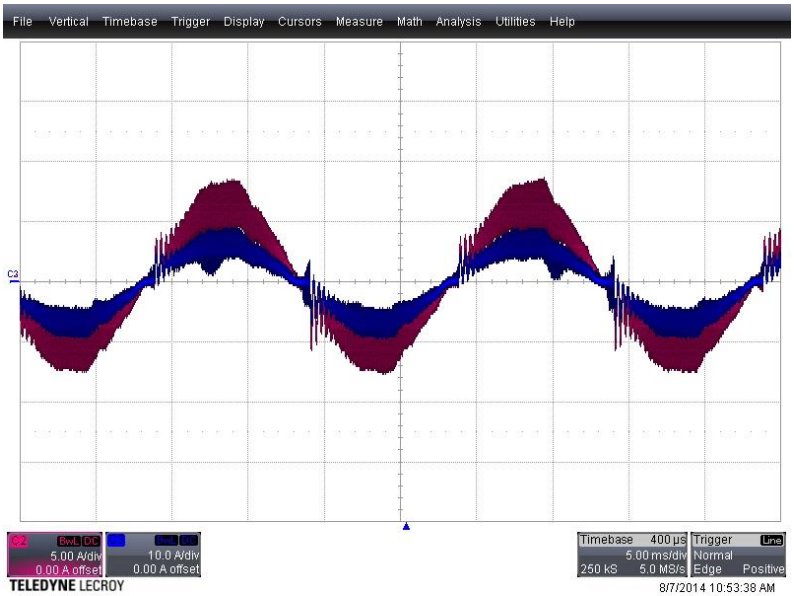

Figure 7.10: ***A repeat of Figure 6.9, with different scaling for the two modules, module A (5 A/div) and module B (10 A/Div) (time 5 ms/div)***

The benefit of interleaving on inductor current ripple reduction is demonstrated in Figure 7.11.

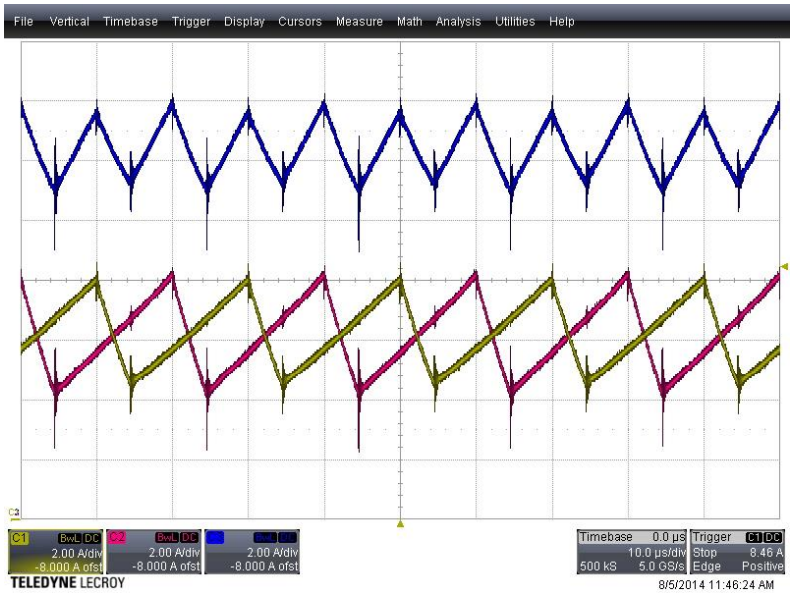

Figure 7.11: ***Close-up in inductor currents for Module A(yellow) and current in module B (red) and the total output inductor current at 2 kW (blue) in 2 A/div (time 10 µs/div)***

The bottom waveform in Figure 7.11 shows the output inductor currents for modules A and B, whilst the top waveform shows the sum of these two currents, which is fed to the output capacitor. The PWM signals generated by the FPGA for the two modules are phase shifted by 180°, and it can be seen that the total output current seen by the VCU output capacitor then has half the ripple magnitude at twice the frequency of the individual inductor currents. This so-called interleaving strategy reduces the size of the output capacitor and a similar effect occurs at the VCU input, which also allows the input capacitor to be minimised.

The interleaved AC chopper output voltage and current waveforms when supplying a 2 kW, lagging 0.98 power-factor load are shown in Figure 7.12.

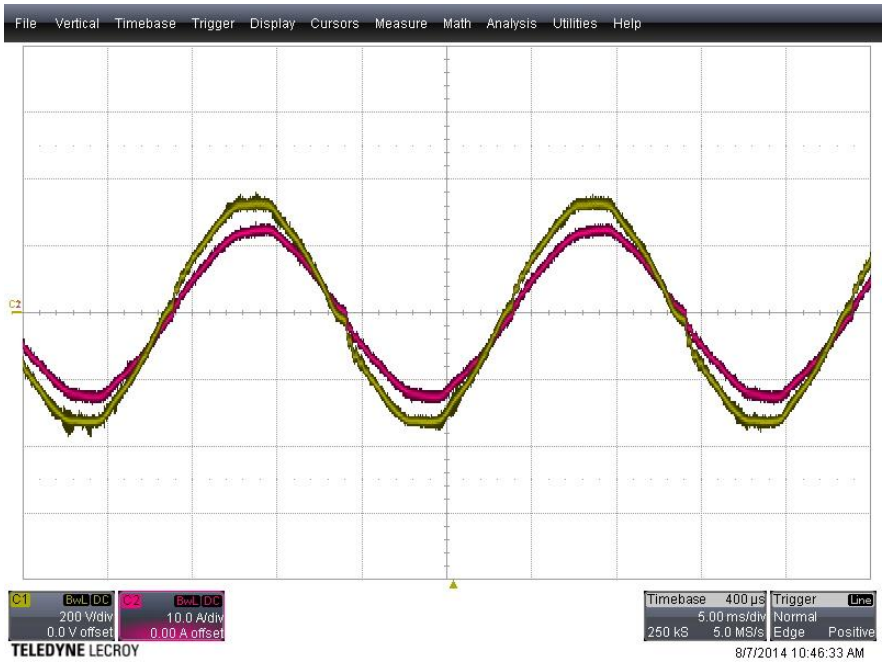

Figure 7.12: Module output voltage (200 V/div) and output current (10A/div) waveforms for 2 kW, 0.98 power factor output power (time 5 ms/div)

The performance of the AC Chopper with a reactive load was investigated experimentally. Three 10 mH, 50 Hz inductors in series with variable resistors were employed to reproduce a 1 kVA, 0.87 power factor load. As can be seen in Figure 7.13, the output voltage is near-sinusoidal, but the distortion on the input current has increased when compared the 0.98 power factor load. A possible reason for this that the errors in the current-sign detector circuit, which occur at the current zero-crossings, now coincides with point on the supply voltage waveform that is relatively large. Whereas, when the load power factor is high, as was the previous case, the zero-crossing occurs when the input supply voltage is close to zero.

Figure 7.13: ***Module output voltage (200 V/div) and input current (5 A/div) waveforms for 1 kVA, 0.87 power factor output power (time 5 ms/div)***

7.3 Converter Power Loss Measurement

The input and output power for one SiC based module when operating at 300 V/230 V, input/output voltage and a 50 kHz switching frequency was measured using two Voltech PM 1000 power analysers. The module was tested over a range of output powers from 500 W to 1000 W and the semiconductor and inductor losses were estimated by calculating the difference between the power analyser measurements. These results are shown by the blue diamond curve in Figure 7.14, where the losses have been multiplied by 15 to give an indication of the overall losses for a complete 15 kW converter.

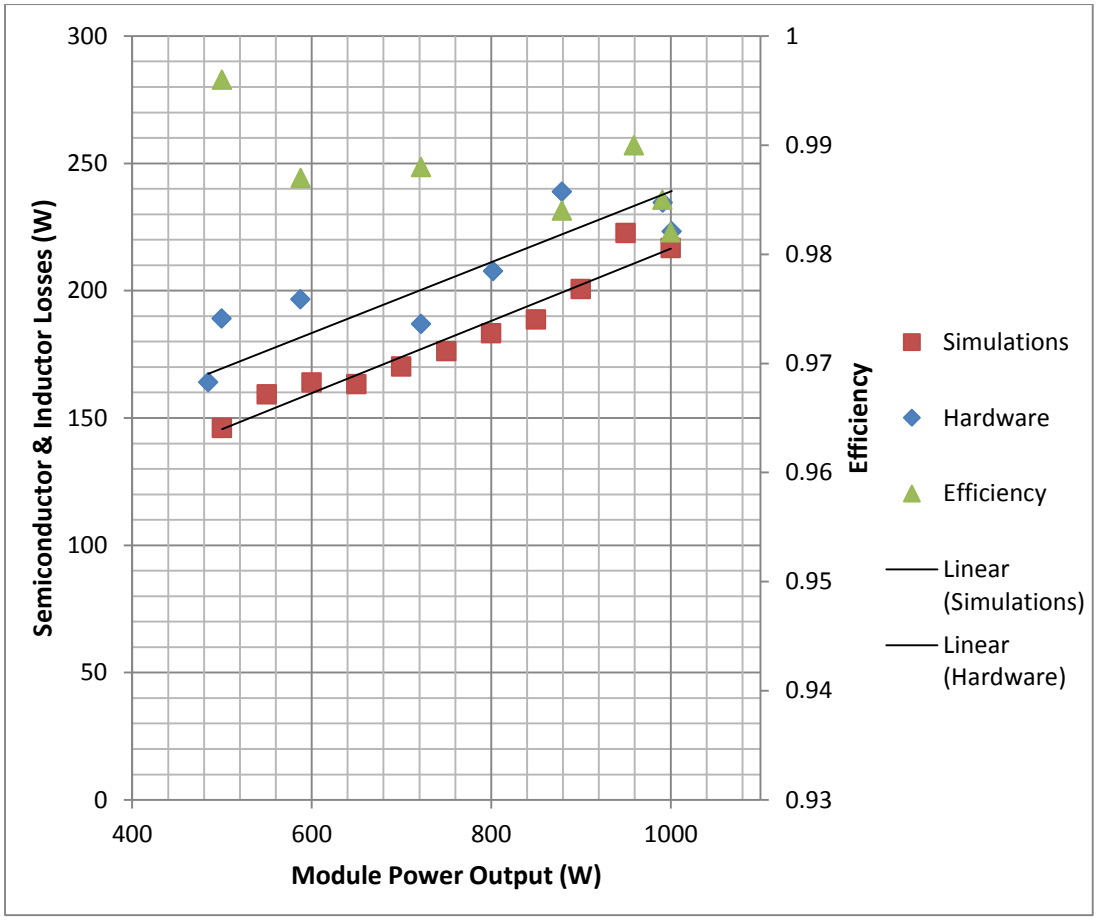

Figure 7.14: Measured (Hardware – blue diamonds) and predicted (Spice Simulation – red squares) semiconductor and inductor losses (W) as a function of individual module power rating (W) and corresponding converter efficiency (Hardware - green triangles)

The measured converter efficiency is also shown in Figure 7.14 by the green triangle curve. It can be seen that using 15 off, 1 kW modules the losses are approximately 225 W, which exceeds the target of 150 W. The 225 W losses correspond to an efficiency of 98.5 %. Lower overall losses can be obtained with more modules, for example 30 off 500 W modules would give losses of just above 150 W. A further increase in the number modules has a diminishing benefit as then switching losses tend to dominate.

Also shown in Figure 7.14 are the predicted Spice semiconductor losses, which were presented in Chapter 3. It can be seen that there is close agreement between the measured and predicted loss curves, the constant offset error being due to the fact that the Spice results do not include the inductor losses. These results therefore validate the simulation results and hence justified the conclusion that was drawn from the simulation studies that the AC Chopper was the most efficient topology when compared with the 2-leg and 3-leg converters.

At this point in the project the CREE CMF20120 Cree SiC MOSFETs that were used in the hardware prototype tests and the Spice simulations, became obsolete without any warning.

However, suppliers immediately replaced them with a new CREE SiC MOSFET device the C2M0080120D having a very similar specification. The SiC MOSFETs were therefore replaced in the converter prototype and subsequent tests were carried out using the newer devices.

Due to the limited accuracy of the power analysers, which was 0.3% or e=0.3/100, the differential method of measuring losses is not accurate enough for a high-efficiency converter. Since the losses are calculated as the difference between the input and output power measurements respectively, the maximum error in this calculation is potentially $e(\xi+1)/(\xi-1)$, where ξ is the converter efficiency and it is assumed that one analyser is reading high and one is reading low – see Appendix E for Mathematica derivation. With a target efficiency of $\xi=0.99$, and e=0.3/100 this gives a worst-case error of 60%, which is unacceptable. In practice the assumption of a maximum high and low reading on the two power analysers is not statistically realistic and the actual error will be somewhat lower than this value. For example, in Figure 7.15 illustrates the results of the measurement of the efficiency of the 2 kW interleaved AC Chopper using the new C2M0080120D MOSFETs against individual module power, where the red-curve is with power analyser 1 connected to the input and analyser 2 connected to the output, and the green-curve with the two meters swapped over.

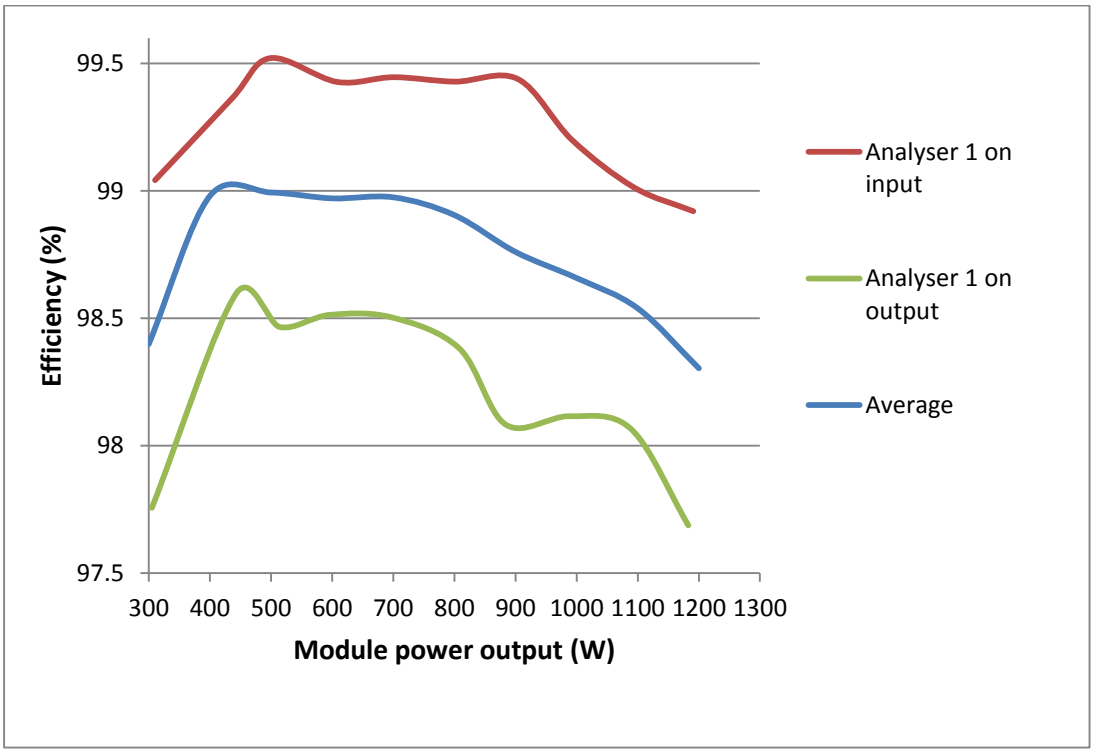

Figure 7.15: Converter efficiency as a function of module power rating (W) using the difference between two Voltech PM 1000 power analyser measurements, (red-curve) meter 1 input, meter 2 output, (green curve) meter 2 input, meter 1 output

It can be seen in Figure 7.15 and in Table 7-1 that there is a variation at the measured efficiency between the two configurations of the power analysers. The mean of these two configurations is shown by the blue curve and from Appendix E the maximum error of the mean is e=0.3/100 or 0.3 %. Assuming the mean is therefore a fairly accurate measurement of losses, the original measurements – the red and green curves in Figure 7.15 – are in error from the mean by approximately 0.5% efficiency, which corresponds to 75 W losses or a 50% error in the measurement of losses.

	Pin (W)	**Pout (W)**	**n (%)**
Power Analyser 1 on output	313.2	310.2	99.04215
	438	435.2	99.36073
	501	498.6	99.52096
	611.5	608	99.42764
	704.2	700.3	99.44618
	805.3	800.7	99.42878
	909	903.9	99.43894
	1000.3	992.3	99.20024
	1104.9	1094	99.01349
	1203.9	1190.9	98.92018
Power Analyser 2 on output	312	305	97.75641
	450	443.7	98.60000
	521.6	513.6	98.46626
	605.5	596.5	98.51363
	708.3	697.7	98.50346
	821.6	808.3	98.38121
	901.9	884.6	98.08183
	1008.4	989.4	98.11583
	1110.9	1089.4	98.06463
	1210.8	1182.8	97.68748

Table 7-1: **Voltech PM 1000 power analyser input and output power measurements**

However, there was no way to validate this analysis and alternative methods for measuring losses were investigated. For example a thermal-camera measurement was taken of the converter as shown in Figure 7.16. MOSFETs Q1 and Q2 shown in the figure are the upper MOSFETs of the chopper circuit, and because of the duty cycle associated with operating the converter at 300/230, input/output voltage these have higher losses than the lower devices. It is interesting to note the dissipation in the main power devices at 1 kW is similar to the DC-DC converters used for the gate drives and also the +/- 15V linear regulators used for the control electronics. The total power supplied to all four gate-drives used in the prototype was measured

from meter readings as 2.5 W and the gate-drive DC-DC converters had an efficiency of 85 % and the high dissipation from these devices can clearly be seen. In the final converter these losses would contribute significantly to the overall efficiency of the equipment and again, further work is needed to look at more efficient gate drive and auxiliary circuits. Unfortunately, whilst the camera method gave an accurate measurement of device temperatures, there was no way of relating this back to individual component losses.

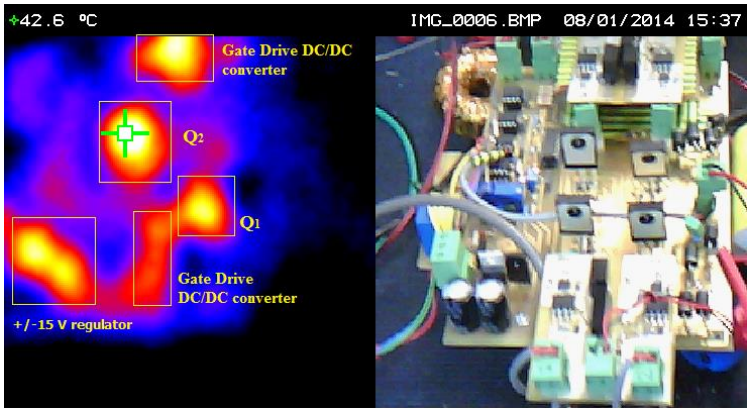

Figure 7.16: ***Thermal image of the module operating at 1 kW***

7.3.1 Calorimetric Method

In order to get a more accurate measurement of the VCU efficiency a calorimetric approach was utilised. This method consisted of first calibrating the temperature rise of the SiC MOSFETs and the inductor using known power dissipation in each device. This was achieved by injecting a DC current into each component to generate a conduction loss through the on-state resistance and winding resistance of the MOSFETs and inductor respectively. Since the device voltage and current was DC then these were easily measured to a high-accuracy using bench-top multi-meters. The measured DC voltage and current was then multiplied to calculate device power loss and a plot of loss against steady-state temperature rise was generated. Note that the MOSFETs remained on the PCB during these tests in order to ensure the thermal resistance of the environment around the devices did not change, whereas the inductor was placed inside a thermally insulated polystyrene box. Figure 7.17 and 7.18a show the power dissipation of each device against temperature rise above ambient (ΔT) and Figure 7.18b shows the open insulated box with the inductor placed inside – the insulated lid with thermometer can also be seen.

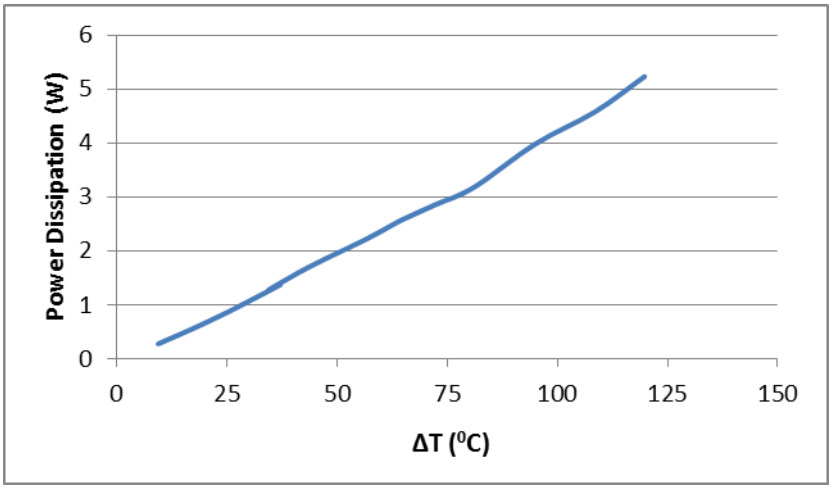

Figure 7.17: ***SiC MOSFET power dissipation against surface temperature rise***

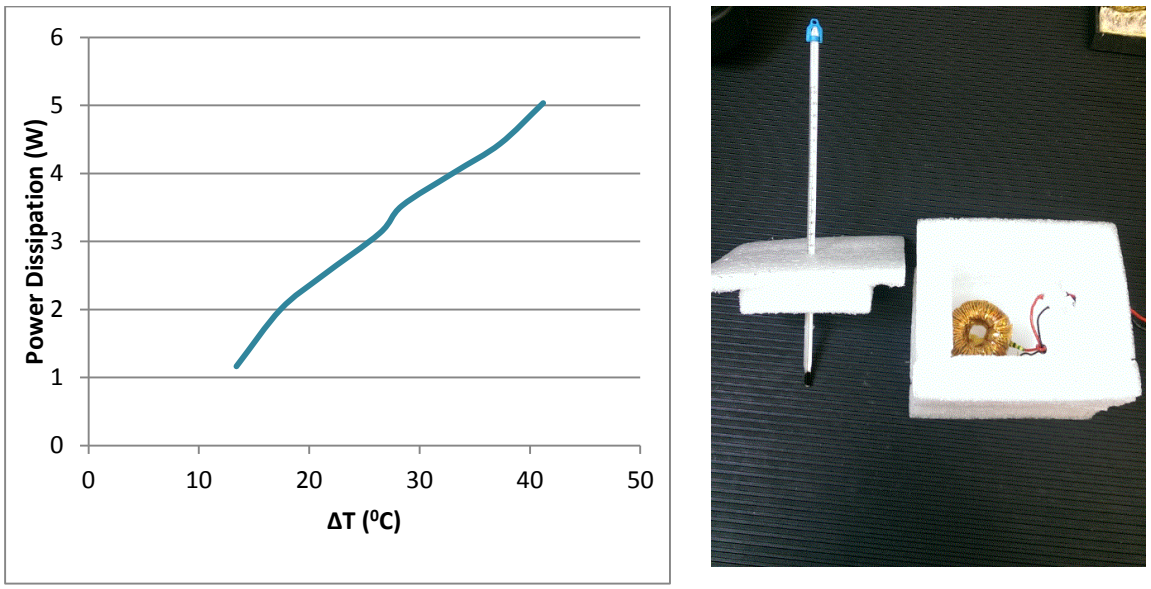

(a) ***(b)***

Figure 7.18: ***Calorimetric box (a) and Inductor power dissipation against surface temperature rise (b)***

From Figure 7.17 and 7.18a it can be seen that the temperature rise is almost linear with power dissipation for both the MOSFET and inductor, which give them an approximate equivalent thermal conductance of 0.044W/ ^{0}C and 0.133 W/ ^{0}C respectively.

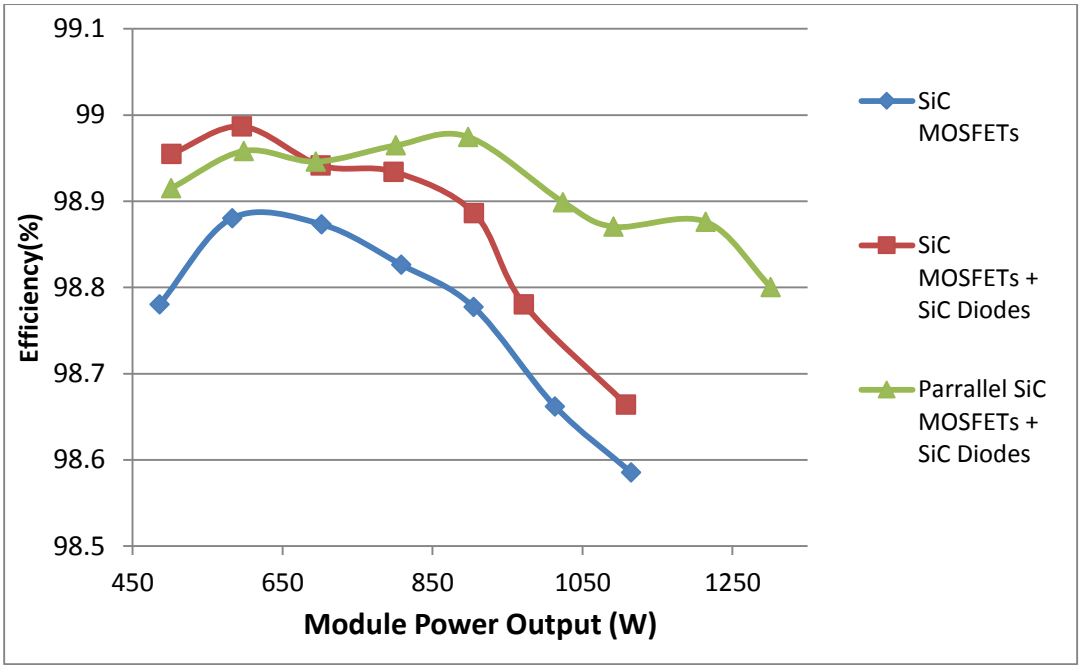

Figure 7.19: ***Total measured semiconductor and inductor losses (W) as a function of individual module power rating (W) using calorimetric method (blue curve) SiC MOSFETs only (red curve) SiC MOSFETs plus SiC anti-parallel diodes (green curve) two parallel MOSFETs***

The converter losses using the new CREE C2M0080120D MOSFETs were re-measured with the calorimeter method for a single 1 kW module. This involved measuring the temperature rise for each device and using the previously measured thermal conductance curves to estimate losses. Figure 7.19 illustrates the total measured semiconductor and inductor losses for three different scenarios. The blue curve shows the measured converter efficiency with the SiC MOSFETs, whereas the red curve shows the same configuration but with external SiC C4D20120A anti-parallel diodes, which have a superior reverse-recovery characteristic when compared to the MOSFET body-diode. Finally the green curve shows measurements when using two SiC MOSFETs connected in parallel with external SiC anti-parallel diodes.

	Pin (W)	Pout (W)	n (%)
SiC MOSFETs	492	486	98.78049
	589.5	582.9	98.88041
	710	702	98.87324
	818	808.4	98.82641
	916	904.8	98.77729
	1027	1013.26	98.66212
	1131	1115	98.58532
SiC MOSFETs & SiC Diodes	507.2	501.9	98.95505
	602	595.9	98.98671
	708.5	701	98.94143
	806.9	798.3	98.93419
	915.7	905.5	98.88610
	984	972	98.78049
	1123	1108	98.66429
Parallel SiC MOSFETs & SiC Diodes	507	501.5	98.91519
	604.8	598.5	98.95833
	702	694.6	98.94587
	809.5	801.12	98.96479
	907	897.7	98.97464
	1035.4	1024	98.89898
	1104	1091.53	98.87047
	1228	1214.2	98.87622
	1317	1301.2	98.80030

Table 7-2: Total measured input and output power and efficiency using calorimetric method

It can be seen also from Figure 7.19 and Table 7-2 which gives the exact measurement results that there is a significant improvement when utilising the SiC anti-parallel diodes. However, whilst these measurements do not include the external SiC diode losses, there was no discernible temperature rise in these diodes, indicating that their losses were negligible.

Comparing the red and green curves, the additional parallel MOSFET have again significantly reduced converter losses at power levels of 850 W and above. The improvement increases with power level indicating lower conduction losses, which is to be expected with the lower overall R_{DSon} that results from utilising two MOSFETs in parallel. The above measurements do not include the total gate drive losses which were measured to be 3 W for the red and blue curves and this increased to 4 W with the two parallel MOSFET case.

The effect of gate-drive resistance R_g, which influences the switching time of the MOSFETs, was investigated next. The converter efficiency when using a gate resistance of 4 Ω and 6 Ω is shown in Figure 7.20. This configuration is with two parallel MOSFETs and SiC anti-parallel diodes.

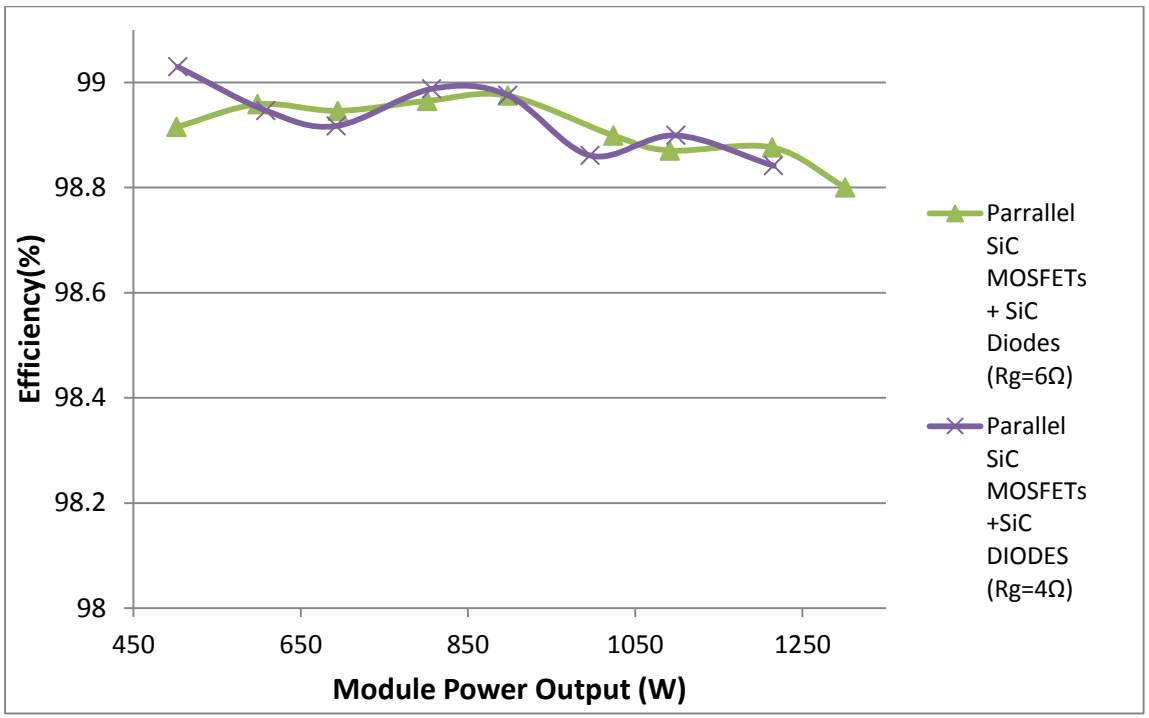

Figure 7.20*: Total measured semiconductor and inductor losses (W) as a function of individual module power rating (W) using calorimetric method (green curve) Rg=6 Ω and (purple curve) Rg=4 Ω*

Figure 7.20 shows that whilst there is some variation in losses between the use of a 4 Ω and 6 Ω gate resistor, the overall difference is negligible between loads of 450 W and 1250 W.

Again CREE released a newer improved device toward the very end of the project. This was the C2M0025120D, which has a lower on-state resistance of 25 mΩ when compared with 80 mΩ for the existing C2M0080120D. The converter efficiency was compared for a module containing 2 parallel C2M0080120D MOSFETs against a configuration with single C2M0025120D MOSFETs, and is shown in Figure 7.21. Both configurations had SiC anti-parallel diodes.

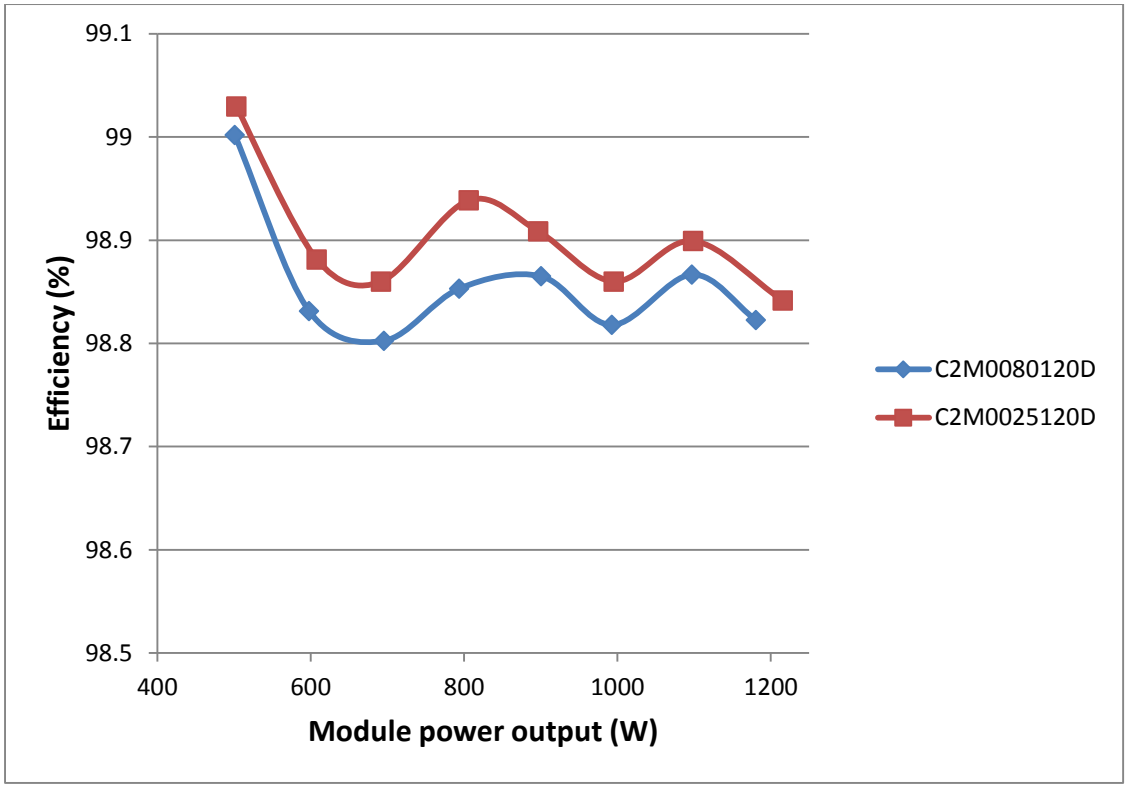

Figure 7.21: ***Total measured semiconductor and inductor losses (W) as a function of individual module power rating (W) using calorimetric method for (blue curve) the 80 mΩ C2M0080120D MOSFET and (red curve) the newer 25 mΩ C2M0025120D MOSFET***

Figure 7.21 shows an improvement in losses for the converter when using the newer 25 mΩ C2M0025120D MOSFET. The converter efficiency has improved by approximately 0.05%, when using single 25 mΩ devices compared with 2 parallel 80 mΩ devices. This improvement equates to 7.5 W overall losses.

7.4 Summary

To demonstrate the proposed VCU hardware using SiC power devices a single-phase AC chopper prototype was built and tested in the laboratory. In this chapter, the potential benefits that SiC power semiconductor devices can offer such as, high switching frequency and low power losses has been demonstrated by experimental verification. The important issues which require consideration when utilising SiC power devices was found to be:

- The fast switching of SiC MSOFETs generates undesirable noise in the electronics.
- This caused the current-sign detector to operate incorrectly around the zero-crossing of the output inductor current waveform.

- Errors in the current-sign detector led to large voltage spike across the MOSFETs, and it is hypothesised that this is what led to the low quality converter input current waveform.
- By using 2 of 80 mΩ MOSFETs in parallel for each device in the Chopper leg, the efficiency of the converter is very close to the target value of 99%.
- For newer C2M0025120D 25 mΩ MOSFETs the efficiency improves further and exceeds 99% for a module power rating of 500 W.

It was noted that all of the efficiency measurements shown in the above figures have an oscillatory shape; however it is not known what causes this effect.

8 Conclusion

This thesis has discussed the drive toward electricity as the dominant form of energy supply in the UK within the context of the so-called energy trilemma. LCTs will play a key role in future electricity generation and consumption profiles as a contribution towards a decarbonised electric future. The rapid increase in LCT systems installed in the LV distribution network will result in significant power and voltage regulation issues for DNOs. The solution proposed in this thesis was to raise the phase voltage in LV networks from 230 V to around 300 V, which will avoid the need for re-conductoring and hence provide benefits in terms of cost savings and the avoidance of disruption that re-conductoring produces. A device is then needed to step down the voltage from 300V to within the statutory limits at customer's premises. This device was termed a Voltage Control Unit (VCU). A power electronic based solution was found to be the strongest candidate for the VCU. In particular simulation studies and analysis showed that the single-phase AC Chopper utilising SiC MOSFETs and diodes could achieve the targeted efficiency and VA rating. The design and implementation of a 2 kW interleaved SiC AC Chopper module with an efficiency of 99 % as part of a total 15 kW VCU proved the concept of such a solution.

8.1 Enabling Low Carbon Technologies using SiC based converters

Most of the energy policies developed in the last decade in the UK are driven from initiatives around energy economics, energy security of the country and its future sustainability. All these drivers reflect a shift towards a low carbon energy infrastructure, where electricity will become a key part in solving the energy trilemma. Towards 2020 and according to policy makers, the UK will remain a leader among developing and developed economies in solving the energy trilemma. This will be through a push to being less dependent on fossil fuels and their imports and moving to a high penetration of LCTs such as DG, EVs and electro-heating. The DNOs in the UK will face significant challenges in the near future towards this shift to decarbonised electricity generation and consumption. Since it was first designed the LV network has been considered a passive network where the electricity flows in one direction from the bulk supply points to the end user. As the load demand and the installation of DG such as PV units increases, DNOs must start considering the LV network as being active and therefore will need to find solutions around capacity constraints and associated power quality issues. The conventional solution to these problems is reinforcement of the grid by utilising higher rating conductors. Besides the cost and the disruption to the public and business that this solution causes, it does not exploit the potential of new developments in power related technology. A number of "smarter" solutions have been proposed in the literature or have already been implemented in the LV networks. Automatic,

on-load tap-changers for distribution substation transformers, dynamic asset ratings, demand side management and energy storage schemes are just a few such "smart-grid" methodologies.

The work described in this thesis, which was funded by WPD who are the largest UK DNO covering the regions of the Midlands, the South West and South Wales, proposes a solution to the ease the congestion and power quality problems within the LV network. This proposal is to increase the existing local 230 V LV network phase-to-neutral voltage to at least 300 V, which is within the existing underground cable rating of 600 V. A VCU is then installed at each property to step the voltage down to the statutory 230 V. The location of the VCU is to be the electricity meter-box, which raises certain challenges. In particular, in order to avoid a significant temperature increase inside in the meter box which will affect the operation of the electricity meter and de-rate the existing 100 A service fuse, the VCU design must have extremely low losses. Furthermore, as the space and weight bearing capacity in the location is limited the VCU requires a high power density and low weight.

To assess the increase in LV network capacity that a higher network voltage would provide a basic analysis followed by a detailed load-flow analysis was carried out. These studies looked at three distinct types of LV network and proposed higher operating voltage levels were scored against the subsequent increased hosting capacity of slow, fast or rapid EV charging scenarios. The three networks that were investigated were Very Rural, Rural and Urban, and the load profiles for these networks were derived from stochastic energy models. Moreover, overvoltage issues occurring due to PV generation was also considered. The use of DC distribution was also investigated but was found not to be viable on the existing underground cabling due to capacity limits of the neutral conductor. Whilst it was found that 400 V AC was the optimum network voltage level in terms of a trade-off between increasing capacity and voltage stress on the VCU, no such voltage was available for prototype testing within the university laboratories. A voltage of 300 V was therefore used in the VCU simulation and designs.

A study of several topologies was carried out in order to determine the optimum configuration for this particular application in terms of efficiency and size/weight constrains. In addition, all the topologies under study were evaluated in terms of secondary benefits such as power quality improvement for the DNO and/or the end user. Conventional solutions such as wound transformers were found to have to low a power density and efficiency. Therefore a power electronic solution was investigated where several circuits were appraised and compared in terms of their VA rating. For unity VCU input power factor, the independent shunt series configuration (I-SHUSE) was found to have the lowest VA rating, followed by the dependent series/shunt and shunt series (D-SHUSE and D-SESHU). The non-isolated

back-to-back topology were also excluded from further investigation due to that fact the it does not provide a continuous neutral/earth link between the supply and the load.

Four candidate topologies proceeded for further detailed Spice simulation studies namely, the I-SHUSE, 2-Leg converter, the 3-Leg converter and the AC Chopper. However, due it's more complex structure and cost, it was decided to leave any further investigations of the I-SHUSE to the end of the project if time allowed.

If the 2 and 3-Leg represent the highest performance in terms of power quality, then the AC chopper is an example of low performance device however it is a near-optimum solution in terms of voltage step-down capability in the context of reduced converter size, weight and control complexity. However, in terms of power quality, the basic chopper circuit only provides a regulated, sinusoidal voltage to the load.

Manufacturer's Spice models were used for three different types of semiconductor devices, Si IGBTs, Si MOSFETs and SiC MOSFETs in order to calculate losses. This work concluded that the targeted efficiency could only be met by (a) the utilisation of SiC devices and (b) using the AC Chopper, which produced the lowest semiconductor losses from the three candidate circuits. In particular, the total semiconductor losses for a 15 kW single-phase SiC AC Chopper found to be 148 W, which was the target specification for the VCU. It was decided that a prototype Chopper would be built using a parallel modular approach to allow the use of available TO247 package CREE MOSFETs. This method could then also exploit the ability to interleave the switching of individual models to reduce input and output capacitor sizes and also permit the hot-swapping or by-passing of faulty modules.

The experimental verification of the AC Chopper was considered a key part of the project in order to demonstrate the feasibility of the proposed technology. A 2 kW interleaved SiC based prototype was built and tested in the laboratory. The design of the prototype included the consideration of the auxiliary circuits such as the FPGA 4-step commutation control, the protection and current-sign detection circuit, the gate drive circuits and the design of passive components such as the output inductor and input and output filter capacitors. Power quality issues around the distortion of the input current were found to be a problem and this was thought to be due to MOSFET high-speed switching, which was contaminating the current-sign detector circuit.

Various methods of measuring the efficiency of the VCU prototype were investigated. The differential power analyser method was found to be too inaccurate, and therefore an alternative calorimetric approach was used. The overall efficiency of the converter power electronics and filter inductor achieved 98.95% with two parallel 80 mΩ CREE SiC MOSFETS and SiC anti-parallel diodes, which corresponds to a VCU loss of 158 W.

8.2 Contributions of this Research

The research described in this thesis helps identify what the drivers are for a change towards a higher utilisation of electricity as a means of energy supply, what problems these changes cause to the distribution network and what are the potential solutions. In addition, an important impact of this research project is to motivate key stakeholders for example regulators, DNOs, manufacturers, and consumers, to create the necessary conditions and incentive mechanisms so that the added benefits from LCT deployment can be sufficiently exploited.

The main contributions of the research presented in this thesis are that it:

- Proposes a solution to facilitate the penetration of LCTs in LV networks by increasing the capacity of the network without changing the existing infrastructure. This is achieved by increasing the AC voltage in the LV distribution networks.
- Investigates the most appropriate voltage step-down topologies among a number of conventional power electronic circuits by deriving VA rating analysis.
- Introduces a new topology for this application termed the I-SHUSE, which is able to step-down the voltage at unity input factor and provide secondary power quality benefits such as removing currents harmonics in LV networks. The combination of a shunt CSI and a series VSI with the above features has not been reported in the literature.
- Introduces a new application of an existing topology with a voltage ratio of 300 V to 230 V.
- Demonstrates the application of SiC devices in a 2kW prototype to achieve efficiency above 99%.

Finally, it is worth to mention that this research work constituted the basis for a follow-on research project titled “A Low Cost, High Capacity, Smart Residential Distribution Network Enabled By SiC Power Electronics” InnovateUK Project Number 101994, with company partners Exception EMS, Schneider Electric, Western Power Distribution, Anvil Semiconductors, Turbo Power Systems and Aston University. The project value is around £1 million and lasts from January 2015 to January 2018. The project will look at taking the SiC based Chopper concept developed in this project toward a commercial product.

8.3 Publications arising from this Work

- **Zacharis, E**.; Cross, A.M.; Godfrey, B.; Safari, S.; Castellazzi, A.; Ward, P.; Mosely, I., "High efficiency SiC AC chopper for LV networks," Power Electronics, Machines and Drives (PEMD 2014), 7th IET International Conference on , vol., no., pp.1,6, 8-10 April 2014
- **Zacharis, E.**; Cross, A.M.; Godfrey, B., "Power electronic interfaces for low voltage residential networks," Power Electronics and Applications (EPE), 2013 15th European Conference on , vol., no., pp.1,10, 2-6 Sept. 2013
- **Zacharis, E.**; Cross, A.M.; Godfrey, B., "Power quality improvements for LV networks," Power Quality, IET Seminar on , vol., no., pp.1,2, 6-6 Nov. 2012

8.4 Future work

In terms of future work, then firstly a consideration of the integration of energy storage into the VCU would provide a fault ride-through capability during power outages, which would bring benefits to the customer – a more secure supply – and DNOs who would benefit from avoiding financial penalties applied by the regulator.

Moreover, EVs in this work were considered as additional loads on the LV network. It would be interesting to investigate their behaviour during the reverse power flow operation when they provide extra power to the grid if it is needed under the Vehicle to Grid (V2G) scheme. The implementation of a VCU communication network in an LV network would facilitate a "selective" fast-charging scheme for EVs on a residential network. Here power usage information would be shared between VCUs on a local network. The VCU would provide a separate charging outlet, which would only be enabled providing the total number of fast-charges being used on the network at any one time does not overload the main feeder cable.

In this work an open-loop voltage control was implemented for the single-phase AC/AC Chopper converter. Time constrains and research prioritisation didn't allow the researcher to implement a closed loop control. However, by adding a closed-loop output voltage control, this would allow a higher relaxation of the voltage limits on the sub-station side of the VCU, which would benefit the DNOs in terms of voltage regulation requirements. For example, the current problem of voltage rise on the network caused by the increased use of domestic PV arrays would be alleviated since the VCU at each house would ensure the voltage at the property was kept within statutory limits. The ability of the DNO to adjust the VCU output voltage via a communications network would also be beneficial in terms of reducing the demand from resistive loads at peak times, so- called demand-side-management (DSM).

The analysis conducted in this work has resulted in the proposal for the I-SHUSE topology for this application. This device promises to be more power-dense than the AC Chopper, whilst having a more robust design and providing functions for power-quality improvement. Further investigation into the feasibility of this topology may be lead to a more suitable AC/AC converter.

The problem of the noise entering the current-sign detector needs further work. In fact one of the main issues discovered when using SiC MOSFETs is the noise generated by the fast switching of these devices and methods of controlling this problem need careful consideration. A more robust solution for the current-sign detector may be to insert two back-back SiC diodes in the main current path and use the sign of the on-state voltage across these diodes as an indication of current direction. This is a technique currently used in high-power matrix converters. The solution to filter the harmonic(s) by using an enhanced passive filter at the input and the output of the VCU will cause an increase in the size of the converter module. At this point further work needed to evaluate the trade-off between the size, the efficiency and the power quality requirements. If, the power quality is the first priority other candidate topologies - not selected for this application, but presented in Table 4-3 would appear to be more functional in comparison with the AC Chopper.

Conventional 4H SiC has a high cost compared with conventional Si devices such as MOSFETs. The viability of new 3C SiC based semiconductors needs further investigation as they promise better performance at a much lower cost than existing 4H devices. This work is currently being undertaken by the follow-on InnovateUK project described in section 7.1, where Anvil Semiconductors are trialling their new 3C-SiC on Si technology. Moreover, a high-power module based, bidirectional-switch structure using a combined SiCMOSFET/Schottky diode would be beneficial in terms of reducing stray parasitic inductance so that even higher switching frequency operation could be achieved.

The protection scheme used in this work for the VCU was very basic consisting of just VCU overcurrent detection and an input and output voltage clamp circuits. A consideration of the co-ordination of the VCU with the existing circuit-breakers in a house under faulted operation needs further investigation. For example, the VCU must be able to source enough fault current to trip the devices in the house if needed.

References

[1] UK Government (2008), `Climate Change Act'. Available online: http://www.legislation.gov.uk/

[2] Department of Energy and Climate Change (2012*c*), Updated energy and emissions projections 2012, Technical Report October.

[3] Council Directive 2001/80/EU (2001), `DIRECTIVE 2001/80/EC OF THE EUROPEAN PARLIAMENT AND OF THE COUNCIL of 23 October 2001 on the limitation of emissions of certain pollutants into the air from large combustion plants'.

[4] Department of Energy and Climate Change (2013*c*), `Electricity Market Reform: Delivering UK Investment'.

[5] The Stationary Office (2002), `The Renewables Obligation Order'.

[6] The Stationary Office (2008), `The Enegy Act'.

[7] World Energy Trilemma Time to get real – the myths and realities of financing energy systems World Energy Council 2014

[8] Costantini, V. and Martini, C. (2010), `The causality between energy consumption and economic growth: A multi-sectoral analysis using non-stationary cointegrated panel data', *Energy Economics* 32(3), 59-603.

[9] Stern, D. I. (2011), `The role of energy in economic growth.', *Annals of the New York Academy of Sciences* 1219, 26-51.

[10] Cleveland. (2014). Energy quality. Available online: http://www.eoearth.org/view/article/152555

[11] Hall, C., Cleveland, C. and Kaufmann, R. (1986), *Energy and resource quality: the ecology of the economic process*.

[12] Jorgenson, D. W. (1984), `The role of energy in productivity growth', *Energy Journal* 5(3), 11-26.

[13] Kaufmann, R. K. (1994), `The relation between marginal product and price in US energy markets Implications for climate change policy', *Energy Economics* 16(2), 145{158.

[14] Mackay, D. (2009), *Sustainable Energy without the hot air*, UIT Cambridge.

[15] Schurr, S. and Netschert, B. (1960), `Energy and the American Economy, 1850-1975', *Johns Hopkins University Press. Baltimore.*

[16] Stern, D. I. and Cleveland, C. (2004), `Energy and Economic Growth', *Rensselaer Working Papers in Economics No. 0410* (April)

[17] Speirs, J., Gross, R., Deshmukh, S., Heptonstall, P., Leach, M. and Torriti, J. (2010), Heat delivery in a low carbon economy, Technical Report Opsi 2008.

[18] UK Government (2012) Electricity Market Reform: policy overview

[19] Sims, R. E. H., Schock, R. N., Adegbululgbe, A., Fenhann, J., Konstantinaviciute, I., Moomaw, W., Nimir, H. B., Schlamadinger, B., Turner, C., Uchiyama, Y., Wamukonya, N., Zhang, X., Davidson, O. R., Bosch, P. R., Dave, R. and Kingdom, U. (2007), Energy supply, *in* `Climate Change 2007: Working Group III: Mitigation of Climate Change', Cambridge University Press.

[20] Levine, M., • Urge Vorsatz, D., Blok, K., Geng, L., Harvey, D., Lang, S., Levermore, G Mehlwana, A. M., Mirasgedis, S., Novikova, A., Rilling, J. and Yoshino, H. (2007), Residential and comer cial buildings, *in* B. Metz, O. R. Davidson, P. R. Bosch, R. Dave and L. A. Meyer, eds, `Climate Change 2007: Mitigation. Contribution of Working Group III to the Fourth Assessmen Report of the Intergovernmental Panel on Climate Change', Cambridge University Press.

[21] UNFCCC. Fact sheet: Climate change science - the status of climate change science today Available Online: http://unfccc.int/press/fact_sheets/items/4987.php

[22] Blanco G., R. Gerlagh, S. Suh, J. Barrett, H.C. de Coninck, C.F. Diaz Morejon, R. Mathur, N. Nakicenovic, A. Ofosu Ahenkora, J. Pan, H. Pathak, J. Rice, R. Richels, S.J. Smith, D.I. Stern, F.L. Toth, and P. Zhou, 2014: Drivers, Trends and Mitigation. In: Climate Change 2014: Mitigation of Climate Change. Contribution of Working Group III to the Fifth Assessment Report of the Intergovernmental Panel on Climate Change [Edenhofer, O., R. Pichs-Madruga, Y. Sokona, E. Farahani, S. Kadner, K. Seyboth, A. Adler, I. Baum, S. Brunner, P. Eickemeier, B. Kriemann, J. Savolainen, S. Schlömer, C. von Stechow, T. Zwickel and J.C. Minx (eds.)]. Cambridge University Press, Cambridge, United Kingdom and New York, NY, USA

[23] Bruckner T., I.A. Bashmakov, Y. Mulugetta, H. Chum, A. de la Vega Navarro, J. Edmonds, A. Faaij, B. Fungtammasan, A. Garg, E. Hertwich, D. Honnery, D. Infield, M. Kainuma, S. Khennas, S. Kim, H.B. Nimir, K. Riahi, N. Strachan, R. Wiser, and X. Zhang, 2014: Energy Systems. In: Climate Change 2014: Mitigation of Climate Change. Contribution of Working Group III to the Fifth Assessment Report of the Intergovernmental Panel on Climate Change [Edenhofer, O., R. Pichs-Madruga, Y. Sokona, E. Farahani, S. Kadner, K. Seyboth, A. Adler, I. Baum, S. Brunner, P. Eickemeier, B. Kriemann, J. Savolainen, S. Schlömer, C. von Stechow, T. Zwickel and J.C. Minx (eds.)]. Cambridge University Press, Cambridge, United Kingdom and New York, NY, USA.

[24] UNFCCC. Kyoto Protocol [Online]. Available online: http://unfccc.int/kyoto_protocol/items/2830.php

[25] Grubb, M., Haites, E., Omassoli, S., Bremner, C., Vincent, D., Purvis, N., Muller, B., Butler, N., Kameyama, Y., Sato, M. and Safonov, Y. (2008), `Energy and Climate : Opportunities for the G8', *Cambridge Centre for Energy Studies* .

[26] CEC (2008*)* Proposal for a directive on the promotion of the use of energy from renewable sources. Technical report, Technical report, European Commission, Brussels.

[27] A Roadmap for moving to a competition low carbon economy in 2050," European Commission, available online at http://ec.europa.eu/clima/policies/roadmap/index_en.htm., Brussels, 2011.

[28] "The EU's Target for Renewable Energy: 20% by 2020 - Volume I: Report," House of Lords, European Union Committee, London, 2008.

[29] "The UK Renewable Energy Strategy," ed: The Secretary of State for Energy and Climate Change, HM Government, 2009.

[30] MacLeay, I., Harris, K. and Michaels, C. (2007), Digest of United Kingdom Energy Statistics, Technical report.

[31] Barnacle, M., Robertson, E., Galloway, S., Barton, J. and Ault, G. (2013), `Modelling generation and infrastructure requirements for transition pathways', *Energy Policy* 52, 60-75.

[32] Foxon, T. J. (2013), `Transition pathways for a UK low carbon electricity future', *Energy Policy* 52, 10-24.

[33] Energy Statistics Team, Energy Trends June 2013. Available online: https://www.gov.uk/government/uploads/system/uploads/attachment_data/file/208560/et_june_2013.PDF

[34] EIA, "International Energy Outlook," U.S. Energy Information Administration, Office of Integrated Analysis and Forecasting, 2010.

[35] DECC, "UK Energy in Brief," Department for Energy & Climate Change, A National Statistics Publication, 2014.

[36] Hinnells, M. (2008), `Technologies to achieve demand reduction and microgeneration in buildings', *Energy Policy* 36(12), 4427{4433.

[37] Council Directive 2001/80/EU (2001), `DIRECTIVE 2001/80/EC OF THE EUROPEAN PARLIAMENT AND OF THE COUNCIL of 23 October 2001 on the limitation of emissions of certain pollutants into the air from large combustion plants'.

[38] Department of Energy and Climate Change (2012), Gas Generation Strategy, Technical Report December 2012.

[39] Electricity Capacity Assessment Report 2013 Report to the Secretary of State, Technical report. Ofgem (2013)

[40] Skea, J., Green, T., Heptonstall, P., Leach, M., Anderson, D. and Gross, R. (2007), `Renewables and the grid: understanding intermittency', *Proceedings of the ICE - Energy* 160(1), 31-41.

[41] Watson, J. (2003), UK Electricity Scenarios for 2050, Technical Report November.

[42] Ault, G., Frame, D., Hughes, N., Strachan, N., Watson, J. and Pollitt, M. (2008), Electricity Network Scenarios for Great Britain in 2050 Final Report for Ofgem's LENS Project, Technical Report 157.

[43] Foxon, T. J., Hammond, G. P. and Pearson, P. J. G. (2010), `Developing transition pathways for a low carbon electricity system in the UK', *Technological Forecasting and Social Change* 77(8), 1203{1213.

[44] Electricity Networks Strategy Group (2010), A Smart Grid Routemap, Technical Report February, UK Government.

[45] Department of Energy and Climate Change (2010), 2050 Pathways Analysis, Technical Report July.

[46] National Grid (2010), National Electricity Transmission System Seven Year Statement, Technical report.

[47] National Grid (2014), National Electricity Transmission System Ten Year Statement, Technical report.

[48] Ault, G., Elders, I., Mcdonald, J., Burt, G. and Tumilty, R. (2006), SuperGen Future Network Technologies Consortium Electricity Network Scenarios for 2020, Technical Report July.

[49] 2014 Future Energy Scenarios, National Grid Company, 2014.

[50] Electricity System: assessment of future challenges – annex, DECC, 2012

[51] Ault, G., Frame, D., Hughes, N., Strachan, N., Watson, J. and Pollitt, M. (2008), Electricity Network Scenarios for Great Britain in 2050 Final Report for Ofgem's LENS Project, Technical Report 157.

[52] Ekins, P., Strachan, N., Keppo, I., Skea, J., Usher, W. and Anandarajah, G. (2013), The UK energy system in 2050: Comparing Low-Carbon, Resilient Scenarios, Technical report, UKERC.

[53] H.L. & Scott, W.G., 2000. *Distributed Power Generation Planning and Evaluation* 1st ed., New York, Basel: Marcel Dekker Inc.

[54] Digest of United Kingdom Energy Statistics, 2014

[55] THE DISTRIBUTION CODE and THE GUIDE TO THE DISTRIBUTION CODE OF LICENSED DISTRIBUTION NETWORK OPERATORS OF GREAT BRITAIN, 2012

[56] DTI, "Review of Distributed Generation," DTI (now Department for Business Innovation and Skills, BIS), London U.K.May 2007 2007.

[57] ENA, "Distributed Generation Connection Guide " Energy Network Association, London, 2010

[58] T. Ackermann, G. Andersson, and L. Söder, "Distributed generation: a definition," *Electric Power Systems Research,* vol. 57, pp. 195-204, 2001.

[59] Carmen LT Borges and Djalma M Falcao. Optimal distributed generation allocation for reliability, losses, and voltage improvement. *International Journal of Electrical Power & Energy Systems*, 28(6):413–420,2006.

[60] Dondi, P., Bayoumi D., Haederli C., Julian D., Suter M. Network integration of distributed power generation. *Journal of Power Sources*, (1-2):1–9, April 2002.

[61] J. Lopes, N. Hatziargyriou, J. Mutale, P. Djapic, and N. Jenkins. Integrating distributed generation into electric power systems: A review of drivers, challenges and opportunities. *Electric Power Systems Research*, 77(9):1189–1203, July 2007.

[62] L. F. Ochoa, A. Padilha-Feltrin, and G. P. Harrison. Evaluating distributed generation impacts with a multiobjective index. *Power Delivery, IEEE Transactions on*, 21(3):1452–1458, July 2006.

[63] PasseyR., Spooner T., MacGill I., Watt M., and Syngellakis K.. The potential impacts of grid-connected distributed generation and how to address them: A review of technical and nontechnical factors. *Energy Policy*, 39(10):6280–6290, October 2011.

[64] Pepermans, G., Driesen, J., Haeseldonckx, D., Belmans, R., & D'haeseleer, W. (2005). Distributed generation: definition, benefits and issues. Energy policy, 33(6), 787-798.

[65] Cavlovic M., Challenges of optimizing the integration of distributed generation into the distribution network. In *2011 8th International Conference on the European Energy Market (EEM)*, pages 419–426. IEEE, May 2011.

[66] E. J. Coster, J. M. A. Myrzik, B. Kruimer, and W. L. Kling. Integration Issues of Distributed Generation in Distribution Grids. *Proceedings of the IEEE*, 99(1):28–39, January 2011.

[67] Rajkumar Viral and D. K. Khatod. Optimal planning of distributed generation systems in distribution system: A review. *Renewable and Sustainable Energy Reviews*, 16(7):5146–5165, September 2012.

[68] I. Burdon, "Implementation of a medium-scale CHP scheme," *Power Engineering Journal*, vol. 8, no. 6, pp. 265–271, 1994.

[69] C. Williams, "CHP systems," *Distributed Energy*, pp. 57-59, 2003.

[70] Handbook for implementing the RIIO model, OFGEM, 2010.

[71] F. Pilo, G. Celli, and S. Mocci, "Improvement of reliability in active networks with Intentional islanding," in *IEEE Electric Utility Deregulation, Restructuring and Power Technologies*, in Hong Kong, 2-5 April, 2004, vol. 2, pp. 474-479.

[72] P. Fuangfoo, W.-J. Lee, and M.-T. Kuo, "Impact Study on Intentional Islanding of Distributed Generation Connected to a Radial Subtransmission System in Thailand's Electric Power System," *IEEE Trans. on Industry Applications*, vol. 43, pp. 1491-1498, 2007.

[73] W. Helmy, Y. G. Hegazy, M. A. Mostafa, and M. A. Badr, "Strategic Placement of Distributed Generation Units to Avoid Load Shedding in Overloaded Power Systems," in *WSEAS Trans. on POWER SYSTEMS*, in Venice, Italy, 2007, pp. 261-270.

[74] Fritz, J. & Russ, D.H., 2002. *Non-Technical Losses in Electrical Power Systems*.Ohio University.

[75] P. Chiradeja, "Benefit of distributed generation: A line loss reduction analysis," in *Transmission and Distribution Conference and Exhibition*, Asia and Pacific, 2005.

[76] Dugan and T McDermott, "Distributed generation impact on reliability and power quality," in *IEEE*, 2002

[77] González-Longatt, F.M., 2007. Impact of Distributed Generation over Power Losses on Distribution System. In *9th International Conference, Electrical Power Quality and Utilisation*. Barcelona.

[78] Delfanti, M., Falabretti, D. & Merlo, M., 2013. Dispersed generation impact on distribution network losses. *Electric Power Systems Research*, 97, pp.10–18.

[79] Costa, P.M. & Matos, M.A., 2009. Avoided losses on LV networks as a result of microgeneration. *Electric Power Systems Research*, 79(4), pp.629–634.

[80] A. Rathnayaka, V. Potdar, O. Hussain, and T. Dillon, “Identifying prosumer’s energy sharing behaviours for forming optimal prosumer-communities,” in *Cloud and Service Computing (CSC), 2011 International Conference on*, dec. 2011, pp. 199 –206.

[81] Bertini, D. et al., 2011. Hosting Capacity of Italian Distribution Networks. In *CIRED 21st International Conference on Electricity Distribution*. Frankfurt, Germany, pp. 6–9.

[82] HMSO, 2002. *The Electricity Safety, Quality and Continuity Regulations 2002*, UK: HMSO, no 2665

[83] BS EN 50160:2007 Voltage characteristics of electricity supplied by public distribution networks

[84] Demirok, E. et al., 2011. Local Reactive Power Control Methods for Overvoltage Prevention of Distributed Solar Inverters in Low-Voltage Grids. *IEEE Journal of Photvoltaics*, 1(2), pp.174–182.

[85] Canova, A. et al., 2009. Electrical Impact Of Photovoltaic Plant In Distributed Network. *IEEE Transactions on Industry Applications*, 45(1), pp.341–347.

[86] Masters, C.L., 2002. Voltage rise the big issue when connecting embedded generation to long 11 kV overhead lines. *Power Engineering Journal*, 16(1), pp.5–12.

[87] Ali, S., Pearsall, N. & Putrus, G., 2012. Impact of High Penetration Level of Grid- Connected Photovoltaic Systems on the UK Low Voltage Distribution Network. In *International Conference on Renewable Energies and Power Quality*. Santiago de Compostela, Spain.

[88] Alam, M.J.E., Muttaqi, K.M. & Sutanto, D., 2013. Mitigation of Rooftop Solar PV Impacts and Evening Peak Support by Managing Available Capacity of Distributed Energy Storage Systems. *IEEE Transactions on Power Systems*, 28(4), pp.3874 – 3884.

[89] Masoum, A.S. et al., 2012. Impact of Rooftop PV Generation on Distribution Transformer and Voltage Profile of Residential and Commercial Networks. In *IEEE PES Innovative Smart Grid Technologies*. Washington DC, pp. 1–7.

[90] C. Gonzalez et al., "LV distribution network feeders in Belgium and power quality issues due to increasing PV penetration levels," in *Innovative Smart Grid Technologies (ISGT Europe), 2012 3rd IEEE PES International Conference and Exhibition on*, 2012, pp. 1-8.

[91] Thomson, M. & Infield, D.G., 2007. Impact of widespread photovoltaics generation on distribution systems. *IET Renewable Power Generation*, 1(1), pp.33–40.

[92] Conti, S. et al., 2003. Integration of multiple PV units in urban power distribution systems. *Solar Energy*, 75(2), pp.87–94.

[93] Assessing the impact of low carbon technologies on Great Britain's power distribution networks, Ofgem 2012

[94] González-Longatt, F.M., 2007. Impact of Distributed Generation over Power Losses on Distribution System. In *9th Internation Conference, Electrical Power Quality and Utilisation*. Barcelona.

[95] Navarro, A., Ochoa, L.F. & Randles, D., 2013. Monte Carlo-Based Assessment of PV Impacts on Real UK Low Voltage Networks. In *IEEE Power and Energy Society General Meeting*. Vancouver, BC, pp. 1–5.

[96] Singh, A.K., Singh, G.K. & Mitra, R., 2007. Some Observations on Definitions of Voltage Unbalance. In *2007 39th North American Power Symposium*. IEEE, pp.473–479.

[97] Shahnia, F. et al., 2011. Voltage imbalance analysis in residential low voltage distribution networks with rooftop PVs. *Electric Power Systems Research*, 81(9), pp.1805–1814.

[98] Low Voltage Network Solutions. A First Tier Low Carbon Networks Fund Project Closedown Report, ENW, 2014

[99] Woyte, A. et al., 2006. Voltage Fluctuations on Distribution Level Introduced by Photovoltaic Systems. *IEEE Transactions on Energy Conversion*, 21(1), pp.202– 209.

[100] Latheef, A.A., Gosbell, V.J. & Smith, V., 2006. Harmonic Impact of Residential Type Photovoltaic Inverters on 11kV Distribution System. In *Australian Universities Power Engineering Conference*. Melbourne, Victoria.

[101] Papaioannou, I.T. et al., 2008. Harmonic Impact of Small Photovoltaic Systems Connected to the LV Distribution Network. In *5th International Conference on European Electricity Market, 2008. EEM 2008.* Lisbon.

[102] Jegathesan, V. & Jerome, J., 2011. Elimination of lower order harmonics in Voltage Source Inverter feeding an induction motor drive using Evolutionary Algorithms. *Expert Systems with Applications*, 38(1), pp.692–699.

[103] Fekete, K., Klaic, Z. & Majdandzic, L., 2012. Expansion of the residential photovoltaic systems and its harmonic impact on the distribution grid. *Renewable Energy*, 43, pp.140–148.

[104] I.T. and Bouhouras, A.S. and Marinopoulos, A.G. and Alexiadis, M.C. and Demoulias, C.S. and Labridis, D.P. Papaioannou, "Harmonic impact of small photovoltaic systems connected to the LV distribution network," in *Electricity Market, 2008. EEM 2008. 5th International Conference on European*, 2008, pp. 1-6.

[105] Moeed Amjad, A. & Salam, Z., 2014. A review of soft computing methods for harmonics elimination PWM for inverters in renewable energy conversion systems. *Renewable and Sustainable Energy Reviews*, 33, pp.141–153.

[106] Department of Energy and Climate Change, 2014d. Electricity Market Reform: Capacity Market design - News stories - GOV.UK.

[107] Mancarella, P., Gan, C.K. & Strbac, G., 2011. Evaluation of the impact of electric heat pumps and distributed CHP on LV networks. In *IEEE PowerTech*. Trondheim, pp. 1–7.

[108] Papadopoulos, P. et al., 2009. Distribution Networks with Electric Vehicles. In *Universities Power Engineering Conference*. Glasgow.

[109] Wu Q., Jensen, J. M., Hansen L, H., Bjerre A., Nielsen A. H., Stergaard J., EV portfolio management and grid impact study. Project report, EDISON, 2012.

[110] Hassett, B., E. Bower, and M. Alexander. "MERGE WP 3 task 3.2: evaluation of the impact that progressive deployment of EV will provoke on electricity demand, steady state operation,

market issues, generation schedules and on the volume of carbon emissions." *Ricardo, European Commission* (2011).

[111] Shao S; Pipattanasomporn, M.; Rahman, S., "Grid Integration of Electric Vehicles and Demand Response With Customer Choice," Smart Grid, IEEE Transactions on , vol.3, no.1, pp.543,550, March 2012

[112] Marra, F., Jensen, M. M., Garcia-Valle, R., Traholt, C., & Larsen, E. (2011, October). Power quality issues into a Danish low-voltage grid with electric vehicles. In *Electrical Power Quality and Utilisation (EPQU), 2011 11th International Conference on* (pp. 1-6).

[113] Papadopoulos, P., Skarvelis-Kazakos, S., Grau, I., Cipcigan, L. M., & Jenkins, N. (2012). Electric vehicles' impact on British distribution networks. *IET Electrical Systems in Transportation*, *2*(3), 91-102.

[114] Kutt, L., Saarijarvi, E., Lehtonen, M., Molder, H., & Niitsoo, J. (2013, May). A review of the harmonic and unbalance effects in electrical distribution networks due to EV charging. In *Environment and Electrical Engineering (EEEIC), 2013 12th International Conference on* (pp. 556-561). IEEE.

[115] N. Bottrell, E. Ortega, M. Bilton, T. Green, G. Strbac, "Impact of low voltage – connected low carbon technologies on power quality", Report B3 for the "Low Carbon London" LCNF project: Imperial College London, 2014.

[116] M Akmal, B Fox, D.J Morrow, and T. Littler, "Impact of high penetration of heat pumps on low voltage distribution networks," in *PowerTech, 2011 IEEE Trondheim*, 2011.

[117] Chris Thompson, Preston Foster, Liam Wardley, Robert Stubbs, Richard Davis, Dean Naylor, Northern Powergrid. CLNR-L260, Case Study: Heat pump disruptive load on a low-voltage overhead line network, Northern Powergrid (Northeast) Limited, Northern Powergrid (Yorkshire) Plc, 2015

[118] C. Oates; A. Barlow and Victor Levi, , "Tap changer for distributed power," *2007 European Conference on Power Electronics and Applications* , pp.1-9, 2007.

[119] Brewin, B.O., Jupe, S.C.E., Bartlett, M.G., Jackson, K.T., Hanmer, C. (2011). New technologies for low voltage distribution networks. 2011 *2nd IEEE PES International Conference and Exhibition on Innovative Smart Grid Technologies (ISGT Europe)*, 05-07 Jan. 2011, Manchester, UK.

[120] Liu Xiaohu; A. Aichhorn,; Liu Liming and Li Hui, "Coordinated Control of Distributed Energy Storage System With Tap Changer Transformers for Voltage Rise Mitigation Under High Photovoltaic Penetration," *IEEE Transactions on Smart Grid, vol.3, no.2, pp.897-906,* June 2012.

[121] Qi, S., et al. "Assessment of Voltage Control Techniques for Low Voltage Networks." (2014): 12-11.

[122] Zidan, A. & El-Saadany, E.F., 2013. Distribution system reconfiguration for energy loss reduction considering the variability of load and local renewable generation. Energy, 59, pp.698–707.

[123] Kalambe, Shilpa, and Ganga Agnihotri. "Loss minimization techniques used in distribution network: bibliographical survey." *renewable and sustainable energy reviews* 29 (2014): 184-200.

[124] Zhang, Y. et al., 13. Quantification of Low Voltage Network Reinforcement Costs : A Statistical Approach. IEEE Transactions on Power Systems, 28(2), pp.810–818.

[125] Mokhtari, G. et al., 2013. Overvoltage prevention in LV smart grid using customer resources coordination. *Energy and Buildings*, 61, pp.387–395

[126] P., Crow, M.L. & Yang, Z., 2000. STATCOM control for power system voltage control applications. *IEEE Transactions on Power Delivery*, 15(4), pp.1311–1317.

[127] Clement-Nyns, K., Haesen, E. & Driesen, J., 2011. The impact of vehicle-to-grid on th distribution grid. Electric Power Systems Research, 81(1), pp.185–192.

[128] Ghassem, M. et al., 2013. A New Voltage Support Approach for Distribution Networks. IEEE Transactions on Smart Grid.

[129] Demirok, E. et al., 2011. Local Reactive Power Control Methods for Overvoltage Prevention of Distributed Solar Inverters in Low-Voltage Grids. *IEEE Journal of Photvoltaics*, 1(2), pp.174–182.

[130] R. Tonkoski; L. A C Lopes; T. H M and EL-Fouly, , "Coordinated Active Power Curtailment of Grid Connected PV Inverters for Overvoltage Prevention," *IEEE Transactions on Sustainable Energy*, vol.2, no.2, pp.139-147, 2011

[131] Madureira, A.G. e as Lopes, .A.,2009 . Coordinated voltage support in distribution networks with distributed generation and microgrids. *IET Renewable Power Generation*, 3(4), p.439.

[132] Yeoh Chee-Min; Tan Hee-Yuan; Kok Choon-Keat; Lee Hoon-Jae and Lim Hyotaek., "e2Home: A Lightweight Smart Home Management System," *Third International Conference on Convergence and Hybrid Information Technology*, 2008, pp. 82-87.

[133] F. C. Schweppe, *Spot pricing of electricity*. Boston: Kluwer Academic, 1988.

[134] Pina, A., Silva, C. & Ferrão, P., 2011. The impact of demand side management strategies in the penetration of renewable electricity. *Energy*, 41(1), pp.128–137.

[135] Papaioannou, I.T., Purvins, A. & Tzimas, E., 2013. Demand shifting analysis at high penetration of distributed generation in low voltage grids. International Journal of Electrical Power & Energy Systems, 44(1), pp.540–546.

[136] Balta-Ozkan, N. et al., 2013. The development of smart homes market in the UK. *Energy*, 60, pp.361–372.

[137] M.J.E Alam, K.M Muttaqi. and D Sutanto, "Effectiveness of traditional mitigation strategies for neutral current and voltage problems under high penetration of rooftop PV," *IEEE Power and Energy Society General Meeting (PES)*, 2013, vol., no., pp.1,5, 21-25 July 2013

[138] Melnik, I., Provoost, F., Bos, W. (2011). Intelligent distribution substation improves powe quality. *21st Cired International Conference on Electricity Distribution*, Frankfurt, Germany, 6-9 June 2011.

[139] Hazelrigg, G.A.; Adler, R.B.; Kirn, W.G., "Higher Voltage Distribution and Utilization Systems Benefits and Problems," Power Apparatus and Systems, IEEE Transactions on , vol.PAS-101, no.6, pp.1679,1688, June 1982

[140] Jones, A.I.; Smith, B.E.; Ward, D.J., "Considerations for higher voltage distribution," Power Delivery, IEEE Transactions on , vol.7, no.2, pp.782,788, Apr 1992

[141] Ozay, N.; Guven, A.N.; Tureli, A.; Demiroglu, M., "Technical and economic feasibility of conversion to a higher voltage distribution," Generation, Transmission and Distribution, IEE Proceedings- , vol.142, no.5, pp.468,472, Sep 1995

[142] Söderberg, D.; Engdahl, H., "Using 1kV low voltage distribution for connection of plug-in vehicles," Innovative Smart Grid Technologies Conference Europe (ISGT Europe), 2010 IEEE PES , vol., no., pp.1,5, 11-13 Oct. 2010

[143] J. Lohjala, T. Kaipia, J. Lassila, J. Partanen, and P. Jarventausta, "Potentiality and effects of the 1 kV low voltage distribution system," in Proc. IEEE Future Power Syst. Conf., 2005, pp. 1–6.

[144] Kaipia, T.; Lassila, J.; Partanen, J.; Lohjala, J.; Sahko, S.-S., "Experiences of using the 1 kV three phase supply in rural electricity distribution," Rural Electric Power Conference, 2006 IEEE , vol., no., pp.1,6

[145] Chin Kim Gan; Pudjianto, D.; Djapic, P.; Strbac, G., "Strategic Assessment of Alternative Design Options for Multivoltage-Level Distribution Networks," Power Systems, IEEE Transactions on , vol.29, no.3, pp.1261,1269, May 2014

[146] Connor, G.; Jones, C.E.; Finney, S.J., "End user voltage regulation to ease urban low-voltage distribution congestion," Generation, Transmission & Distribution, IET , vol.8, no.8, pp.1453,1465, August 2014

[147] Connor, G.; Jones, C.E.; Finney, S.J., "Easing future low voltage congestion with an AC chopper voltage regulator," Power Electronics, Machines and Drives (PEMD 2014), 7th IET International Conference on , vol., no., pp.1,6, 8-10 April 2014

[148] (ER) G81 - Part 1: Design and Planning, "Framework for design and planning, materials specification, installation and record for low voltage housing development installations and associated new HV/LV distribution substations"

[149] Willis, H. Lee. *Power distribution planning reference book*. CRC press, 2004.

[150] Haggis, T.; *"Network Design Manual" Eon/Central Networks Report, December 2006*

[151] Scaddan, Brian. *IEE Wiring Regulations: Explained and Illustrated*. Routledge, 2011.

[152] Engineering Recommendation G81 Part 4 "Framework for design and planning, of industrial and commercial underground connected loads up to and including 11kV.

[153] IEC 60038 IEC Standard Voltages

[154] Dept. of Energy and Climate Change (DECC), "Energy consumption in the UK 2011," UK government, London, UK, Jul. 2012. Available Online: https://www.gov.uk/government/publications/energy-consumption-in-the-uk

[155] Singh, R.; Singh, A.; , "Energy loss due to harmonics in residential campus — A case study," *Universities Power Engineering Conference (UPEC), 2010 45th International* , vol., no., pp.1-6, Aug. 31 2010-Sept. 3 2010

[156] Stephens, Mark. "Power Quality and Utilisation Guide." *PQ in continuous manufacturing* (2006).

[157] Hardie, S.; Watson, N.; , *"The effect of new residential appliances on Power Quality," Universities Power Engineering Conference (AUPEC), 2010 20th Australasian , vol., no., pp.1-6, 5-8 Dec. 2010*

[158] I.Richardson, M. Thomson, D. Infield, C. Clifford, "Domestic electricity use: A high resolution energy demand model, Energy and Buildings, 42(10), pp.1878-1887," (2010)

[159] I. Richardson, M. Thomson, Domestic electricity demand model - simulation example, Loughborough University Institutional Repository, http://hdl.handle.net/2134/5786 (2010).

[160] ENATS 35-1 Distribution transformers (from 16 kVA to 100 kVA)

[161] Western Power Distribution Company Directive, "STANDARD TECHNIQUE: SD5A/1, Design of Low Voltage Domestic Connections", April 2012, Table 2 and section 3.3.1

[162] Effective HVDC solutions, Alstom. Accessed online http://www.alstom.com/grid/products-and-services/engineered-energy-solutions/hvdc-transmission-systems/

[163] Hammerstrom, D.J., "AC Versus DC Distribution Systems. Did We Get it Right?," Power Engineering Society General Meeting, 2007. IEEE , vol., no., pp.1,5, 24-28 June 2007

[164] Peltoniemi, P.; Nuutinen, Pasi; Salonen, P.; Niemela, M.; Pyrhonen, J., "Output filtering of the customer-end inverter in a low-voltage DC distribution network," *Power Electronics and Motion Control Conference, 2008. EPE-PEMC 2008. 13th* , vol., no., pp.1763,1770, 1-3 Sept. 2008

[165] Salonen, Pasi; Nuutinen, Pasi; Peltoniemi, Pasi; Partanen, Jarmo, "Protection scheme for an LVDC distribution system," Electricity Distribution - Part 1, 2009. CIRED 2009. 20th International Conference and Exhibition on , vol., no., pp.1,4, 8-11 June 2009

[166] Mattsson, A.; Lana, A.; Nuutinen, P.; Vaisanen, V.; Peltoniemi, P.; Kaipia, T.; Silventoinen, P.; Partanen, J., "Galvanic Isolation and Output LC Filter Design for the Low-Voltage DC Customer-End Inverter," *Smart Grid, IEEE Transactions on* , vol.5, no.5, pp.2593,2601, Sept. 2014

[167] Kaipia, T.; Karppanen, J.; Mattsson, A.; Lana, A.; Nuutinen, P.; Peltoniemi, P.; Salonen, P.; Partanen, J.; Lohjala, J.; Wookyu Chae; Juyong Kim, "A system engineering approach to low voltage DC distribution," *Electricity Distribution (CIRED 2013), 22nd International Conference and Exhibition on* , vol., no., pp.1,4, 10-13 June 213

[168] Antoniou, D.; Tzimas, A.; Rowland, S.M., "DC utilization of existing LVAC distribution cables," Electrical Insulation Conference (EIC), 2013 IEEE, vol., no., pp.518,522, 2-5 June 2013

[169] Electricity meter type approval certificates Annex MI-003. Available Online: https://www.gov.uk/government/publications/electricity-meter-type-approval-certificates-annex-mi-003

[170] http://ukevse.org.uk/charge-points-chargers

[171] http://www.meterboxes.co.uk/products/domestic-meter-boxes/gas.html

[172] SLEMON, G. R. (1992). *Electric machines and drives*. Reading, Mass, Addison-Wesley Pub.

[173] http://www.powerperfector.com/Product/technical-info.htm

[174] http://powerstar02.wsiefusion.net/index.html

[175] http://vo4home.com/

[176] http://www.vphase.co.uk/

[177] Pal, Y.; Swarup, A.; Singh, B.; , "A Review of Compensating Type Custom Power Devices for Power Quality Improvement," *Power System Technology and IEEE Power India Conference, 2008. POWERCON 2008. Joint International Conference on* , vol., no., pp.1-8, 12-15 Oct. 2008

[178] A. Ghosh and G. Ledwich, "Power Quality Enhancement Using Custom Power Devices": Kluwer Academic Publishers, 2002

[179] Barriviera, R.; da Silva, S.A.O.; Modesto, R.A.; Goedtel, A.; Kaster, M.; , "Power quality conditioner with series-parallel compensation applied to single-phase systems," *Power Electronics and Applications (EPE 2011), Proceedings of the 2011-14th European Conference on* , vol., no., pp.1-10, Aug. 30 2011-Sept. 1 2011

[180] Singh, B.; Al-Haddad, K.; Chandra, A.;, "A review of active filters for power quality improvement," *Industrial Electronics, IEEE Transactions on* , vol.46, no.5, pp.960-971, Oct 1999

[181] El-Habrouk, M.; Darwish, M.K.; Mehta, P.;, "Active power filters: a review," *Electric Power Applications, IEE Proceedings* - , vol.147, no.5, pp.403-413, Sep 2000

[182] Ghosh, Arindam, and Gerard Ledwich. "Compensation of distribution system voltage using DVR." Power Delivery, IEEE Transactions on 17.4 (2002): 1030-1036.

[183] M.J. Newman; D.G. Holmes; J.G. Nielsen and F. Blaabjerg, , "A dynamic voltage restorer (DVR) with selective harmonic compensation at mediumvoltage level," IEEE Transactions on Industry Applications, vol.41, no.6, pp.1744,1753, 2005.

[184] Singh, B.; Saha, R.; Chandra, A.; Al-Haddad, K.; , "Static synchronous compensators (STATCOM): a review," *Power Electronics, IET* , vol.2, no.4, pp.297-324, July 2009

[185] Yao Shu-jun; Song Xiao-yan; Wang Yan; Yan Yu-xin; Yan Zhi; , "Research on dynamic characteristics of Unified Power Flow Controller (UPFC)," *Electric Utility Deregulation and Restructuring and Power Technologies (DRPT), 2011 4th International Conference on* , vol., no., pp.490-493, 6-9 July 2011

[186] Khadkikar, Vinod. "Enhancing electric power quality using UPQC: a comprehensive overview." Power Electronics, IEEE Transactions on 27.5 (2012): 2284-2297.

[187] Mohamed, B. S., et al. "Performance Evaluation of R-UPQC and L-UPQC Based on a Novel Voltage Imperfections Detection Algorithm." International Review of Electrical Engineering (IREE) 8.4 (2013): 1311-1323.

[188] Brenna, M.; Faranda, R.; Tironi, E., "A New Proposal for Power Quality and Custom Power Improvement: OPEN UPQC," Power Delivery, IEEE Transactions on , vol.24, no.4, pp.2107,2116, Oct. 2009

[189] Jou, H.-L.; Wu, J.-C.; Tsai, C.; Wu, K.-D.; Huang, M.-S.; , "Novel line-interactive uninterruptible power supply," *Electric Power Applications, IEE Proceedings* - , vol.151, no.3, pp. 359- 364, 8 May 2004

[190] Wheeler, P.W.; Rodriguez, J.; Clare, J.C.; Empringham, L.; Weinstein, A.; , "Matrix converters: a technology review," *Industrial Electronics, IEEE Transactions on* , vol.49, no.2, pp.276-288, Apr 2002

[191] Jose, P.S.; Deepika, N.C.; Nisha, S.N.; , "Applications of single phase matrix converter," Emerging Trends in Electrical and Computer Technology (ICETECT), 2011 International Conference on , vol., no., pp.386-391, 23-24 March 2011

[192] Zuckerberger, A.; Weinstock, D.; Alexandrovitz, A.; , "Single-phase matrix converter," *Electric Power Applications, IEE Proceedings* - , vol.144, no.4, pp.235-240, Jul 1997

[193] Vorobyov, Maxym. "Overview of single phase matrix converter application." Publication of Doctoral School of Energy and Geotechnology (2011).

[194] Idris, Zahirrudin, Mustafar Kamal Hamzah, and Ahmad Maliki Omar. "Implementation of Single-Phase Matrix Converter as a Direct AC-AC Converter Synthesized Using Sinusoidal Pulse Width Modulation with Passive Load Condition." Power Electronics and Drives Systems, 2005. PEDS 2005. International Conference on. Vol. 2. IEEE, 2005.

[195] Singh, B.; Singh, B.N.; Chandra, A.; Al-Haddad, K.; Pandey, A.; Kothari, D.P.; , "A review of single-phase improved power quality AC-DC converters," *Industrial Electronics, IEEE Transactions on* , vol.50, no.5, pp. 962- 981, Oct. 2003

[196] Jacobina, C.B.; de Freitas, I.S.; da Silva, E.R.C.; Lima, A.M.N.; de Oliveira, T.M.; , "AC-AC single-phase to single-phase two-leg converters," Industry Applications Conference, 2005. Fourtieth IAS Annual Meeting. Conference Record of the 2005 , vol.4, no., pp. 2388- 2394 Vol. 4, 2-6 Oct. 2005.

[197] Han-Woong Park; Sung-Jun Park; Jin-Gil Park; Cheul-U Kim; , "A novel high-performance voltage regulator for single-phase AC sources," Industrial Electronics, IEEE Transactions on , vol.48, no.3, pp.554-562, Jun 2001

[198] Krishnaswami, H.; Ramanarayanan, V.;, "Control of high-frequency AC link electronic transformer," *Electric Power Applications, IEE Proceedings* - , vol.152, no.3, pp. 509- 516, 6 May 2005

[199] She, Xu, et al. "Review of solid state transformer in the distribution system: From components to field application." Energy Conversion Congress and Exposition (ECCE), 2012 IEEE. IEEE, 2012.

[200] Banaei, M.R.; Salary, E.; , "Power quality improvement based on novel power electronic transformer," *Power Electronics, Drive Systems and Technologies Conference (PEDSTC), 2011 2nd* , vol., no., pp.286-291, 16-17 Feb. 2011]

[201] Jih-Sheng Lai; Fang Zheng Peng; , "Multilevel converters-a new breed of power converters," *Industry Applications, IEEE Transactions on* , vol.32, no.3, pp.509-517, May/Jun 1996

[202] Kouro, S.; Malinowski, M.; Gopakumar, K.; Pou, J.; Franquelo, L.G.; Bin Wu; Rodriguez, J.; Pérez, M.A.; Leon, J.I.; , "Recent Advances and Industrial Applications of Multilevel Converters," *Industrial Electronics, IEEE Transactions on* , vol.57, no.8, pp.2553-2580, Aug. 2010

[203] J. Biela, M. Schweizer, S. Waffler, and J. W. Kolar, "SiC versus Si;Evaluation of Potentials for Performance Improvement of Inverter and DC-DC Converter Systems by SiC Power Semiconductors," *Industrial Electronics, IEEE Transactions on*, vol. 58, pp. 2872-2882, 2011.

[204] N.C.Durham, "Cree launches industry's first commercial silicon carbide power mosfet," Available online: http://www.cree.com/news-and-events , Jan, 2011.

[205] Cree Silicon Carbide Power White Paper: Highly Efficient, and Compact ZVS Resonant Full Bridge Converter Using 1200V SiC MOSFETs. Available online: http://www.cree.com/

[206] Whitaker, B.; Barkley, A.; Cole, Z.; Passmore, B.; Martin, D.; McNutt, T.R.; Lostetter, A.B.; Jae Seung Lee; Shiozaki, K., "A High-Density, High-Efficiency, Isolated On-Board Vehicle Battery Charger Utilizing Silicon Carbide Power Devices," Power Electronics, IEEE Transactions on , vol.29, no.5, pp.2606,2617, May 2014

[207] J.H. Alimeling, W.P. Hammer, "PLECS-piece-wise linear electrical circuit simulation for Simulink", Proceedings of the IEEE 1999 International Conference on Power Electronics and Drive Systems, 1999. PEDS '99, Vol. 1, pp. 355-360.

[208] A.V. Thompson, "Micro-CAP: An Analog Circuit Design System for Personal Computers", IEEE Computer Graphics and Applications, 1984, Vol. 4, Iss: 4, pp: 30 – 32.

[209] R. Jaeger, T. Blalock, "Microelectronic Circuit design", McGraw Hill, 4th ed., p. 191.

[210] Mestha, L.K.; Evans, P.D.; , "Analysis of on-state losses in PWM inverters," Electric Power Applications, IEE Proceedings B , vol.136, no.4, pp.189-195, Jul 1989

[211] Mohan, Ned, and Tore M. Undeland. *Power electronics: converters, applications, and design*. John Wiley & Sons, 2007.

[212] Zhang, M.T.; Jovanovic, M.M.; Lee, F.C.Y., "Analysis and evaluation of interleaving techniques in forward converters," *Power Electronics, IEEE Transactions on* , vol.13, no.4, pp.690,698, Jul 1998

[213] Gerber, M.; Ferreira, J.A.; Hofsajer, I.W.; Seliger, N., "Interleaving optimization in synchronous rectified DC/DC converters," *Power Electronics Specialists Conference, 2004. PESC 04. 2004 IEEE 35th Annual* , vol.6, no., pp.4655,4661 Vol.6, 20-25 June 2004

[214] Burany, N., "Safe control of four-quadrant switches," *Industry Applications Society Annual Meeting, 1989., Conference Record of the 1989 IEEE* , vol., no., pp.1190,1194 vol.1, 1-5 Oct. 1989

[215] SiC MOSFET Isolated Gate Driver. Available online: **http://www.cree.com**

Appendix A

1. LV service cables Characteristics

	Phase	Neutral	Loop	Maximum rating	Maximum Current	Phase Reactance	Neutral Reactance
	Ω/km	Ω/km	Ω/km	kVA	A	Ω	Ω
35mm^2 Hybrid	**0,851**	**0,900**	**1,751**	**18**	**115**	**0,041**	**0,041**

Table1: Typical Values of a LV service cable

2. Very Rural Network Asset Characteristics

Size (kVA)	L/N R	L/N X	L/N Imp	Preferred fuse size (A)	Nameplate kVA	Maximum fuse size (A)
100	**0.0371**	**0.0810**	**0.0891**	**200**	**100**	**200**

Table 2: Typical values of a Pole Transformer

	Phase	Neutral	Loop	Maximum rating	Maximum Current	Phase Reactance	Neutral Reactance
	Ω/km	Ω/km	Ω/km	kVA	A	Ω	Ω
50ABC	**0,641**	**0,641**	**1.282**	**100**	**144**	**0,083**	**0,083**

Table 3: Typical values of the 50ABC conductors

3. Rural Network Assets Characteristics

	Phase	Neutral	Loop	Maximum rating	Maximum Current	Phase Reactance	Neutral Reactance
	Ω/km	Ω/km	Ω/km	kVA	A	Ω	Ω
95ABC	**0,320**	**0,320**	**0.640**	**100**	**228**	**0,077**	**0,077**

Table 4: Typical values of the 95ABC conductors

4. Urban Network Assets Characteristics

Size (kVA)	L/N R	L/N X	L/N Imp	Preferred fuse size (A)	Nameplate kVA	Maximum fuse size (A)
800	**0.0029**	**0.0107**	**0.0111**	**400**	**800**	**630**

Table 5: Typical values of a Ground Mounted Transformer

	Phase	Neutral	Loop	Maximum rating	Maximum Current	Phase Reactance	Neutral Reactance
	Ω/km	Ω/km	Ω/km	kVA	A	Ω	Ω
185 CNE	**0,164**	**0,164**	**0.328**	**800**	**292**	**0.074**	**0.014**

Table 6: Typical values of the 185ABC conductors

Appendix B

B.1 Low Voltage Network Losses Analysis

Figure B.1 illustrates a residential LV network with a number of houses n, connected to the main feeder via service cables. In some cases the service cable is shared between two houses.

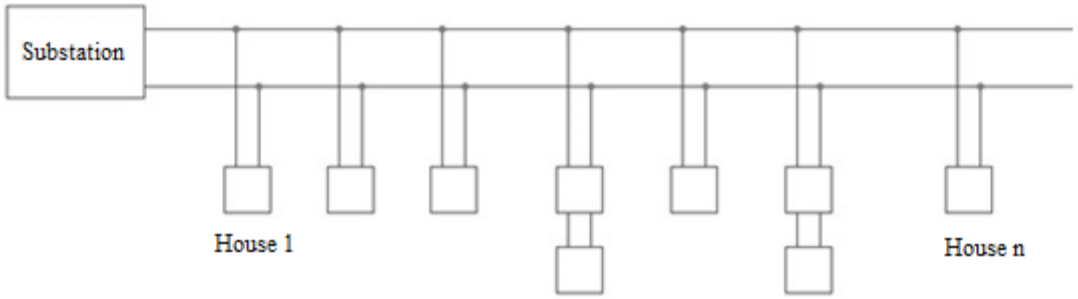

Figure B.1: Low Voltage network schematic

Here it is assumed that houses can be lumped together at the mid-point of the cable, which typically has length of 400 m and is shown in Figure B.2. It is also assumed that the power factor is unity – typical residential properties have power factors of between 0.95 and 1.0.

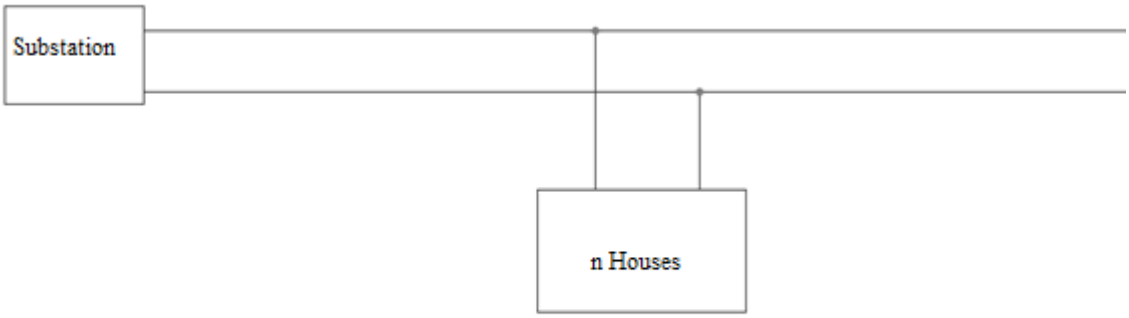

Figure B.2: Simplified Low Voltage Network schematic

The losses of the main cable and service cable P_{cable}, are given by the following expression:

$$P_{cable} = I_s^2 L R_c \qquad \text{(B.1)}$$

Where, I_S is the supply current flowing in the main cable, R_C is the total resistance of the main and service cable per metre and L is the cable length.

I_s can be approximated from the balance of supply and load power, assuming losses are small,

$$I_S V_S = I_L V_L \tag{B.2}$$

where V_L and I_L are the voltage and total current supplied to the loads respectively and V_S is the supply voltage. If the supply voltage is increased above the load voltage by a factor N where $V_S=NV_L$, then the above equation for cable losses becomes,

$$P_{cable} = \left(\frac{1}{N}\frac{P_L}{V_L}\right)^2 LR_C \tag{B.3}$$

where P_L is the total load power. We can also include a figure for the VCU losses, so that the total network losses P_{LVCU} are,

$$P_{LVCU} = P_{cable} + VCU\ losses \tag{B.4}$$

The losses of the VCU depend on its efficiency ε, $(1-\varepsilon)P_L$ so that

$$P_{LVCU} = \left(\frac{P_L}{V_L N}\right)^2 LR_C + (1-\varepsilon)\,P_L \tag{B.5}$$

If the after diversity maximum demand (ADMD) is a, then the Equation (B.5) becomes,

$$P_{LVCU} = a\left[a\left(\frac{1}{N}\right)^2 \frac{LP_L R_C}{V_L} + (1-\varepsilon)\right]P_L \tag{B.6}$$

and the maximum power drawn by a house is P_{HOUSE}, then equations (B.6) becomes,

$$P_{LVCU} = a\left[a\left(\frac{1}{N}\right)^2 n\frac{LR_C}{R_L} + (1-\varepsilon)\right]nP_{HOUSE} \tag{B.7}$$

where R_L is the minimum equivalent load resistance for a single house. Equation (B.5) is plotted for various values of N and L, with typical, urban residential values of R_C=0.164 Ω/km, n=100 houses, ε =0.99, an ADMD of a=0.2 and a maximum domestic load of P_{HOUSE}=15 kW, which represents a house with electric heating, shower, and cooker and slow electric vehicle charging and gives R_L=3.53 Ω at V_L=230 V.

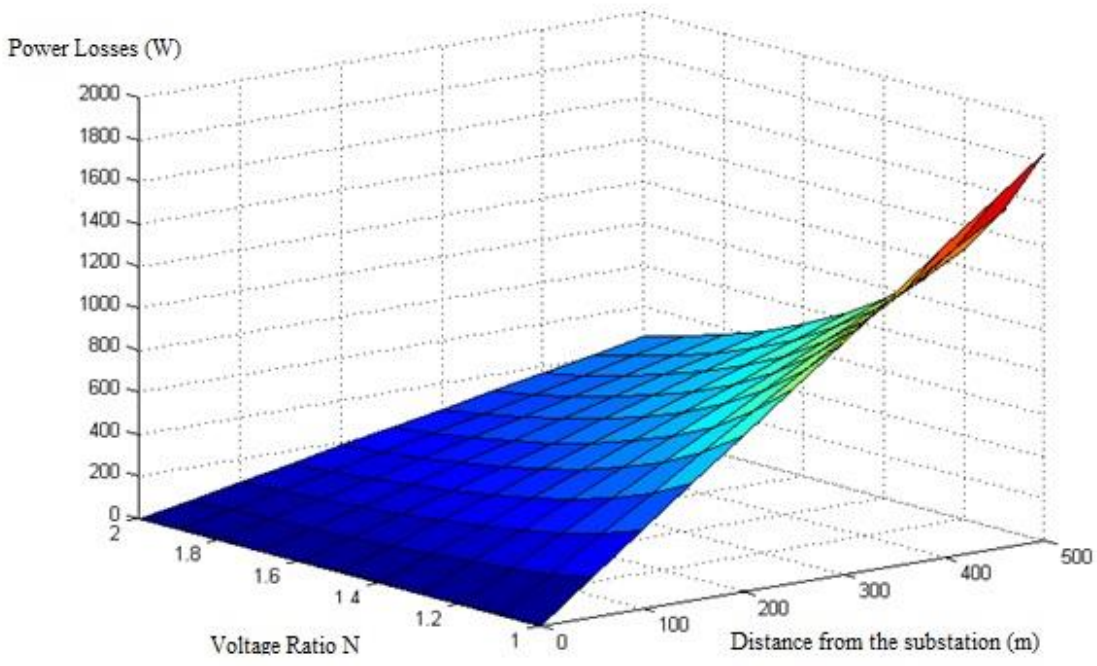

Figure B.3: Typical cable power loss (W) for m=100 house load, with an ADMD of 3 kW per house against distance L from sub-station (m) and step-up supply voltage conversion ratio N

Figure B.3 shows that for the proposed voltage ratio of N=1.3, which corresponds to a network voltage of 300V and household supply voltage of 230 V, the losses are reduced by 40% from the N=1 value. In other words the capacity of the LV network can be increased by a factor of 1.4.

Appendix C
Mathematica Derivation

```
Remove["Global`*"]

Element[{Vs, VL, VSERIES, Iis, IiL, IiSHUNT, Nn, SL, ϕs, ϕL, ϕVL}, Reals];

vs = Vs Exp[i 0];
iis = Iis Exp[i ϕs];

vL = VL Exp[i ϕVL];
iiL = IiL Exp[i (ϕL + ϕVL)];

iiSHUNT = iiL - iis;
vSERIES = vs - vL;

Iis = (VL IiL Cos[ϕL])/(Vs Cos[ϕs]); (* Active input/output power balance *)

Vs = Nn VL;

ϕs = 0; (*Assume unity pf at input *)

IiL = SL/VL; (* define the load VA as SL, which is fixed for all configurations *)

VAR = Abs[vSERIES] Iis + VL Abs[iiSHUNT]; (* VA rating UPQCR *)
VAL = Abs[vSERIES] IiL + Vs Abs[iiSHUNT]; (* VA rating UPQCL *)


VAR = FullSimplify[ComplexExpand[VAR], Assumptions → {Vs > 0, VL > 0, Abs[vSERIES] > 0, Iis > 0, IiL > 0, Nn > 0, SL > 0}];
VAL = FullSimplify[ComplexExpand[VAL], Assumptions → {Vs > 0, VL > 0, Abs[vSERIES] > 0, Iis > 0, IiL > 0, Nn > 0, SL > 0}];

(* normalise to SL *)

VARNORM = Simplify[VAR / SL] (* Independent *)
VALNORM = Simplify[VAL / SL]

(* Dependent VA equation is the same as independant but needs additional active power link *)

VARNORM = Simplify[VAR / SL + 2 (VL IiL Cos[ϕL])/SL] (* Dependent includes 2 off inverters for *)
VALNORM = Simplify[VAL / SL + 2 (VL IiL Cos[ϕL])/SL] (* isolation rated at the active power    *)

VABB = Simplify[(Vs Iis + SL) / SL + 2 (VL IiL Cos[ϕL])/SL] (* Back to back with isolated link *)
```

```
Remove::rmnsm : There are no symbols matching "Global`*". »
```

$$\frac{2\,\text{Cos}[\phi_L]\,\sqrt{1+\text{Nn}^2-2\,\text{Nn}\,\text{Cos}[\phi_{VL}]}+\sqrt{2}\,\sqrt{1+2\,\text{Nn}^2+\text{Cos}[2\,\phi_L]-4\,\text{Nn}\,\text{Cos}[\phi_L]\,\text{Cos}[\phi_L+\phi_{VL}]}}{2\,\text{Nn}}$$

$$\sqrt{1+\text{Nn}^2-2\,\text{Nn}\,\text{Cos}[\phi_{VL}]}+\frac{\sqrt{1+2\,\text{Nn}^2+\text{Cos}[2\,\phi_L]-4\,\text{Nn}\,\text{Cos}[\phi_L]\,\text{Cos}[\phi_L+\phi_{VL}]}}{\sqrt{2}}$$

$$\frac{2\,\text{Cos}[\phi_L]\left(2\,\text{Nn}+\sqrt{1+\text{Nn}^2-2\,\text{Nn}\,\text{Cos}[\phi_{VL}]}\right)+\sqrt{2}\,\sqrt{1+2\,\text{Nn}^2+\text{Cos}[2\,\phi_L]-4\,\text{Nn}\,\text{Cos}[\phi_L]\,\text{Cos}[\phi_L+\phi_{VL}]}}{2\,\text{Nn}}$$

$$2\,\text{Cos}[\phi_L]+\sqrt{1+\text{Nn}^2-2\,\text{Nn}\,\text{Cos}[\phi_{VL}]}+\frac{\sqrt{1+2\,\text{Nn}^2+\text{Cos}[2\,\phi_L]-4\,\text{Nn}\,\text{Cos}[\phi_L]\,\text{Cos}[\phi_L+\phi_{VL}]}}{\sqrt{2}}$$

$$1+3\,\text{Cos}[\phi_L]$$

Appendix D

D.1 Schematics and PCB layouts

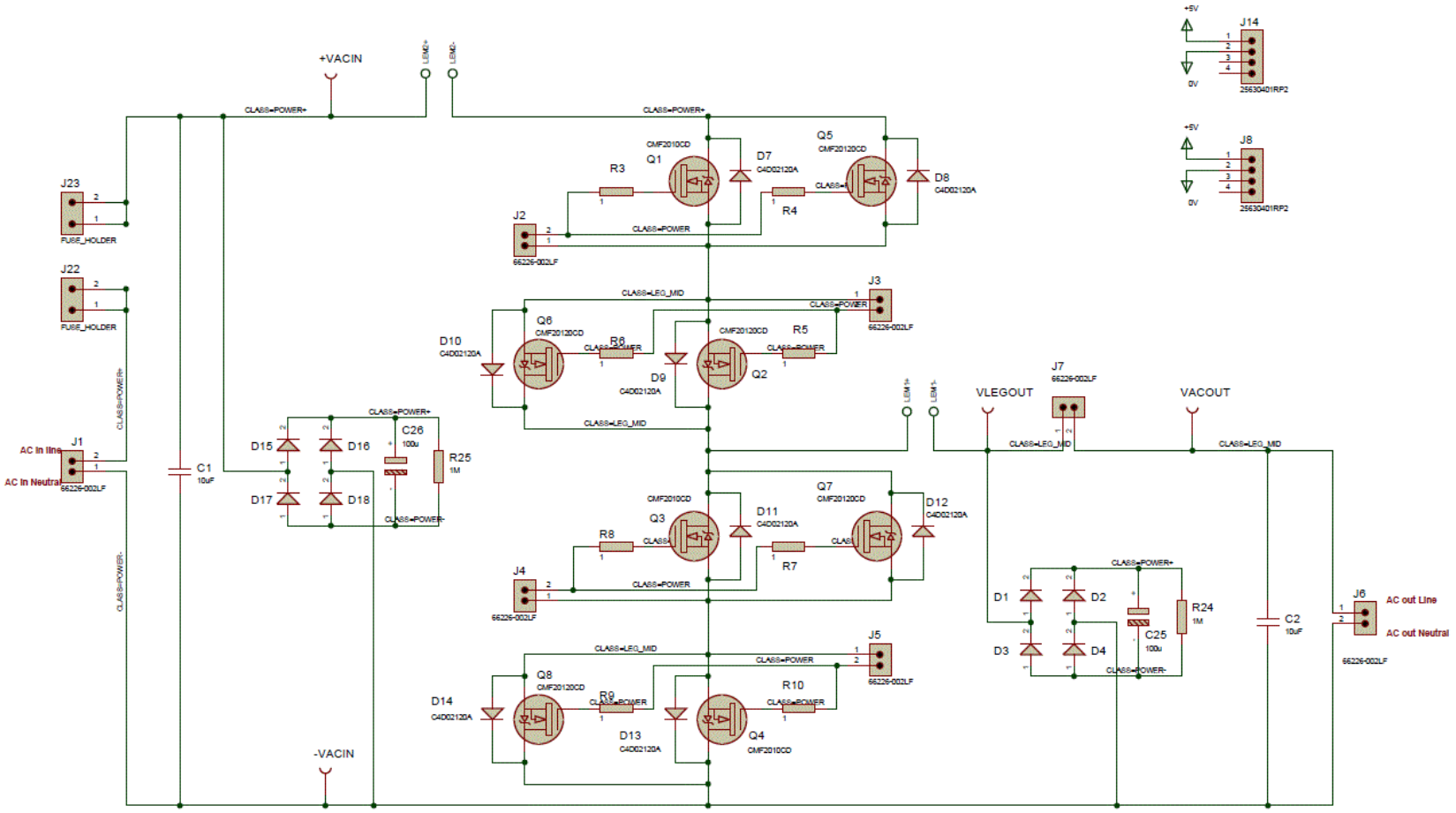

Figure D.1: AC Chopper prototype schematic from Proteus software

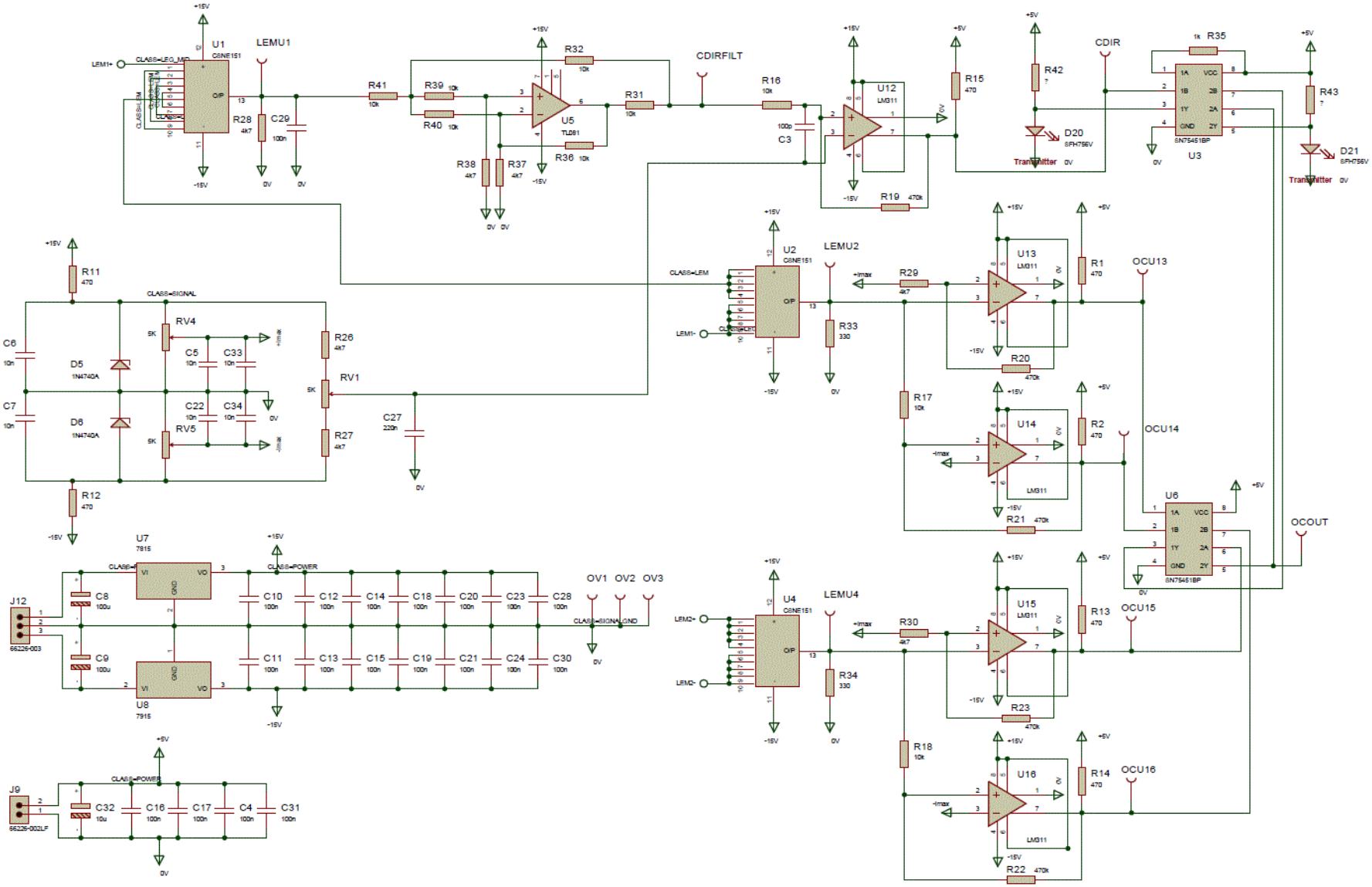

Figure D.2: AC Chopper prototype protection and current direction detection schematic from Proteus software

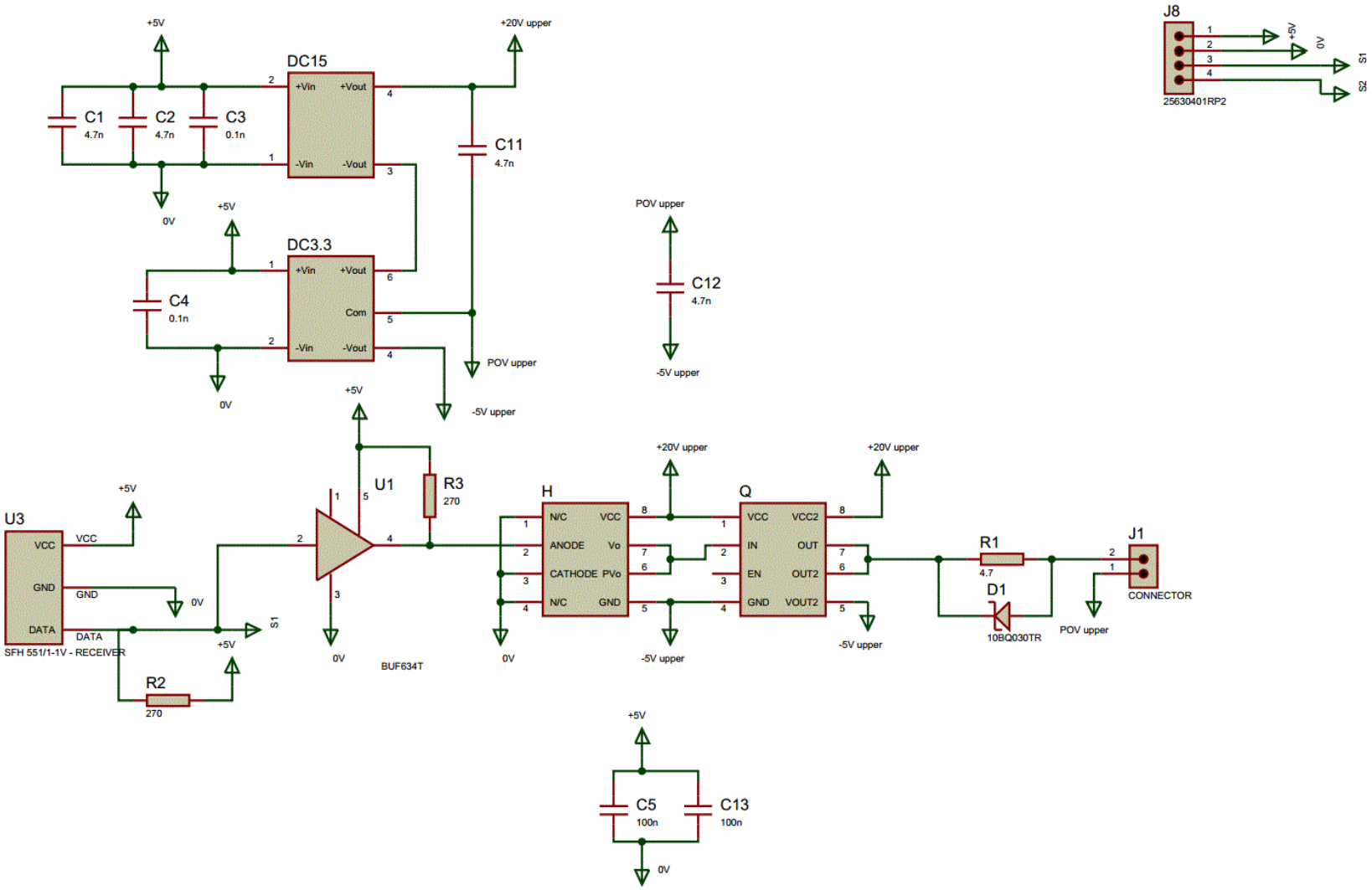

Figure D.3: SiC Gate drive circuit from Proteus Software

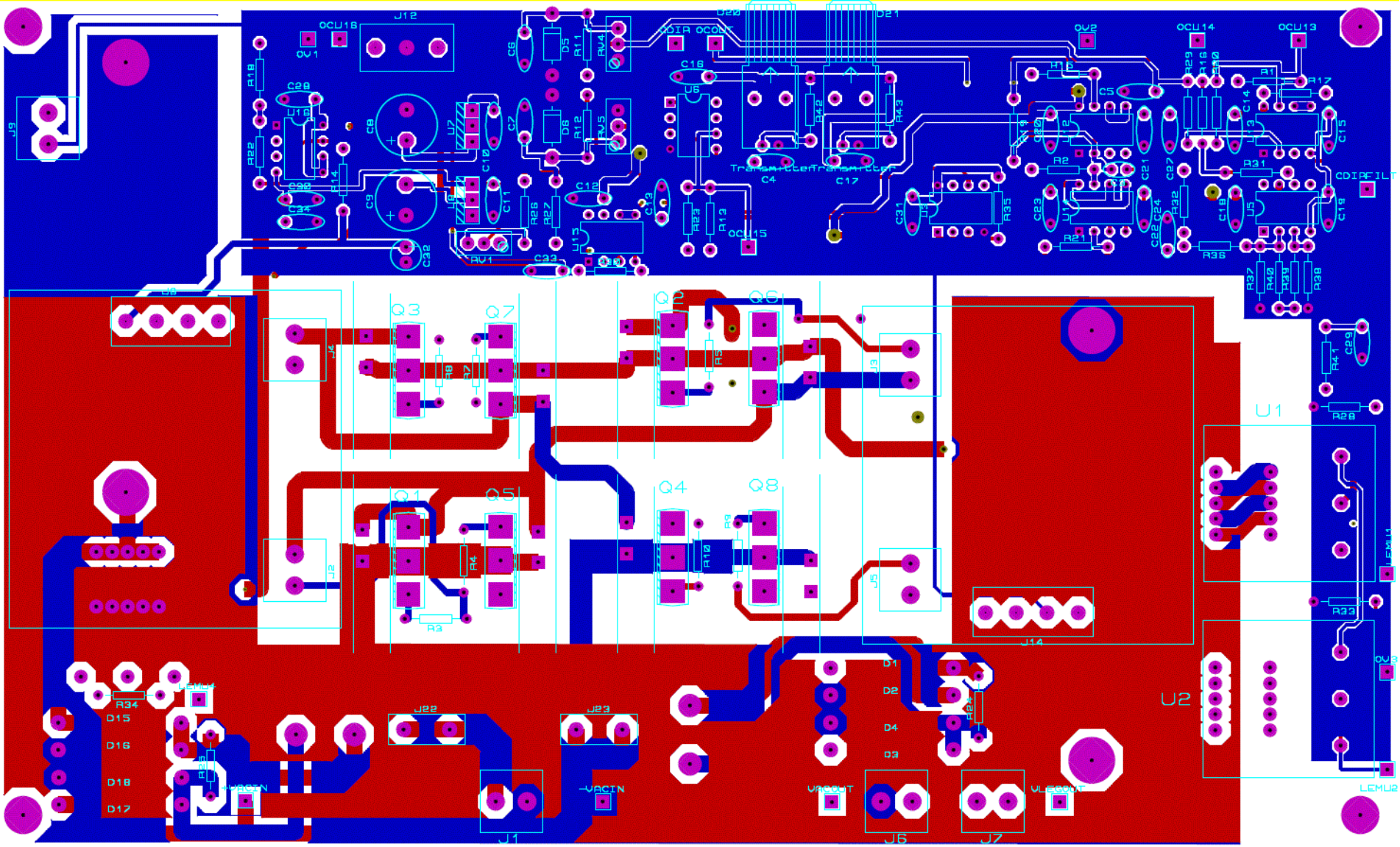

Figure D.4: AC Chopper prototype top and bottom power planes from Proteus software

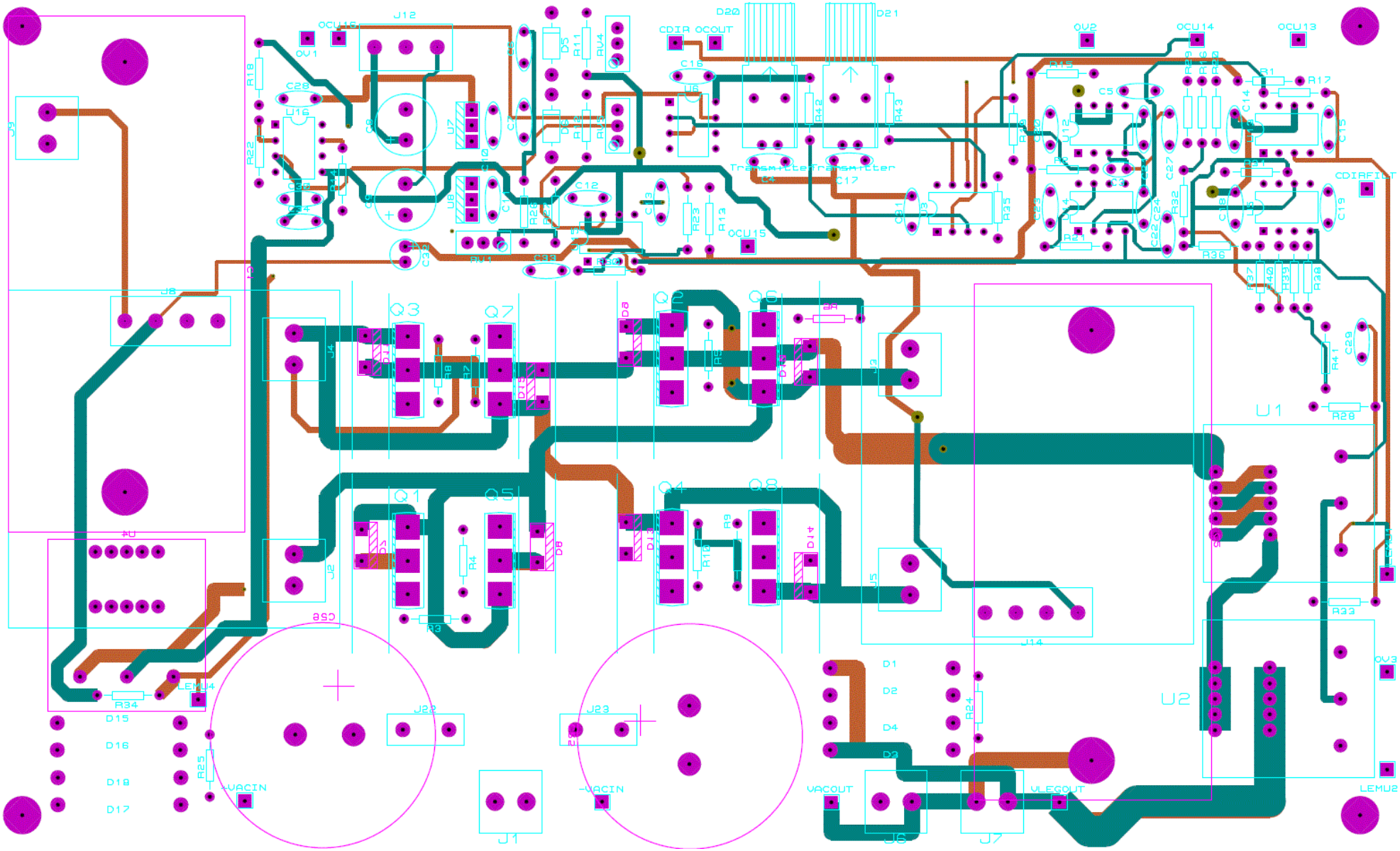

Figure D.5: AC Chopper prototype inner power planes from Proteus software

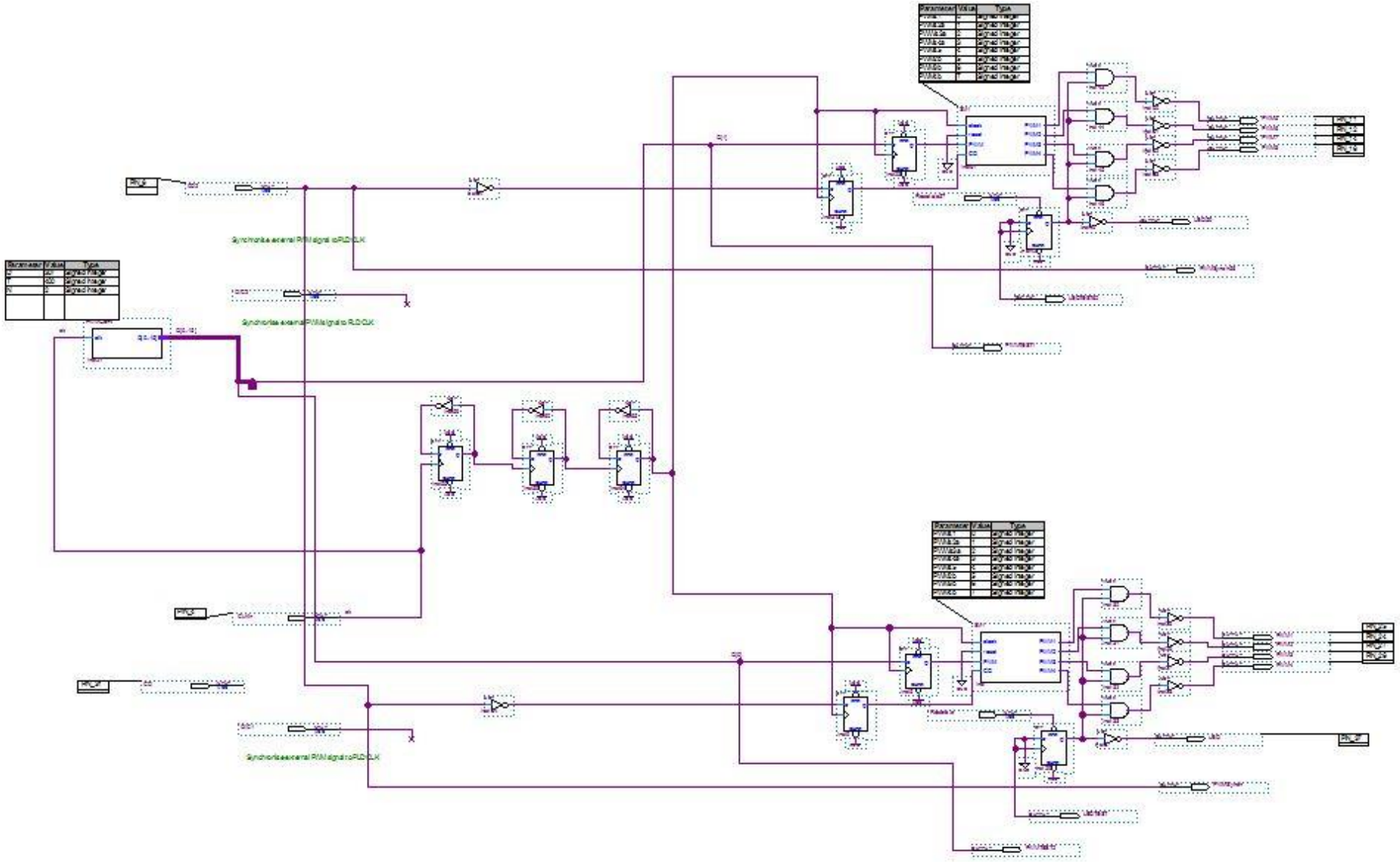

Figure D.6: AC Chopper prototype CPLD control circuit from Alterra Quartus software

C.2 CPLD CODE

```
`timescale 1ns/1ns
module SM1 (clock,reset,PWM,CD,
   PWM1,PWM2,PWM3,PWM4);
   input clock;
   input reset;
   input PWM;
   input CD;
   tri0 reset;
   tri0 PWM;
   tri0 CD;
   output PWM1;
   output PWM2;
   output PWM3;
   output PWM4;
   reg PWM1;
   reg reg_PWM1;
   reg PWM2;
   reg reg_PWM2;
   reg PWM3;
   reg reg_PWM3;
   reg PWM4;
   reg reg_PWM4;
   reg [7:0] fstate;
   reg [7:0] reg_fstate;
   parameter PWMs1=0,PWMs2a=1,PWWs3a=2,PWMs4a=3,PWMs5=4,PWM2b=5,PWM3b=6,PWM4b=7;
   initial
   begin
      reg_PWM1 <= 1'b0;
      reg_PWM2 <= 1'b0;
      reg_PWM3 <= 1'b0;
      reg_PWM4 <= 1'b0;
   end
   always @(posedge clock)
   begin
      if (clock) begin
         fstate <= reg_fstate;
      end
   end
   always @(fstate or reset or PWM or CD or reg_PWM1 or reg_PWM2 or reg_PWM3 or reg_PWM4)
   begin
      if (reset) begin
         reg_fstate <= PWMs1;
         reg_PWM1 <= 1'b0;
         reg_PWM2 <= 1'b0;
         reg_PWM3 <= 1'b0;
         reg_PWM4 <= 1'b0;
         PWM1 <= 1'b0;
         PWM2 <= 1'b0;
         PWM3 <= 1'b0;
         PWM4 <= 1'b0;
      end
      else begin
         reg_PWM1 <= 1'b0;
         reg_PWM2 <= 1'b0;
         reg_PWM3 <= 1'b0;
         reg_PWM4 <= 1'b0;
         PWM1 <= 1'b0;
         PWM2 <= 1'b0;
         PWM3 <= 1'b0;
         PWM4 <= 1'b0;
         case (fstate)
            PWMs1: begin
               if (((PWM == 1'b1) & (CD == 1'b1)))
                  reg_fstate <= PWMs2a;
               else if (((PWM == 1'b1) & (CD == 1'b0)))
                  reg_fstate <= PWM2b;
               else if ((PWM == 1'b0))
                  reg_fstate <= PWMs1;
               // Inserting 'else' block to prevent latch inference
               else
                  reg_fstate <= PWMs1;
               reg_PWM1 <= 1'b0;
```

```
    reg_PWM2 <= 1'b0;
    reg_PWM3 <= 1'b1;
    reg_PWM4 <= 1'b1;
  end
  PWMs2a: begin
    if ((PWM == 1'b0))
      reg_fstate <= PWMs1;
    else if ((PWM == 1'b1))
      reg_fstate <= PWWs3a;
    // Inserting 'else' block to prevent latch inference
    else
      reg_fstate <= PWMs2a;
    reg_PWM1 <= 1'b0;
    reg_PWM2 <= 1'b0;
    reg_PWM3 <= 1'b0;
    reg_PWM4 <= 1'b1;
  end
  PWWs3a: begin
    if ((PWM == 1'b0))
      reg_fstate <= PWMs2a;
    else if ((PWM == 1'b1))
      reg_fstate <= PWMs4a;
    // Inserting 'else' block to prevent latch inference
    else
      reg_fstate <= PWWs3a;
    reg_PWM1 <= 1'b1;
    reg_PWM2 <= 1'b0;
    reg_PWM3 <= 1'b0;
    reg_PWM4 <= 1'b1;
  end
  PWMs4a: begin
    if ((PWM == 1'b1))
      reg_fstate <= PWMs5;
    else if ((PWM == 1'b0))
      reg_fstate <= PWWs3a;
    // Inserting 'else' block to prevent latch inference
    else
      reg_fstate <= PWMs4a;
    reg_PWM1 <= 1'b1;
    reg_PWM2 <= 1'b0;
    reg_PWM3 <= 1'b0;
    reg_PWM4 <= 1'b0;
  end
  PWMs5: begin
    if (((PWM == 1'b0) & (CD == 1'b1)))
      reg_fstate <= PWMs4a;
    else if (((PWM == 1'b0) & (CD == 1'b0)))
      reg_fstate <= PWM4b;
    else if ((PWM == 1'b1))
      reg_fstate <= PWMs5;
    // Inserting 'else' block to prevent latch inference
    else
      reg_fstate <= PWMs5;
    reg_PWM1 <= 1'b1;
    reg_PWM2 <= 1'b1;
    reg_PWM3 <= 1'b0;
    reg_PWM4 <= 1'b0;
  end
  PWM2b: begin
    if ((PWM == 1'b0))
      reg_fstate <= PWMs1;
    else if ((PWM == 1'b1))
      reg_fstate <= PWM3b;
    // Inserting 'else' block to prevent latch inference
    else
      reg_fstate <= PWM2b;
    reg_PWM1 <= 1'b0;
    reg_PWM2 <= 1'b0;
    reg_PWM3 <= 1'b1;
    reg_PWM4 <= 1'b0;
  end
  PWM3b: begin
    if ((PWM == 1'b1))
      reg_fstate <= PWM4b;
```

```
            else if ((PWM == 1'b0))
               reg_fstate <= PWM2b;
            // Inserting 'else' block to prevent latch inference
            else
               reg_fstate <= PWM3b;
            reg_PWM1 <= 1'b0;
            reg_PWM2 <= 1'b1;
            reg_PWM3 <= 1'b1;
            reg_PWM4 <= 1'b0;
         end
         PWM4b: begin
            if ((PWM == 1'b1))
               reg_fstate <= PWMs5;
            else if ((PWM == 1'b0))
               reg_fstate <= PWM3b;
            // Inserting 'else' block to prevent latch inference
            else
               reg_fstate <= PWM4b;
            reg_PWM1 <= 1'b0;
            reg_PWM2 <= 1'b1;
            reg_PWM3 <= 1'b0;
            reg_PWM4 <= 1'b0;
         end
         default: begin
            reg_PWM1 <= 1'bx;
            reg_PWM2 <= 1'bx;
            reg_PWM3 <= 1'bx;
            reg_PWM4 <= 1'bx;
            $display ("Reach undefined state");
         end
      endcase
      PWM1 <= reg_PWM1;
      PWM2 <= reg_PWM2;
      PWM3 <= reg_PWM3;
      PWM4 <= reg_PWM4;
   end
 end
endmodule // SM1
```

Appendix E

Mathematica derivation

```
Remove["Global`*"]

(* Pin input power *)
(* Pin output power *)

(* ein error in power analyser at input *)
(* ein error in power analyser at output *)

(* ζ converter efficiency *)

ActualLoss = Pin - Pout;
Pout = Pin ζ;

MeasuredLoss = Pin (1 + ein) - Pout (1 + eout);

LossError = 1 - MeasuredLoss / ActualLoss;

Simplify[LossError]  (* Expression for the error in the loss measurement *)

(* Result = *)

(* Now examine the effect of swapping the two meters *)
(* over and taking the mean of the loss measurements *)


LossErrorTranspose = ( (ein - eout ζ)/(-1 + ζ) + (eout - ein ζ)/(-1 + ζ) ) / 2;
Simplify[LossErrorTranspose]
```

Out[60]= $\frac{\text{ein} - \text{eout}\,\zeta}{-1 + \zeta}$

Out[62]= $\frac{1}{2}\,(-\text{ein} - \text{eout})$